

RADC-TR-82-21
Final Technical Report
March 1982



ACROSS FIVE (ACTIVE CONTROL OF SPACE STRUCTURES) PHASE 1A

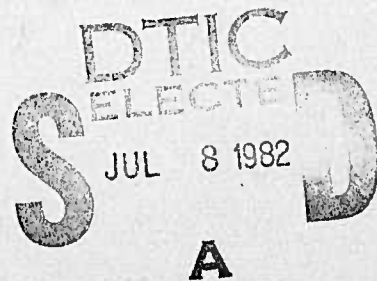
Lockheed Missiles & Space Company, Inc.

Sponsored by
Defense Advanced Research Projects Agency (DoD)
ARPA Order No. 3654

APPROVED FOR PUBLIC RELEASE; DISTRIBUTION UNLIMITED

The views and conclusions contained in this document are those of the authors and should not be interpreted as necessarily representing the official policies, either expressed or implied, of the Defense Advanced Research Projects Agency or the U.S. Government.

ROME AIR DEVELOPMENT CENTER
Air Force Systems Command
Griffiss Air Force Base, New York 13441



82 07 07 002

AD A116655

ACROSS FIVE

DTIC FILE COPY

This report has been reviewed by the RADC Public Affairs Office (PA) and is releasable to the National Technical Information Service (NTIS). At NTIS it will be releasable to the general public, including foreign nations.

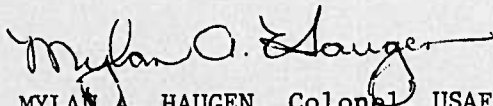
RADC-TR-82-21 has been reviewed and is approved for publication.

APPROVED:



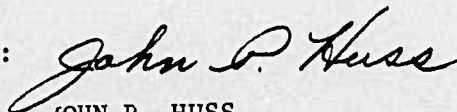
RICHARD W. CARMAN
Project Engineer

APPROVED:



MYLAN A. HAUGEN, Colonel, USAF
Chief, Surveillance Division

FOR THE COMMANDER:



JOHN P. HUSS
Acting Chief, Plans Office

If your address has changed or if you wish to be removed from the RADC mailing list, or if the addressee is no longer employed by your organization, please notify RADC. (OCSE) Griffiss AFB NY 13441. This will assist us in maintaining a current mailing list.

Do not return copies of this report unless contractual obligations or notices on a specific document requires that it be returned.

ACOSS FIVE (ACTIVE CONTROL OF SPACE STRUCTURES) PHASE 1A

Jean N. Aubrun
John A. Breakwell
Narendra K. Gupta
Michael G. Lyons
Gabriel Margulies

Contractor: Lockheed Missiles & Space Company, Inc.
Contract Number: F30602-80-C-0102
Effective Date of Contract: 13 March 1980
Contract Expiration Date: 3 September 1981
Short Title of Work: ACOSS FIVE (ACTIVE CONTROL OF SPACE
STRUCTURES) PHASE 1A
Program Code Number: OE20
Period of Work Covered: Mar 80 - Sep 81

Principal Investigator: Michael G. Lyons
Phone: (415) 493-4411 x45155

Project Engineer: Richard Carman
Phone: (315) 330-3148

Approved for public release; distribution unlimited.

This research was supported by the Defense Advanced
Research Projects Agency of the Department of Defense
and was monitored by Richard Carman (OSCE), Griffiss
AFB NY 13441 under Contract F30602-80-C-0102.



Accession For	
NTIS GRA&I	<input checked="checked" type="checkbox"/>
DTIC TAB	<input type="checkbox"/>
Unannounced	<input type="checkbox"/>
Justification	
By	
Distribution/	
Availability Codes	
Avail and/or	
Dist	Special
A	

UNCLASSIFIED

SECURITY CLASSIFICATION OF THIS PAGE (When Data Entered)

REPORT DOCUMENTATION PAGE		READ INSTRUCTIONS BEFORE COMPLETING FORM
1. REPORT NUMBER RADC-TR-82-21	2. GOVT ACCESSION NO. AD-A116655	3. RECIPIENT'S CATALOG NUMBER
4. TITLE (and Subtitle) ACROSS FIVE (ACTIVE CONTROL OF SPACE STRUCTURES) PHASE 1A		5. TYPE OF REPORT & PERIOD COVERED Final Technical Report 13 Mar 80 - 3 Sep 81
		6. PERFORMING ORG. REPORT NUMBER LMSC-D811889
7. AUTHOR(s) J. N. Aubrun M. G. Lyons J. A. Breakwell G. Margulies N. K. Gupta		8. CONTRACT OR GRANT NUMBER(s) F30602-80-C-0102
9. PERFORMING ORGANIZATION NAME AND ADDRESS Lockheed Missiles & Space Company, Inc. Lockheed Palo Alto Research Laboratory 3251 Hanover Street, Palo Alto CA 94304		10. PROGRAM ELEMENT, PROJECT, TASK AREA & WORK UNIT NUMBERS C6540105
11. CONTROLLING OFFICE NAME AND ADDRESS Defense Advanced Research Projects Agency 1400 Wilson Blvd Arlington VA 22209		12. REPORT DATE March 1982
		13. NUMBER OF PAGES 130
14. MONITORING AGENCY NAME & ADDRESS (if different from Controlling Office) Rome Air Development Center (OCSE) Griffiss AFB NY 13441		15. SECURITY CLASS. (of this report) UNCLASSIFIED
		15a. DECLASSIFICATION/DOWNGRADING SCHEDULE N/A
16. DISTRIBUTION STATEMENT (of this Report) Approved for public release; distribution unlimited.		
17. DISTRIBUTION STATEMENT (of the abstract entered in Block 20, if different from Report) Same		
18. SUPPLEMENTARY NOTES RADC Project Engineer: Richard Carman (OCSE)		
19. KEY WORDS (Continue on reverse side if necessary and identify by block number) Control Theory Micro-vibration Suppression Large Space Structures Low and High Authority Control Structural Dynamics Steady-State Disturbance Rejection Flexible Vehicles Optimal Regulators <u>Stability Augmentation</u> Multivariable Control		
20. ABSTRACT (Continue on reverse side if necessary and identify by block number) The theory of steady-state disturbance rejection for large space structures is developed and tested analytically on a complex optical strawman configuration (CSDL Model #2). It is shown that active control is potentially feasible for micro-vibration stabilization of precision large structures. A number of brassboard experiments have been carried out to illustrate the theory and to address implementation and mechanization of active control systems.		

DD FORM 1 JAN 73 1473

EDITION OF 1 NOV 65 IS OBSOLETE

UNCLASSIFIED

SECURITY CLASSIFICATION OF THIS PAGE (When Data Entered)

PREFACE

This final report for ACOSS FIVE (Active Control of Space Structures) Phase 1A represents work performed by the Lockheed Missiles & Space Co., Inc., and its principal consulting subcontractor Integrated Systems, Inc., for the Defense Advanced Research Project Agency under Contract No. F30602-80-C-0102. Hardware integration for experimental data acquisition and control law implementation was provided by Synergistic Technology, Inc. Prof. R. E. Skelton, Purdue University, served as consultant on the initial activities of Phase 1A.

The authors would like to express their gratitude to the LMSC personnel who have contributed to various tasks of this extensive study project. Listed in order of functional activity, they are: M. J. Ratner (control design and synthesis); D. D. Durante, T. R. Havas, Jr., and A. S. Benson (structural mechanics design and modal analysis); G. J. Chambers (modal testing and experimental hardware integration for TOYSAT); T. P. Winarske (large-scale software development and support); C. R. Denison and E. J. Clisham (hardware, optics, and electronics integration for Palo Alto brassboards); C. C. Huang (development of microphase optical sensor); and L. J. Ritzmann (technical publications).

CONTENTS

Section	Page
	v
	ix
1	1-1
1.1	1-1
1.2	1-1
1.3	1-2
1.4	1-2
2	2-1
2.1	2-1
2.2	2-1
2.3	2-1
3	3-1
3.1	3-1
3.2	3-1
3.3	3-2
3.4	3-2
3.4.1	3-2
3.4.2	3-3
3.4.3	3-10
3.5	3-12
3.5.1	3-12
3.5.2	3-23
3.5.3	3-28

(cont.)

CONTENTS (cont.)

Section	Page
4	
TECHNOLOGY PRIMER	4-1
4.1 Introduction	4-1
4.1.1 Objectives of Structural Control (ACOSS FIVE)	4-1
4.1.2 Peculiarities and Pathologies of LSS	4-1
4.1.3 Motivation for New Synthesis Techniques	4-2
4.1.4 Road Map of New Methodology	4-3
4.2 Modeling of Flexible Spacecraft	4-3
4.2.1 State-Space Models	4-4
4.2.2 Nonlinear Models	4-5
4.2.3 Model Reduction	4-8
4.3 Control Design Methodology	4-9
4.3.1 Low-Authority Control (LAC) Design	4-9
4.3.2 High-Authority Control (HAC) Design	4-11
4.3.3 Controller Simplification	4-14
4.3.4 Actuators and Sensors	4-14
4.3.5 Stability and Performance Evaluation	4-15
4.3.6 Strengths and Weaknesses	4-15
4.4 Application of ACOSS Design Methodology to a Simple Example.	4-15
4.4.1 The Two-Mode Example	4-16
4.4.2 HAC Controller Evaluation on Full-Order Model	4-16
4.4.3 LAC Design and HAC/LAC Controller Evaluation	4-17
4.4.4 Frequency-Shaped Control Laws for Roll-Off	4-17
4.4.5 Evaluation of Frequency-Shaped Roll-Off Control on Full- Order Model	4-18
4.4.6 Frequency Shaping for Rejection of Single-Frequency Disturbance	4-19
4.5 Application of ACOSS Design Methodology to a Complex Optical Structure	4-19
4.5.1 The CSDL No. 2 Structural Model and Disturbances	4-19
4.5.2 The CSDL No. 2 Line-of-Sight Control Problem	4-22
4.5.3 Control Design for CSDL No. 2	4-23
4.5.4 Performance Evaluation for CSDL No. 2 Nominal and Perturbed Models	4-28
4.5.5 Matrix Computational Algorithms for CSDL No. 2	4-31

CONTENTS (cont.)

Section		Page
5	PROGRAM CONCLUSIONS AND RECOMMENDATIONS	5-1
References	R-1
Appendix		
A	CIRCULAR PLATE EXPERIMENT - SIMULATION RESULTS	A-1
B	HAC GAIN MATRICES	B-1

ILLUSTRATIONS

Figure		Page
3-1	Proof-Mass Actuator Concept	3-3
3-2	PPM Actuator Photograph	3-4
3-3	Pivoted Proof-Mass Actuator Schematic	3-4
3-4	Actuator Servo-Loop	3-4
3-5	Velocity Response of PPM Actuator	3-5
3-6	Equivalent Force Actuator	3-5
3-7	PPM Actuator Dynamics Model	3-6
3-8	PPM Actuator Design No. 1 - Performance Region (f, ℓ)	3-7
3-9	Contactless Actuator Principle	3-8
3-10	Octopolar Magnetic Stabilization	3-8
3-11	Contactless Stabilizer Schematic	3-8
3-12	PPM Actuator Calibration	3-9
3-13	Microphase-Optic Ten-Channel Package	3-10
3-14	Toysat Test Setup	3-12
3-15	Measurement and Control Flow Diagram	3-12
3-16	Matrix for Eigenvalues of Six-State Controller	3-14
3-17	Open-Loop Kalman Filter Output (Response to 4-s Chirp)	3-15
3-18	Measured and Predicted Open-Loop Central Body Rotation (Response to 4-s Chirp)	3-16
3-19	Measured and Predicted Open-Loop Rotational Tip Acceleration (Response to 4-s Chirp).	3-16
3-20	Open- and Closed-Loop Central Body Measurements	3-17
3-21	Open- and Closed-Loop Tip Acceleration Measurement	3-18
3-22	Open- and Closed-Loop Kalman Filter Output (Response to 4-s Chirp)	3-18
3-23	Open- and Closed-Loop Transfer Functions; Translational Tip Acceleration/ Input Chirp.	3-19
3-24	Open- and Closed-Loop Transfer Functions; Rotational Tip Acceleration/ Input Chirp	3-20
3-25	Closed-Loop Pole Location; Predicted vs. Test	3-20
3-26	Measurements for Case With Provoked Spillover	3-21
3-27	Transfer Function; Spillover Case Rotational Tip Acceleration/ Input Chirp	3-21
3-28	Measured and Predicted Open-Loop Central Body Rotation for a 20-Hz Sample Rate Kalman Filter	3-22
3-29	Measured Tip Acceleration for Two Closed-Loop Tests, One With Nominal Configuration, One With 2-lb Tip Mass Removed	3-22
3-30	Slim Beam Hardware Setup	3-23
3-31	Slim Beam Sensors/Actuators	3-23

ILLUSTRATIONS (cont.)

Figure		Page
3-32	Slim Beam Experiment Setup	3-24
3-33	LAC Control Loop Parameters	3-24
3-34	Slim Beam Structural Model	3-24
3-35	Slim Beam Principal Modes Analyzed	3-25
3-36	Slim Beam Experimental Versus Theoretical Results	3-26
3-37	Slim Beam Experimental Versus Theoretical Results	3-27
3-38	Parameter Variation Study: Power Spectra	3-28
3-39	Parameter Variation Study: Model Identification by Curve Fitting	3-28
3-40	Circular Plate Experimental Setup	3-29
3-41	Circular Plate Optical Sensing System	3-29
3-42	Photograph of Circular Plate Experiment	3-30
3-43	Circular Plate PPM Actuator Compensation	3-30
3-44	Sensor and Actuator Type and Location for Circular Plate Experiment	3-31
3-45	Overall System Configuration	3-31
3-46	ACOSS System	3-32
3-47	Finite-Element Grid for 60-cm Radius Plate Experiment	3-32
3-48	Modal Frequencies (Hz) and Patterns of the Circular Plate Experiment	3-33
3-49	VAMP Spectral Analysis: Open-Loop Response	3-35
3-50	Stabilization of Rigid Body Controller (HAC) by LAC Controller	3-36
3-51	Array Processor Timing Sequence	3-37

ILLUSTRATIONS (cont.)

Figure		Page
4-1	Flexible Structure Mode Location and Controller Bandwidth	4-2
4-2	Road Map of New Methodology	4-3
4-3	Need to Integrate High-Authority Controller (HAC) and Low-Authority Controller (LAC).	4-9
4-4	A Frequency-Shaped Controller to Reduce High-Frequency Spillover	4-12
4-5	A Frequency-Shaped Filter to Reduce High-Frequency Spillover	4-13
4-6	A Frequency-Shaped Controller to Eliminate the Effect of Disturbance at ω on Output y	4-13
4-7	CSDL No. 2 Model (Artist's Conception).	4-20
4-8	Principal Lumped Masses in CSDL No. 2 (Masses in Relative Proportional Size)	4-20
4-9	Computer-Graphic Display of CSDL No. 2 (All Beam Elements Shown)	4-20
4-10	CSDL No. 2 Model Perturbation (Qualitative)	4-21
4-11	Disturbances and Actuator/Sensor Locations for CSDL No. 2	4-22
4-12	Ratio of Transfer Functions (30% damping/0.1% damping) (See Text)	4-24
4-13	Control Design Approach for Disturbance Rejection	4-24
4-14	Frequency-Shaped Weights for Disturbance Rejection	4-25
4-15	LOX Frequency Response to Sinusoidal Disturbance of Upper-Support Truss, Nominal (P0) and Perturbed (P2, P4) Models	4-29
4-16	A Robust Controller for P_2	4-30
4-17	Total System Equations (CSDL No. 2 Control System).	4-32
4-18	Block Diagram for Combined HAC/LAC Control System	4-32
4-19	Closed-Loop System/Evaluation Model (CSDL No. 2 Control System)	4-32

TABLES

Table		Page
3-1	Characteristic Parameters of Prototype PPM Actuator	3-7
3-2	PPM Actuator Bench Test Results	3-9
3-3	Microphase-Optic Ten-Channel Package	3-10
3-4	Slim Beam Test Matrix	3-10
3-5	Toysat: HAC Estimator Design	3-10
3-6	Toysat: HAC Controller Experiments	3-11
3-7	Circular Plate Test Matrix	3-11
3-8	Toysat Modal Frequencies, Dampings, Mode Shapes, and Influence Coefficients.	3-13
3-9	80-Hz Controller Design Parameters	3-17
3-10	80-Hz Controller Design Parameters	3-17
3-11	Slim Beam System Matrices	3-25
3-12	Slim Beam Open-Loop Characterization	3-26
3-13	Gain Combinations Tested	3-26
3-14	ACOSS System Capabilities	3-32
3-15	Circular Plate Frequencies (Hz)	3-34
3-16	Control and Measurement Vector Definition	3-34
3-17	Control Synthesis Model for the Plate	3-34
3-18	First Open-Loop Characterization	3-36
4-1	Modal Partitioning and Approximate Transfer Functions.	4-7
4-2	Description of Member Perturbations	4-21
4-3	Description of Mass Perturbations	4-21
4-4	System Modes and Their Contributions to the Line-of-Sight Error	4-23
4-5	Effect of Passive Damping on LOS Performance	4-23
4-6	Mode Selection for HAC (12 Modes).	4-25
4-7	Frequency-Shaped Controller/Filter Structure	4-25
4-8	Control and Filter Weighting Used in the Design (Nonzero Elements)	4-26
4-9	Closed-Loop High-Authority Control (HAC) Design	4-26
4-10	Mode Selection for High-Authority (HAC) and Low-Authority (LAC) Control	4-27
4-11a	Closed-Loop Low-Authority Control (LAC) Design	4-28
4-11b	LAC Gains C_L	4-28
4-12	Closed-Loop Poles With HAC/LAC Controller	4-28
4-13	Frequency and LOS Observability Comparisons - Nominal and Perturbed Models	4-29
4-14	LOS Error and Control Efforts for Nominal and Perturbed Models	4-30
4-15	Comparison of Open-Loop and Closed-Loop LOS Errors	4-30
4-16	Closed-Loop Controller Simplification	4-30

Section 1 INTRODUCTION

1.1 BACKGROUND

Deployment of large space structures for communications, space defense, power generation, manufacturing, and research has become a major objective of space mission planners for the mid-1980s and beyond. These systems typically combine large size with extremely rigorous pointing and surface figure performance requirements. There is a clear need to achieve diffraction-limited performance with large apertures exemplified by antennas operating above 10 GHz and by large precision optical systems. Boresight jitter stabilization well below 1 μ rad and dynamic surface figure error near one twentieth of a wavelength are necessary to realize the performance capability of these large systems.

Coupled to these ultrahigh performance requirements are the obvious needs to minimize spacecraft mass and construction and launch costs. High system mass may entail multiple launches and on-orbit assembly, greatly increasing system cost. In addition, structural design and materials limitations may in many cases make high performance unreachable with any mass in a passive system. In general, such constraints result in highly flexible spacecraft which exhibit poor dimensional precision. Our current ability to conceptualize space systems, to select structural materials, and to build mechanisms for on-orbit construction and deployment has now far outstripped our demonstrated ability to control the resulting structures. This observation has in recent years given impetus to the idea of building control-configured spacecraft using active stability-augmentation systems, integrated with the spacecraft structure in the design process, to achieve what passive methods alone cannot accomplish.

Integration of structural and control design is, of course, a well-established discipline for high-performance aircraft, but its extension to flexible spacecraft is by no means straightforward. Not only are the control requirements quite different, but spacecraft structural dynamics also give rise to a dense spectrum of nearly undamped, partly identified modes, some of which must be significantly controlled without destabilizing the closed-loop system. Control requirements for large structures may be broadly divided into three categories: (1) attitude control in the presence of structural bending; (2) transient vibration suppression (usually required during maneuvering); and

(3) suppression of steady-state vibration propagation due to onboard disturbance sources. Stability augmentation and flight control system configurations are dictated by mission-dependent mixes of these objectives. Passive structural damping can in some cases provide the desired performance or enhance active system performance. Such passive methods, however, have unpredictable performance characteristics, address only a small subset of the main control objectives, and in some cases can degrade system performance (see Section 4). Control requirements are an essential ingredient in proper modeling, synthesis, and evaluation activities, and, indeed, the form which the control systems take is highly dependent on the performance requirements.

The purpose of the DARPA/ACOSS program is to investigate the feasibility of control-configured spacecraft by developing and testing control synthesis procedures and performance evaluation techniques and by assessing hardware requirements (through brassboard demonstrations) for flight experiment programs. Specific requirements for Phase 1A are detailed below. During Phase 1, and subsequently in Phase 1A, the Lockheed Missiles & Space Company, Inc. (LMSC) team developed a basic synthesis methodology, described in detail in Section 4 of this report, which incorporated a two-level control synthesis approach. At one level, specific structural mode shapes and modal dampings were significantly modified by plant-dependent estimator/controller forms referred to as high-authority controllers. At the other level, small amounts of damping were introduced by colocated actuator/sensor pairs using rate-feedback (output feedback) control laws synthesized with very little dependence on knowledge of plant parameters. These low-authority control mechanizations provided the basis for reducing spillover instability created by high-authority controls.

1.2 OBJECTIVES FOR PHASE 1A

The extension of Phase 1 activities into Phase 1A (ACOSS FIVE) at LMSC sought to advance the basic synthesis procedures to more complex examples and to provide an experimental basis on which to assess the validity of the synthesis and performance evaluation techniques. Toward this end, the Phase 1A objectives naturally divide into analytical and brassboard demonstration activities. The analytical objectives include:

1. INTRODUCTION

1.4 REPORT FORMAT

1. The formalization of the controls synthesis procedure
2. Application to a complex structure
3. Demonstration of the integration of low- and high-authority control techniques
4. Assessment of robustness
5. Investigation of performance limits

These activities were centered on the analysis of a test structure, CSDL No. 2, representative of a precision optical space system. The brassboard activities included three experiments to address fundamental analytical concepts, viz:

1. Verification of low-authority control synthesis on a two-axis vertical beam
2. Digital mechanization of high-authority control on a test structure using twin flexible beams.
3. Verification of transient suppression using integrated low- and high-authority techniques on a highly resonant circular plate

1.3 SCOPE

This report summarizes the work of Phase 1A by collecting the significant experimental data and interpretations in light of the theoretical developments begun in Phase 1 and continued into Phase 1A. Sufficient detail is provided to assess the depth of the experimental investigation and to motivate the findings, but not to replicate the experiments. Analytical studies are developed in detail and control gains and plant dynamics are provided so that interested researchers may reproduce the analytical results.

1.4 REPORT FORMAT

The report begins in Section 2 with an overview of program achievements with several comments on the role of existing technology. A summary of technical activities follows in Section 3 with a review of the methodology and an explanation of the experimental results. The report concludes with an extensive technology primer which gathers together analytical work on the CSDL No. 2 model and explains the details of the controls approach.

Section 2 TECHNOLOGY ACHIEVEMENTS

2.1 MAJOR FINDINGS AND RESULTS

Basic substantiation of the LAC/HAC control synthesis procedures was achieved in Phase 1A. In particular, analytical work on the complex CSDL No. 2 model showed that LAC and HAC mechanizations, synthesized using different models, could be combined by including LAC control outputs in the HAC estimator equations. This allowed both systems to be synthesized independently without the controllers "working against each other." Independent synthesis of the LAC output feedback mechanization is particularly advantageous. It means that:

1. HAC control synthesis need not consider LAC closed-loop evaluation models.
2. Spillover suppression using LAC can be assured by basing LAC synthesis on a model of much higher order than is convenient or appropriate for HAC synthesis.

Furthermore, this technique allows extremely high-performance steady-state vibration suppression while retaining robustness vis-à-vis spacecraft parameter changes. A fundamental theorem for LAC stability is established which sets limits to maximum LAC performance vis-à-vis structural or actuator passive damping.

Experimental evidence now provides a basis for LAC robustness claims. Cross-coupling errors in multiple degree-of-freedom systems appear to cause no problems for LAC performance. Conversely, noncollocation or nonconsistency errors in the output feedback mechanization can cause significant instability, usually at high frequency. Good sensor/actuator selection and design can eliminate these problems, however. A major performance improvement was achieved in Phase 1A with the development of the pivoted proof-mass actuator (PPM) using high-bandwidth electrodynamic motors. This design is inherently flight-qualifiable.

2.2 RELATIONSHIP TO EXISTING TECHNOLOGY

Methodologies closest to ACOSS involve stability augmentation of control-configured aircraft, ride control, and load alleviation. The LAC output feedback approach (identically located acceleration and force (ILAF) technique) has been used successfully on numerous aircraft. Modal control techniques there can be much simpler than those for space structures, since fewer modes participate in performance degradation or HAC spillover. Also, transient vibration suppression is the only case of interest there. In general, evaluation models for spacecraft are not nearly as well-defined, the control objectives are more complex, and the performance requirements are more difficult to achieve, from both sensor/actuator and algorithm points of view.

2.3 IMPACT ON FUTURE SYSTEMS

Achievement of goals for space-based advanced communication, military surveillance, and weapons systems will necessarily depend on control-configured spacecraft. After feasibility is demonstrated by actual flight experiments, a synergistic approach using combined controls and structural methods will be adopted to effect new systems. Spacecraft missions, now impractical, may become reality in the 1990 time frame.

Methodologies currently being explored for LSS are still developmental and will continue to be that way until flight experiments can confirm the validity of the engineering approach. Engineering proof-of-concept experiments will reduce flight experiment risks, but there is inherently no way to completely verify performance of a system which cannot be ground-tested; and the test would be meaningless in any event. This is currently the major difficulty in achieving acceptance of this technology to the same extent as it has been accepted in the aviation community.

Section 3 TECHNICAL ACTIVITIES

3.1 OBJECTIVES AND APPROACH

The ACOSS FIVE effort encompassed both analytical and experimental activities, which are described in this section. The objectives that motivated those activities were described in Section 1 and are repeated here. Since analytical details are contained in Section 4, only a very brief summary of the procedures will be included here. Experimental results, however, will be fully detailed in Sections 3.4 and 3.5 below.

The project objectives divide into analytical and experimental goals. Analytical objectives include:

1. Development of a procedural organization for the synthesis and evaluation techniques
2. Demonstration of the viability of integrated low- and high-authority control (LAC/HAC)
3. Limited evaluation of LAC/HAC robustness
4. Evaluation of Stability Augmentation Systems (SAS) and disturbance rejection performance limits for control-configured spacecraft.

These objectives are addressed in detail in Section 4.

Experimental objectives are based on requirements for verification of fundamental concepts using realizable sensors and actuators on simple test structures. Following the theoretical development, these objectives are:

1. Verification of LAC synthesis and performance prediction formulas on simple structures
2. Investigation of digital HAC mechanization characteristics
3. Practical integration of LAC and HAC techniques for transient vibration suppression.

The approach to these objectives consists of treating a few control problems in considerable detail by limiting both the number of system models to be investigated and the performance requirements of interest. For the analytical objectives, a single structure, CSDL No. 2, was selected by DARPA for study of synthesis procedures, modeling difficulties, and performance assessments. For the experimental work, three test structures were used: (1) a vertical tubular beam (Slim Beam) to verify multi-axis LAC mechanization using proof-mass inertial force actuators; (2) a multiple beam (Toysat) to assess digital control problems using

noncollocated actuators and sensors; and (3) a vertically suspended highly resonant circular plate using inertial actuators, optical sensing, and combinations of analog LAC and digital HAC. These mechanizations were selected to verify fundamental ideas while demonstrating brassboard-mounted actuator/sensor concepts which could be employed on actual spacecraft. Thus, actuation methods which rely on reactions against the laboratory reference frame were mostly avoided.

3.2 TASKS RELATED TO SOW

The original ACOSS Phase 1A SOW was substantially modified over the course of the contract to reflect changes in experimental objectives. The main SOW objectives for analytical and experimental development are listed below, using the original task numbering.

Task 4.1 Development and Demonstration of Control Strategies

The analytical work, including control law synthesis for brassboards, was included in this task. Although not performed in serial order, the individual tasks included, as required by the Task 4.1 SOW:

- Modeling
- System identification
- Model reduction
- Control law synthesis methodology development
- LAC/HAC synthesis.

Task 4.2 Fabrication

All test articles, including actuators, were fabricated in this task. They included:

- Pivoted-proof-mass actuator construction
- Slim Beam fabrication and assembly
- Toysat fabrication, suspension, and assembly
- Circular Plate fabrication, suspension, and assembly.

Task 4.3 Experiments and Testing

All brassboard testing was accomplished under this task, including:

- Actuator/sensor testing
- Slim Beam data generation and reduction
- Toysat testing
- Circular Plate testing.

3. TECHNICAL ACTIVITIES

3.4.1 ANALYTICAL EXAMPLES AND EXPERIMENT DESCRIPTIONS

During these tests system identification methods were given limited evaluation tests.

3.3 CONTROL THEORY AND METHODOLOGY SUMMARY

In Section 4 a detailed account is given of the theory and methodology subsequently applied to a large complex optical structure (CSDL No. 2) to illustrate the procedures developed in the ACOSS program. In summary form, these steps are (see Fig. 4-2 in Section 4.1.4):

1. Definition of the structural model, the disturbances, and the control objectives. For nontrivial applications finite-element structural modeling is used, providing a specially formatted output tape containing modal frequencies and mode shape values at nodal stations on the structure.
2. Creation of the state-space model to prepare the structure for control systems. This requires a preliminary selection of sensors and actuators based on engineering judgment arising from examining the physics of the problem and refined by the use of controllability, observability, and various modal cost criteria. This initial model is taken to be the "truth-model" or evaluation model, and is generally of large dimension. All control laws subsequently designed are tested against this model for stability and performance.
3. Reduction of the previous model to a workable size for control synthesis. This reduction process also involves controllability, observability, and modal cost criteria. In general, the first reduction is used for LAC synthesis and a further reduction for HAC synthesis.
4. Control synthesis is carried out for HAC, and the spillover, evaluated in the evaluation model, is used to synthesize the LAC gains.
5. The LAC control law is then incorporated into the HAC state estimator, and the combined HAC/LAC control laws are evaluated for stability (spillover correction) and performance on the evaluation model. For robustness tests, the same controller is evaluated on perturbed evaluation models.

3.4 IMPLEMENTATION

Control methodologies developed for the ACOSS program have been implemented and tested on both computer models and real hardware brassboard

experiments. This section briefly summarizes these implementations, which are discussed in detail in subsequent sections. The components used for the brassboard experiments are described in this section, and accompanying numerical data are presented. The matrix of experiments constituting the test plan is examined, and achievements and problems are discussed.

3.4.1 Analytical Examples and Experiment Descriptions

Two computer models have been used to demonstrate the LMSC ACOSS technology. First, a "simple" example consisting of a two-mode model was created for the purpose of demonstrating in its simplest form the theory that had been developed and described. Since one of the most important aspects of LSS control is the handling of unmodeled modes, this example had to be at least a two-mode model, one mode being controlled and the other one uncontrolled, so that the HAC/LAC two-level approach could be demonstrated.

The HAC controller in the simple example involves a state estimator which is of second order if only one mode is to be estimated. The evaluation model of the total system is thus of sixth order - two for the controller plus four for the original two-mode model. Consequently, pure analytical solutions are impossible, since eigenvalues and eigenvectors for a sixth order system are required. Some computing is necessary to determine optimal gains and the stability of the total system even in that simple case. Inclusion of frequency shaping methods, which involve a state augmentation procedure, inflates the size of the example even more. Therefore, this example should not be construed as being representative of the actual control methodology, since the controller order ends up being much higher than that of the original model. This does not happen with a real structure, where the number of modes far exceeds the size of the control system. However, the example will help the reader to follow the various procedures of the control synthesis.

The second example, generated by Charles Stark Draper Laboratory, is more representative of a real spacecraft with high performance optical capabilities. This model, referred to as CSDL No. 2, is a wide-angle, three-mirror optical space system, together with a line-of-sight (LOS) model giving the law of displacement of the image in the focal plane when the structure deforms. The control problem is to reduce the LOS error in the presence of structural vibrations induced by two independent onboard sinu-

sinusoidal disturbances acting simultaneously. The evaluation (truth) model contains 44 modes (or 88 states), and the controller is of order 32, leading to a total system order of 120. The size and complexity of this example is representative of the actual problems encountered for LSS control.

The dynamic analysis, control synthesis, and performance evaluation of such a model requires the use of large-scale computer programs without which the LSS control problem cannot even be addressed. Indeed, the simplest model which is of sufficient size to illustrate fundamental generic approaches (e.g., model reduction, in-band and out-of-band spillover, disturbance rejection, etc.) would be about 20th order for only a five mode system with no actuator or sensor dynamics. In effect then, for the LSS control methodology the difference between models of order 10, 20, or 120 is purely academic except for the additional numerical accuracy problems which result from large-scale computation.

Experimental verifications of the control strategies demonstrated on these computer models have been undertaken using three different test structures. These experiments are referred to as the Slim Beam, Toysat, and Circular Plate experiments.

The Slim Beam is a vertically suspended flexible beam. Actuators and sensors are mounted with no connection (other than electrical) to the laboratory. This experiment adequately represents a free structure in space and is mainly devoted to testing the LAC approach.

Toysat is a horizontal flexible beam with a massive rigid body in its center. The beam is suspended to allow only rotations (or bending) in the horizontal plane. Actuators mounted on the ground impart forces and torque to the central body, and the sensors are linear variable displacement transducers and accelerometers. This experiment demonstrates the capabilities of a digital HAC system for imparting a significant amount of damping in the first few bending modes.

Finally, the Circular Plate is a vertically suspended thin aluminum plate in nearly free-free conditions. The actuators are of two types: 1) proof-mass, and 2) contactless (they have a ground-based part but provide no extraneous friction or damping). The sensors are 1) optical, with ground reference, and 2) inertial (accelerometers). This experiment is the closest of the three to a real LSS because of its

high modal density, low natural damping, and three-dimensional characteristics. It is controlled by a high-speed digital optimal controller capable of handling a large number of states (16 in this current phase). Control operates on pointing as well as vibration. Hardware failure prevented the full testing of this controller, but successful tests were conducted with a purely analog rigid body controller.

3.4.2 Components

Proof-mass actuators. These actuators produce a force on the structure by inertial reaction on a small mass (proof-mass), as shown in Fig. 3-1. Although an exact linear momentum counterpart of the angular momentum storage devices does not exist, the "proof-mass" actuator comes closest to the linear analog of a gyro.

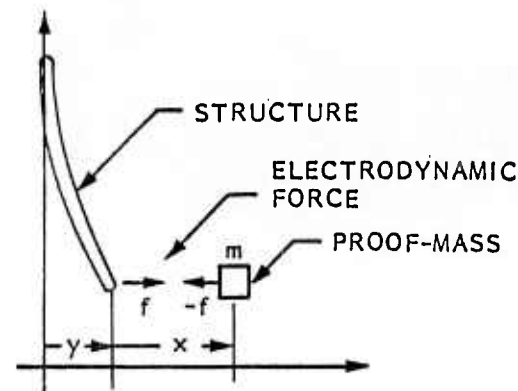


Fig. 3-1 Proof-Mass Actuator Concept

An important feature is that the force f applied to the structure is the opposite of the force acting on the mass m of the actuator. Thus, this mass will accelerate with the acceleration $-f/m$, and, unless the force is reversed, the mass will continue to travel. This seems an obvious point, but it is an important distinction from the CMG case, where the gimbal angle stays constant when no torque is generated. This means that proof-mass actuators cannot be used for rigid-body control; their main purpose is to control vibrations, since in this case they will produce a force with no DC content. In fact, in practical implementations these actuators will always be AC coupled to remove any possible bias, and the mass will have to be physically restrained by a weak spring so it will not drift.

3. TECHNICAL ACTIVITIES

3.4.2 COMPONENTS: PROOF-MASS ACTUATORS

Existing linear actuators (i.e., those which provide a translational motion, such as the Ling Shaker) are plagued by three main disadvantages: considerable weight, stiff guiding/suspension systems with inherent friction, and weakness of the suspension system in transverse loadings. To remedy these difficulties a new actuator was recently developed, the so-called pivoted proof-mass (PPM) actuator. In this actuator the linear motion of the proof-mass is approximated by a small circle of arc about a pivot point realized by a flexure. This type of flex-pivot has three advantages: 1) it is very strong in transverse loadings; 2) it has no stiction; and 3) it is extremely accurate mechanically. The actuation is obtained by a light electrodynamic motor. Figure 3-2 shows a picture of an actual PPM prototype, and Fig. 3-3 shows a schematic of the device.



Fig. 3-2 PPM Actuator Photograph

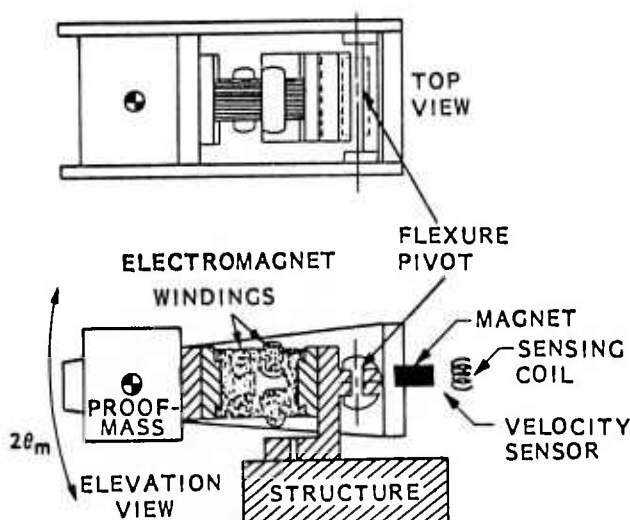


Fig. 3-3 Pivoted Proof-Mass Actuator Schematic

Despite its much improved performances, the PPM actuator still has some residual undesirable dynamics characteristics, mostly due to non-linearities and the flexure spring constant. In order to eliminate these characteristics, the velocity of the proof-mass is controlled by the servo-loop shown in Fig. 3-4. The behavior of this velocity-controlled actuator is described in the following discussion.

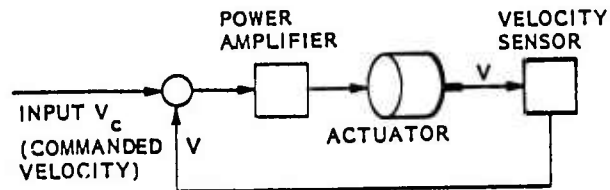


Fig. 3-4 Actuator Servo-Loop

Let m be the mass of the proof-mass, k the stiffness of the suspension system, and x the relative displacement of the proof-mass. The actuator is attached to some structure where displacement is denoted by y . Thus, the transformed equations of the system in the s -plane are

$$\left. \begin{aligned} ms^2(x + y) + kx &= -f + G(v_c - v) \\ v &= sx \\ y &= z(s)f \end{aligned} \right\} \quad (3.1)$$

where $z(s)$ is a transfer function characteristic of the structure and may be very small in the frequency range of interest if the structure is very rigid (e.g., the actuator mounted on a test bench). Solving Eq. (3.1) for v gives the transfer function

$$v/v_c = \left[1 + \frac{k + ms^2}{Gs(1 + ms^2 z(s))} \right]^{-1} \quad (3.2)$$

Thus, for G large enough, the influence of m , k , and z are washed out, and v basically follows the commanded velocity v_c . The bandwidth of such systems is given approximately by

$$\omega_0 \approx G/m, \quad (3.3)$$

and the minimum achievable velocity is

$$v_0 \approx f_0/G \quad (3.4)$$

3. TECHNICAL ACTIVITIES

where f_0 is the friction force in the actuator system. Thus, linearity in both frequency response and amplitude is greatly improved by the velocity feedback. Figure 3-5 shows a typical example of open- and closed-loop transfer functions of this actuator.

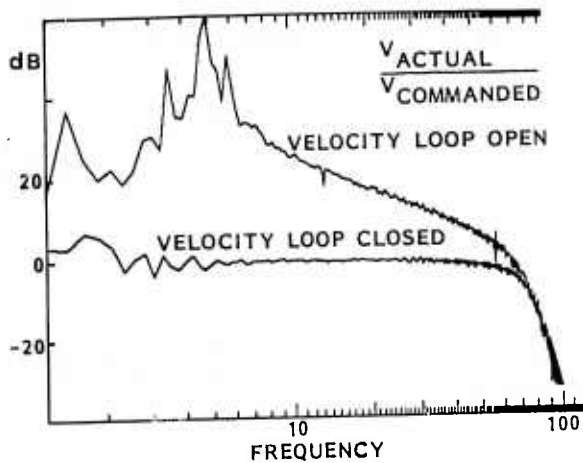


Fig. 3-5 Velocity Response of PPM Actuator

Velocity-controlled (VC) actuators are quite different from force actuators and therefore must be used differently. For LAC implementation, the usual control law in its simplest form is

$$f = -D\dot{y} \quad (3.5)$$

If the structural displacement y is relatively small compared to the displacement of the proof-mass*, then

$$f = -m\ddot{x} \quad (3.6)$$

and Eqs. (3.5) and (3.6) can be combined to give

$$\ddot{x} \approx \frac{D}{m} \dot{y} \quad (3.7)$$

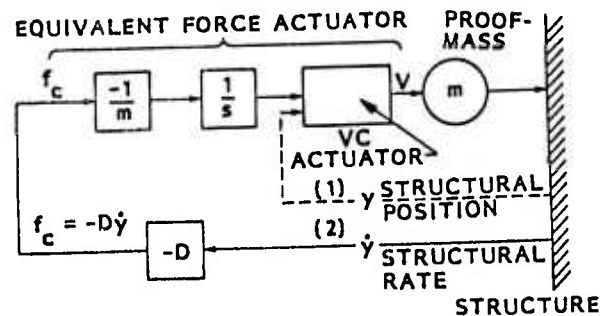
*This is normally the case because the structure's local apparent mass is usually larger than the mass of the proof-mass.

3.4.2 COMPONENTS: PROOF-MASS ACTUATORS

Integrating once leads to

$$v \approx \frac{D}{m} y + \text{constant} \quad (3.8)$$

This shows that the velocity of the actuator must be proportional to the structural displacement. Therefore, when using a VC actuator, one should feed back position and not rate as for force actuators. This is an unusual but very important point to be noted. For example, consider the electronic compensator shown in Fig. 3-6. The commanded force f_c goes through a gain $-1/m$ and is integrated before going to the VC actuator. The velocity of the proof-mass is then $v = -f_c/ms$ and the force output is $f = -msv = f_c$. Thus, the integrating circuit has transformed the VC actuator into a force actuator. In practical applications, however, it is important to remember that proof-mass actuators must be AC coupled, and thus the integration in Fig. 3-6 must be replaced by a compensation of the type $s/(s+a)(s+b)$ where a and b are small compared to the frequency of the lowest mode to be controlled.



- (1) DIRECT USE OF VC ACTUATOR
- (2) USE OF VC ACTUATOR AS A FORCE ACTUATOR

Fig. 3-6 Electronic Compensation for Velocity-Controlled (VC) Actuators

The dynamics of the PPM actuator are not as straightforward as those of the linear type. A dynamic model of the actuator is shown in Fig. 3-7.

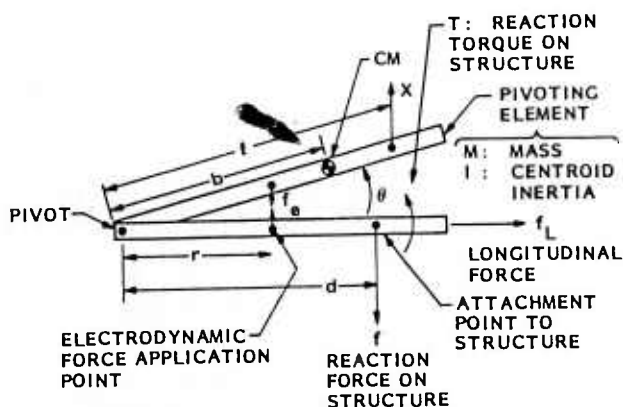


Fig. 3-7 PPM Actuator Dynamics Model

Because of pivoting, both reaction force and torque are produced on the structure.

Application of D'Alembert's principle shows that

$$\left. \begin{aligned} f_L &= -mb(\ddot{\theta}^2 \cos \theta + \ddot{\theta} \sin \theta) \\ f &= mb(\ddot{\theta} \cos \theta - \dot{\theta}^2 \sin \theta) \\ T &= (I + mb^2)\ddot{\theta} - mbd(\ddot{\theta} \cos \theta - \dot{\theta}^2 \sin \theta) \end{aligned} \right\} \quad (3.9)$$

Since the angular displacement θ is usually limited to a few degrees, the above equations may be conveniently linearized. The longitudinal force f_L may be ignored, so that the force and torque applied to the structure by the actuator are given by

$$\left\{ \begin{aligned} f &\approx mb\ddot{\theta} \\ T &\approx (I + mb^2 - mbd)\ddot{\theta} \end{aligned} \right. \quad (3.10)$$

$$(3.11)$$

where

$$\ddot{\theta} = \frac{rf_e}{I + mb^2} \quad (3.12)$$

Equation (3.11) shows that it is possible to have no torque transmitted to the structure by choosing the attachment point at the distance

$$d_0 = (I + mb^2)/mb \quad (3.13)$$

Varying d above or below this value will change the sign of the output torque as well as

its magnitude. The mass of the PPM actuator and its CM may be adjusted by changing the position and mass of a lead piece situated at a distance ℓ from the pivot point.

Let b_0 , m_0 , and I_0 be, respectively, the position of the CM, the mass, and the moment of inertia with respect to the pivot of the "unloaded" actuator, and let m_1 be the mass of the lead piece with which it is loaded. Then

$$\begin{aligned} m &= m_0 + m_1 \\ b &= \frac{m_0 b_0 + m_1 \ell}{m} \\ I + mb^2 &= I_0 + m_1 \ell^2 \end{aligned} \quad (3.14)$$

Using Eqs. (3.10) and (3.12) the ratio of the output force to the electrodynamic force can be expressed as

$$f/f_e = \left(\frac{1 + m_0 b_0 / m_1 \ell}{1 + I_0 / m_1 \ell^2} \right) \frac{r}{\ell} \quad (3.15)$$

In addition to the mass/inertia properties mentioned previously, two important parameters must be considered in the design and use of PPM actuators:

- (1) f_{em} = maximum electrodynamic force
- (2) θ_m = maximum angular displacement.

Since the angular displacement θ depends upon the frequency, optimal choices for the design parameters will depend upon the frequency range of application. From the two conditions

$$|f_e| \leq f_{em} \quad (3.16)$$

$$|\theta| \leq \theta_m \quad (3.17)$$

and Eqs. (3.10), (3.14) and (3.15), two more conditions, namely

$$|f| \leq \left(\frac{1 + m_0 b_0 / m_1 \ell}{1 + I_0 / m_1 \ell^2} \right) \frac{r}{\ell} f_{em} \quad (3.18)$$

$$|f| \leq (1 + m_0 b_0 / m_1 \ell) m_1 \ell^2 \omega_m^2 \theta_m \quad (3.19)$$

are found when $\omega/2\pi$ is the frequency of the output force.

3. TECHNICAL ACTIVITIES

Design regions may be derived from these conditions. The quantities ℓ/r and ω may be chosen as main parameters, and regions of possible values of f may be plotted as functions of them. Typical plots were obtained for the prototype PPM actuator, whose characteristic parameters are shown in Table 3-1.

Table 3-1 CHARACTERISTIC PARAMETERS OF PROTOTYPE PPM ACTUATOR		
Mass	Geometry	Electro- dynamics
$I_0 = 1.5 \cdot 10^{-5} \text{ kg m}^2$ $m_0 = 0.088 \text{ kg}$	$b_0 = 0.016 \text{ m}$ $r = 0.021 \text{ m}$ $\theta_m = 0.067 \text{ rad}$	$f_{em} = 1 \text{ N}$

The actuator used in the experiments has a proof-mass $m_1 = 0.08 \text{ kg}$. Figure 3-8 shows the output force f as a function of ℓ/r . Depending on the lever arm, more or less force can be obtained. The zero point (obtained for a negative value of ℓ) corresponds to locating the composite center of mass at the pivot point.

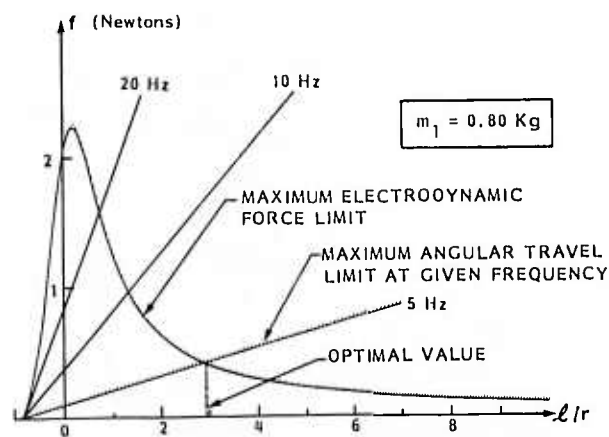


Fig. 3-8 PPM Actuator Design No. 1 - Performance Region ($f, \ell/r$)

The fact that the curve in Fig. 3-8 does not go to infinity for $\ell/r = 0$ but has a maximum is due to the inertia of the unloaded actuator,

3.4.2 COMPONENTS: CONTACTLESS ACTUATORS

which absorbs part of the energy going to the proof-mass m_1 . The straight lines represent the limits, at various frequencies, due to the angular travel limitation. It is thus seen that at a given frequency there is an optimum value for ℓ/r corresponding to the intersection of the curve and the straight line. If this value of ℓ/r is chosen for a given frequency, then the actuator will perform properly at all higher frequencies. For instance, if this actuator has to control vibrations at or above 5 Hz, a value close to 3 is optimal for ℓ/r , leading to the corresponding values:

$$\left. \begin{aligned} \ell &= 0.062 \text{ m} \\ b &= 0.038 \text{ m} \\ m &= 0.168 \text{ kg} \\ I &= 8.2 \times 10^{-5} \text{ kg m}^2 \end{aligned} \right\} \text{Optimal for 5 Hz. (3.20)}$$

The effect of increasing the mass m_1 is to increase the angular travel limit, thus allowing the actuator to work at lower frequencies with basically the same force output. Obviously the increase in mass can be traded off against an increase of ℓ/r , but at the expense of the force level.

Contactless Actuators. This type of actuator was designed to provide small but continuous forces for rigid body control purposes in the laboratory. Attitude control in ground experiments usually presents a special problem because the PPM actuators saturate almost immediately at any DC level needed to compensate for external disturbances (air currents, suspension stiffness, or unbalance).

For small specimens, gyros are not feasible because they would have to be miniaturized or because they too will tend to saturate after a while.

Electrodynamic actuators connected to the ground usually introduce too much friction and damping and interfere with the six-degrees-of-freedom suspension system. One simple way to produce forces without mechanical contact is by the interaction of a small permanent magnet with a fixed-base magnetic field created by a coil as shown in Fig. 3-9. Passive stabilization of the specimen may be obtained by a purely magnetic system as shown in Fig. 3-10, where the magnet attached to the structure has a neutral equilibrium position. (This is not a stable equilibrium along the magnet axis, but the structure's motion along this axis is usually stabilized by the mechanical suspension itself.)

3. TECHNICAL ACTIVITIES

3.4.2 COMPONENTS: ELECTROSEIS ACTUATORS

The contactless stabilizer used in the plate experiment is a combination of the devices in Figs. 3-9 and 3-10 and is depicted in Fig. 3-11.

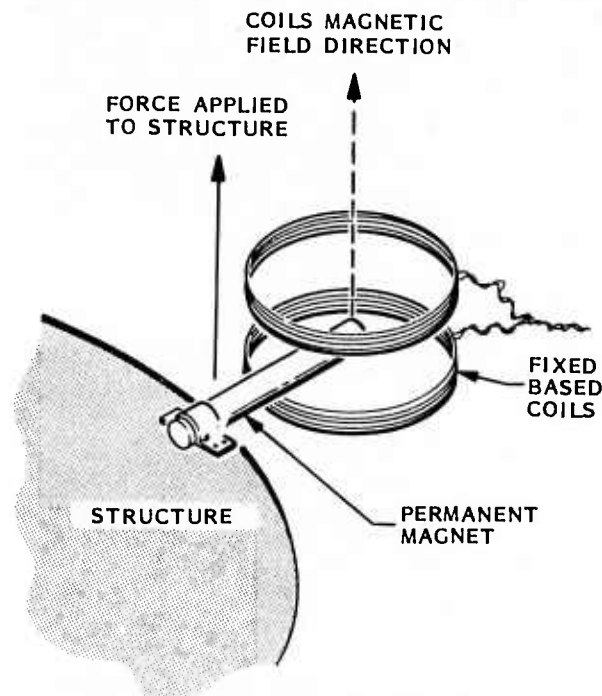


Fig. 3-9 Contactless Actuator Principle

Electroseis Actuators. These actuators are made by Acoustic Power Systems, and their primary function is to provide excitation for testing structures. They are of the linear type, i.e., the force is transmitted through a rod which is moving along its own axis. The force is produced by a coil/permanent magnet system. The constrained translation of the moving part is provided by rollers.

The use of electroseis actuators in a control system is made difficult by their friction characteristics, their nonlinear behavior at high force level or frequency, their large weight (80 lb), and the fact that they must have their base mounted on the ground. The output stroke is ± 6 in., and they can provide a maximum of 30 lb output. Their frequency range is between 1.0 Hz and 30.0 Hz. Since the moving part weighs about 5 lb, it affects the characteristics of the structure to which it is attached and has to be taken into account in the analytical model of the structure. This type of actuator was used for the Toysat experiment and worked reasonably well, given its pathologies.

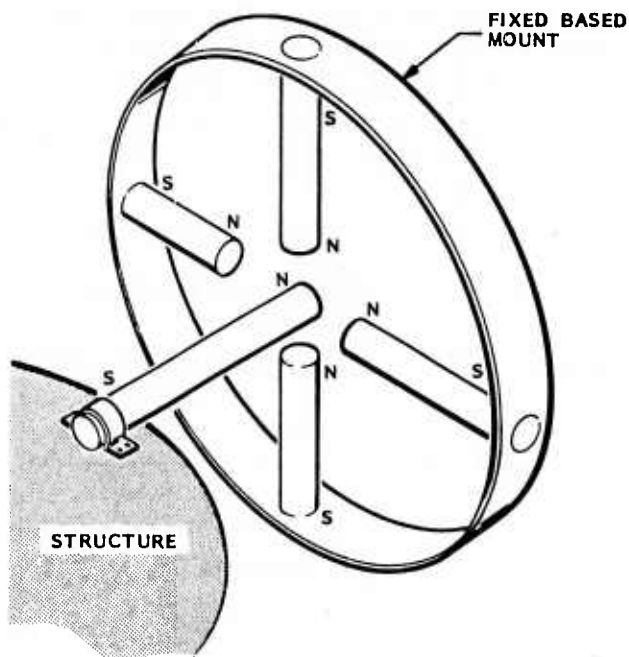


Fig. 3-10 Octopolar Magnetic Stabilization

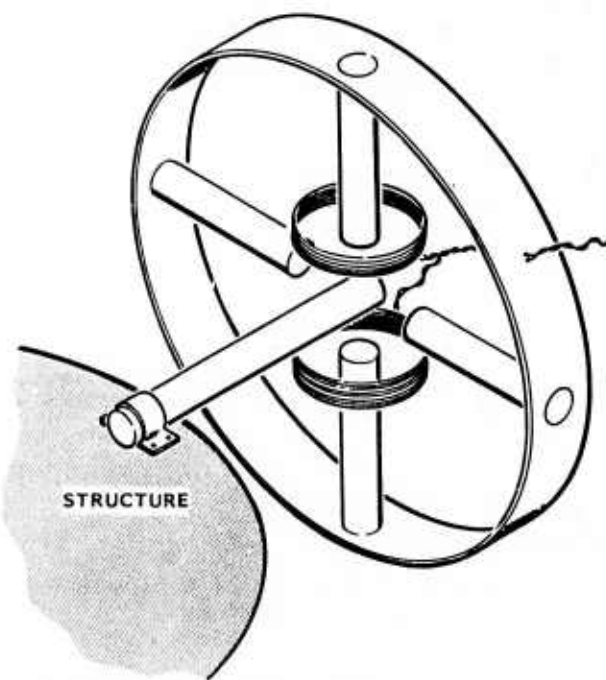


Fig. 3-11 Contactless Stabilizer Schematic

3. TECHNICAL ACTIVITIES

3.4.2 COMPONENTS: ACTUATOR CALIBRATION

Actuator Calibration. Calibration of a PPM actuator is performed with the actuator tightly mounted on an optical bench. Angular motions are detected optically (by a laser beam, mirror, and linear detector), inertially (by an accelerometer), and electromagnetically (by the velocity sensor coil) as shown in Fig. 3-12. The primary measurement is the optical one because of its accuracy and sensitivity. The accelerometer provides a way to cross-check the data in the high frequency range. These measurements, along with those of voltages and currents in the servo-loop, allow for the calibration of the velocity sensor, the output force of the actuator (versus input current), and the various gains in the servo-loop. The principal results are shown in Table 3-2.

Table 3-2 PPM ACTUATOR BENCH TEST RESULTS		
f/I	0.12	N/amp
K_v	0.124	V/ms ⁻¹
G_v	1200	

Note that the force calibration is indirect, obtained from the measurement of the angular amplitude θ_m and the relation

$$f = mb \omega^2 \theta_m$$

where $\omega/2\pi$ is the excitation frequency, and m and b are the quantities defined in Eqs. (3.14) and computed from the (measured) values given in Table 3-1.

The contactless actuators were calibrated directly on the circular plate from observations of the rigid-body response under low-frequency sinusoidal excitation. The force was obtained from the relation

$$f = \frac{M}{4} \omega^2 \theta_m$$

where M is the mass of the plate, and θ_m is the rigid-body rotation angle. For these actuators the force/current relation was found to be:

$$f/I = 0.1 \text{ N/amp}$$

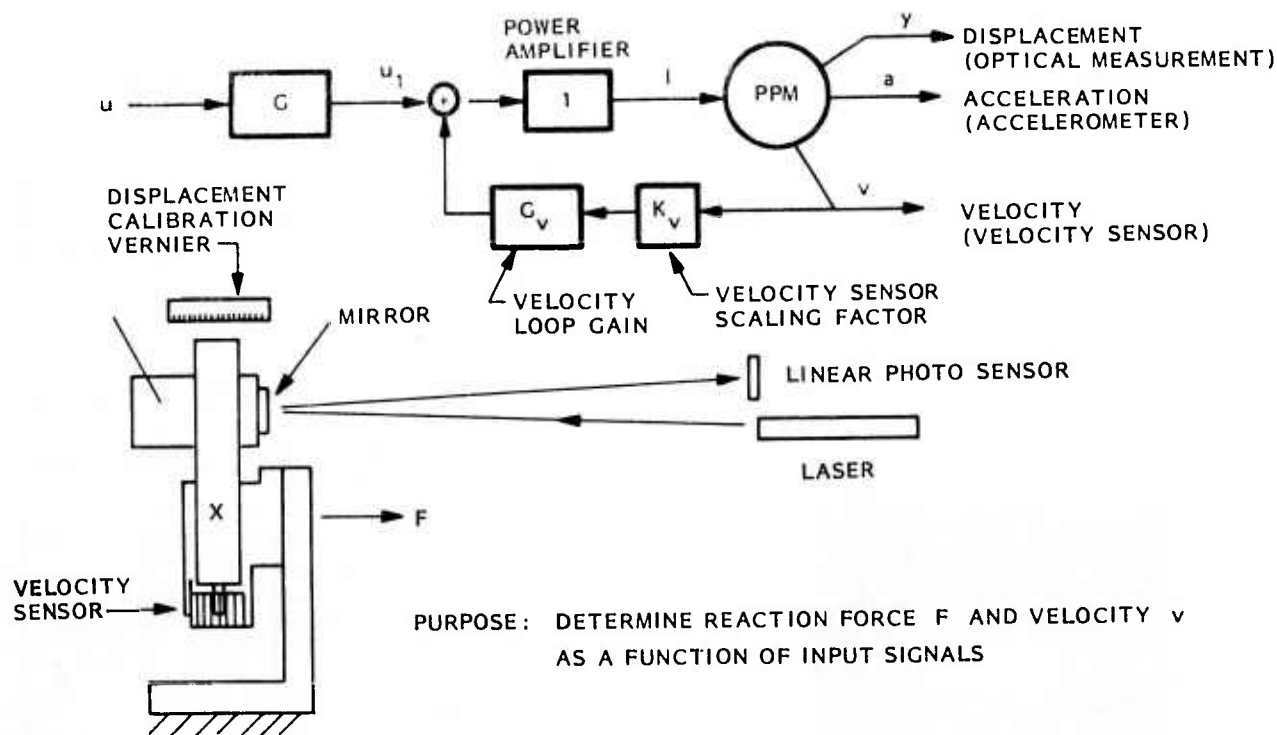


Fig. 3-12 PPM Actuator Calibration

Finally, the electroseis actuators were calibrated on the bench by means of load cells.

Sensors. Two types of sensors were used in all the brassboard experiments - accelerometers and optical angular sensors. However, a new optical sensor, the "microphase optic" sensor, was developed and tested during this phase of the contract. The accelerometers are Unholtz-Dikie piezoelectric accelerometers with an output of 1 V/g. Their sensitivity above 3 Hz is about 1 mg.

The optical angular sensor uses three elements:

1. A low-power He-Ne laser producing a beam used as a reference for angle measurements
2. A small mirror mounted on the structure, reflecting the laser beam
3. A linear photodetector measuring the displacement of the reflected beam.

Such a device was used to calibrate the PPM actuators shown in Fig. 3-12.

For long optical paths (10 to 40 ft or more) it is customary to add a beam expander to the laser to ensure good convergence of the spot on the detector. The detectors used in the experiments were United Detector Technology two-axis photodetectors. Their active area is 0.74×0.74 (in.²), and their sensitivity is 0.0001 in. Special low-noise amplifiers are used in conjunction with them. With a 1 mW laser the output at maximum deflection is about ± 12 V.

The principle of the microphase optics sensing system was described previously in the ACOSS THREE Phase 1 final report (Ref. 1). This system is capable of simultaneously measuring the position of several points on a structure by sending laser beams to corner mirrors and measuring the phase of the return beams. A ten-channel package was built, and preliminary tests were made. Figure 3-13 shows a picture of the optical package. Its external dimensions are $24\frac{3}{4} \times 14\frac{1}{4} \times 5$ (in.).



Fig. 3-13 Microphase Optics Ten-Channel Package

Because of the sensor's extreme sensitivity ($0.08 \mu\text{m}$), dynamic range (2 cm), and wide bandwidth (5 kHz), it appears very promising for complex structures (e.g., dynamic figure control of large optical systems).

3.4.3 Test Plan

The experimental objectives of this study are summarized in Table 3-3 below.

Table 3-3 EXPERIMENTAL OBJECTIVES		
CONTROL TYPE	BRASSBOARD	OBJECTIVES
Low-Authority (LAC)	Slim Vertical Beam	<ul style="list-style-type: none"> • 2-Axis LAC • Comparison with Prediction • Cross-Coupling/Noncollocation Effects • Robustness Tests • Fundamental Stability Theorem
High-Authority (HAC)	Toysat Structure (Flexible Multiple Beams)	<ul style="list-style-type: none"> • Robustness Demonstration • Rigid-Body/Bending Mode Control • Spillover Demonstration
HAC with LAC	Circular Plate	<ul style="list-style-type: none"> • Multi-Mode/Multi-Actuator Digital Control • Analog LAC • Frequency-Shaped Controls • Interaction Between LAC and HAC

In order to reach these objectives, a test plan was established for each of the experiments. These test plans are described in Tables 3-4 to 3-7.

Table 3-4 SLIM BEAM TEST MATRIX				
TEST NO.	PURPOSE	ROLL-OFF	PLANT	COMMENTS
0	ACTUATOR CHARACTERISTICS	NOMINAL (70 Hz)	-	
1 + 10	PERFORMANCE PREDICTION/ GAIN ROBUSTNESS		NOMINAL	EXTREMELY GOOD AGREEMENT
11 + 20	GAIN VARIATION WITH LOW-FREQ. ROLLOFF	LOW (30 Hz)	NOMINAL	NO EFFECT
21 + 30	GAIN VARIATION WITH PLANT PARAMETER CHANGE	NOMINAL	PERTURBED (50% OF MASS)	HIGH ROBUSTNESS

Table 3-5 TOYSAT: HAC ESTIMATOR DESIGN				
TEST	SAMPLE RATE (Hz) 10 20 40 80	ESTIMATED MODES	ANTIALIASING FILTER	COMMENTS
1.	X	Rigid Body + 4 Bending Modes	No Filters	Unsuccessful
2.	X			Satisfactory
3.	X			
4.	X			
5.	X			
6.	IN-BAND UNMODELED MODES TESTS REMOVED		X {100 Hz} X {150 Hz}	No Effect
7.				
8.				
9.	Selectee Rate			
10.	Selected Rate			

3. TECHNICAL ACTIVITIES

3.4.3 TEST PLAN

The Slim Beam test matrix is shown in Table 3-4. The most important tests were Nos. 1 to 10. The effects of noncolocation and nonconsistency of the sensor/actuator system were also shown in the tests. These effects precluded the observation of the fundamental LAC theorem, which presupposes colocation and consistency. Digital state estimator studies conducted on the Toysat experiments are shown in Table 3-5, and the digital optimal controller (HAC) experiments are listed in Table 3-6.

The circular plate experiment test matrices are shown in Table 3-7. Because of hardware problems, digital controller tests could not be performed. However, successful tests were obtained with an analog two-axis rigid body controller using two contactless actuators,

Table 3-6
TOYSAT: HAC CONTROLLER EXPERIMENTS

CONTROLLER GAIN				SAMPLE RATE (Hz)		MODES CONTROLLED	PLANT VARIATION		COMMENTS
TEST	LOW	NOMINAL	HIGH	80	40		NONE	1	
1.		X		X		X	X		Nominal Case (with tip masses)
3.		X		X		Y		X	Effect of Plant Variations on Stability (one tip mass removed)
5.	X			X		X	X		Eventually Provoked Spillover
6.			X	X		X	X		
11. 12. 13.	X		X		X	X X X	X X X		Low Frequency Instability

Table 3-7
CIRCULAR PLATE TEST MATRIX

REPEAT EXPERIMENT WITH CONTROLLER FOR HAC FORMULATED WITH SHARP ROLL-OFF FILTER FOR OUT-OF-BAND DISTURBANCES

TEST	PURPOSE	CONTROLLER		NUMBER OF ACTUATORS		MODES 2 RIGID + 5 BENDING	DISTURBANCES TYPE LOC		PLANT ^b	REMARKS
		HAC	LAC	2	4		1 ^a	1		
1	BASELINE RUNS	1	STABLE	X		X	1	1	1	ANALOG CONTROLLER ONLY - 2 RIGID BODY MODES CONTROLLED
2		2	MARGINALLY UNSTABLE	X		X	1	1	1	ANALOG CONTROLLER ONLY - 2 RIGID BODY MODES CONTROLLED
3	EFFECTS OF DISTURBANCE LOCATION CHANGE ON PERFORMANCE	1			X	X	1	1	1	NOT AVAILABLE
4		2			X	X	1	2	1	NOT AVAILABLE
5		1			X	X	1	1	2	NOT AVAILABLE
6	PLANT SENSITIVITY TO PERTURBATION WITHOUT LAC	2			X	X	1	1	2	NOT AVAILABLE
7		1			X	X	1	1	3	NOT AVAILABLE
8		2			X	X	1	1	3	NOT AVAILABLE
9	EFFECTS OF LAC ON HAC	1			X	X	1	1	1	PERFORMANCE INCREASED OUT OF BAND NOT AVAILABLE
10		2		X	X	X	1	1	1	UNSTABLE CASE STABILIZED ANALOG CONTROLLER ONLY - 2 RIGID BODY MODES CONTROLLED

^a TYPE 1 DISTURBANCES ARE ACTUALLY TWO TESTS. THE FIRST TEST IS WITH BROAD-BAND DISTURBANCES WITHIN THE CONTROLLER BANDWIDTH. THE SECOND TYPE IS BROAD-BAND PAST THE CONTROLLER BANDWIDTH.

^b PLANT 1 IS BASELINE PLATE. PLANT 2 IS SMALL VARIATION. PLANT 3 IS A LARGE VARIATION.

3. TECHNICAL ACTIVITIES

demonstrating the fundamental spillover problem and its stabilization by an LAC system.

3.5 VERIFICATION

3.5.1 Toysat Experiment

Phase 1A Objectives. In Phase 1, the Toysat experiment was used to demonstrate optimal slewing, Low Authority Control, and High Authority Control.

For Phase 1A, the Toysat objective was to delve into the mechanics of the digital High Authority Control. Areas of concern were: 1) agreement between analytical prediction and experimental results; 2) spillover; 3) low sample rate systems; and 4) sensitivity to parameter errors.

These were all investigated experimentally, and the results are presented here.

Hardware Setup. A drawing of the Toysat experimental setup is shown in Fig. 3-14. The test setup consists of a 12-ft flexible beam fastened to the side of a 1.3-ft square block of aluminum. To accentuate bending, a 2-lb weight is attached to each end of the beam. The beam is suspended from the ceiling in such a way as to allow free motion in the horizontal plane.

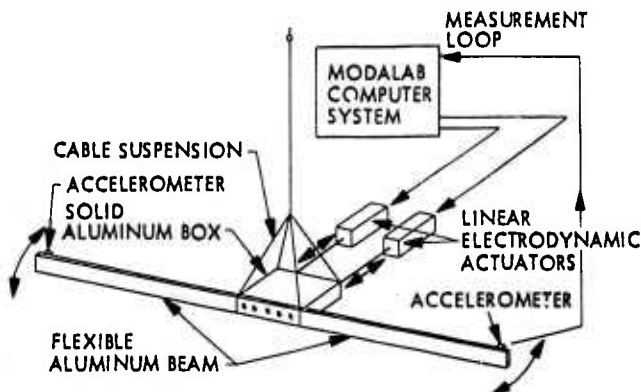


Fig. 3-14 Toysat Test Setup

Control of the motion of the specimen is provided by two linear actuators. When the actuators act together, translational motion results, and when equal but opposite commands are given, pure rotational motion results. Sensing is provided by accelerometers mounted at the ends of the flexible beam and by linear position sensors mounted in tandem with the linear actuators. The average of the two accelerometer measurements indicates the translational motion,

3.5.1 TOYSAT EXPERIMENT: CONTROLS SYNTHESIS

and their difference measures the rotational motion. The same holds true for the position sensors. The separation of rotation and translation in both controller and sensor, as well as in the physical behavior of the Toysat, allows independent and separate design of translational and rotational control laws.

Figure 3-15 shows how the Toysat is connected by way of A/D and D/A converters to a computer where the digital control law is implemented. The large number of computations necessary to carry out the control law is handled by an array processor which allows a sampling rate of 80 Hz.

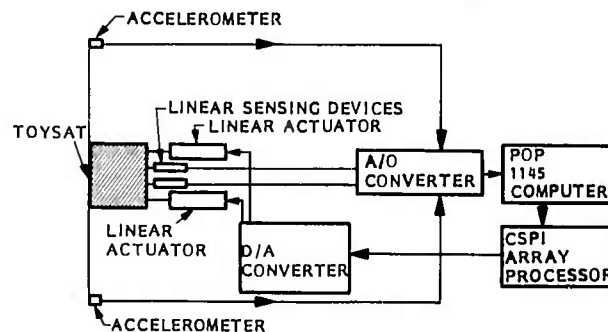


Fig. 3-15 Measurement and Control Flow Diagram

The frequencies, dampings, and mode shapes for the assembled system are shown in Table 3-8. These data result from a judicious combination of analysis and testing. The rigid body modes and the first two bending modes in both translation and rotation are used in controls synthesis and implementation. The remaining modes are used to evaluate the effect of spillover. The frequencies and dampings (ω_i , ξ_i) are assembled in the usual block diagonal form to give the F matrix, the η_i give the G matrix, and the $\phi_i(0)$ and $\phi_i(L)$ give the H_1 and H_2 matrix components corresponding to the linear sensors and accelerometers respectively. (For definitions of these matrices, see Section 4.2.1.)

Controls Synthesis. The controller implemented in the hardware has the form:

$$\begin{aligned}\hat{x}_{n+1} &= \Phi' \hat{x}_n + \Gamma' u_n + K z_n \\ u_n &= C x_n,\end{aligned}\quad (3.21)$$

where Φ' denotes the transition matrix, and Γ' , K , C are constant matrices to be determined. This deceptively simple form conceals a

3. TECHNICAL ACTIVITIES

multitude of complexities involved in choosing the gains K and C. The controller separates naturally into a part which estimates the modal amplitudes and another part which outputs these estimates, multiplied by some gain, to the control actuators. In accordance with this separation we will present first the estimator synthesis and then the control gains synthesis.

Filter Synthesis. The problem is defined in the continuous domain by Eqs. (3.22) below. (The state covariance is specified in the continuous domain.)

$$\begin{aligned}\dot{x} &= Fx + Gu + w_c \\ z &= H_1x + H_2\dot{x} + v_c\end{aligned}\quad (3.22)$$

w_c is white noise, zero mean, covariance Q_c ;
 v_c is white noise, zero mean, covariance R_c .

The extra term H_2 is necessary because the standard form does not allow for acceleration measurements. The specific entries in the matrices for the separate translation and rotation plants are given in Table 3-8.

Table 3-8 TOYSAT MODAL FREQUENCIES, DAMPINGS, MODE SHAPES, AND INFLUENCE COEFFICIENTS					
	ω_i (Hz)	ξ_i (%)	ϕ_i (o)	ϕ_i (el)	η_i
Trans R.B.					
1	0.19	70.0*	1.0	1.0	3.24
2	0.98	0.58	0.0842	-0.952	4.21
3	9.06	0.29	0.0365	0.365	1.83
4	28.02	0.54	0.0210	-0.229	1.05
5	57.69	0.74	0.0147	0.0164	0.735
6	98.15	0.1	0.0113	-0.128	0.565
	149.38	0.1	0.0092	0.105	0.460
RT R.B.					
1	0.0	0.0	1.0	72.0	0.00712
2	2.64	0.33	0.252	-0.471	1.54
3	9.87	0.30	0.127	0.335	0.774
4	28.4	0.54	0.055	-0.226	0.335
5	57.94	0.88	0.033	0.163	0.201
6	98.33	0.1	0.022	-0.127	0.134
	149.53	0.1	0.017	0.104	0.104
Total Mass = 3.708 slugs Total Inertia = 140.47 in.-lb-s ²					
*An approximation for a phenomenon that cannot be accounted for by modal damping.					

3.5.1 TOYSAT EXPERIMENT: FILTER SYNTHESIS

The first step in the synthesis process is to convert the continuous system given in Eqs. (3.22) to a discrete system,

$$\begin{aligned}x_{n+1} &= \Phi x_n + \Gamma u_n + w_d \\ z_n &= H_1x_n + H_2\dot{x}_n + v\end{aligned}\quad (3.23)$$

w_d is zero mean white noise, covariance Q_d ;
 v is zero mean white noise, covariance R .
 Q_d is derived from Q_c by the formula

$$Q_d = E \{ w_d w_d^T \} = \int_0^T \Phi(t) Q_c \Phi^T(t) dt. \quad (3.24)$$

Φ and A are derived from F and G using standard numerical matrix exponential procedures. T is the step length. The covariance of the discrete noise R is taken as an input and is not derived from the continuous measurement noise R_c . Equations (3.23) are put into standard Kalman filter form in two steps. First x_n is substituted for in the z_n equation by means of Eq. (3.22), leaving

$$z_n = H_1x_n + H_2Fx_n + H_2Gu_n + H_2w_c + v. \quad (3.25)$$

Then to the first of Eqs. (3.23) we add the identically zero quantity

$$\begin{aligned}L \{ z_n - H_1x_n - H_2Fx_n \\ - H_2Gu_n - H_2w_c - v \}\end{aligned}\quad (3.26)$$

where L is to be determined later. The result is

$$\begin{aligned}x_{n+1} &= [\Phi - LH_1 - LH_2F] x_n \\ &+ [\Gamma - LH_2G] u_n + Lz_n \\ &+ w_d - LH_2w_c - Lv.\end{aligned}\quad (3.27)$$

Equations (3.25) and (3.27) together constitute the usual Kalman filter problem if L is chosen so that the measurement noise ($H_2w_c + v$) and the state noise ($w_d - LH_2w_c - Lv$) are uncorrelated. Equation (3.28) shows the choice of L that accomplishes this.

$$L = \Phi(T) Q_c H_2^T [H_2 Q_c H_2^T + R]^{-1} \quad (3.28)$$

3. TECHNICAL ACTIVITIES

3.5.1 TOYSAT EXPERIMENT: SPECIFIC CONTROLS DESIGN

Standard optimal techniques may now be used to obtain the filter gains K . The resulting filter has the form

$$\begin{aligned} \hat{x}_{n+1} = & [\Phi - (L + K)(H_1 + H_2 F)] \hat{x}_n \\ & + [\Gamma - (L + K) H_2 G] u_n + (L + K) z_n. \end{aligned} \quad (3.29)$$

Φ and Γ shown in Eq. (3.21) are just the appropriate coefficients of x_n and u_n from Eq. (3.29).

Control Gains. The control segment of the problem is specified by

$$\dot{x} = Fx + Gu \quad (3.30)$$

with the cost functional

$$J = \int_0^\infty (x^T A x + u^T B u) dt.$$

Again, as with the filter, this problem is converted to a discrete problem

$$x_{n+1} = \Phi x_n + \Gamma u_n, \quad (3.31)$$

but now the cost function is specified by

$$J = \sum_{n=1}^{\infty} (x_n^T \tilde{Q} x_n + u_n^T \tilde{S} u_n + 2 u_n^T \tilde{R} x_n), \quad (3.32)$$

where the weights \tilde{Q} , \tilde{S} , \tilde{R} of the discrete problem are given by

$$\tilde{Q} = \int_0^T \Phi^T(t) A \Phi(t) dt \quad (3.33a)$$

$$\tilde{S} = \int_0^T \Gamma^T(t) A \Phi(t) dt \quad (3.33b)$$

$$\tilde{R} = \int_0^T \{ B + \Gamma^T(t) A \Gamma(t) \} dt. \quad (3.33c)$$

Equations (3.31) and (3.32) specify a standard discrete optimal control problem that is easily solved by standard methods. The resulting gains C are those implemented in the controller specified by Eq. (3.21).

Evaluation of controller. When the six-state controller for either translation or rotation is completed, it is tested on an augmented fourteen-state evaluation model. The eigenvalues of the six-state controller operating on the fourteen-state plant are investigated for signs of spillover. These eigenvalues are those of the matrix shown in Fig. 3-16. The superscripts 14 in this figure refer to the fourteen-state evaluation model.

Specific Controls Design. The actual gain selection procedure, like the theory, divides into separate estimator and control gains selections. First a filter was designed and tested on the open-loop system. When that seemed to be working, the loop was closed with an appropriate set of control gains.

To obtain filter gains, the parameters to be selected were the continuous state noise covariance matrix Q_C (defined in Eq. (3.22)) a six-by-six matrix for either translation or rotation, and the state noise covariance matrix R (defined in Eq. (3.23)), a two-by-two matrix assumed to be diagonal.

The approach to choosing Q_C and R was to pick Q_C so as to maximize the separation of the estimator poles. When done correctly this assures that the separate states in the Kalman filter contain just the intended modal amplitude

$$\left[\begin{array}{c|c} \Phi^{14} & \Gamma^{14} C \\ \hline (K + L) [H_1^{14} + H_2^{14} F^{14}] & \Phi - (K + L) (H_1 + H_2 F) + [\Gamma - (K + L) H_2 G] C \\ & + (K + L) H_2^{14} G^{14} C \end{array} \right]$$

Fig. 3-16 Matrix for Eigenvalues of Six-State Controller

3. TECHNICAL ACTIVITIES

3.5.1 TOYSAT EXPERIMENT: EXPERIMENTAL RESULTS

and very little of the others. That is, Q_c is picked to minimize cross-talk between modes in the Kalman filter.

Figure 3-17 shows the time history of the estimates of the state vector for a good choice of Q_c . The specimen had been excited by a four-second chirp (a fast sine sweep varying linearly in frequency), and the outputs of the estimator were recorded. The rigid-body channels contain all the low-frequency movement, while the modal channels separate the remaining frequencies nicely.

The measurement covariance matrix R was chosen to force good convergence of a modal reconstruction of the measurements with the actual measurements. That is, individual components of R are increased until corresponding components of Hx converge with the actual measurements fairly quickly. Figures 3-18 and 3-19 show that the modal reconstruction of the rotational displacement and tip acceleration converge quite quickly with the actual measurements. Again, in this case the specimen had been perturbed by a four-second chirp and then allowed to settle.

Once a filter design has been established, the selection of control gains is straightforward. Since there was no obvious physical quantity such as a line of sight on the Toysat, the control weights were picked to give fast and roughly equal settling times for all modes. The values for the covariance matrices and control weighting matrices which generated the nominal controller are shown in Table 3-9 for the translation controller and in Table 3-10 for the rotation controller. Also shown are the resulting filter and control pole locations.

Toysat Experimental Results. The hardware tests of the control system described in the previous section are slight variations of standard modal identification tests. A four-second chirp containing frequencies from 0 to 40 Hz is applied simultaneously in rotation and translation through the Electro-seis shakers. This open-loop command is superimposed upon any feedback commands which may be generated by the control law given in Eq. (3.21). The open-loop chirp command is also communicated to the estimator. Data are taken for twelve seconds. Since the chirp begins sometime in the first second, this allows for roughly eight seconds of data after the chirp has expired. Data saved during

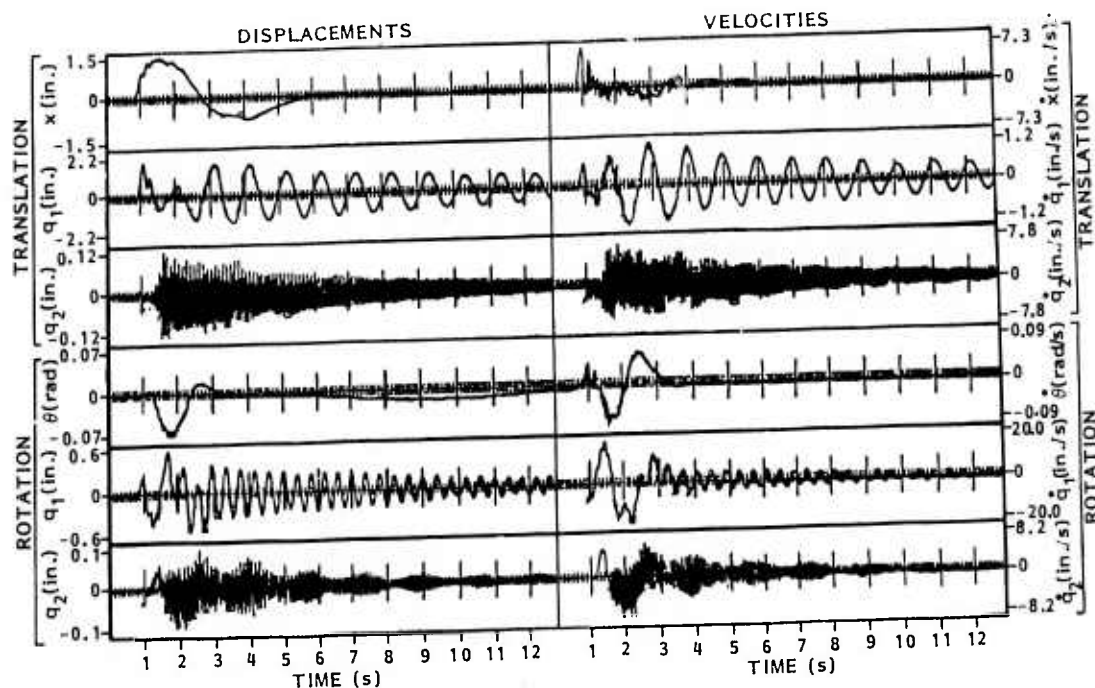


Fig. 3-17 Open-Loop Kalman Filter Output (Response to 4-s Chirp)

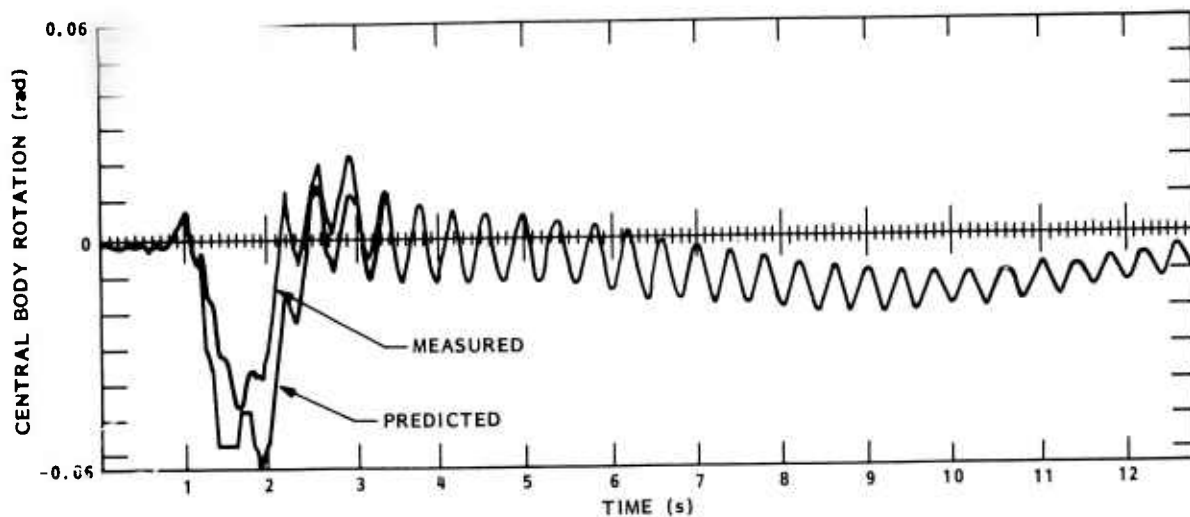


Fig. 3-18 Measured and Predicted Open-Loop Central Body Rotation (Response to 4-s Chirp)

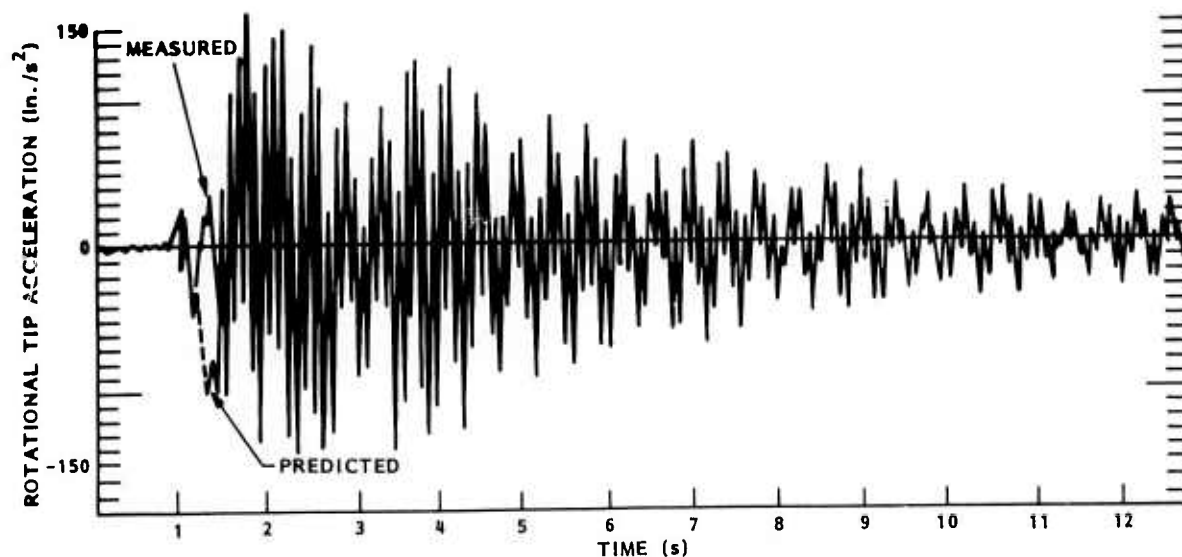


Fig. 3-19 Measured and Predicted Open-Loop Rotational Tip Acceleration (Response to 4-s Chirp)

the test run include the open- and closed-loop control commands, all four measurements, and the twelve Kalman filter states during the run. Post-experiment processing allows analysis of the data in the frequency domain as well as in the time domain.

Figures 3-20 through 3-25 illustrate various forms of results from the control system test described in Tables 3-9 and 3-10. Figures 3-20 and 3-21 show comparisons of the four measurements taken during two separate test runs; one without controls, and one with the control

3. TECHNICAL ACTIVITIES

3.5.1 TOYSAT EXPERIMENT: EXPERIMENTAL RESULTS

Table 3-9
80-Hz CONTROLLER DESIGN PARAMETERS

$$A = \begin{bmatrix} 1 & 0 & -2 & 0 & -3.7 & 0 \\ & 0 & 0 & 0 & 0 & 0 \\ & & 3.8 & 0 & -0.71 & 0 \\ & & & 0 & 0 & 0 \\ \text{symmetric} & & & 833 & 0 & 0 \end{bmatrix}$$

TRANSLATION

$$B = 3 \times 10^{-3}$$

$$Q_C = \text{Diag. } (0, 5 \times 10^{-3}, 0, 0.02, 3 \times 10^{-6})$$

$$R = \text{Diag. } (8 \times 10^{-5}, 8 \times 10^{-1})$$

CONTROL POLES

$$-4.2 \pm i \ 0.808$$

$$-5.1 \pm i \ 9.1$$

$$-6.7 \pm i \ 56.7$$

FILTER POLES

$$5.2 \pm i \ 5.3$$

$$-9.8 \pm i \ 5.8$$

$$-28.7 \pm i \ 50.2$$

Table 3-10
80-Hz CONTROLLER DESIGN PARAMETERS

ROTATION

$$A = \begin{bmatrix} 718 & & & & \\ & 0 & & & 0 \\ & & .22 & & \\ & & & 0 & 12 \\ & 0 & & & 0 \end{bmatrix}$$

$$B = 1 \times 10^{-5}$$

$$Q_C = \text{Diag } (0, 1.0 \times 10^{-3}, 0, 1.0, 0, 3 \times 10^{-3})$$

$$R = \text{Diag } (5 \times 10^{-4}, 5 \times 10^{-4})$$

CONTROL POLES

$$-4.5 \pm i \ 4.9$$

$$-6.4 \pm i \ 17.1$$

$$-5.7 \pm i \ 60.1$$

FILTER POLES

$$-2.4 \pm i \ 2.5$$

$$-12.3 \pm i \ 10.4$$

$$-33.8 \pm i \ 54.9$$

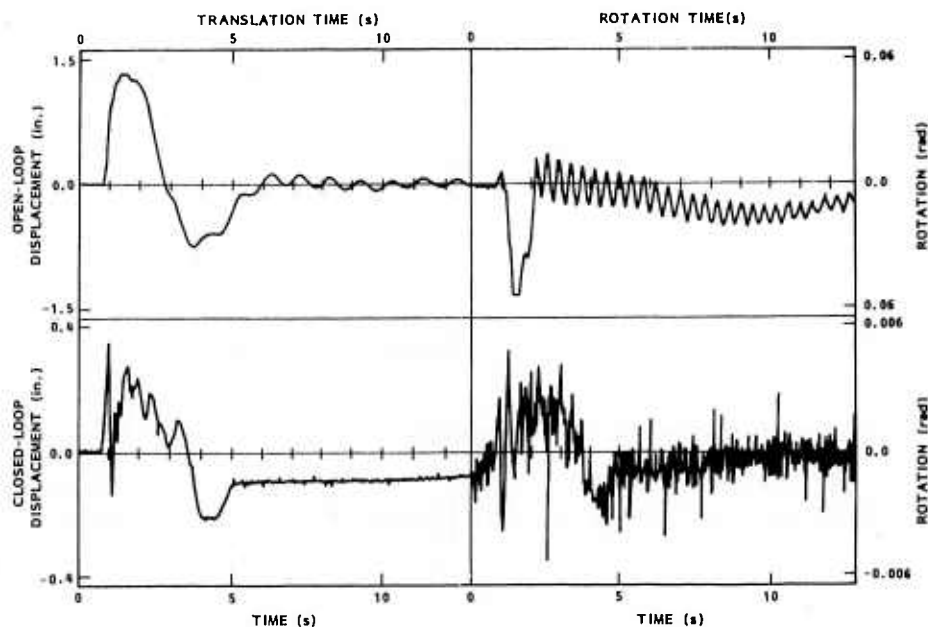


Fig. 3-20 Open- and Closed-Loop Central Body Measurements

3. TECHNICAL ACTIVITIES

3.5.1 TOYSAT EXPERIMENT: EXPERIMENTAL RESULTS

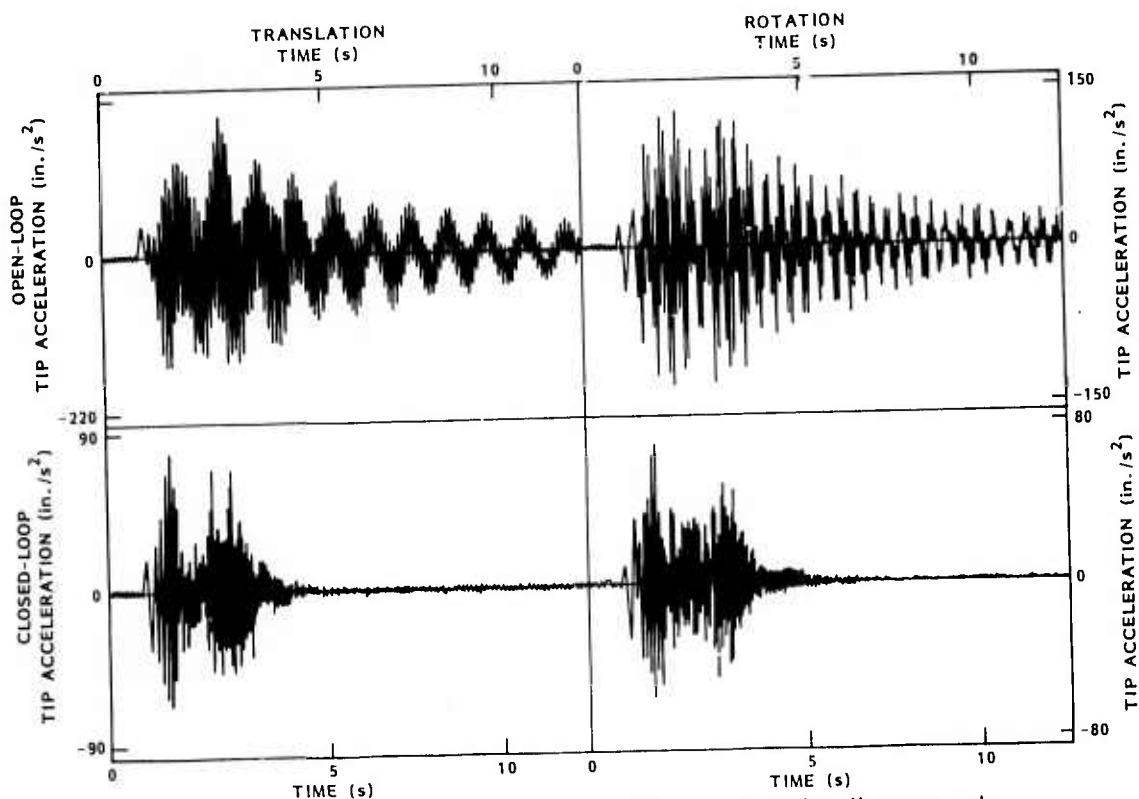


Fig. 3-21 Open- and Closed-Loop Tip Acceleration Measurements

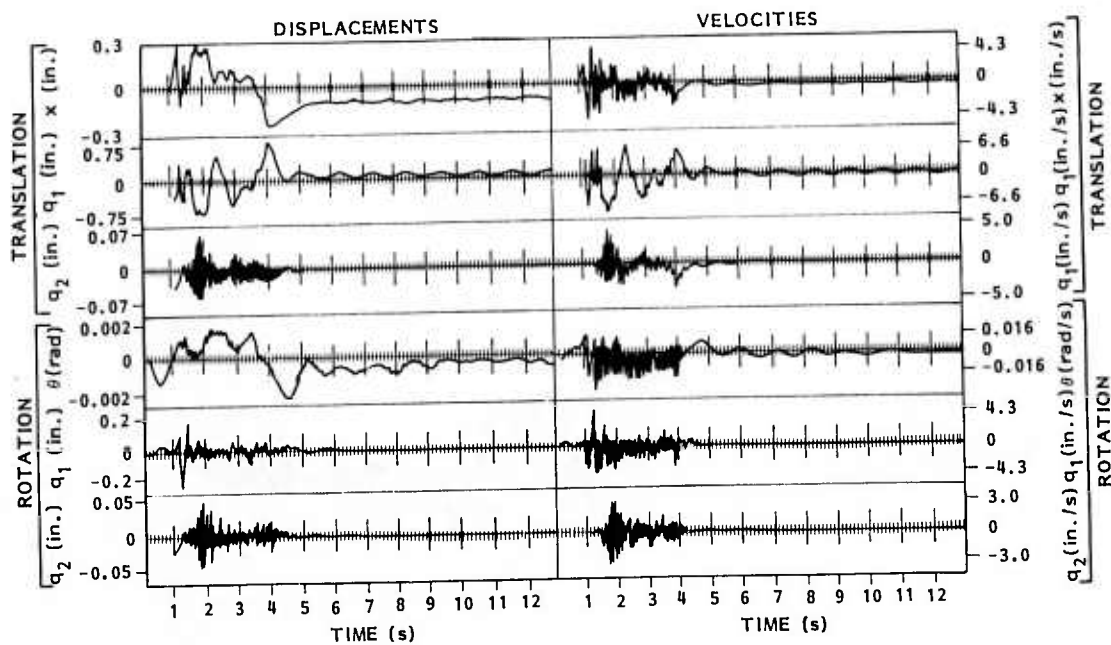


Fig. 3-22 Closed-Loop Kalman Filter Output (Response to 4-s Chirp)

system loop closed. The closed-loop data show much faster settling time than do the data from the open-loop test. Also, peak excursions during the chirp excitation are considerably smaller. Figure 3-22 shows the Kalman filter states during the closed-loop test. This may be compared with Fig. 3-17 which describes the same states during the open-loop test.

Figures 3-23 and 3-24 present frequency domain comparisons of open- and closed-loop transfer functions for tip accelerations to inputs through the central shakers. Figure 3-23 shows that the translation controller reduces the response of the first two bending modes (at 1 and 9 Hz) to below the level of the third unmodeled bending mode (28 Hz). The first mode amplitude is reduced by a factor of eight, a number which is proportional to the increase in damping. The damping was measured by fitting second order models to the transfer function. The closed-loop was roughly 4 percent for the first mode (versus 0.29 percent open-loop) and

11 percent for the second mode (versus 0.54 percent open-loop). For the rotation controller, the first and second modes (2.6 and 9.8 Hz) were also reduced below the level of the third mode (28 Hz). Again, the ratio of the reduced amplitude was proportional to the increase in damping. The first mode closed-loop damping was roughly 6 percent (versus 0.33 percent open-loop), and the second mode was 12 percent (versus 0.3 percent open-loop).

The damping measured from test data does not exactly agree with the analytically predicted pole locations shown in Tables 3-9 and 3-10. The predictions for the second mode behavior were reasonably close, but the first mode predictions were quite inaccurate. These differences are dramatically illustrated by the charts in Fig. 3-25. The failure of the first mode to behave as expected may almost certainly be attributed to poor low-frequency response of the Electro-seis actuators.

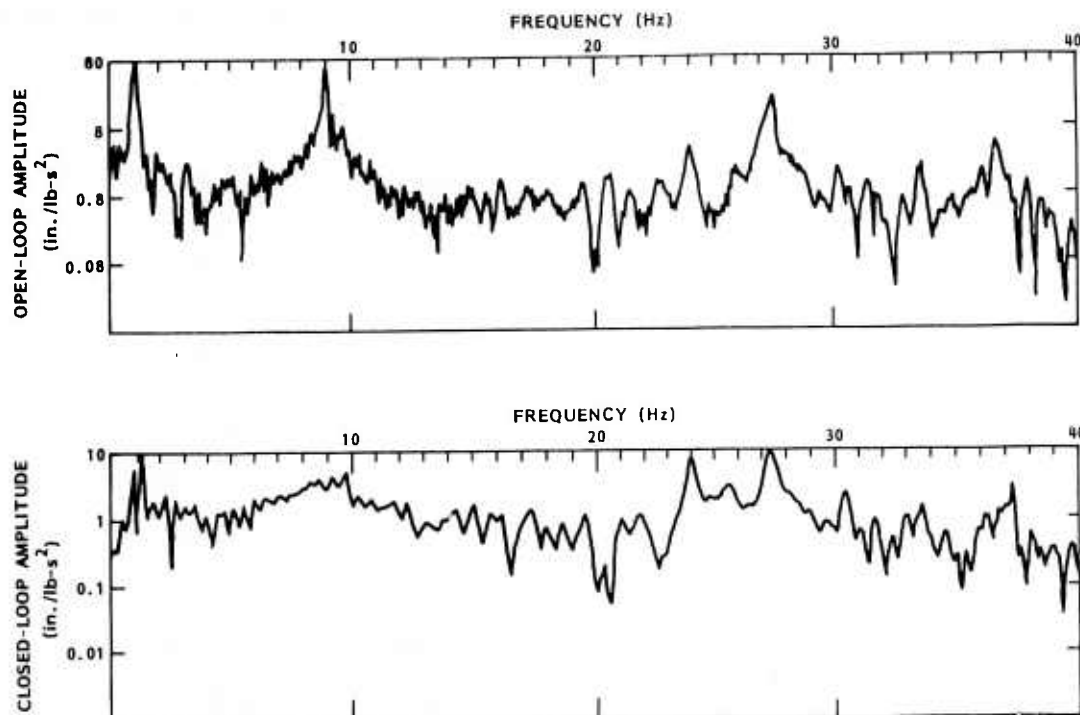


Fig. 3-23 Open- and Closed-Loop Transfer Functions; Translational Tip Acceleration/Input Chirp

3. TECHNICAL ACTIVITIES

3.5.1 TOYSAT EXPERIMENT: EXPERIMENTAL RESULTS

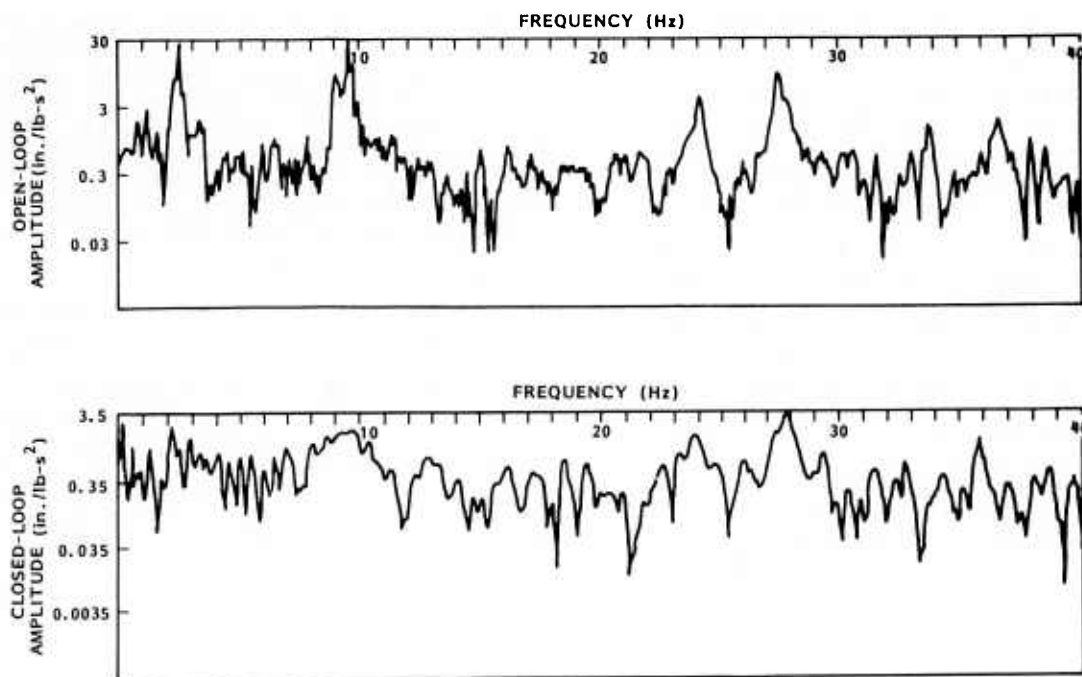


Fig. 3-24 Open- and Closed-Loop Transfer Functions; Rotational Tip Acceleration/Input Chirp

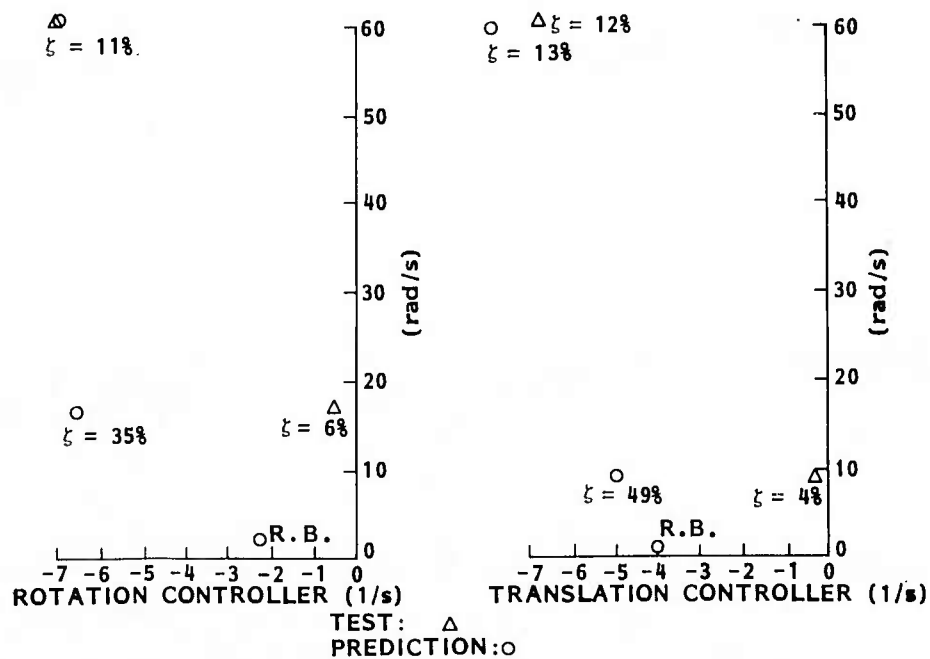


Fig. 3-25 Closed-Loop Pole Location; Predicted vs. Test

3. TECHNICAL ACTIVITIES

3.5.1 TOYSAT EXPERIMENT: EXPERIMENTAL RESULTS

Figure 3-26 shows the result of a deliberate attempt to provoke the phenomena commonly known as spillover. A new control system was generated by reducing the weight on the translation control by a factor of one hundred from that given in Table 3-9. The analysis predicted that this controller would cause the first

unmodeled mode (at 29 Hz) to go unstable. Test results given in Fig. 3-26 demonstrate that indeed something did go unstable. The frequency domain transfer function in Fig. 3-27 confirms that it was the 29-Hz mode which dominated the instability.

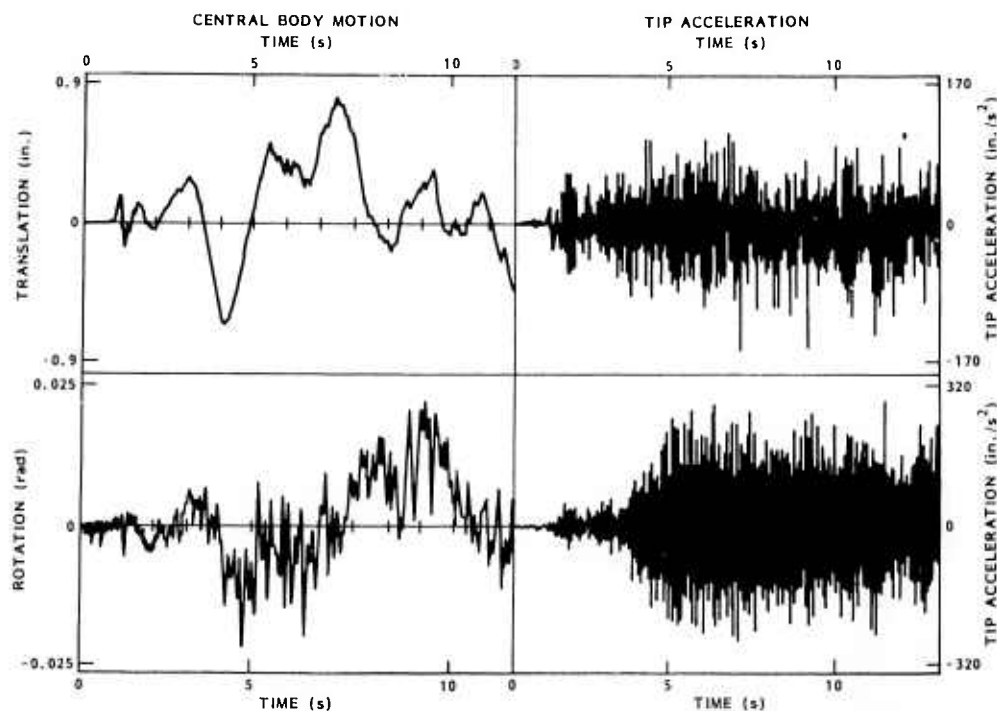


Fig. 3-26 Measurements for Case With Provoked Spillover

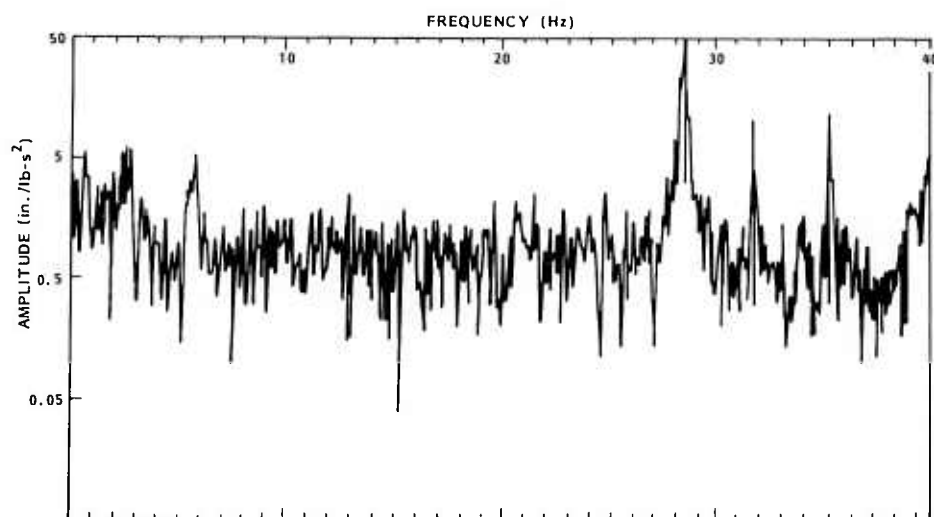


Fig. 3-27 Transfer Function; Spillover Case Rotational Tip Acceleration/Input Chirp

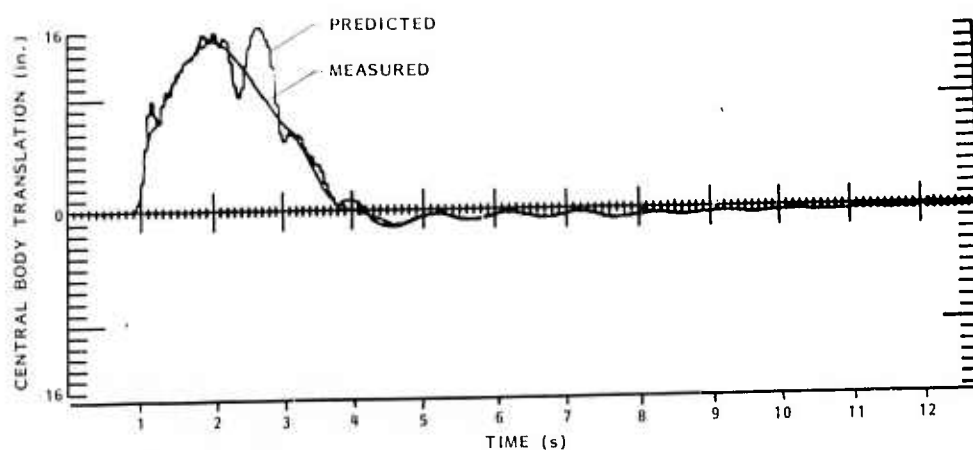


Fig. 3-28 Measured and Predicted Open-Loop Central Body Rotation for a 20-Hz Sample Rate Kalman Filter

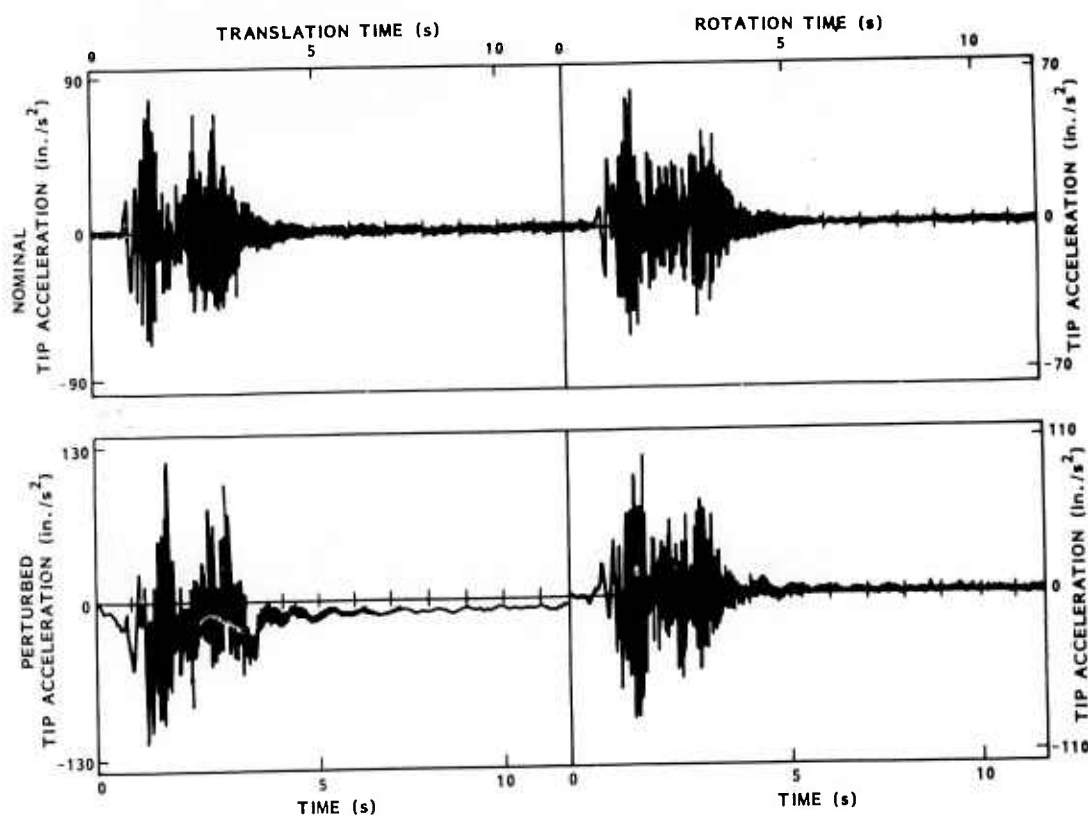


Fig. 3-29 Measured Tip Acceleration for Two Closed-Loop Tests, One With Nominal Configuration, One With One 2-lb Tip Mass Removed

3.5.2 Slim Beam Experiment

Objectives. The main objective of the Slim Beam experiment is the verification of Low Authority Control (LAC) theory using a simple three-dimensional structure. The main features of interest are: 1) comparison between predicted and actual damping; 2) effects of cross-axis coupling, noncolocation, and nonconsistency of sensors and actuators; and 3) robustness of the LAC controller under significant parameter variations. A secondary (but nonetheless important) objective of this experiment is the demonstration of the use of proof-mass actuators for vibration control. Thus, correct modeling and calibration of these actuators is an important

part of this experiment and a determinant factor in its success. A third objective of the Slim Beam experiment is to verify the LAC stability theorem, i.e., the relationship between the internal passive damping of the actuator and the maximum achievable active damping in the structure. The first two objectives of this experiment have been achieved. However, as will be shown later, it was not possible to accomplish the third objective due to certain characteristics of the experimental setup and the particular nature of the actuators.

Hardware Mechanizations. The structure to be controlled is a 5.3-ft long thin-wall stainless steel tube (3/8 in. OD, 10 mil thick) suspended vertically by string and spring (Fig. 3-30). Rigid mounting pieces are attached on both ends of the beam: at the upper end an aluminum cylinder, at the lower end, a square aluminum plate. The suspension string is attached directly to the cylinder.

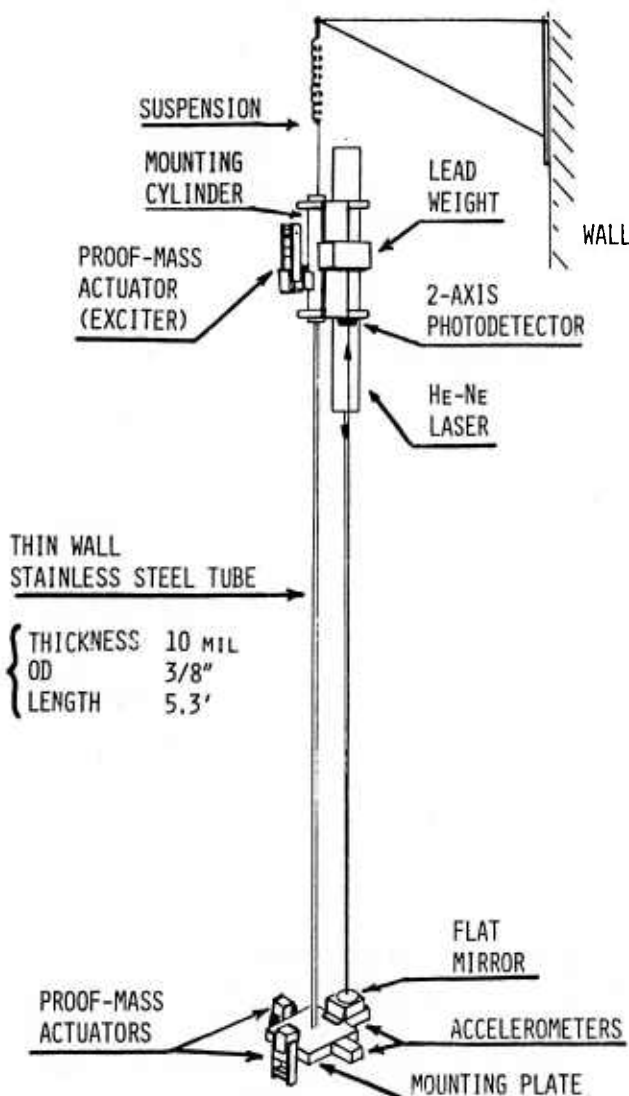


Fig. 3-30 Slim Beam Hardware Setup

The sensing system consists of a laser attached to the cylinder with a linear photodetector on its side. The laser beam is reflected by a small mirror mounted on top of the square plate. The beam hits the detector, which measures the beam's displacements along the 1- and 2- axes. Thus, this sensor measures the difference between the rotations of the plate and the laser about the 1- and 2-axes. However, because the laser assembly is very massive (lead weights were added to balance the laser and increase the rotational inertia), the major contribution comes from the plate rotations.

In addition, two Unholz-Dikie accelerometers are mounted on the square plate. These measure acceleration along the 1- and 2-axes (Fig. 3-31).

LIGHT BEAMS

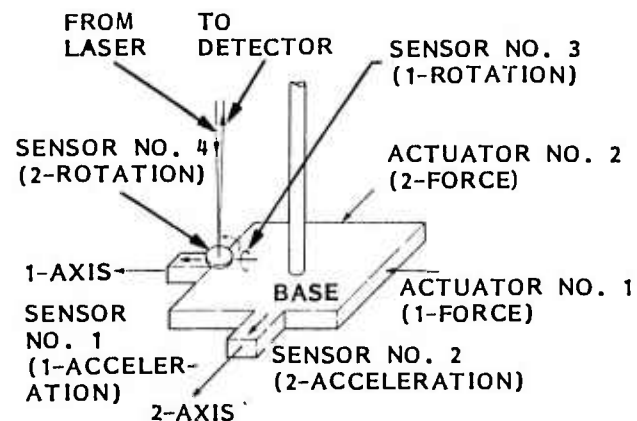


Fig. 3-31 Slim Beam Sensors/Actuators

3. TECHNICAL ACTIVITIES

3.5.2 SLIM BEAM EXPERIMENT: CONTROL SYNTHESIS/SIMULATION

This sensing system is, to the first order, insensitive to torsion modes, i.e., rotation of the beam about its own axis (vertical 3-axis).

Actuation is provided by two PPM actuators mounted on the square plate. These exert reaction forces along the 1- and 2-axes respectively. In addition, a third PPM actuator is mounted on the cylinder. It provides excitation forces in both the 1- and 2-axes directions.

The control (LAC) system uses analog compensators connected to the optical (laser) sensor and the two bottom actuators. The testing system is based on the Vibration Analysis and Measurement Program (VAMP) and uses the top actuator as an exciter and both optical and inertial sensors. In this way the beam can be tested independently of the control system, both in open- and closed-loop configurations. The system's overall configuration is shown in Fig. 3-32. Figure 3-33 depicts the compensation circuits of the LAC system.

Control Synthesis/Simulation Results. In order to formulate the control problem, a finite element model of the slim beam/suspension system was created as shown in Fig. 3-34. Base plate and laser assembly were treated as lumped mass/inertias, but massless nodal points were added to the model (e.g., points 13, 16, 17, 18), so that actuator and sensor influence coefficients could be obtained.

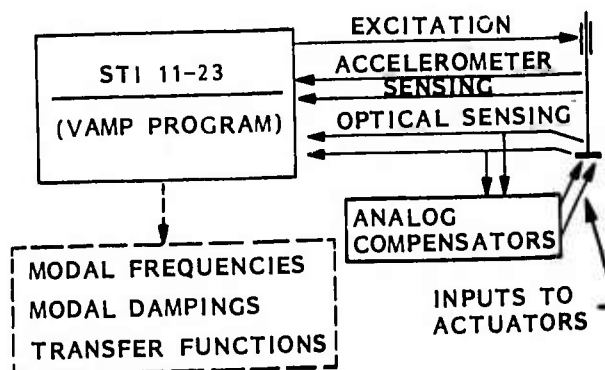


Fig. 3-32 Slim Beam Experiment Setup

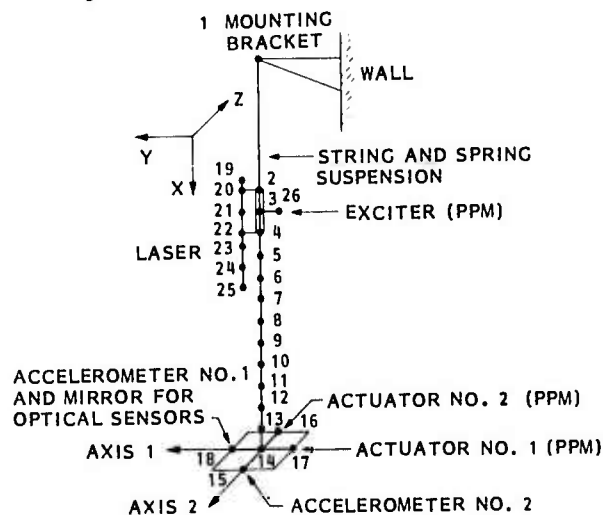
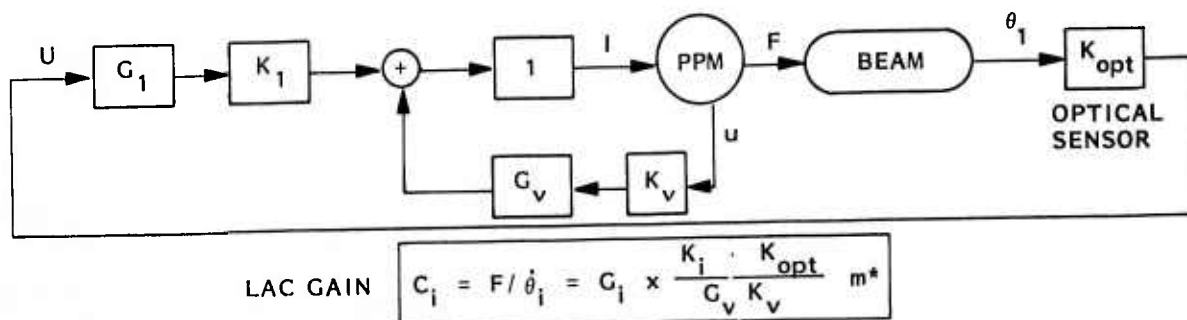


Fig. 3-34 Slim Beam Structural Model



$$m^* = 0.086 \text{ (kg)}$$

$$K_1 = 2.65$$

$$K_2 = 2.24$$

$$K_{opt} = 682 \text{ (V/RAD)}$$

$$K_v = 0.124 \text{ (V/ms}^{-1}\text{)}$$

$$G_v = 1200$$

$$\begin{cases} C_1 = 1.04 G_1 \text{ (AXIS 1)} \\ C_2 = 0.88 G_2 \text{ (AXIS 2)} \end{cases}$$

Fig. 3-33 LAC Control Loop Parameters

3. TECHNICAL ACTIVITIES

From frequencies and mode shapes, the system's F, G, D, and H matrices were obtained. They are listed in Table 3-11. The system's equations are:

$$\begin{cases} \dot{x} = Fx + Gu + Du_e \\ y = Hx \end{cases} \quad (3.33)$$

Table 3-11
SLIM BEAM SYSTEM MATRICES

** F 15 30X30

1, 1	-9.126-04	1, 2	-1.382-02	2, 1	1.000+00	3, 3	-1.039-02
3, 4	-5.254+00	4, 3	1.000+00	5, 5	-1.042-02	5, 6	-5.302+00
6, 5	1.000+00	7, 7	-3.219-02	7, 8	-1.619+01	8, 7	1.000+00
9, 9	-3.219-02	9, 10	-1.619+01	10, 9	1.000+00	11, 11	-1.005-01
11, 12	-1.579+02	12, 11	1.000+00	13, 13	-2.516-01	13, 14	-9.910+02
14, 13	1.000+00	15, 15	-2.989-01	15, 16	-1.322+03	16, 15	1.000+00
17, 17	-3.025-01	17, 18	-1.430+03	18, 17	1.000+00	19, 19	-6.774-01
19, 20	-7.170+03	20, 19	1.000+00	21, 21	-6.049-01	21, 22	-7.330+03
22, 21	1.000+00	23, 23	-1.466+00	23, 24	-3.359+04	24, 23	1.000+00
25, 25	-1.504+00	25, 26	-3.536+04	26, 25	1.000+00	27, 27	-3.231+00
27, 28	-1.631+05	28, 27	1.000+00	29, 29	-3.244+00	29, 30	-1.644+05
30, 29	1.000+00						

** G 15 30X 2

1, 1	9.626-05	1, 2	-7.301-06	3, 1	1.705-01	3, 2	7.077-01
5, 1	7.007-01	5, 2	-1.791-01	7, 1	-3.909-01	7, 2	3.245-02
9, 1	-3.437-02	9, 2	-3.093-01	11, 1	2.000-03	11, 2	2.014-03
13, 1	-0.020-03	13, 2	9.290-02	15, 1	1.031-01	15, 2	-1.105-02
17, 1	-5.976-02	17, 2	2.060-03	19, 1	-1.421-02	19, 2	-9.909-03
21, 1	5.416-03	21, 2	-2.519-02	23, 1	-5.702-02	23, 2	-1.079-03
25, 1	2.535-03	25, 2	-5.150-02	27, 1	-5.326-02	27, 2	-3.675-03
29, 1	-4.051-03	29, 2	5.213-02				

** H 15 2X30

1, 1	1.966-06	1, 3	1.324-03	1, 5	5.264-03	1, 7	-2.203-02
1, 9	-1.006-03	1, 11	3.012-03	1, 13	0.337-02	1, 15	0.422-01
1, 17	2.234-01	1, 19	-7.303-01	1, 21	2.619-01	1, 23	1.045+00
1, 25	-4.599-02	1, 27	3.192-01	1, 29	2.094-02	1, 31	1.750-06
2, 3	-5.202-03	2, 5	1.310-03	2, 7	-1.026-03	2, 9	1.000-02
2, 11	3.009-04	2, 13	-7.160-01	2, 15	5.333-02	2, 17	1.091-01
2, 19	3.203-01	2, 21	0.501-01	2, 23	-4.105-02	2, 25	-1.140+00
2, 27	-3.429-02	2, 29	4.104-01				

** D 15 30X 1

1, 1	-2.067-02	3, 1	5.311-02	5, 1	1.409-01	7, 1	2.992-01
9, 1	5.401-02	11, 1	-1.076-04	13, 1	9.401-03	15, 1	6.256-02
17, 1	3.249-02	19, 1	1.056-02	21, 1	-1.036-02	23, 1	5.951-03
25, 1	-2.245-03	27, 1	-5.711-04	29, 1	-1.313-03		

The term x is the vector of modal amplitudes (and their time derivatives). Fifteen modes were generated by the finite element program. Thus, x is a 30-dimensional vector here. The first six modes are suspension and pendulum type modes and of little interest for the experiment. The next three modes are bending and torsion modes and have been studied in detail in this experiment. Figure 3-35 shows the corresponding mode shapes. The vector u contains the inputs to the two PPM actuators, while u_e is the input to the exciter. The measurement vector y represents the time rate of change of the two angular sensors' outputs.

Computation of the H matrix involves the construction of the difference between the rotation angles of the base and of the laser for the angular sensor. In the analog mechanization of

3.5.2 SLIM BEAM EXPERIMENT: CONTROL SYNTHESIS/SIMULATION

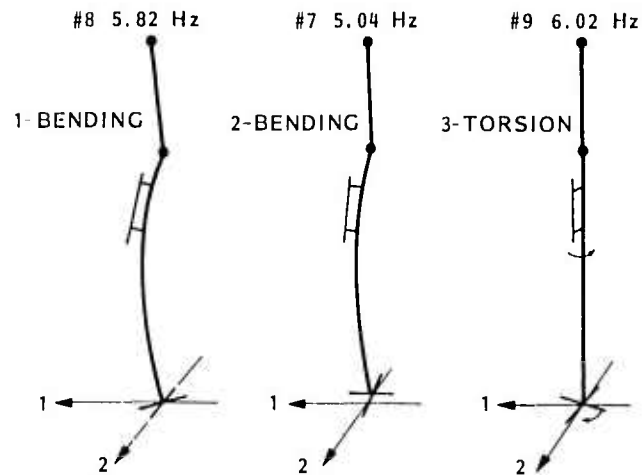


Fig. 3-35 Slim Beam Principal Modes Analyzed

LAC for the slim beam experiment, the angular sensor truly measures angles and the implemented control law has the form $v = C\theta$, where v is the velocity of the proof-mass of the PPM actuator. However, this form of control is difficult to represent in the state-space formulation. Therefore, in the off-line digital computational model, the control law is given the equivalent form $f = -C$ (see Section 3.4.2), where f is the force applied by the PPM actuator. This forms the basis for the LAC gain synthesis computations. Thus, y_1 and y_2 are defined as angular rates rather than angles. Finally, the computation of the G matrix includes both force and torque effects of the PPM actuators, using the model described in Section 3.4.2.

The LAC control law has the form

$$u = Cy \quad (3.34)$$

where C is diagonal. The relationship between the gains C_i and the electronic compensator gains is described in Fig. 3-33.

Forming the closed-loop equations from Eqs. (3.33) and (3.34) leads to

$$\dot{x} = (F + GCH)x + Du_e$$

The eigenvalues of $(F+GCH)$ are the closed-loop poles of the LAC system. A set of values for the C matrix was chosen and the corresponding poles computed for later comparison with the experimental values.

3. TECHNICAL ACTIVITIES

3.5.2 SLIM BEAM EXPERIMENT: EXPERIMENTAL PERFORMANCE

Experimental Performance. The open- and closed-loop eigenvalues of the slim beam were determined experimentally using the full set of sensors and the VAMP program. The VAMP program provides a curve fit between the measured transfer functions y/u_e and modal analytical expressions of the form

$$\sum_i \frac{A_i + B_i \omega}{\omega_i^2 + 2j\zeta_i \omega_i \omega - \omega^2}$$

where A_i and B_i are complex coefficients, ω_i is the frequency of i th mode, and ζ_i is the mode's damping ratio ($j \triangleq \sqrt{-1}$).

Table 3-12 shows a comparison between computed and measured open-loop characteristics. This comparison shows that the analytical (finite element) model was quite accurate in predicting the modal frequencies. However, the damping ratios were unknown and were assumed to be 0.4 percent. Although the measurement shows some significant departures from this value, the order of magnitude is in the expected range.

Table 3-12 SLIM BEAM OPEN-LOOP CHARACTERIZATION					
MODE NO.		FREQUENCIES		DAMPING RATIOS	
		COMPUTED	MEASURED	COMPUTED (ASSUMED)	MEASURED
RIGID	1	0.02	—	0.004	—
BODY/	2	0.36	—	0.004	—
SUSPENSION	3	0.36	—	0.004	—
MODES	4	0.64	—	0.004	—
	5	0.64	—	0.004	—
	6	2.00	2.00	0.004	—
Y BEND	7	5.00	5.04	0.004	0.012
X BEND	8	5.78	5.82	0.004	0.004
TORSION	9	6.02	6.06	0.004	0.003
Y BEND	10	13.48	13.36	0.004	0.008
X BEND	11	13.63	13.65	0.004	0.006
Y BEND	12	29.16	—	0.004	—
X BEND	13	29.92	29.53	0.004	0.003
Y BEND	14	64.28	—	0.004	—
X BEND	15	64.52	64.69	0.004	0.005

For the closed-loop tests, various combinations of the adjustable gains G_1 and G_2 were used (see Fig. 3-33), corresponding to various feedback gains C_1 and C_2 :

$$\begin{aligned} C_1 &= 1.04 G_1 \\ C_2 &= 0.88 G_2 \end{aligned}$$

The combinations tested are given in Table 3-13 below.

Table 3-13 GAIN COMBINATIONS TESTED										
DATA POINT	1	2	3	4	5	6	7	8	9	10
G_1	0.0	0.0	0.0	1.0	1.0	1.5	1.5	2.0	2.0	4.39
G_2	1.0	1.5	2.0	0.0	1.0	0.0	1.5	0.0	2.0	3.30

Figure 3-36 shows the comparison between predicted and measured frequencies, and Fig. 3-37 compares predicted and measured damping ratios. The vertical arrows in these two figures indicate the effect of changes in the plant parameters which will be discussed later. Mode No. 9, which is almost a pure torsion, is poorly controlled as expected.

The last data point (No.10) was obtained by increasing G_1 and G_2 until the system became unstable, then backing off just enough to recover stability. Thus, the values of G_1 and G_2 shown in Table 3-13 for this data point are the maximum achievable gains in the LAC system. To these gains correspond maximum achievable damping ratios in the modes studied.

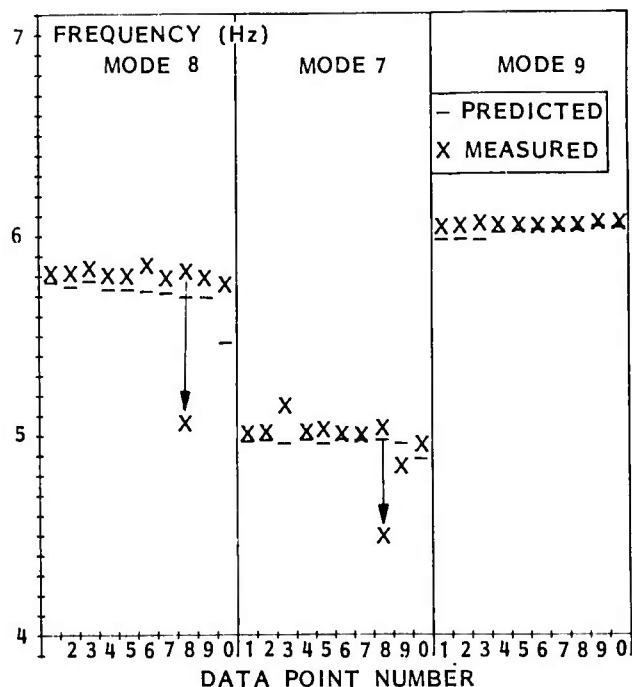


Fig. 3-36 Slim Beam Experimental versus Theoretical Results

3. TECHNICAL ACTIVITIES

3.5.2 SLIM BEAM EXPERIMENT: EXPERIMENTAL PERFORMANCE

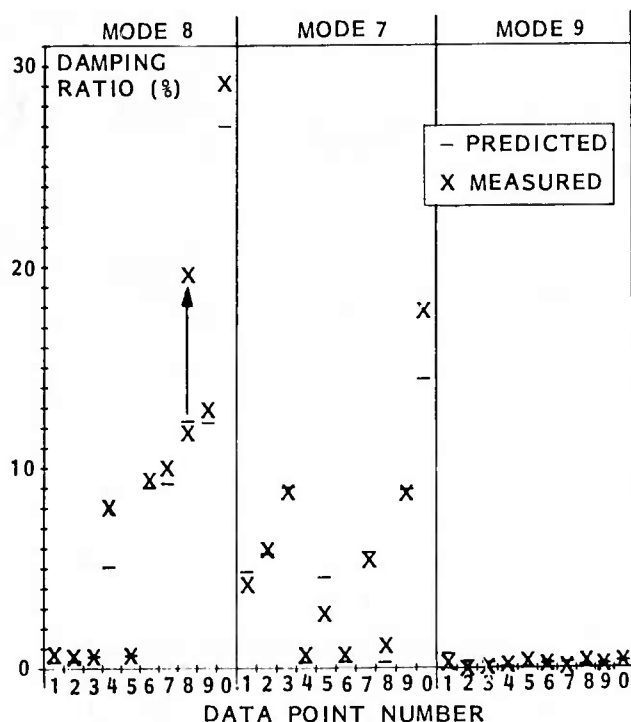


Fig. 3-37 Slim Beam Experimental versus Theoretical Results

The existence of a gain limit with the LAC system was expected from the stability theorem shown in Section 4.3.1. However, in this particular case another phenomenon was involved that prevented the experimental verification of the theorem by creating a much more severe stability problem. This phenomenon is the noncollocation and nonconsistency of the sensors and actuators.

Colocation implies that sensing and actuation are performed at the same location on the structure. This was not the case, since the sensor output corresponding to the i th axis ($i = 1, 2$) was

$$y_i = \theta_j - \gamma_j \quad (j = 2, 1)$$

where θ_j was the rotation angle about the perpendicular axis at the actuator location, but γ_j was the rotation at the laser location. The LAC control law was thus

$$f_i = -C_i (\dot{\theta}_j - \dot{\gamma}_j)$$

The term γ_j , though much smaller than θ_j because of the large inertia associated with the laser system, introduces a colocation error. Moreover, instead of a displacement x_i , an angle is measured, violating the consistency requirement (displacement/force, rotation/torque). Although θ_j and x_i are proportional and of the same sign for the low-frequency modes, at some higher frequencies they become of opposite sign, thus leading to instability. However, such instability is predictable by the LAC theory using the fundamental LAC formula (see Section 4.3.1)

$$2\zeta_n \omega_n = \sum_{ar} C_{ar} \phi_{an}^A \phi_{rn}^R$$

The following expressions for the damping ratios of modes 7 and 8 (i.e., the first two bending modes studied) and modes 12 and 13 (higher frequency bending modes which went unstable) were obtained:

Mode No.	Frequency	
7	5.00 Hz	$2\zeta_7 \omega_7 \approx -0.016 C_1 - 3.37 C_2$
8	5.78 Hz	$2\zeta_8 \omega_8 \approx +4.53 C_1 - 0.036 C_2$
12	29.16 Hz	$2\zeta_{12} \omega_{12} \approx -1.6 C_1 + 0.007 C_2$
13	29.93 Hz	$2\zeta_{13} \omega_{13} \approx -0.003 C_1 + 4.34 C_2$

Two phenomena can be seen in these expressions. First, as emphasized by arrows (1), a small cross-axis coupling exists due to the fact that the actuators are not exactly in the planes of the bending modes. Thus actuator No. 1, which controls mostly the 1-axis where mode 8 is the most active, also has some effect on mode 7 (as shown by the negative coefficient -0.016 in front of C_1). This has a destabilizing effect. However, the existence of the second actuator with the gain C_2 is enough to override this instability.

The more important problem is the noncollocation/nonconsistency effect which is shown by arrows (2). When C_2 is chosen with a sign compatible with a stable root (here C_2 must be negative to ensure a positive damping ratio ζ_7), it has the wrong sign for mode 13. (See Table 3-12 for ordering of modes.) The same can be seen of the gain C_1 , which must be positive to ensure stability of mode 8, but then destabilizes mode 12. Assuming that there already exists some (natural) damping in modes 12 and 13, it is possible to use the above set of equations to determine the maximum values for C_1 and C_2 and thus for ζ_7 and ζ_8 . The

3. TECHNICAL ACTIVITIES

3.5.3 CIRCULAR PLATE: OBJECTIVES

values obtained are as follows where ξ_{12} and ξ_{13} represent existing natural damping:

$$\begin{aligned}\xi_7 &< 4.6 \xi_{13} \\ \xi_8 &< 15 \xi_{12}\end{aligned}$$

The open-loop damping in modes 12 and 13 was thus measured and found to be about 1.6 percent. The following set of values summarizes the agreement between the predicted and experimental measurements:

	G_1	G_2	ξ_7	ξ_8
Predicted	3.52	1.57	7.4	23
Measured	4.39	3.3	29	18

It is believed that mode shape inaccuracies are responsible for the numerical discrepancies observed, since these numbers are particularly sensitive to the values in the H and G matrices, which are basically constructed with the normalized mode shapes.

The LAC control loop was implemented with a first order roll-off at 70 Hz in the hope of observing the instability predicted by the theorem. Because of the colocation/ consistency effect, instability was observed at about 30 Hz. Attempts to roll-off the controller around 30 Hz did not change the results significantly.

Finally, a robustness test was made by simply attaching an 80-g lead mass near the middle of the beam. Figure 3-38 shows the spectra of excitation and sensor responses in nominal and perturbed cases. This perturbation does not affect the 6-Hz mode (torsion) but affects the first two bending modes quite strongly. However, the system remains very stable. Figure 3-39 shows how the frequency response was fitted by VAMP to obtain the perturbed frequencies and dampings. The effect of the perturbation is displayed in Figs. 3-36 and 3-37 by the arrow showing the corresponding changes in damping and frequencies.

3.5.3 Circular Plate

Objectives. The main objective of this experiment is the demonstration and verification of digital optimal control strategies applied to a

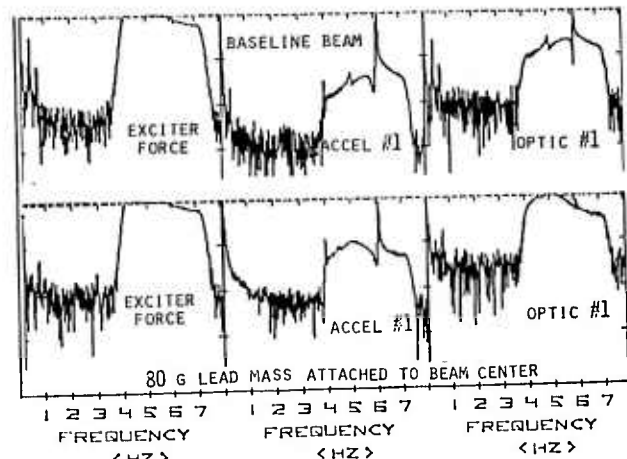
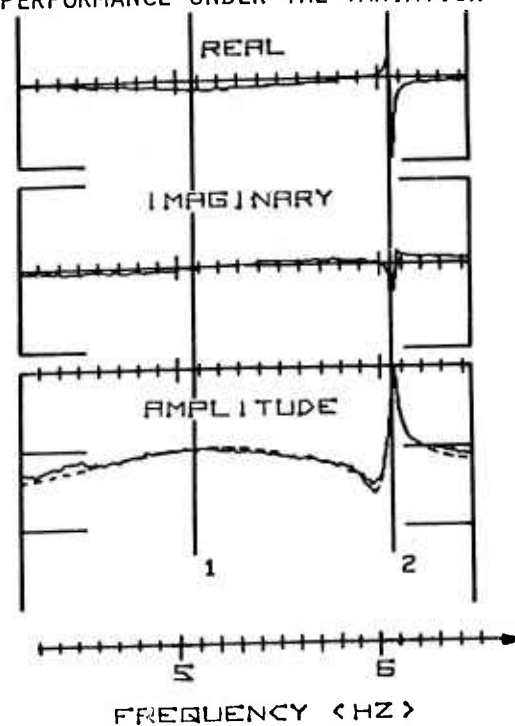


Fig. 3-38 Parameter Variation Study: Power Spectra

PERFORMANCE UNDER THE VARIATION



— MEASURED
-- FITTED

RESULTS

M	FREQ	DAMP
1	5.079	0.196
2	5.059	0.002

Fig. 3-39 Parameter Variation Study: Modal Identification by Curve Fitting

3. TECHNICAL ACTIVITIES

specimen with more realistic spacecraft-like features, e.g., free body in space, dense spectrum of vibratory modes, very low natural damping, etc. The main features of interest are: 1) design, implementation, and modeling of the specimen; 2) synthesis, implementation, and testing of various optimal digital controllers (HAC) to control both rigid body (attitude) and a certain number of flexible modes; and 3) study of the HAC spillover problem and its cure by adjoining an LAC system.

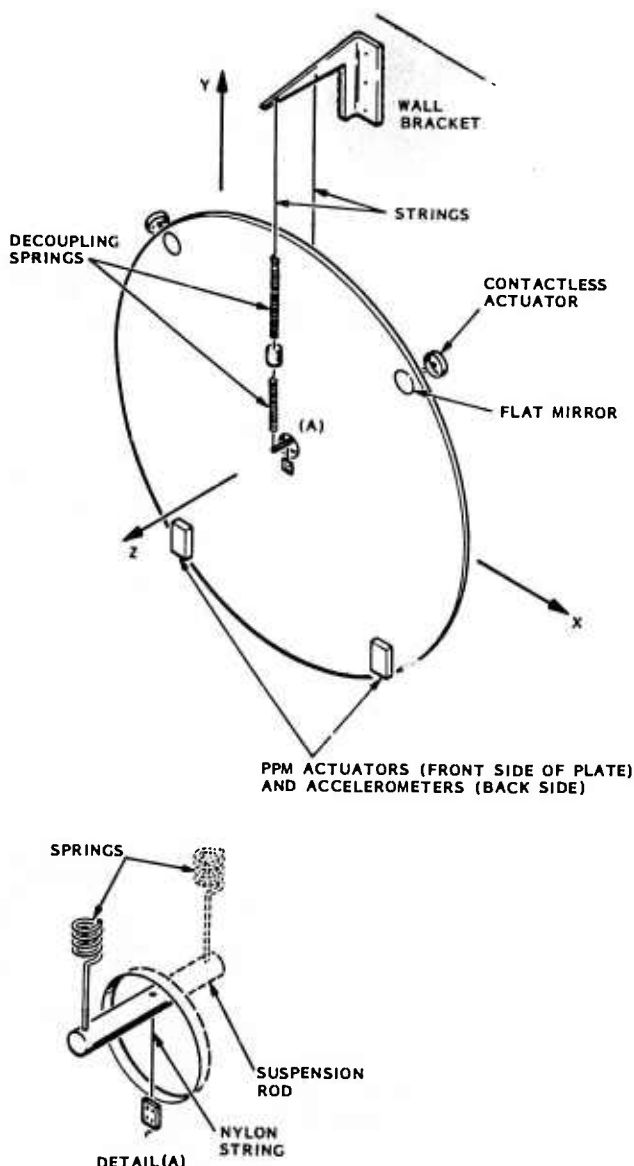


Fig. 3-40 Circular Plate Experimental Set-Up

3.5.3 CIRCULAR PLATE: HARDWARE MECHANIZATIONS

A secondary objective is the testing of methods for incorporation of velocity-controlled PPM actuators in optimal controller mechanizations. Most of the objectives were accomplished, except for the actual testing of the digital controller. This was not performed due to persistent microprocessor hardware failures. However, these failure problems have since been solved and understood and have provided valuable information for future digital mechanizations.

Hardware Mechanizations. The structure to be controlled is a flat circular aluminum plate of 1.2-m diameter and 1/8-in. thickness. It is suspended vertically by two spring and string systems attached near its center (Fig. 3-40). This device provides nearly unrestrained conditions for the plate, with the rigid body modes being below 1 Hz, while the first bending occurs at about 19 Hz. The lead masses in series with the suspension springs provide an additional attenuation of the vibrations transmitted to the plate by the laboratory wall. The use of nylon strings also helps to reduce vibration transmission. A picture of this system is shown in Detail A of Fig. 3-40.

The main sensing system is provided by optical sensors. Two flat mirrors are mounted on the plate and reflect the light beams of a fixed-based laser and two-axis detector system (Fig. 3-41).

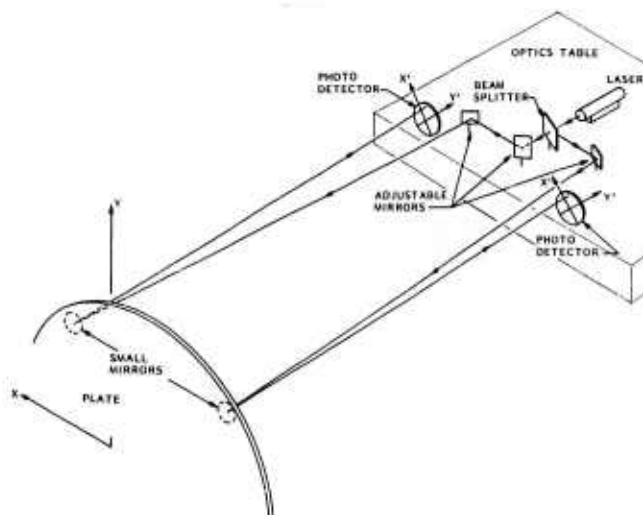


Fig. 3-41 Circular Plate Optical Sensing System

Each detector measures the displacement of the spot in the x' and y' direction (the axes (x', y') are rotated 45 deg from the plate (x, y) axes). Thus each detector measures the

rotations about the y' and x' axes of the corresponding mirror on the plate. If d is the distance from the plate to the detectors, the spot displacement x is related to the plate rotation θ by:

$$x = 2d \theta$$

With a detector sensitivity of 14 V/cm, and $d = 16.5$ ft, the sensor sensitivity is then

$$V/\theta = 14.1 \times 10^3 \text{ V/rad}$$

or $V/\theta = 14 \text{ mV}/\mu\text{rad}$

Since the detector noise is less than 1mV p/p, this optical sensor is potentially capable of measuring pointing errors as small as 100 nrad.

In addition to this sensor, accelerometers are mounted directly on the back side of the plate (see Fig. 3-40). They provide measurements of the local velocity along the z -axis when used in conjunction with an integrating network. A photograph of the experiment is shown in Fig. 3-42.

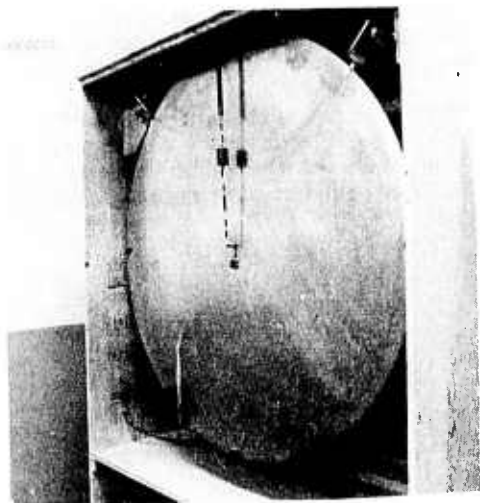


Fig. 3-42 Photograph of Circular Plate Experiment

Actuation is provided by two sets of actuators. The first set consists of two contactless actuators (see Section 3.4.2) mounted on the edge of the plate (Fig. 3-40). These actuators provide forces along the z -axis and constitute the main attitude (pointing) control system, since they can operate at DC levels. The second set of actuators consists of two velocity-controlled PPM actuators located on the lower part of the plate (Fig. 3-40). These actuators can only operate in AC conditions and thus can only provide vibration control. For optimal control mechanizations, it is necessary to make these actuators behave like force actuators, i.e., a control input u should correspond to a force and not to a linear momentum as is the case when the PPM has the velocity servo-loop wrapped around it. This is realized by the compensating circuit shown in Fig. 3-43.

A general schematic of the actuator/sensor system is shown in Fig. 3-44. This arrangement of actuators and sensors is basically colocated. However, the actuators and sensors are not consistent, and for HAC application each sensor will feed back to all actuators via the Kalman filter. Thus, colocation is in effect lost.

The overall system configuration for this experiment is shown in Fig. 3-45. Two microprocessors are involved. The STI/DEC 11-23 system is the host processor which handles the data acquisition system (for open- and closed-loop characterization) and sets up the other processor, the CSPI MAP 300 array processor in which the control algorithms are mechanized.

This array processor has its own D/A and A/D converters and is thus autonomous, which allows it to process a large amount of data at relatively high sampling rates. Control gains computed off-line by large-scale programs residing in the UNIVAC 1110 are directly transferred to

●FOR OPTIMAL CONTROL DESIGNS ACTUATORS CIRCUIT MODIFIED TO MIMIC FORCE ACTUATORS

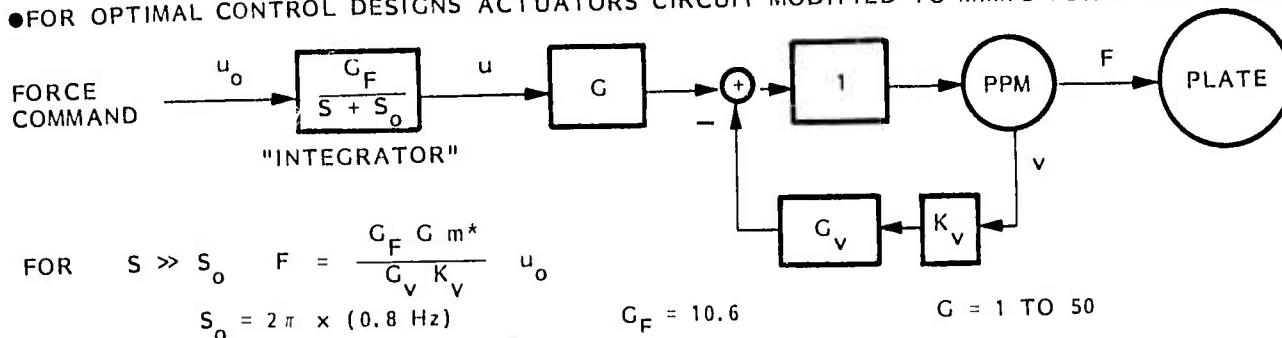


Fig. 3-43 Circular Plate PPM Actuator Compensation

3. TECHNICAL ACTIVITIES

3.5.3 CIRCULAR PLATE: HARDWARE MECHANIZATIONS

①, ② : INERTIAL SENSING/
ACCELEROMETERS
(1 D.O.F. Z-MEASUREMENT)

③, ④ } OPTICAL SENSING/MIRRORS
⑤, ⑥ } (2 D.O.F. $\theta_{x'}$, $\theta_{y'}$ ANGULAR
MEASUREMENT

(x' , y') are 45° W.R.T. (x , y)

A_1 , A_2 PPM ACTUATORS

A_3 , A_4 CONTACTLESS ACTUATORS

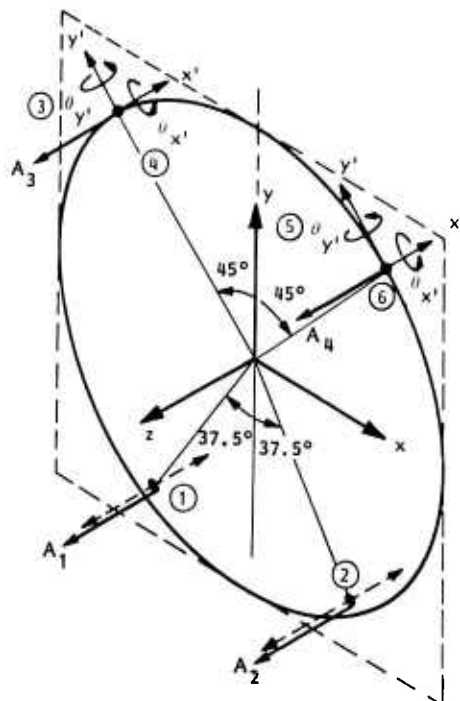


Fig. 3-44 Sensor and Actuator Type and Location for Circular Plate Experiment

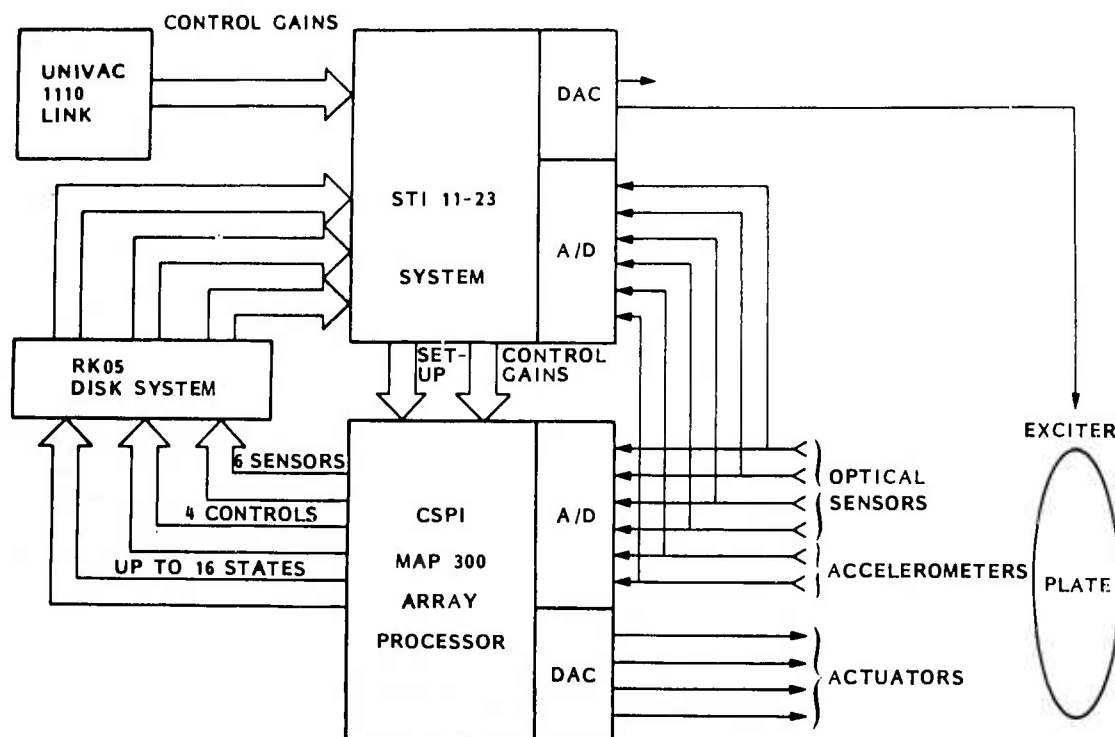


Fig. 3-45 Overall System Configuration

the 11-23 and then loaded into the array processor. Sensor signals, control inputs, and state estimates computed by the array processor can be stored on disk for later processing by the 11-23. A more detailed structure of the system is shown in Fig. 3-46, and a summary of the system's capabilities is given in Table 3-14. More specific characteristics of the array processor will be discussed later in this section.

Control Synthesis/Simulation Results

Finite Element Model. The plate finite element model was created using the SPAR program. It consists of 120 plate elements of triangular and trapezoidal shapes, since SPAR can handle this type of element (See Fig. 3-47). The boundary conditions were treated as unrestrained because the interaction with the suspension system was found to be negligible. A first test was made to determine the accuracy of the model by comparing the computed modal frequencies with those obtained directly from analytical formulas. The agreement was good to three-digit accuracy for the first seven modes. The masses of the actuators and accelerometers were then

Table 3-14
ACOSS SYSTEM CAPABILITIES

ARRAY PROCESSOR

Analog Input (ADC)

12 Bit
± 10V F.S.
8 Channels
31 K Samples/Channel/Second Max (252 K Throughput)

Analog Output (DAC)

12 Bit
± 10V F.S.
4 Channels
64 K Samples/Channel/Second Max (256 K Throughput)

HOST CPU

Analog Input (ADC)

12 Bit
± 10V F.S.
16 Channels
4 K Samples/Channel/Second Max (64 K Throughput)

Analog Output (DAC)

12 Bit
± 10V F.S.
2 Channels
100 K Samples/Channel/Second Max (200 K Throughput)

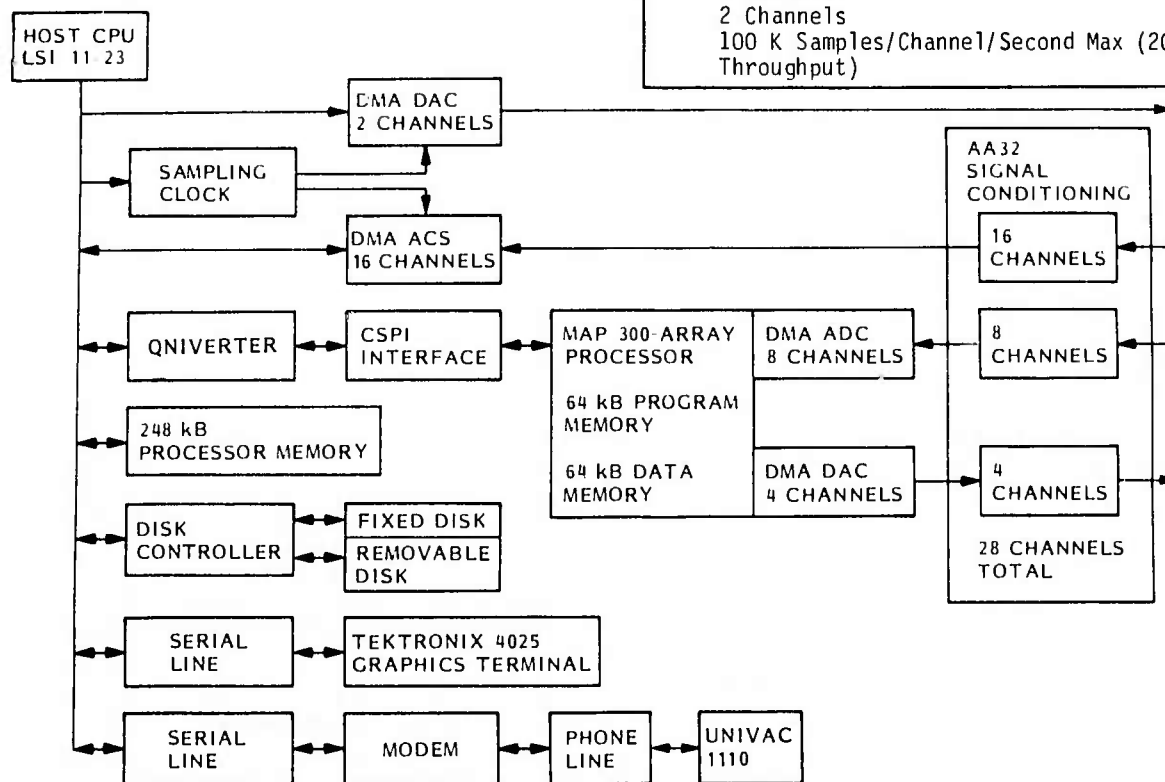


Fig. 3-46 ACOSS System

3. TECHNICAL ACTIVITIES

3.5.3 CIRCULAR PLATE: CONTROL SYNTHESIS/ SIMULATION

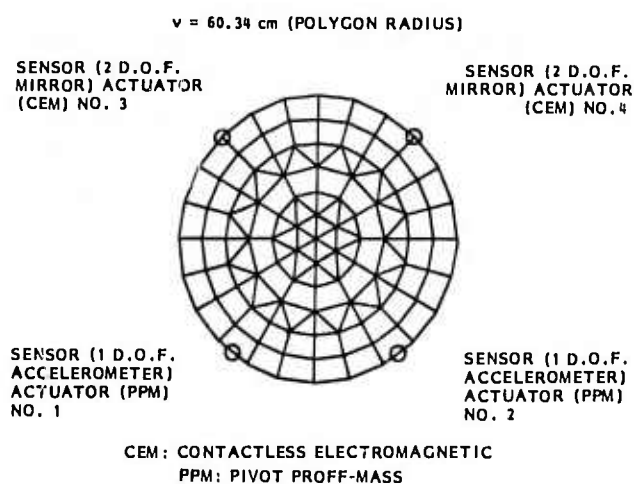


Fig. 3-47 Finite-Element Grid for 60-cm Radius Plate Experiment

added to the finite element model. The effect of these masses is to break the symmetry of the plate and cause the double roots to split, since the horizontal and vertical axes are no longer equivalent. The mode shape patterns associated with the first 11 bending modes of the plate are shown in Fig. 3-48. Table 3-15 shows a comparison between the modal frequencies of a uniform circular plate and those corresponding to the plate with actuator masses.

Control Synthesis Model. From the SPAR finite element model, system matrices were generated corresponding to the usual state equations

$$\begin{cases} \dot{x} = Fx + Gu \\ y = Hx \end{cases} \quad (3.35)$$

(ATTACHED SENSORS AND ACTUATORS PRODUCE SMALL "SEPARATION" OF CLASSICAL "DOUBLE-ROOT" MODES)

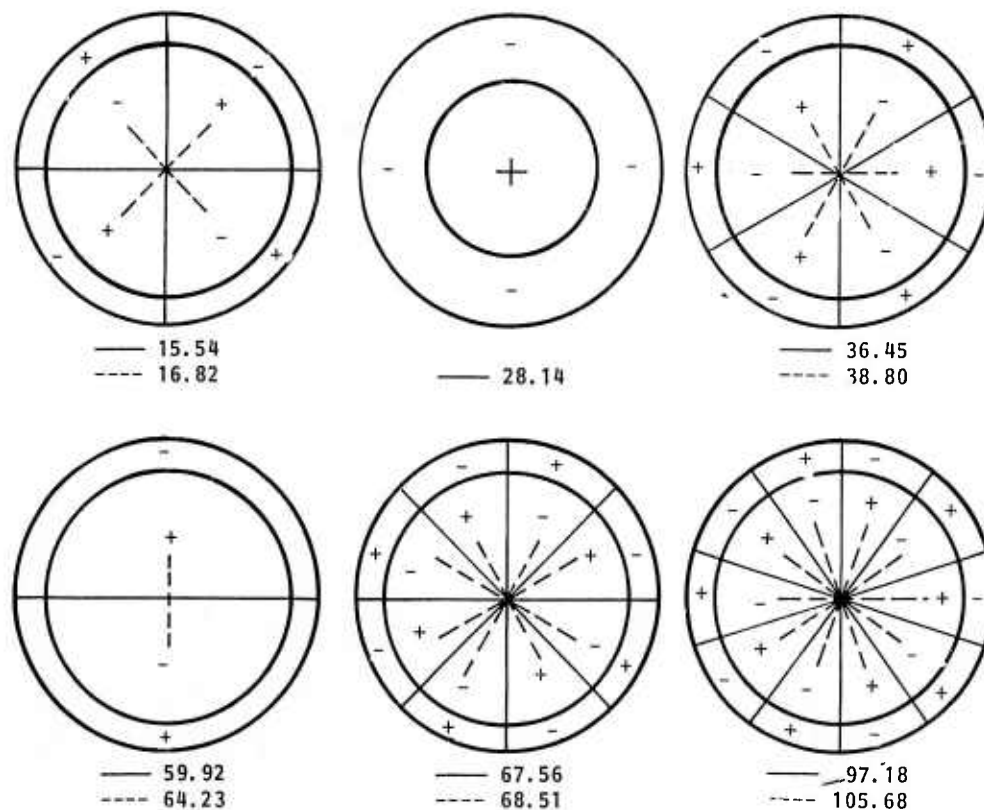


Fig. 3-48 Modal Frequencies (Hz) and Patterns of the Circular Plate Experiment

3. TECHNICAL ACTIVITIES

3.5.3 CIRCULAR PLATE: CONTROL SYNTHESIS/ SIMULATION

Table 3-15
CIRCULAR PLATE FREQUENCIES (Hz)

UNIFORM PLATE	WITH MASSES ADDED
16.9	15.54
16.9	16.82
29.3	28.14
39.4	36.45
39.4	38.80
66.1	59.92
66.1	64.23
69.3	67.56
69.3	68.51
106.4	97.18
106.4	105.68

where x is the vector of modal coordinates and their derivatives, with the added attitude variables:

$$x \triangleq [\dot{\theta}_x \ \theta_x \ \dot{\theta}_y \ \theta_y \ \dot{q}_1 \ q_1 \ \dot{q}_2 \ q_2 \ \dots \ \dot{q}_n \ q_n]^T$$

The initial model includes five flexible modes and two rigid-body modes. Thus, a 14th-order model is obtained. The control vector u is 4 x 1, and the measurement vector y is 6 x 1. Their components are shown in Table 3-16.

Table 3-16
CONTROL AND MEASUREMENT VECTOR DEFINITION

CONTROL VECTOR:

	Actuator Number	Type	Action
u_1	1	PPM	z-force
u_2	2	PPM	z-force
u_3	3	Contactless	z-force
u_4	4	Contactless	z-force

MEASUREMENT VECTOR:

	Sensor Number	Type	Sensed Quantity
y_1	1	Accelerometer	z
y_2	2	Accelerometer	z
y_3	3	Optical	θ_y
y_4	3	Optical	θ_x
y_5	4		θ_y
y_6	4		θ_x

In order to be able to use the PPM actuators in an integrated attitude/vibration control scheme, saturation from DC inputs must be avoided. To do so, the actuators are AC-coupled electronically, and it is important that this coupling be included in the controller synthesis. One way of achieving this is to use the frequency-shaping method for the control effort. The idea is to put a heavy penalty at zero frequency on the control inputs of the PPMs. Thus, the cost functional used for synthesizing the optimal controller is of the form:

$$J = \int_0^{\infty} (x^T A x + u_C^T B_C u_C + u_P^T B_P u_P) dt$$

where u_C and u_P are the control inputs for the contactless and PPM actuators respectively. The frequency-dependent weight B_P is then chosen to be of the form:

$$B_P = \frac{1}{\omega^2}$$

To implement this frequency shaping, Eqs. (3.35) must be augmented with the equations:

$$\begin{aligned} \dot{x}_{15} &= u_1 \\ \dot{x}_{16} &= u_2 \end{aligned} \quad (3.36)$$

Thus, the final model for control synthesis has the same form as Eq. (3.35), but the state vector now has 16 components, and the F , G , and H matrix dimensions are changed correspondingly. Entries for these matrices are shown in Table 3-17.

Table 3-17
CONTROL SYNTHESIS MODEL FOR THE PLATE

** F 15 16x16															
1, 2	-2.467+00	2, 1	1.000+00	3, 4	-2.274+00	4, 3	1.000+00	5, 5	-1.156+00	5, 6	-1.327+04	6, 5	1.000+00	7, 7	-1.200+00
7, 8	-1.440+04	8, 7	1.000+00	9, 9	-1.014+00	9, 10	-2.857+04	10, 9	1.000+00	11, 11	-4.313+00	11, 12	-6.025+04	12, 11	1.000+00
12, 13	-2.192-01	13, 14	-7.505+04	14, 13	1.000+00	15, 15	-1.000-03	16, 16	-2.000-03						
** G 15 16x4															
1, 1	-3.069-01	1, 2	-3.069-01	1, 3	2.977-01	1, 4	2.977-01	2, 1	-3.069-01	2, 2	-3.069-01	2, 3	2.977-01	2, 4	2.977-01
3, 1	2.523-01	3, 2	-2.523-01	3, 3	2.956-01	3, 4	-2.956-01	5, 1	5.302-01	5, 2	-5.302-01	5, 3	-5.732-01	5, 4	5.732-01
7, 1	1.474-01	7, 2	1.474-01	7, 3	1.149-02	7, 4	1.148-02	9, 1	3.636-01	9, 2	3.636-01	9, 3	3.720-01	9, 4	3.720-01
11, 1	4.732-01	11, 2	-4.731-01	11, 3	5.253-01	11, 4	-5.255-01	13, 1	-2.253-01	13, 2	-2.254-01	13, 3	4.869-01	13, 4	4.867-01
15, 1	1.000+00	15, 2	1.000+00												
** H 15 6x16															
1, 1	-4.576-01	1, 3	3.642-01	1, 5	5.302-01	1, 7	1.474-01	1, 9	3.636-01	1, 11	4.732-01	1, 13	-2.253-01	2, 1	-4.576-01
2, 3	-3.642-01	2, 5	-5.302-01	2, 7	1.474-01	2, 9	3.636-01	2, 11	-4.731-01	2, 13	-2.254-01	3, 2	-7.071-01	3, 4	7.071-01
3, 6	-1.059-02	3, 8	-2.031-01	3, 10	-4.389-03	3, 12	-2.018-01	3, 14	2.244-01	4, 2	7.071-01	4, 4	7.071-01	4, 6	-1.494-01
4, 8	4.308-03	4, 10	1.803-01	4, 12	1.857-01	4, 14	1.828-01	5, 2	-7.071-01	5, 4	7.071-01	5, 6	-1.494-01	5, 8	-4.305-03
5, 10	-1.803-01	5, 12	1.857-01	5, 14	-1.828-01	6, 2	7.071-01	6, 4	7.071-01	6, 6	-1.058-02	6, 8	2.031-01	6, 10	4.408-03
6, 12	-2.017-01	6, 14	-2.244-01												

3. TECHNICAL ACTIVITIES

The next step is to transform the continuous equations Eq. (3.35) into discrete equations of the form

$$\begin{aligned} x_{n+1} &= \Phi_0 x_n + \Gamma_0 u_n \\ y_n &= H_0 x_n \end{aligned} \quad (3.37)$$

The state estimator has the form

$$\hat{x}_{n+1} = \Phi_0 \hat{x}_n + \Gamma_0 u_n + K (y_n - H_0 \hat{x}_n) \quad (3.38)$$

and the control law is

$$u_n = C \hat{x}_n \quad (3.39)$$

The values of the gain matrices C and K are obtained by standard optimal control synthesis programs. Equations (3.38) and (3.39) constitute the controller equations and can be rewritten in the single matrix operation form

$$\begin{bmatrix} x_{n+1} \\ u_{n+1} \\ y_{n+1} \end{bmatrix} = \mathcal{A} \begin{bmatrix} x_n \\ u_n \\ y_n \end{bmatrix} \quad (3.40)$$

where

$$\mathcal{A} \triangleq \begin{bmatrix} \Phi_0 - K H_0 & \Gamma & K \\ \text{---} & \text{---} & \text{---} \\ C (\Phi_0 - K H_0) & C \Gamma & C K \end{bmatrix} \quad (3.41)$$

Simulations. The dynamics of the total system are evaluated by combining the plate evaluation model, which contains two rigid body modes, 11 flexible modes, and the controller equations. The evaluation model must first be translated into its discrete equivalent

$$\begin{cases} x_{n+1} = \Phi x_n + \Gamma u_n \\ y_n = H x_n \end{cases} \quad (3.42)$$

Then Eqs. (3.42), (3.38), and (3.39) are combined into the single equation

$$\begin{bmatrix} x_{n+1} \\ \hat{x}_{n+1} \end{bmatrix} = S \begin{bmatrix} x_n \\ \hat{x}_n \end{bmatrix} + D u_e \quad (3.43)$$

3.5.3 CIRCULAR PLATE: EXPERIMENTAL PERFORMANCE

where

$$S = \begin{bmatrix} \Phi & \Gamma C \\ \text{---} & \text{---} \\ K H & \Phi_0 + \Gamma_0 C - K H_0 \end{bmatrix} \quad (3.44)$$

and D is a matrix corresponding to external disturbance inputs.

Stability may be determined by the roots of S (in the z-plane) and performance by computing the time sequences defined by Eq. (3.43) for given initial conditions or for a given disturbance u_e . An example of such a simulation (for initial conditions corresponding to a unit value in all modal amplitudes) is shown in Appendix A.

Experimental Performance.

Open-Loop Characterization. The open-loop characteristics of the data were determined using the VAMP program. The data were generated by exciting one of the contactless actuators with a chirp and observing the signals from optical and inertial sensors. (A chirp is a fast sine sweep varying linearly in frequency.) Figure 3-49 shows the resulting spectrum corresponding to the velocity sensor no. 2 (i.e., integrated signal from accelerometer no. 2). Several peaks corresponding to various bending modes can be seen. The first mode at 9.8 Hz is identified as a spurious resonance in the suspension system. A comparison between computed and measured frequencies and dampings is shown in Table 3-18. Two interesting phenomena can be observed: first, the agreement becomes very poor as frequency goes up; and second, the natural damping is extremely small. These two

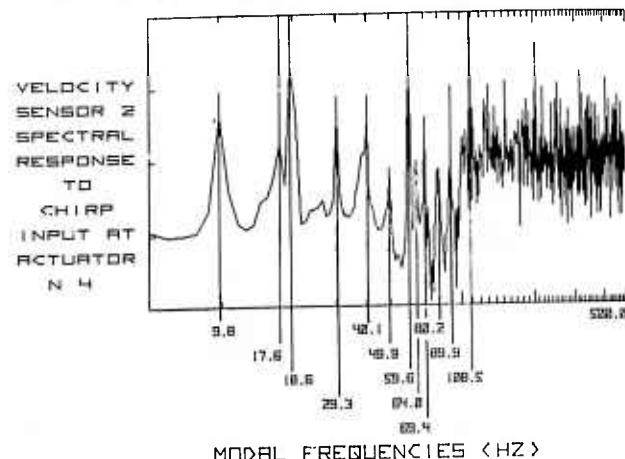


Fig. 3-49 VAMP Spectral Analysis: Open-Loop Response

3. TECHNICAL ACTIVITIES

3.5.3 CIRCULAR PLATE: EXPERIMENTAL PERFORMANCE

Table 3-18 FIRST OPEN-LOOP CHARACTERIZATION				
MODAL FREQUENCIES (Hz)		DAMPING RATIOS		
(COMPUTED)	(MEASURED)	RELATIVE CONTROLLABILITY (COMPUTED)	(MEASURED)	
1 0	.4			CONTROLLER MODEL
2 0	.4			
3 15.5	17.6	15	0.0003	
4 16.8	18.6	1	-	
5 28.1	29.3	4	0.0013	
6 36.5	40.1	5	0.0004	UNCONTROLLED MODES
7 38.8	49.9	1	-	
8 59.9	59.6	-	-	
9 64.2	64.0	-	-	
10 67.5	69.4	-	-	
11 68.5	80.2	-	-	
12 97.2	89.9	-	-	
13 105.7	108.5	-	-	

features are typical of large space structures and justify the use of this particular test structure for vibration control studies.

The open-loop measurements were initially hampered by environmental disturbances acting on the plate - mainly air currents preventing the plate from remaining pointed at the optical sensors. This was solved by the magnetic stabilization (described in Section 3.4.2) and by enclosing the plate in a cabinet with a plexiglass window. Also, an analog rigid-body controller was designed to keep the plate correctly pointed.

Although the main purpose of the experiment was the study of digital control, this analog (and classical) controller was useful in demonstrating two main points of the theory of LSS control: 1) the interaction between rigid-body

control and flexible modes; and 2) the stabilization of the spillover by an LAC system. Indeed, though this analog controller had a bandwidth of about 2 Hz, it was able to destabilize the first bending mode at 17.6 Hz. This was the result of the low damping in this mode preventing gain stabilization of the controller. This problem was cured by closing the inner velocity servoloop on the PPM actuators. This closure makes the actuators behave as passive mass/dashpot systems. Although such systems do not introduce much damping in the structure unless specifically tuned, their effect is sufficient to stabilize the controller. Simulations of this result were made and are displayed in Fig. 3-50. The equations of the controller are given below:

$$\dot{z}_1 = -az_1 + ay_6$$

$$\dot{z}_2 = z_1$$

$$\dot{z}_3 = -az_3 + ay_5$$

$$\dot{z}_4 = z_3$$

$$u = -c_3(\dot{dz}_1 + pz_1 + rz_2)$$

$$u_4 = -c_4(\dot{dz}_3 + pz_3 + rz_4)$$

where u and y retain the same meanings they had in the equations set forth above. Nominal values for the parameters are:

$$\begin{cases} a = 16.0 \\ d = 1.0 \\ p = 4.0 \\ r = 8.0 \\ c_3 = -c_4 = 1.0 \end{cases}$$

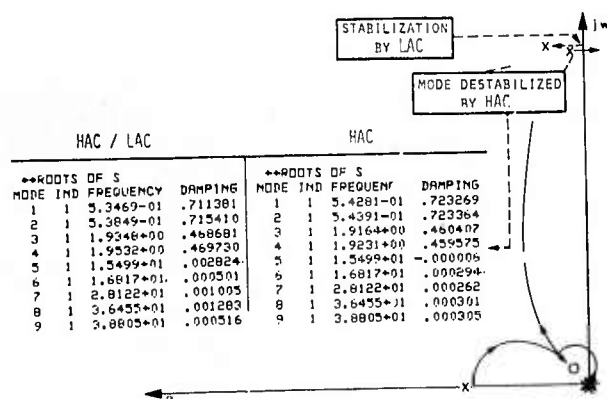


Fig. 3-50 Stabilization of Rigid-Body Controller (HAC) by LAC Controller

Digital Controller Implementation. Control Eqs.(3.40) and (3.41) were implemented in the array processor. The main reason for this mechanization is that the array processor is capable of effecting matrix multiplications in a very short time. It is designed for handling large size matrices such as occur in image processing. However, the arithmetic processor is controlled by another processor, the CSPU processor, which functions in the usual sequential fashion. Thus, each operation requested from

3. TECHNICAL ACTIVITIES

3.5.3 CIRCULAR PLATE: CONCLUSIONS AND RECOMMENDATIONS

the arithmetic unit requires some setup time. In the present application to digital control, this setup time becomes a major restriction in computational speed and thus in sampling rate. Fig. 3-51 shows a simplified model of the sequence of operations needed for this control experiment. The actual calculation takes only 1.4 ms, while 4.4 ms are spent on overhead.

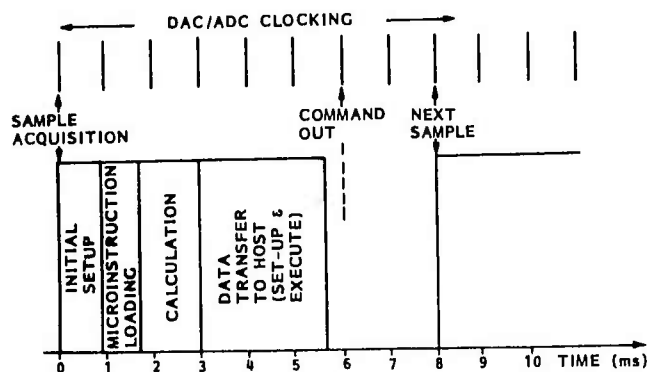


Fig. 3-51 Array Processor Timing Sequence

The additional time necessary to transfer the data to the host processor created a serious problem which took specialized hardware and tests to recognize. The original sampling rate of 200 Hz was selected on the basis of manufacturer specifications and the intent of controlling modes up to 100 Hz. However, the 5-ms

sampling time conflicted with the total processing time, and unpredictable failures occurred constantly. Other synchronization problems between the DAC and the algorithm clocks prevented the testing of the control algorithm. Finally, the hardware was found to be extremely temperature sensitive, which caused other catastrophic failures. All these problems have finally been solved, and the system is now operational for the next contract phase. The maximum sampling rate with a 16th order system is about 170 Hz.

Conclusions and Recommendations. With the present level of disturbances (air currents, building vibrations, acoustic noise) and the simple rigid-body analog controller, the total (i.e., rigid and flexible) pointing error of the plate is about 20 μ rad rms, of which about 5 μ rad is due to bending mode excitation. The use of the more sophisticated digital controller is expected to reduce this error significantly and thus make this experiment very relevant to actual optical space systems. Already, new problems associated with microvibration levels have been observed (e.g., nonlinear damping effects, microlimit cycles), and more are expected at lower amplitudes. Finally, it appears that yet-to-be-developed dedicated LQG microprocessors would be more appropriate for digital control than the present array processor. However, the advantage of the latter (the only processor in existence today) is its flexibility as a research tool.

Section 4 TECHNOLOGY PRIMER

4.1 INTRODUCTION

The control of structural flexibility implies, in some sense, the ability to construct and/or deploy in space large structures whose behavior is predominantly determined not by passive characteristics but by active control systems. The role such ACOSS systems can play in modifying structural and attitude dynamics is the subject of the ACOSS FIVE research study.

In the context of preliminary investigations, it is often useful to restrict consideration to a few simple models (examples) in the hope that generic characteristics of the control process will emerge and be directly applicable to more detailed, realistic systems. Experience with detailed structural models, however, has already indicated that system performance metrics, such as optical or rf LOS performance measures, rms surface shape, modal damping, etc., can be extremely sensitive to changes in the structural model, actuator and sensor placement, sensor measurement error, etc. These sensitivities may also result from the detailed way a portion or all of the structure is built, the limitations of sensor measurements in general, or the disturbances associated with specific actuator implementations. Therefore, while consideration of quite simple structures and examples is a necessary first step in obtaining knowledge of fundamentals, it should not generally be expected that control strategies developed in this way (i.e., limited to small, simple examples) can be immediately implemented on real, high-detail large space structures (LSS). For the latter, questions of local versus global control, sensor/actuator placement strategy and error, model accuracy and identification, modal density, model order-reduction schemes, computational requirements, etc., will be the dominant considerations.

The intended purpose of this technology primer is to describe in a systematic manner the new controls technology developed by LMSC under the ACOSS program. While the material is presented in a relatively detailed, tutorial fashion in order to make possible the transfer of this technology, several requirements must be met by the potential user in order to make this transfer effective in real applications. Because of the high level of interconnectedness between the various disciplines involved in this technology, e.g., structures, dynamics, controls,

numerical analysis, etc., a strong integration of these disciplines is required. This entails in particular the availability of interconnected large-scale software which allows the user to construct and manipulate the various models which arise during the different phases of control synthesis and evaluation.

The individual computer programs required for this task are generic in nature, and are generally available in different forms, e.g., finite-element structural programs, complex eigen-solvers, optimal control synthesis programs, etc. However, it is the user's responsibility to assemble and organize these various codes to best suit his particular needs and to recognize that the intrinsic size of the LSS controls problem, even for the simplest cases, precludes the manual handling of data.

4.1.1 Objectives of Structural Control (ACOSS FIVE)

The general objective of ACOSS is to develop a technology for the design and implementation of active control systems to meet the high performance requirements inherent in the new generation of space systems. Particular objectives include high-precision pointing in the presence of structural flexibility, suppression of transient vibrations induced by attitude maneuvers (ACOSS THREE), and attenuation of vibration induced by onboard disturbances, with special emphasis in ACOSS FIVE on sinusoidal steady-state disturbance sources. The main objective present in all these control problems is the development of techniques to properly eliminate instabilities created by spillover, which is the interaction of the controller with the unmodeled modes.

4.1.2 Peculiarities and Pathologies of LSS

Problems associated with vibration control and accurate pointing of large space structures (LSS) are quite different from those posed by traditional rigid spacecraft, even if the latter have flexible appendages. LSS systems typically combine large size with extremely rigorous pointing and surface figure error requirements, so that the peculiarities and pathologies of LSS become meaningful only by comparison with the control of traditional spacecraft. Differences in control requirements and constraints, synthesis and evaluation methodologies, etc., must be addressed in the context of the flight control system design.

Control design is principally driven by spacecraft dynamic characteristics, performance considerations, on-board or environmental disturbances, and sensor/actuator availability. The special features of large flexible spacecraft in these four categories are summarized below.

1. There are an infinite number of elastic modes, usually with low natural damping, and the controller bandwidth extends over a significant number of these modes (Fig. 4-1). This last feature is taken to be the defining characteristic of a large space structure.
2. Flexible modes interact not only with the attitude controller but contribute directly to the deformation geometry of the structure which itself may require accurate control. Performance criteria must then be precisely formulated or the control problem is ill-posed.
3. A variety of disturbances may excite the structure and degrade its performance. Again, the formulation of the control problem will be strongly affected by the type of the disturbances and their spatial and spectral characteristics.
4. Most of the actuators and sensors currently envisioned for large space structures have been studied only theoretically. Ground experiments in active vibration control and hardware development are just beginning, and it is safe to state that there is no available flight-qualified hardware. The control designer must therefore rely on believable extrapolation of available data.

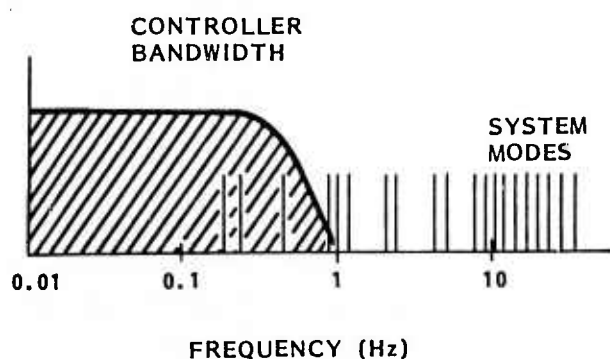


Fig. 4-1 Flexible Structure Mode Location and Controller Bandwidth

The major problems encountered in the control design of large flexible spacecraft are directly due to the first three characteristics. The truly infinite-dimensional character

of the structure has to be approximated by a finite-dimensional model. A good structural analysis usually generates modal models with a large number of modes which provide a reasonable representation of the spacecraft. However, such models have two fundamental drawbacks: (1) their size is much beyond the computational capability of current control synthesis methods; and (2) the higher frequency modes of a structural model are known only imprecisely.

Modes are usually accurate in the low-frequency part of the total spectrum. They depart more and more often from the actual spacecraft modes as frequency increases and can only be used in a qualitative manner in the design process. Thus, the control design must be based on a reduced-order model containing only selected low-frequency modes. This is not by itself a major limitation, since low-frequency modes usually require the most control because of their longer settling times and larger contribution to performance degradation. Nevertheless, the control design approach must properly handle the poorly known higher-frequency modes by not destabilizing them while controlling the low-frequency modes. Indeed, no matter where the controller roll-off frequency is situated, the infinite nature of the modal spectrum implies that there will be modes within and beyond the roll-off region. It has been shown (Ref. 2) that destabilization is likely and almost certain to occur in the roll-off region, a situation which can only worsen for closely packed modes and low natural damping. This so-called "spillover" phenomenon is one of the most crucial problems faced by the control designer.

4.1.3 Motivation for New Synthesis Techniques

Traditional control synthesis techniques have primarily addressed single-input/single-output (SISO) systems, and numerous frequency-domain procedures have been developed to handle such systems. For multi-input/multi-output (MIMO) systems, the usual approach is to decompose them into separate SISO control systems and synthesize controllers for them individually. This has been typical, for instance, of attitude control systems where pitch and roll-yaw behavior are assumed to be decoupled. For the LSS control problem, the large number of degrees-of-freedom affected by a single actuator (or those measured by a single sensor) precludes any simplifying decoupling assumptions, and both actuators and sensors have to be treated together in multi-dimensional representations.

Modern control techniques are particularly well suited to handle such multi-dimensional systems for which, in fact, they were originally developed. These techniques, primarily formulated in the time-domain, put special emphasis on performance which is quantified in a quadratic cost functional. Control synthesis procedures are then derived from the optimization of the performance, and in this sense are particularly useful in the multi-faceted LSS control problem.

Even though these optimal techniques automatically guarantee the existence of a stable solution to any control synthesis for a perfectly known dynamic plant, serious stability problems arise when there are uncertainties in the plant parameters or when only a partial (reduced) model of the plant is used. These features, characteristic of the LSS control problem, motivated the development of new synthesis techniques beyond the straightforward application of modern optimal control. These new techniques, such as the two-level HAC/LAC approach and the frequency-shaping of the roll-off, have incorporated some frequency domain considerations into the state-space time-domain optimal formulations.

4.1.4 Road Map of New Methodology

The major steps of the new methodology are depicted in Fig. 4-2. The procedure starts with the finite-element structural model of the spacecraft which yields frequencies and open-loop mode shapes. This allows construction of the state-space model (see Section 4.2.1), which also requires the performance and disturbance models for proper actuator and sensor definition. Then the state-space model is reduced for controller synthesis into lower order models for High and Low Authority Control.

The HAC law is designed first, and the spillover is evaluated on the evaluation model. This model is constructed from the original state-space model and the various control laws which have to be tested against it. The degree of spillover due to the HAC controller is then used to determine the LAC damping ratios necessary to prevent the spillover from creating instabilities. Then the combined HAC/LAC control law is evaluated again for stability and performance.

In any of the sequences described above, some iteration may take place. The control design

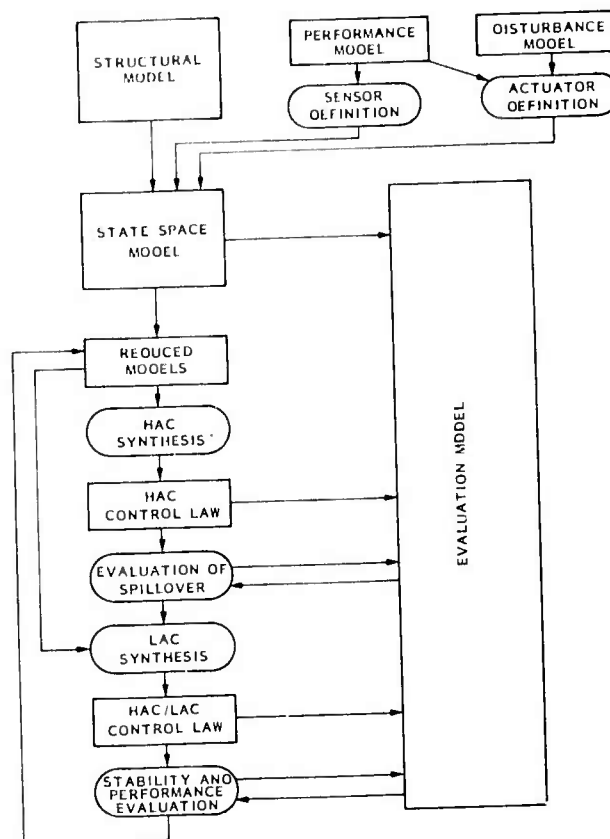


Fig. 4-2 Road Map of New Methodology

methodology is discussed in detail in Section 4.3

4.2 MODELING OF FLEXIBLE SPACECRAFT

A central issue in the active control of space structures is the development of "correct" mathematical models for the open- and closed-loop dynamical plants. While a great deal of controversy has been generated recently over finite-element methods and their assorted pitfalls, programs such as NASTRAN and SPAR are nevertheless the primary current tools for generating dynamical models of conceptual spacecraft whose structure cannot be idealized by simple models of beams, plates, and beams with lumped masses.

Finite-element structural programs generally provide the control designers with a set of

modal frequencies ω_n and a set of mode shapes (eigenvectors) ϕ_n corresponding to appropriate boundary values.* These eigenvectors are given in discretized form, i.e., a set of modal displacements in the x, y, and z directions at each nodal station. In some cases, modal rotations, $\theta_x, \theta_y, \theta_z$ are also required. In addition, coordinates and a "map" of the structure's nodes must be provided to allow the reconstruction of physical displacements in terms of their modal expansions.

The important point here is that, for any non-trivial flexible satellite configuration, the volume of information is so large that the data handling must remain entirely within the computer and its mass-storage facilities. Development of this data base, in a form usable by control synthesis software, is a fundamental necessity for the synthesis and evaluation of complex controls which require modal truncation, actuator/sensor location and type changes, and evaluation of system performance for parameter and system order changes. Preparation of a structure for controls is a major part of the overall effort required to develop structural control systems.

4.2.1 State-Space Models

As an example, consider the dynamic equations of a structure, which are linear for small displacements and are written as

$$M\ddot{\delta} + K\delta = f, \quad (4.1)$$

where δ is a column vector obtained by "stacking" the components of the displacements at all nodes, f is a similar vector of (control) forces applied at those nodes, and M and K are generalized mass and stiffness matrices of appropriate dimensions. The usual procedure (Ref. 3) is then to diagonalize Eq. (4.1) by solving the eigenproblem:

$$M^{-1}K\Phi = \Phi \begin{bmatrix} -\omega_n^2 \\ \vdots \\ -\omega_n^2 \end{bmatrix}, \quad (4.2)$$

where Φ is the matrix whose columns ϕ_n are the mode shapes corresponding to the modal cyclic frequencies ω_n (i.e., eigenvalues of $M^{-1}K$). Because of reciprocity properties, K and M are symmetric matrices (M is a diagonal for lumped-mass models if δ is the vector of

displacements at lumped-mass locations). It is known that there exists a normalization of Φ (whose columns are only determined up to a multiplicative constant by Eq. (4.2)) such that $\Phi^T M \Phi = I$, and hence, from Eq. (4.2),

$$\Phi^T K \Phi = \begin{bmatrix} -\omega_n^2 \\ \vdots \\ -\omega_n^2 \end{bmatrix}. \quad (4.3)$$

Using then the basic modal transformation $\delta = \Phi q$ (where q is a vector of modal amplitudes), one can transform Eq. (4.1) into the classical modal equations

$$\ddot{q} + \begin{bmatrix} -\omega_n^2 \\ \vdots \\ -\omega_n^2 \end{bmatrix} q = \Phi^T f. \quad (4.4)$$

In general, forces are applied only at a few nodal points of the structure, via specific actuators, and there are linear relations between the set of command inputs, represented by some vector u , and the vector f or control forces, such as:

$$f = \mathcal{A} u.$$

In the same way, sensor measurements may be stacked in a vector y which is linearly related to the position and rates of the nodal points, i.e.,

$$y = \mathcal{R} \begin{bmatrix} \dot{\delta} \\ \delta \end{bmatrix} = \mathcal{R} \begin{bmatrix} \Phi & 0 \\ 0 & \Phi \end{bmatrix} \begin{bmatrix} \dot{q} \\ q \end{bmatrix}.$$

Defining the modal state vector as

$$x \triangleq \begin{bmatrix} \dot{q} \\ q \end{bmatrix}, \quad (4.5)$$

one can finally write the equations describing the dynamics of the spacecraft in the usual first-order form:

$$\begin{aligned} \dot{x} &= Fx + Gu, \\ y &= Hx, \end{aligned} \quad (4.6)$$

where

$$F \triangleq \begin{bmatrix} -2\zeta_n\omega_n & -\omega_n^2 \\ I & 0 \end{bmatrix}, \quad G \triangleq \begin{bmatrix} \Phi^T \mathcal{A} \\ -\Phi \end{bmatrix}$$

and $H \triangleq \mathcal{R} \begin{bmatrix} -\Phi & \Phi \end{bmatrix}. \quad (4.7)$

The diagonal elements $-2\zeta_n\omega_n$ are added in the F matrix to represent the (usually small) natural modal damping. The F matrix is the state-space form of the (open-loop) dynamics

*For single-body monolithic spacecraft configurations, unrestrained modes are appropriate. For gimbaled multi-body structures, see discussion at the end of this subsection.

matrix and now has complex eigenvalues and eigenvectors. The calculation of the matrices F, G, and H from the structural data and the actuator/sensor definitions usually require direct handling and processing of the data by digital computers, since hand calculations rapidly become prohibitive for large systems. The introduction of actuator or sensor dynamics may further complicate the construction of these matrices. Nevertheless, Eqs. (4.6) along with the definitions (4.5) and (4.7) constitute the basic model for preliminary control design.

Although modern control synthesis methods are principally formulated in the time domain, frequency-domain methods provide a useful complement, especially when steady-state responses are sought. In particular, combinations of frequency-domain performance criteria with time-domain synthesis methods, discussed in Section 4.3, can produce control designs which can be accurately realized in hardware. Using Eq. (4.4) (with an added term for modal damping) one may easily obtain the open-loop modal amplitude transfer function

$$(q_n/f_i) = \frac{\Phi_{in}}{(\omega_n^2 + 2j\zeta_n\omega_n\omega - \omega^2)} \quad (4.8)$$

where f_i is the force acting on the i th degree of freedom and $j = \sqrt{-1}$. The linear relations between x and q , y and x , and f and u make it easy to compute the other transfer functions of interest, e.g., x_k/u_i and y_k/u_i .

4.2.2 Nonlinear Models

For single-body monolithic structures, the fine-pointing attitude dynamics are subsumed in the rotational rigid body modes included in the modal matrix Φ . When only small motions of a space structure are being considered, the conventional linear structural dynamics analyses (NASTRAN and SPAR) are adequate, and the rigid-body modes are formally handled together with the elastic modes, even though the actuators necessary to control them will in general be different from those used to control elastic vibrations. When larger attitude angles need to be considered, and angular rates remain small, the linear equations (Eqs. (4.6)) are still applicable, provided that the rigid-body modes are now given in terms of three attitude angles which then constitute the first three modal coordinates. The displacements δ_i are then interpreted as the linear deformations of the structure with respect to the rotated frame. This procedure removes the kinematic nonlinearities resulting from the linear stretching of the

structure under the classical rigid-body modes. However, for large angular rates, nonlinear dynamic effects have to be modeled, even though structural deformations can still be represented by linear equations.

For multi-body configurations, such as spacecraft with gimbaled power equipment sections, the dynamics become highly nontrivial. The field of multi-body dynamics was pioneered in the late sixties when, based on the earlier work of Hooker and Margulies (Refs. 4,5), the first N-body attitude dynamics computer software was developed. A number of subsequent extended programs were written in the next few years, and these are documented in Ref. 6. These N-body programs provide a hybrid synthesis of large-angle nonlinear multirigid-body dynamics with the modal representation of linear elastic deformations used in structural mechanics. More recent models, based on T. R. Kane's formulation (Ref. 7), have been developed for monolithic structures containing stored momentum (Ref. 8). However, while those dynamic models and associated computer programs are very useful for evaluation purposes, the associated nonlinear control synthesis problem is still extremely difficult to tackle and will not be discussed in this report.

4.2.3 Model Reduction

Model reduction is a process by which the order of the dynamical system is reduced for a fixed number of actuator inputs and sensor outputs. The traditional structural mechanics approach first approximates the infinite dimensional nature of the real structure by a large but finite number of degrees-of-freedom representation. This approximation may be based on a direct physical interpretation in terms of lumped-masses and interconnecting springs or on the improved "consistent mass matrix" method. Several methods can be used to further reduce the degrees of freedom, and correspondingly, the number of nodal points in the representation of the structure. Most of the techniques used in dynamics and control, however, focus on modal-coordinate reduction. Reducing the number of modes is usually done by modal truncation, whereby modes above a chosen frequency or in an intermediate frequency range are simply discarded. For large space structures control, the frequency criterion is not sufficient in general, and more sophisticated criteria need to be used, resulting in selective deletion of modes. In more general methods, the reduction involves a dimension-reducing coordinate transformation in which the individual meaning of the modes is no longer apparent (Ref. 9).

In general, the requirements for model reduction for active control of large space structures must include the following:

1. The reduced model should be suitable for control design and synthesis. It should incorporate all features critical for the selection of a feedback structure and control gains.
2. The reduced model should accurately incorporate actuator effectiveness, sensor measurements and disturbance distribution.
3. The dynamical characteristics of interest in the structure should be represented in the reduced model.

One usual approach to model reduction is to consider what properties the reduced-model open-loop transfer functions must satisfy so that the corresponding closed-loop transfer functions adequately represent the unreduced closed-loop system. Various criteria for this approach are examined next.

Consider a high-order large space structure model with an $N \times 1$ state vector x , a $q \times 1$ control vector u , and a $p \times 1$ output vector y :

$$\dot{x} = Fx + Gu, \quad (4.9)$$

$$y = Hx + Du. \quad (4.10)$$

The transfer function between y and u is

$$y(s) = [H(sI - F)^{-1}G + D] u(s) \\ \triangleq T(s) u(s). \quad (4.11)$$

The transfer function may be expanded about the N poles of the system. Because of the particular form of Eqs. (4.9) and (4.10), the number of zeros does not exceed the number of poles, and the expansion takes the general form:

$$T(s) = R_0 + \frac{R_1}{(s-\lambda_1)} + \frac{R_2}{(s-\lambda_2)} + \dots \\ + \frac{R_N}{(s-\lambda_N)}, \quad (4.12)$$

where the R 's represent constant coefficient matrices. For any input-output pair (k, ℓ) the transfer function may also be written as a ratio of zeros and poles:

$$T_{k\ell}(s) = \frac{g(s-z_1)(s-z_2) \dots (s-z_M)}{(s-\lambda_1)(s-\lambda_2) \dots (s-\lambda_N)}, \quad (4.13)$$

where the scalar g and the zeros z_i depend upon the choice of k and ℓ . In most representations, the number of zeros is less than or equal to the number of poles.

If the model is to be reduced to n states, the number of poles will drop to n . Criteria have to be developed to determine the set of poles which may be dropped, along with the corresponding set of modes. These criteria must consider the following:

1. Any mode which is uncontrollable and undisturbable or unobservable can be dropped. Either of these conditions corresponds to a zero residue or a perfect pole-zero cancellation in all transfer functions.
2. Controllable modes should not necessarily be discarded even if they are nondisturbable and add nothing to the cost functional, since they may be excited by the control actuators.
3. Highly controllable modes in the bandwidth of interest should be retained even if they are not disturbable or observable. Similarly, highly observable modes should be retained for robustness reasons.
4. Proper mode ordering based on cost analysis (Ref. 9) should include the above factors in addition to performance considerations.

For very small feedback gains, the rate at which the poles migrate depends upon the residues. High-gain, closed-loop behavior is described more accurately by open-loop poles and zeros. Therefore, an ideal reduced-order model should maintain the residues of the retained poles and zeros in the spectrum of interest. Unfortunately, both zeros and residues cannot be preserved simultaneously. The attempt, in reduced-order modeling methods, is to maintain either poles or zeros or provide approximations to both of them.

Retention of Residues. The procedure for retaining residues is implemented as follows. Let F , G , H , and D be in modal form, and assume that the first n modes are retained. The state equations are then written as

$$\begin{bmatrix} \dot{x}_1 \\ \vdots \\ \dot{x}_2 \end{bmatrix} = \begin{bmatrix} F_{11} & 0 \\ 0 & F_{22} \end{bmatrix} \begin{bmatrix} x_1 \\ \vdots \\ x_2 \end{bmatrix} + \begin{bmatrix} G_1 \\ \vdots \\ G_2 \end{bmatrix} u, \quad (4.14)$$

$$y = [H_1 \mid H_2] \begin{bmatrix} x_1 \\ \vdots \\ x_2 \end{bmatrix} + Du. \quad (4.15)$$

Let the average frequency of the retained modes be ω_a . The state x_2 is approximated by

$$x_2 = \text{Re} [(j\omega_a I - F_{22})^{-1} G_2] u, \quad (4.16)$$

where $\text{Re}(\cdot)$ represents the real part of (\cdot) . The real part is selected because it is not feasible to match the imaginary part of the approximation using a reduced model with real coefficients. Therefore, the reduced model is approximated by

$$\dot{x}_1 = F_{11}x_1 + G_1 u,$$

$$y = H_1 x_1 + \{H_2 \text{Re} [(j\omega_a I - F_{22})^{-1} G_2] + D\} u. \quad (4.17)$$

In order to match the dc gain of the reduced model to that of the high-order model, ω_a may be set to zero. Most approximations match only the dc gain because for zero ω_a , the right-hand side of Eq. (4.16) is real. The problem of not being able to match the complex component in Eq. (4.16) then disappears.

Retention of Zeros. To retain the first m zeros and n poles about the average frequency, ω_a , the transfer function given by Eq. (4.13) is simplified to

$$T_{kl}(s) = \frac{g(j\omega_a - z_{m+1}) \dots (j\omega_a - z_M) (s - z_1) \dots (s - z_M)}{(j\omega_a - \lambda_{n+1}) \dots (j\omega_a - \lambda_N) (s - \lambda_1) \dots (s - \lambda_n)} \quad (4.18)$$

The first term is approximated by a real gain. Each input-output transfer function is simplified as in Eq. (4.18). These simplified transfer functions are reconverted into a state-variable description (Ref. 10).

The computation time requirements to obtain reduced-order models which retain zeros are very high. Poles and residues of high-order models are determined much more easily than zeros. This model-reduction procedure, therefore, has not yet been used for large space structures applications.

Table 4-1 shows the partitioning of the infinite series representing the exact transfer function for the case of a general undamped structure. The ϕ_i 's are the mode shapes at the location where the displacement-to-force ratio is measured (or rotation-to-torque, etc.). The number of modes to be controlled is n_c ; the number

of modes retained in the model of the structure is n_r .

Table 4-1
MODAL PARTITIONING AND
APPROXIMATE TRANSFER FUNCTIONS

	MODES	TO BE CONTROLLED	RETAINED IN MODEL	NOT RETAINED IN MODEL
Transfer Function		$s \geq \omega_1$	$s \leq \omega_1$	$s \ll \omega_1$
Exact	$T_c(s) =$	$\sum_{i=1}^{n_c} \frac{\phi_i^2}{\omega_i^2 + s^2}$	$+ \sum_{i=n_c+1}^{n_r} \frac{\phi_i^2}{\omega_i^2 + s^2}$	$+ \sum_{i=n_r+1}^{\infty} \frac{\phi_i^2}{\omega_i^2 + s^2}$
Total Truncation	$T_d(s, n_c) =$	$\sum_{i=1}^{n_c} \frac{\phi_i^2}{\omega_i^2 + s^2}$		
Expanded Truncation	$T_d(s, n_r) =$	$\sum_{i=1}^{n_c} \frac{\phi_i^2}{\omega_i^2 + s^2}$	$+ \sum_{i=n_c+1}^{n_r} \frac{\phi_i^2}{\omega_i^2 + s^2}$	
Rounded	$T_d^R(s, n_r) =$	$\sum_{i=1}^{n_c} \frac{\phi_i^2}{\omega_i^2 + s^2}$	$+ \sum_{i=n_c+1}^{n_r} \frac{\phi_i^2}{\omega_i^2 + s^2}$	$+ \sum_{i=n_r+1}^{\infty} \frac{\phi_i^2}{\omega_i^2 + s^2}$

In the straight truncation case one has $n_r = n_c$, and a substantial error is committed in representing the zeros of the system, leading to erroneous control design. The expanded truncation uses a larger model, but still significant errors may remain. The "rounded" transfer function approximates the remainder of the infinite series by a constant bias term. (For these terms, s is indeed much less than the ω 's, hence the approximation.)

Because all these approximations depend on the convergence of the series, there are open questions regarding the use of other kinds of mode shape functions which may improve convergence. For instance, mode shape derivatives (used to express rotation and torque properties) converge much more slowly than the usual displacement modes when unrestrained modes are used. However, using mode shapes which better reflect the boundary conditions imposed by a torquer may drastically improve convergence.

Mode Selection Criteria. Mode selection may be formally based on modal cost analysis methods developed by Skelton (Ref. 13). An ad hoc approach involving modal controllability, observability, and disturbability is often more physically motivated and can sometimes be related to modal cost. In addition, reduced models are preferably chosen to represent the low-frequency region because: (1) actuators and sensors have finite bandwidth; (2) the model is known more accurately at low frequencies; and

(3) the resulting control law can be implemented adequately with a lower sampling rate than required if high-frequency modes are retained (digital processor requirements are simplified).

The high-order model is used with advantage to evaluate both spillover and the total performance of the controller, since it is this model which reflects the effects of the unmodeled modes. Finally, on-board implementation considerations may require even further reductions of the controller order with minimum degradation of closed-loop performance.

To summarize, large space structure control design usually requires three models:

1. Evaluation model (large order, e.g., 40 or more modes),
2. Control synthesis model (reduced order, e.g., 10-20 modes); and
3. Reduced-controller model (simplified controller, e.g., less than 10 modes).

Correspondingly, the overall control-design procedure includes three major steps:

1. Model reduction. Development of reduced models for control synthesis, which essentially represent accurately the low-frequency behavior while approximating the impact of high-frequency modes on low-frequency response.
2. Control design. Selection of actuator and sensor types, locations, and the controller structure for control synthesis.
3. Controller simplification. Reduction of the controller obtained in the previous step to simplify implementation, and in some cases, to improve robustness.

Finally, steps 2 and 3 must be validated by checking the controller against the large evaluation model, so that spillover effects and performance of the total system may be assessed. These steps may have to be performed iteratively.

4.3 CONTROL DESIGN METHODOLOGY

Design of feedback control laws for large space structures is dictated by the following considerations:

1. Model. Because of modeling accuracy as well as computational considerations, the controller model is of relatively low order. The neglected modes have low damping and can be unstable if not properly considered in control design.

2. Sensors and actuators. Though structures have significant response up to infinite frequency, physical actuators/sensors have finite bandwidth. In addition, actuators and sensors have dead zones, hysteresis, and nonlinearities; their type and placement may be restricted in actual structures.
3. Model uncertainties. The behavior of structures is known only approximately at high frequency. Therefore, control design cannot depend on the behavior of high frequency modes.

To address these issues and to provide adequate robustness, a two-level control-design approach, discussed in Ref. 11, is now described in more detail.

The two-level approach consists of a wide-band, low-authority control (LAC) and a narrow-band, high-authority control (HAC). HAC provides high damping or mode-shape adjustment in a selected number of modes to meet performance requirements. LAC, on the other hand, introduces low damping in a wide range of modes for maximum robustness. Figure 4-2 shows the control-design procedure with integrated LAC and HAC designs.

LAC is usually implemented with colocated sensors and actuators. However, the theory, based on the work of Aubrun, is applicable to multiple actuators/sensors with cross-feedback and possibly filters (Refs. 12,13).

HAC uses a collection of sensors and actuators that are not necessarily colocated. Selecting the increase in damping ratio is realized by use of a state estimator filter. A unique frequency-shaped extension of the linear-quadratic Gaussian (LQG) method has been developed to provide roll-off over desired frequency regions and for selected disturbance rejection (Ref. 14). HAC may destabilize modes not used in the design. LAC is, therefore, necessary to "clean up" problems created by HAC.

The need to integrate HAC with LAC is shown in Fig. 4-3. HAC is based on models valid over a limited frequency region. It produces large increases in damping ratio and disturbance rejection in the frequency range of interest. The effect of the HAC controller on modes not used in the control design and outside the controller bandwidth may be either stabilizing or destabilizing. LAC is designed to provide protection such that adequate damping is provided in the mode most adversely perturbed by HAC. With reference to Fig. 4-3, the LAC moves the entire uncertainty region above the zero level damping ratio.

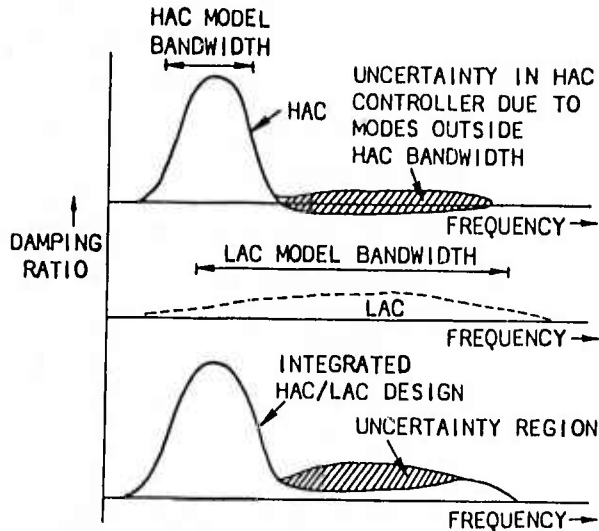


Fig. 4-3 Need to Integrate High-Authority Controller (HAC) and Low-Authority Controller (LAC)

4.3.1 Low-Authority Control (LAC) Design

Low-authority control (LAC) systems (Ref. 13), when applied to structures, are vibration control systems consisting of distributed sensors and actuators with limited damping authority. The control system is allowed to modify only moderately the natural modes and frequencies of the structure. This basic assumption, combined with Jacobi's root perturbation formula, leads to a fundamental LAC formula for predicting algebraically the root shifts produced by introducing an LAC structural control system. Specifically, for an undamped, open-loop structure, the predicted root shift $(d\lambda_n)_p$ is given by

$$(d\lambda_n)_p = \frac{1}{2} \sum_{a,r} C_{ar} \phi_{an} \phi_{rn} \quad (4.19)$$

where the coefficient matrix* $C = [C_{ar}]$ is a matrix of (damping) gains, and ϕ_{an} , ϕ_{rn} denote, respectively, the values of the n th mode shape at actuator station a and sensor station r .

*This LAC gain matrix will subsequently be denoted by C_L in Sections 4.4 and 4.5 to distinguish it from the high-authority control gain matrix C .

Equation (4.19) may also be used to compute the unknown gains C_{ar} if the $d\lambda_n$ are considered to be desired root shifts or, equivalently, desired modal dampings. While an exact "inversion" of Eq. (4.19) does not generally exist, weighted least-squares type solutions can be devised to determine the actuator control gains C_{ar} necessary to produce the required modal damping ratios. This determination of the gains is the synthesis of LAC systems and is achieved by minimizing the special weighted quadratic cost function

$$J(C) = \sum_n W_n [(d\lambda_n)_p - (d\lambda_n)_D]^2 + \sum_{a,r} C_{ar}^2 \quad (4.20)$$

in which the $(d\lambda_n)_p$ denote the predicted root shifts given by formula (4.19), and the $(d\lambda_n)_D$ denote desired root shifts (i.e., given numbers). In the cost function $J(C)$, the modal weights W_n help specify pole locations, and the last term $\sum_{a,r} C_{ar}^2$ improves robustness of the controller.

Since the cost function $J(C)$ is quadratic in $(d\lambda_n)_p$, and hence, in view of Eq. (4.19), also quadratic in the elements of the matrix C , the gains can be obtained algebraically by solving the linear equations

$$\frac{\partial J(C)}{\partial C} = 0 \quad (4.21)$$

for the elements of C . This is an exact algebraic process in which both the modal weights W_n and the desired root shifts (modal dampings) $(d\lambda_n)_D$ play the role of adjustable synthesis parameters, similar to the weights on the control effort and the state error in standard optimal control synthesis procedures.

For structures which already have some damping or control systems in which sensor, actuator, or filter dynamics can either be ignored or are already embedded in the plant dynamics, the root perturbation techniques and cost function minimization methods above can similarly be used to synthesize low-authority controls. In this case, the perturbation method proceeds from the state equations

$$\begin{aligned} \text{Dynamics:} \quad \dot{x} &= Fx + Gu \\ \text{Sensors:} \quad y &= Hx \\ \text{Controls:} \quad u &= Cy, \end{aligned} \quad (4.22)$$

which result in the closed-loop dynamics

$$\dot{x} = (F + GCH)x \quad (4.23)$$

For sufficiently small controls C (Ref. 8), let $GCH \equiv dF$ be considered as a perturbation of F , so that the closed-loop dynamics may now be written as

$$\dot{x} = (F + dF)x \quad (4.24)$$

Let λ_n denote the n th (complex) root of F , and denote by L_n , R_n , respectively, the corresponding left and right eigenvectors of F , i.e.,

$$\begin{aligned} F^T L_n &= \lambda_n L_n \\ F R_n &= \lambda_n R_n \end{aligned} \quad (4.25)$$

normalized so that $L_n^T R_n = 2$ (this normalization makes Eqs. (4.19) and (4.26) below formally compatible).

For small C , let $d\lambda_n$ denote the eigenvalue shift corresponding to dF . Then, as shown in Ref. 13, Jacobi's formula leads to the fundamental root-shift formula:

$$\begin{aligned} d\lambda_n &\approx \frac{1}{2} L_n^T dF R_n = \frac{1}{2} L_n^T G C H R_n \\ &= \frac{1}{2} (\phi_n^A)^T C \phi_n^R, \end{aligned} \quad (4.26)$$

hence,

$$d\lambda_n = \frac{1}{2} \sum_{a,r} C_{ar} \phi_{an}^A \phi_{rn}^R,$$

where

$$\phi_n^A \triangleq G^T L_n \text{ and } \phi_n^R \triangleq H R_n$$

are generalized actuator and sensor modes, respectively. Formula (4.26) is a generalization of formula (4.19) and reduces to Eq. (4.19) when sensors and actuators are complementary (i.e., translation/force, rotation/torque), sensors measure rates, and the structure is undamped.

Robustness of LAC systems. When sensors and actuators are colocated (i.e., $a = r$), are complementary, and only rate feedback is used, formula (4.19) reduces to

$$d\lambda_n = -\xi_n \omega_n = \frac{1}{2} \sum_a C_a \phi_{an}^2, \quad (4.27)$$

which shows that the root shifts are always toward the left of the $j\omega$ -axis if all the gains

are negative. This robustness result is obviously based on the assumption that both sensors and actuators have infinite bandwidth, and also that the structure is initially undamped.*

Several departures from this idealization occur in the actual practical implementation of LAC systems. The most severe of these results from the finiteness of the actuators' bandwidths. More precisely, the second-order roll-off introduced by the actuator dynamics will always destabilize an undamped structure. However, when some natural damping is present in the structure, or when a passive damper is mounted in parallel with the actuator, additional active damping can be obtained without destabilizing the structure. The precise statement of this result is given in the following theorem:

LAC Stability Theorem (Refs. 12,15). Unconditional stability of an LAC system is guaranteed if and only if, for each mode n , the active damping ratio ξ_{cn} is less than a certain maximum ξ_{cn}^* . This maximum damping ratio in any of the modes within the bandwidth of an active LAC controller is proportional to the sum of the natural structural damping ξ_{on} and the damping ξ_{pn} introduced by a passive damper mounted in parallel with the actuator. Specifically,

$$\xi_{cn}^* = R_{\max}(\xi_{on} + \xi_{pn}), \quad (4.28)$$

where the value of the proportionality constant R_{\max} is given by:

$$R_{\max} \equiv \min(K + 2\sqrt{K}, \tau_1 \tau_2 / \tau_0^2), \quad (4.29)$$

where

$$K = \tau_1 / \tau_2 + \tau_2 / \tau_1 + 2, \quad (4.30)$$

and where $1/\tau_1$, $1/\tau_2$ are the poles of the active damper, and $1/\tau_0$ is the pole of the passive damper.

The proof of this theorem is given in Ref. 12.

* Robustness is that quality of a controller of remaining stable in the presence of parameter variations in the structure and/or control system parameters. For example, the above stability condition (negativity of all the root shifts) is independent of mode shapes and frequencies and depends only on the negativity of the gains C_a . Any parameter variation in the controller which modifies the values (but not the signs) of the gains will not affect the stability condition.

4.3.2 High-Authority Control (HAC) Design

The HAC control design procedure is based on linear-quadratic-Gaussian (LQG) methods. Increased penalties in the LQG cost functional are placed at those frequencies where less response is desired. The concept of frequency-shaped cost functionals has been introduced previously (Ref. 14). This section demonstrates the application of these methods to the large space structures problem.

The frequency-shaping methods are useful in several areas of large space structures control. Three principal applications are important: (1) spillover avoidance, (2) state estimation, and (3) disturbance rejection.

Management of spillover. Spillover in closed-loop control of space structures is managed by injecting minimum control power at the natural frequencies of the unmodeled modes. Procedures for controlling spillover at high frequencies will be discussed, although similar techniques are applicable for other regimes.

High-frequency spillover may be controlled by modifying the state or the control weighting. The state weighting $A(j\omega)$ will reduce spillover if it is made a decreasing function of frequency. Three of the possible forms for $A(j\omega)$ are shown in the following:

$$1. \quad A(j\omega) = \frac{1}{\omega^2} A, \quad (4.31)$$

$$2. \quad A(j\omega) = \frac{\omega_0^4}{(\omega_0^2 + \omega^2)^2} A, \quad (4.32)$$

$$3. \quad A(j\omega) = \frac{(\omega_1^2 + \omega^2)^2}{(\omega_0^2 + \omega^2)^2} A, \quad \omega_1 > \omega_0. \quad (4.33)$$

To include the frequency shaping of Eq. (4.31), define additional states \bar{x} as

$$\dot{\bar{x}} = \bar{x}. \quad (4.34)$$

The performance index is then

$$\lim_{T \rightarrow \infty} \frac{1}{T} \int_0^T (\bar{x}^T A \bar{x} + u^T B u) dt, \quad (4.35)$$

and the control law will be of the form

$$u = C_1 x + C_2 \bar{x}. \quad (4.36)$$

The control gain C_2 will ensure that the high-frequency response is minimized. This formulation resembles integral control, but the weighting matrices used in the design are different.

Spillover may also be reduced by placing high control weighting at high frequency. Examples of $B(j\omega)$ which reduce high-frequency spillover are as follows:

$$1. \quad B(j\omega) = \frac{(\omega^2 + \omega_0^2)}{\omega_0^2} B, \quad (4.37)$$

$$2. \quad B(j\omega) = \frac{\omega_1^2 + \omega^2}{\omega_0^2 + \omega^2} B, \quad \omega_1 < \omega_0, \quad (4.38)$$

$$3. \quad B(j\omega) = \frac{\omega^4}{[(\omega^2 + \omega_0^2)^2 + 2\omega_0^2 \omega^2]} B. \quad (4.39)$$

The frequency-shaped parts of these weightings are reciprocals of those used in the state weightings. To implement the weighting function of Eq. (4.37), define a vector u by

$$\dot{u} + \omega_0 u = \omega_0 \bar{u}. \quad (4.40)$$

The performance index then takes the form

$$J = \lim_{T \rightarrow \infty} \frac{1}{T} \int_0^T (x^T A x + \bar{u}^T B \bar{u}) dt, \quad (4.41)$$

and the feedback control law will be

$$\begin{aligned} \dot{u} + \omega_0 u &= \omega_0 \bar{u} = \omega_0 (C_1 x + C_2 u), \\ \text{or} \quad \dot{u} + \omega_0 (1 - C_2) u &= \omega_0 C_1 x. \end{aligned} \quad (4.42)$$

This control law is shown schematically in Fig. 4-4.

4. TECHNOLOGY PRIMER

4.3.2 HIGH-AUTHORITY CONTROL (HAC) DESIGN

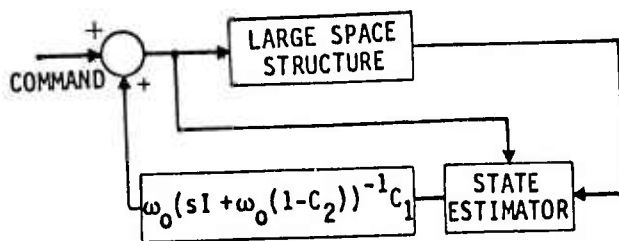


Fig. 4-4 A Frequency-Shaped Controller to Reduce High-Frequency Spillover

During maneuvers and in other missions, there is often a need to avoid exciting a particular mode at ω_0 . Minimization of spillover at one frequency ω_0 is achieved by:

$$A(j\omega) = (\omega^2 - \omega_0^2), \quad (4.43)$$

or by

$$B(j\omega) = \frac{B}{(\omega^2 - \omega_0^2)^2}. \quad (4.44)$$

Spillover reduction in state estimation. The discussion will again address the estimation of low-frequency states when the high-frequency modes are not modeled. Extension to other cases is straightforward.

In the linear systems of Eqs. (4.6), a linear transformation can be used to place all errors caused by unmodeled modes into the measurement equations. Note that when high-frequency modes are not modeled in the state equations, measurement errors in the modified system are also at high frequency. Therefore, errors introduced by lumped-mass modeling at high frequency represents a high-frequency noise measurement with many peaks.

To design a filter with desirable high-frequency behavior, consider the optimal state estimate as the output of an optimization problem with the following performance index:

$$\bar{J} = \lim_{T \rightarrow \infty} \int_0^T (w^T Q w + v^T R v) dt. \quad (4.45)$$

Again, conversion to the frequency domain gives the following performance index:

$$\bar{J} = \int_{-\infty}^{\infty} (w^* Q(j\omega) w + v^* R(j\omega) v) d\omega. \quad (4.46)$$

The problem of model invalidity at high frequency is solved by making Q and R functions of frequency. Since all errors associated with modal truncation are incorporated in the measurements, frequency shaping is used only in R . High-frequency measurement spillover is controlled by increasing $R(j\omega)$ at high frequency. For example, choose $R(j\omega)$ as:

$$R(j\omega) = \frac{(\omega^2 + \omega_0^2)}{\omega_0^2} R. \quad (4.47)$$

Defining a new measurement \bar{y} as

$$\dot{\bar{y}} + \omega_0 \bar{y} = \omega_0 y, \quad (4.48)$$

then

$$\bar{y} = H\bar{x} + v, \quad (4.49)$$

where

$$\dot{\bar{x}} + \omega_0 \bar{x} = \omega_0 x, \quad (4.50)$$

and the state estimator is then of the form:

$$\begin{aligned} \dot{\hat{x}} &= F\hat{x} + Gu + K(y - H\hat{x}), \\ \dot{\bar{x}} &= -\omega_0 \bar{x} + \omega_0 \hat{x} + \omega_0 K(\bar{y} - H\bar{x}), \\ \dot{\bar{y}} &= -\omega_0 \bar{y} + \omega_0 y. \end{aligned} \quad (4.51)$$

This filter is shown schematically in Fig. 4-5. Note that a standard filter is obtained by setting K to zero and $\omega_0/(s + \omega_0)$ to one. In this formulation, filtered measurements are compared with filtered states. The eigenvalues of the closed-loop system are, in general, in the low-frequency region. Low-frequency, closed-loop eigenvalues reduce excitation of high-frequency modes through feedback in the state estimator. The filter shapes may be modified to provide any desired roll-off. The filter, of course, becomes more complex as faster roll-off is obtained. (Note also that the transfer function between the estimated state and the measurements has at least two more poles than zeros.)

4. TECHNOLOGY PRIMER

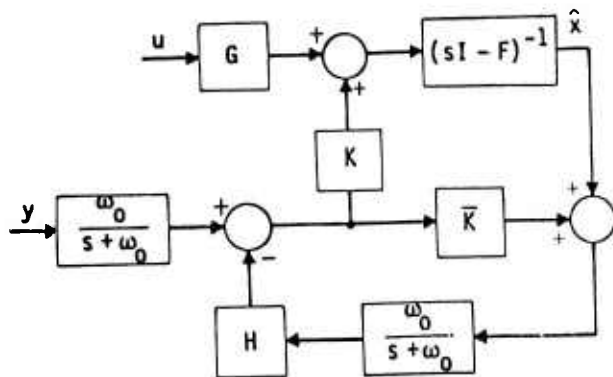


Fig. 4-5 A Frequency-Shaped Filter to Reduce High-Frequency Spillover

Although this filter has been developed for application to large space structures, it is believed to have a wide applicability in the design of practical state estimators.

Disturbance rejection in large space structures. Large space structures are often subject to high disturbance levels caused by rotating machines, combustion devices, rotating antennae, and other onboard equipment. In addition, gravity gradients and solar pressure are external disturbance sources. These sources are usually nonwhite. Frequency-shaping methods may be applied to minimize the effect of these disturbances on the structure. Procedures for realizing disturbance rejection are shown in the following.

Consider a cryogenic cooler or control-moment gyro. The primary disturbance produced by these devices is at one frequency (typically the rotational frequency) and possibly its harmonics. Let the disturbance frequency be $\bar{\omega}$. To minimize the effect of this disturbance on output y , the following term J_1 is included in the performance index:

$$J_1 = \frac{1}{(\omega^2 - \bar{\omega}^2)^2} y^T A_y y. \quad (4.52)$$

Note that the output penalty goes to infinity at the disturbance frequency. Thus, the impact of disturbance on the output is minimized.

The implementation of this frequency-shaped weighting requires definition of additional states as follows:

$$\dot{\bar{x}} = \begin{bmatrix} 0 & I \\ -\omega^2 I & 0 \end{bmatrix} \bar{x} + \begin{bmatrix} 0 \\ I \end{bmatrix} y. \quad (4.53)$$

4.3.2 HIGH-AUTHORITY CONTROL (HAC) DESIGN

The performance index will then take the form

$$J = \lim_{T \rightarrow \infty} \int_0^T (\bar{x}^T A_y \bar{x} + x^T A x + u^T B u) dt, \quad (4.54)$$

and the corresponding control law becomes

$$u = C_1 x + C_2 \bar{x}.$$

The flow chart for this control law is shown in Fig. 4-6.

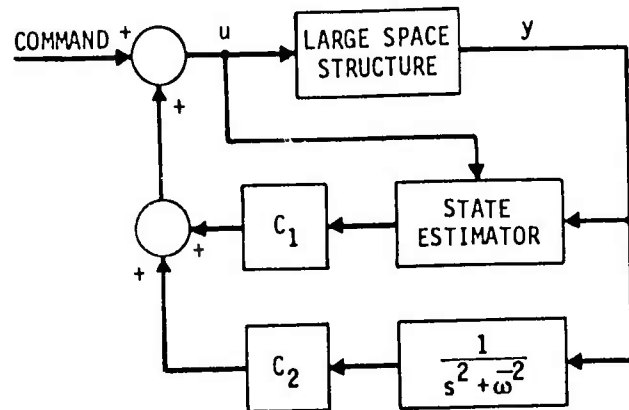


Fig. 4-6 A Frequency-Shaped Controller to Eliminate the Effect of Disturbance at $\bar{\omega}$ on Output y

The control formulation given above may be extended to include disturbance at other frequencies or over a frequency band. In each case, as shown in Fig. 4-6, there is memory in the control portion of the feedback.

Summary. The application of frequency-shaping methods to large space structures leads to a linear controller with memory. However, the additional states needed to represent frequency-dependent weights increase the controller order. The software needed for these controller designs is similar to that for standard LQG problems.

4.3.3 Controller Simplification

The frequency-shaped controllers developed in the previous section are of the form

$$\dot{x}_C = F_C x_C + K y, \quad (4.55)$$

$$u_C = C x_C + D_C y. \quad (4.56)$$

The controller, therefore, has the same form as the system itself, except that: (1) the roles of input and output are switched; (2) the controller state vector depends on the choice of frequency shaping; and (3) the matrices K and C are known exactly (unlike G and H in the design model). Controller simplification is, therefore, similar to model reduction.

All unobservable or uncontrollable modes of the controller should be dropped, since they have no effect on controller performance. In addition, poles with small residues can also be dropped. Note that the residues are physical matrices representing force or moment applied per unit error (Ref. 10).

Further selection of modes or states which should be retained in the low-order controller is a difficult problem. One approach is to drop one or two states at a time to determine the set of states which may be eliminated without loss of performance. To minimize computation time, a stepwise search procedure is needed. A modal cost function could be used in the search (Ref. 9).

4.3.4 Actuators and Sensors

In the initial phases of the control design, actuators and sensors are treated as idealized devices with sufficiently broad bandwidths so that their dynamics can be ignored. The actuators are assumed to produce local forces or torques, whereas sensors are assumed to measure displacements (translations or rotations) and/or their rates. In complex problems, a group of actuators can be driven by a single control input, and similarly a group of sensors can be combined to provide a single measurement output (e.g., the LOS in the CSDL No. 2 example discussed in Section 4.5.2). The problem of type selection is very case-dependent and no universal rules can be given.

The next step in the design procedure is the determination of actuator/sensor locations (and hence quantity) best suited for the particular

control problem being addressed. For structures, this requires an operational dynamical model with well-defined disturbances and measures of performance. In particular, this requires that the physical locations (nodes, lumped elements, etc.) for possible actuator/sensor placement be represented in the model through influence coefficients of some sort. Given this, the problem of determining an effective set of locations remains a difficult problem and entails the use of several criteria which are generally used concurrently.

The most important criterion comes from common sense and examining the physics of the problem. For example, if the performance is determined by the motions of a certain set of structural nodes (e.g., the LOS), these nodes are an obvious choice for actuation in directions associated with the degrees of freedom involved. This procedure is applicable whenever the performance can be expressed in terms of physical coordinates. However, such a set of actuators may be redundant if there are fewer independent variables to be controlled. For example, in CSDL No. 2 (see Section 4.5.2) there are 21 nodal degrees of freedom which determine the three components of the LOS. It can therefore be expected that a minimum of three actuators could control the LOS; for instance the two tilts and translation of the tertiary mirror could provide all the required optical compensation, but at the cost of large control efforts which may be incompatible with actuator capabilities, higher-order optical aberrations, structural strength and redundancy/reliability requirements.

It is precisely because of such interdependent constraints that automated placement procedures are only a design aid and not a solution to the problem. Many such procedures have been proposed and tried, and are usually based on controllability, minimum energy, modal cost considerations (Refs. 1, 9, 16), etc. Most of these procedures, however, are based on modal decomposition whereby the physics of the original problem have been hopelessly scrambled. Finally, the actuator/sensor placement procedure will generally differ for HAC and LAC, since only the latter (usually) requires colocation.

The HAC sensor placement problem is even more complex than its actuator counterpart. This is due to the existence of trade-offs between sensors and state estimators. It is conceivable, for instance, that a single sensor, given sufficient time and low noise level, could be used to estimate all the observable degrees of freedom. It is for this reason that sensor noise,

4. TECHNOLOGY PRIMER

process noise, disturbance spectra, model uncertainty, etc., will all influence the sensor selection and placement choices.

Once a control design has progressed past the initial phases, questions of actuator and sensor dynamics can be looked at within the severe computational constraints of large system performance evaluation. These questions will be addressed more specifically in subsequent study phases.

4.3.5 Stability and Performance Evaluation

The final evaluation of the control system is carried out using the high-order model

$$\dot{X} = FX + Gu + Iw \quad (4.57)$$

to which is added the equation defining the control law $u(t)$. In general, this will result in combined equations of the form

$$\begin{aligned} \dot{X}_s &= F_s X_s + \Gamma_s w \\ y &= H_s X_s \end{aligned} \quad (4.58)$$

where the subscript s denotes the closed-loop system, w the disturbances, and y the vector defining the performance. Stability is evaluated by computing the eigenvalues of F_s . The performance can be evaluated in several ways, depending on the nature of the disturbance. For a transient or initial condition disturbance, time-domain simulation is carried out to obtain $y(t)$, and this can be obtained by closed-form solutions. For a sinusoidal disturbance at frequency ω , the response of y at that frequency is given by the formula

$$y(\omega) = -H_s (F_s - i\omega I)^{-1} \Gamma_s w \quad (4.59)$$

which is obtained from the Fourier transform of the closed-loop system equations. This requires inversion of a generally large complex matrix. For random disturbances specified by their PSD's, analytical expressions for the transfer functions are obtained in the form

$$y_k/w_j = T_{kj}(\omega) = \sum_n A_{k j n} / (s_n + i\omega) \quad (4.60)$$

4.4 APPLICATION OF ACOSS DESIGN METHODOLOGY TO A SIMPLE EXAMPLE

where the poles s_n and the residues $A_{k j n}$ are obtained numerically from the eigensystem decomposition of F_s and the components of H_s and Γ_s .

4.3.6 Strengths and Weaknesses

The control design methodology described in the preceding sections has been applied to two examples - a simple one and a complex one - discussed in detail in the next two sections. In both cases, the application of the new methodology produced excellent results in the sense that the specific problem addressed, viz., a specific control objective for a specific structure (including specific perturbed models thereof) together with a specific set of disturbances, was very successfully solved in each case. For the complex optical structure in particular, the LOS error of the open-loop model was reduced by a factor of 1.3×10^5 by the active control system designed using the new methodology. Furthermore, the controller remained stable and gave comparably good performance on two perturbed models of the spacecraft, establishing robustness with respect to two "point-design" perturbations.

Based on the above results, and in the context of the analysis defined by the scope of the Phase 1A ACOSS contract, no weaknesses in the methodology have been found. It is true, however, that the results obtained at the end of that phase have given rise to a number of open questions, all resulting from "what if" assumptions which strongly relax the specific conditions under which the LSS control problem was initially posed. Included in this category are fundamental questions of robustness-with-performance properties relative to unspecified model perturbations; questions relating to the validity of finite-element models; and questions relating to the effects of unknown disturbances and their possible effects on system performance. While some of these questions are not new, they take on added significance in the context of the LSS control problem and need to be defined more specifically before they can be addressed. This will be undertaken in the next phase of the study.

4.4 APPLICATION OF ACOSS DESIGN METHODOLOGY TO A SIMPLE EXAMPLE

A simple two-mode example is considered to illustrate the high-authority control (HAC) and low-authority control (LAC) design procedures. Spillover problems caused by HAC are demonstrated, as well as the fact that LAC can provide sufficient damping to overcome the effect

4. TECHNOLOGY PRIMER

of the spillover. The frequency-shaped control design demonstrates that the spillover problem can be reduced, thus making it easier for the LAC system to overcome the effects of spillover.

4.4.1 The Two-Mode Example

Consider a hypothetical structure having only two modes (q_i , $i = 1, 2$) with frequencies at 1 rad/s and 5 rad/s, and natural damping of 0.5 percent. Defining the state vector as

$$\dot{X} \equiv [\dot{q}_1 \dot{q}_2 q_1 q_2]^T, \quad (4.61)$$

one can write the dynamical equations as

$$\begin{aligned} \dot{X} &= FX + Gu, \\ y &= HX, \end{aligned} \quad (4.62)$$

where

$$F = \begin{bmatrix} -0.01 & 0 & -1 & 0 \\ 0 & -0.05 & 0 & -25 \\ 1 & 0 & 0 & 0 \\ 0 & 1 & 0 & 0 \end{bmatrix},$$

and

$$\begin{aligned} G &= [1 \ 1 \ 0 \ 0]^T, \\ H &= [1 \ -1 \ 0 \ 0]. \end{aligned}$$

For simplicity, the normalized mode shapes have magnitude 1 at actuator and sensor locations. However, the actuator and the sensor are not colocated, hence the appearance of -1 in the H matrix. This example could represent, for instance, a free-free beam with an actuator at one end and a sensor at the other.

The open-loop eigenvalues are approximately $-0.005 \pm i$ and $-0.025 \pm 5i$. In this simple example the first mode will be controlled, and the spillover into the second mode will be examined. The reduced model for control synthesis is defined by the reduced matrices:

$$\begin{aligned} F_1 &= \begin{bmatrix} -0.01 & -1 \\ 1 & 0 \end{bmatrix}, \quad G_1 = \begin{bmatrix} 1 \\ 0 \end{bmatrix}, \\ \text{and } H_1 &= [1 \ 0]. \end{aligned} \quad (4.63)$$

4.4.2 HAC CONTROLLER EVALUATION ON FULL-ORDER MODEL

The optimal control law for HAC is of the form

$$u = C\hat{X}_1, \quad (4.64)$$

where \hat{X}_1 is the estimate of the reduced state vector $X_1 \equiv (\dot{q}_1 \ q_1)^T$, and the gain matrix C minimizes the weighted quadratic cost functional

$$J = \int_0^\infty (X^T A X + B u^2) dt. \quad (4.65)$$

For the purpose of transient vibration suppression, only the velocity state will be controlled, so that the state penalty weighting matrix is given by

$$A = \begin{bmatrix} 1 & 0 \\ 0 & 0 \end{bmatrix}. \quad (4.66)$$

The control penalty is arbitrarily chosen as $B = 1$. The optimal control gain matrix is found by solving the algebraic Riccati equation using established numerical techniques which yield

$$C = [-1 \ 0]. \quad (4.67)$$

The optimal filter, defined by

$$\dot{\hat{X}}_1 = F_1 \hat{X}_1 + G_1 u + K(y - H_1 \hat{X}_1), \quad (4.68)$$

is designed by similar techniques, and the corresponding gain matrix is

$$K = [1 \ 0]^T. \quad (4.69)$$

The closed-loop eigenvalues of the filter and the controller are at $-0.5 \pm 0.866i$ ($\xi = 50$ percent).

4.4.2 HAC Controller Evaluation on Full-Order Model

The closed-loop dynamics matrix corresponding to the full-order system controlled by the reduced-order HAC controller is given by

$$F_s \equiv \left[\begin{array}{c|c} F & GC \\ \hline KH & F_1 + G_1 C - KH_1 \end{array} \right], \quad (4.70)$$

4. TECHNOLOGY PRIMER

4.4.4 FREQUENCY-SHAPED CONTROL LAWS FOR ROLL-OFF

and is computed to be

$$F_s = \left[\begin{array}{cccc|cccc} -0.01 & 0 & -1 & 0 & -1 & 0 & 0 & 0 \\ 0 & -0.05 & 0 & -25 & -1 & 0 & 0 & 0 \\ 1 & 0 & 0 & 0 & 0 & 0 & 0 & 0 \\ -\frac{1}{0} & -\frac{1}{0} & -\frac{1}{0} & -\frac{1}{0} & -2.01 & -1 & 1 & 0 \end{array} \right] \quad (4.71)$$

The eigenvalues of F_s (poles of the closed-loop system) are

$$\begin{aligned} &0.0164 \pm 4.9084 i \text{ (Spillover roots: unstable)} \\ &-0.4049 \pm 0.8627 i \text{ (Filter roots)} \\ &-0.6466 \pm 0.8512 i \text{ (Controlled roots)} \end{aligned}$$

Clearly, the spillover causes the unmodeled mode to go unstable. A measure of spillover is the distance in the complex plane between the open- and closed-loop poles, i.e., in this case

$$\begin{aligned} d_s &= \sqrt{(-0.025 - 0.0164)^2 + (5 - 4.908)^2} \\ &= 0.10 \text{ rad/s} \end{aligned}$$

This value will be discussed subsequently.

4.4.3 LAC Design and HAC/LAC Controller Evaluation

For the LAC system, a different sensor is used and is colocated with the actuator. The LAC control law is of the form

$$u = C_L y_L, \quad (4.72)$$

where $y_L = G^T x$ represents the measurement of the local displacement rate at the actuator. The LAC system is designed to provide sufficient damping to remove the spillover in the unmodeled mode. The spillover distance $d_s = 0.10$ rad/s, computed at the end of the previous subsection, can be regarded as the radius of an uncertainty circle in the complex plane within which the unmodeled mode root could move under the spillover. Hence, to ensure that the root remains in the left half-plane, the LAC real-part root shift is chosen to be

$$0.10 = \xi \omega = -\frac{1}{2} C_L \phi^2$$

according to the standard LAC formula; in this case $|\phi| = 1$, hence $C_L = -0.20 \text{ N/ms}^{-1}$.

The closed-loop eigenvalues of the LAC system (eigenvalues of $F + G C_L G^T$) are:

$$\begin{aligned} &-0.1052 \pm 0.9953 i \\ &-0.1025 \pm 4.9943 i \end{aligned}$$

For the combined HAC/LAC system, the control law is now

$$u = \hat{C} \hat{x} + C_L G^T x \quad (4.73)$$

and the corresponding closed-loop matrix F_s takes the form:

$$F_s = \left[\begin{array}{ccc|ccc} F + G C_L G^T & & & & & \\ & & & & & \\ & & & & & \\ \hline & & & G C & & \\ & & & & F_1 + G_1 C - K H_1 & \end{array} \right] \quad (4.74)$$

with entries given by:

$$F_s = \left[\begin{array}{cccc|cccc} -0.21 & -0.2 & -1 & 0 & -1 & 0 & 0 & 0 \\ -0.2 & -0.25 & 0 & -25 & -1 & 0 & 0 & 0 \\ 1 & 0 & 0 & 0 & 0 & 0 & 0 & 0 \\ 0 & 1 & 0 & 0 & 0 & 0 & 0 & 0 \\ 0.8 & -1.2 & 0 & 0 & -2.01 & -1 & 0 & 0 \\ 0 & 0 & 0 & 0 & 1 & 0 & 0 & 0 \end{array} \right] \quad (4.75)$$

The eigenvalues of F_s are:

$$\begin{aligned} &-0.0732 \pm 4.8848 i \text{ } (\xi = 1.5\%; \text{ stabilized spillover roots}) \\ &-0.4406 \pm 0.8506 i \text{ } (\xi = 46\%; \text{ filter roots}) \\ &-0.7212 \pm 0.7882 i \text{ } (\xi = 67.5\%; \text{ controlled roots}) \end{aligned}$$

and it is evident that the spillover produced by HAC has been cured by LAC, as expected.

4.4.4 Frequency-Shaped Control Laws for Roll-Off

In order to reduce the HAC spillover, the frequency shaping method is applied to bring about a steeper roll-off of the controls and hence reduce the excitation of the unmodeled mode. This can be achieved by making the control penalty B an increasing function of frequency:

$$B(\omega) = 1 + \omega^4.$$

The state penalty A remains the same as before, i.e.,

$$A = \begin{bmatrix} 1 & 0 \\ 0 & 0 \end{bmatrix}.$$

4. TECHNOLOGY PRIMER

To implement this particular frequency shaping, the reduced-order state vector x_1 is augmented to be

$$x_f = [\dot{q}_1 \ q_1 \ \dot{u} \ u]^T \quad (4.76)$$

and the new control input is u_f . The dynamic equations are modified to be

$$\begin{aligned} \ddot{q}_1 + 0.01 \dot{q}_1 + q_1 &= u \quad (\text{First Mode Dynamics}) \\ \ddot{u} &= u_f \quad (\text{Frequency-Shaped Control}) \end{aligned} \quad (4.77)$$

The control synthesis model, in state-space form, is then

$$\left. \begin{aligned} \dot{x}_f &= F_f x_f + G_f u_f \\ y &= H_f x_f \\ u_f &= C_f x_f \end{aligned} \right\} \quad (4.78)$$

where

$$\begin{aligned} F_f &= \begin{bmatrix} -0.01 & -1 & 0 & 1 \\ 1 & 0 & 0 & 0 \\ 0 & 0 & 0 & 0 \\ 0 & 0 & 1 & 0 \end{bmatrix} \\ G_f &= [0 \ 0 \ 1 \ 0]^T \\ H_f &= [1 \ 0 \ 0 \ 0] \end{aligned}$$

The gain matrix C_f is obtained by standard optimal synthesis as before, and is

$$C_f = [-0.22 \ 0.96 \ -2 \ -1.96]$$

The closed-loop poles (eigenvalues of $F_f + G_f C_f$) are

$$\begin{aligned} -0.3468 \pm 1.0835 i & \text{ (Frequency Shaping Roots)} \\ -0.6582 \pm 0.5827 i & \text{ (System Roots: } \zeta = 50\%) \end{aligned}$$

4.4.5 Evaluation of Frequency-Shaped Roll-Off Control on Full-Order Model

The complete set of equations in this case is given by

$$\begin{aligned} \dot{x} &= FX + Gu \\ \dot{x}_f &= F_f \hat{x}_f + G_f u_f + K_f (y - H_f \hat{x}_f) \\ y &= HX \\ u_f &= C_f x_f \end{aligned} \quad (4.79)$$

4.4.5 Evaluation of Frequency-Shaped Roll-Off Control on Full-Order Model

The first equation may also be written as

$$\dot{x} = FX + GC^* x_f$$

where

$$C^* \triangleq [0 \ 0 \ 0 \ 1]$$

The filter gain matrix K_f is

$$K_f = [1 \ 0 \ 0 \ 0]^T \quad (4.80)$$

and the closed-loop dynamics matrix F_s is now given by

$$F_s = \left[\begin{array}{c|c} F & GC^* \\ \hline K_f H & F_f + G_f C_f - K_f H_f \end{array} \right], \quad (4.81)$$

whose numerical entries are

$$F_s = \begin{bmatrix} -0.01 & 0 & -1 & 0 & 0 & 0 & 0 & 0 & 1 \\ 0 & -0.05 & 0 & -25 & 0 & 0 & 0 & 0 & 1 \\ 1 & 0 & 0 & 0 & 0 & 0 & 0 & 0 & 0 \\ 0 & 1 & 0 & 0 & 0 & 0 & 0 & 0 & 0 \\ -0.22 & 0.96 & -2 & -1.96 & 0 & 0 & 0 & 0 & 0 \\ 0 & 0 & 0 & 0 & -0.01 & -1 & 0 & 0 & 1 \\ 0 & 0 & 0 & 0 & 0 & 0 & 1 & 0 & 0 \\ 0 & 0 & 0 & 0 & 0 & 0 & 0 & -0.22 & 0.96 \\ 0 & 0 & 0 & 0 & 0 & 0 & 0 & 0 & -2 \end{bmatrix}$$

and whose eigenvalues are computed to be:

$$\begin{aligned} -0.0262 \pm 5.0002 i & \text{ (Stabilized Spillover Roots: } \zeta = 0.52\%) \\ -0.3839 \pm 1.0957 i & \text{ (Frequency Shaping Roots: } \zeta = 33\%) \\ -0.4232 \pm 0.8952 i & \text{ (Filter Roots: } \zeta = 43\%) \\ -0.7018 \pm 0.5139 i & \text{ (Controlled Mode Roots: } \zeta = 81\%) \end{aligned}$$

The closed-loop system is now stable, since the small amount of spillover into the unmodeled mode is not enough to destabilize it. The spillover distance d_s in this case is 0.0012. The frequency-shaped roll-off has thus reduced the HAC spillover to about one percent of its original value, and an LAC compensation is therefore not needed in this case. In general, however, there is no guarantee that the frequency-shaped reduction of spillover will maintain stability. LAC will then be used to compensate for the remaining destabilizing effects.

4. TECHNOLOGY PRIMER

4.4.6 Frequency Shaping for Rejection of Single Frequency Disturbance

In this case, the state weighting matrix A must place large penalties at the disturbance frequency. For example, if the disturbance frequency is 0.5 rad/s, and the cost is defined in this case as

$$J = \int_{-\infty}^{\infty} (A_y(\omega) y^2 + B u^2) d\omega, \quad (4.82)$$

then

$$A_y(\omega) = \frac{1}{(\omega^2 - 0.25)^2}.$$

The implementation of this weighting requires the additional equation:

$$\frac{d}{dt} \begin{bmatrix} \dot{\xi} \\ \xi \end{bmatrix} = \begin{bmatrix} 0 & -0.25 \\ 1 & 0 \end{bmatrix} \begin{bmatrix} \dot{\xi} \\ \xi \end{bmatrix} + \begin{bmatrix} 1 \\ 0 \end{bmatrix} y \quad (4.83)$$

The control synthesis model is now of order 6, with the state vector being

$$x_f = [\dot{q}_1 \ q_1 \ \dot{u} \ u \ \dot{\xi} \ \xi]^T.$$

The corresponding evaluation model will then be of order 10: four states for the original system dynamics, and six states for the controller. This illustrates the pitfalls of "simple examples" and emphasizes the fact that these advanced control techniques are primarily relevant for large dynamical systems.

4.5 APPLICATION OF ACOSS DESIGN METHODOLOGY TO A COMPLEX OPTICAL STRUCTURE

The illustration and demonstration of control-design methods for large space structures has been, and remains, a difficult problem. The very nature of large space structures precludes the construction of simple textbook examples to illustrate theory. Control theorists have unfortunately often confused this issue by postulating dynamical plants which are no more than sets of matrices to be immediately processed through a maze of procedures and algorithms developed in theoretical approaches.

Under the Defense Advanced Research Projects Agency (DARPA)-sponsored program on Active Control of Space Structures (ACOSS), an important step toward the resolution of this problem was taken by the Charles Stark Draper Laboratory

4.5.1 THE CSDL NO. 2 STRUCTURAL MODEL AND DISTURBANCES

(CSDL). Early in 1980, DARPA commissioned CSDL to develop a (paper) design of a "generic" optical space structure which embodied the essential characteristics needed to illustrate and demonstrate large space structure control-design methodology, implementation, and performance evaluation. The resulting nontrivial spacecraft model, known today as "CSDL Model No. 2," has been fully documented in Ref. 17. It is available to the dynamics and controls community via a NASTRAN computer tape which contains the entire structural model. References to "CSDL No. 2" are becoming increasingly more frequent, particularly in view of the fact that this model was also recently chosen by Wright-Patterson Air Force Base as the "test bed" for a program they will sponsor and initiate later this year on the Vibration Control Of Space Structures (VCOSS).

4.5.1 The CSDL No. 2 Structural Model and Disturbances

The CSDL No. 2 model (Ref. 17), shown conceptually in Fig. 4-7, represents a wide-angle, three-mirror optical space system, together with a line-of-sight model giving the law of displacement of the image in the focal plane when the structure deforms (see Section 4.5.2). The assumption is made that the mirror surfaces are simply displaced and maintain their nominal (rigid) shapes. The mirror shapes are off-axis sections of rotationally symmetric coaxial surfaces. Since the intent is to derive a first-order optical model (by neglecting the influence of light redistribution in the image), the asphericity of each mirror is disregarded.

The total structure is approximately 28 m high, has a mass of about 9,300 kg, and embodies a structural design based on realistic sizes and weights; the corresponding mass distribution is indicated in Fig. 4-7. Principal lumped masses are graphically displayed in Fig. 4-8. As "seen" by the NASTRAN program input, the structure contains many more structural members than in the artist's conception of Fig. 4-7. The computergraphic display shown in Fig. 4-9 represents the actual structural model which was input to the NASTRAN program, together with its number of nodes, degrees of freedom, nonzero mass elements, and stiffness elements. The structure is configured as a frame, i.e., it is assumed that all joints allow a full moment connection. Thus, bending, axial, and torsional stiffness is included in the model for all structural members.

4. TECHNOLOGY PRIMER

4.5.1 THE CSDL NO. 2 STRUCTURAL MODEL AND DISTURBANCES

HEIGHT ≈ 28 m

TOTAL WEIGHT ≈ 9300 kg

- 51 NODES
- 306 DEGREES-OF-FREEDOM
- 84 NONZERO MASS ELEMENTS
- 137 STIFFNESS ELEMENTS

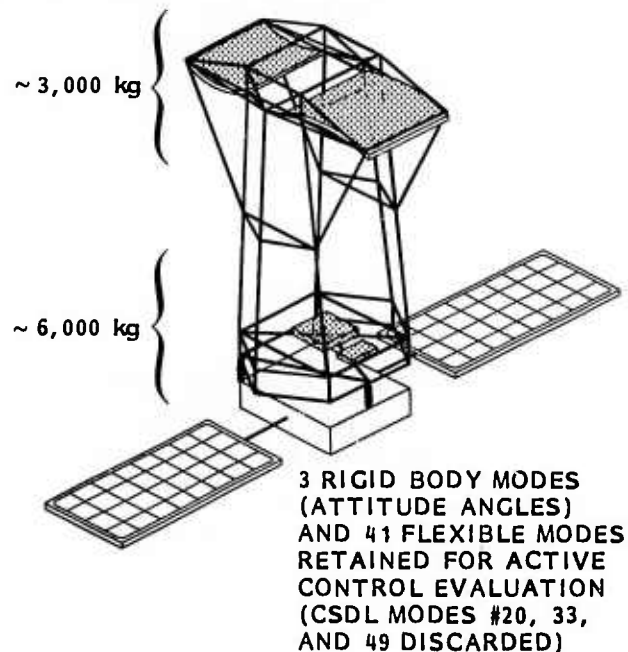


Fig. 4-7 CSDL No. 2 Model (Artist's Conception)

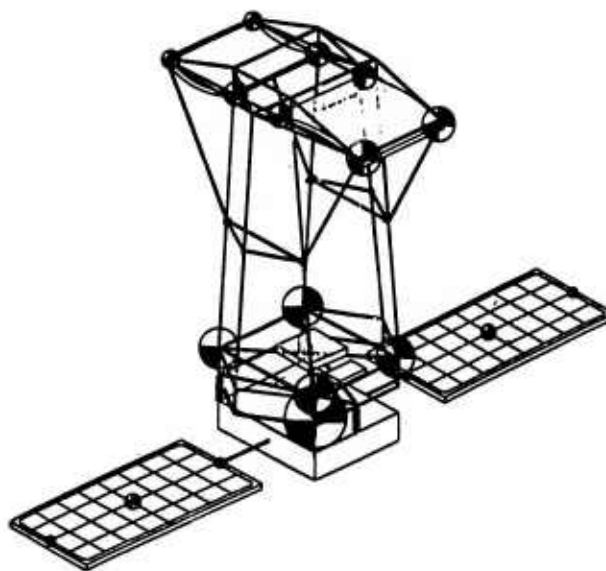


Fig. 4-8 Principal Lumped Masses in CSDL No. 2
(Masses in Relative Proportional Size)

ACROSS DRAPER MODEL

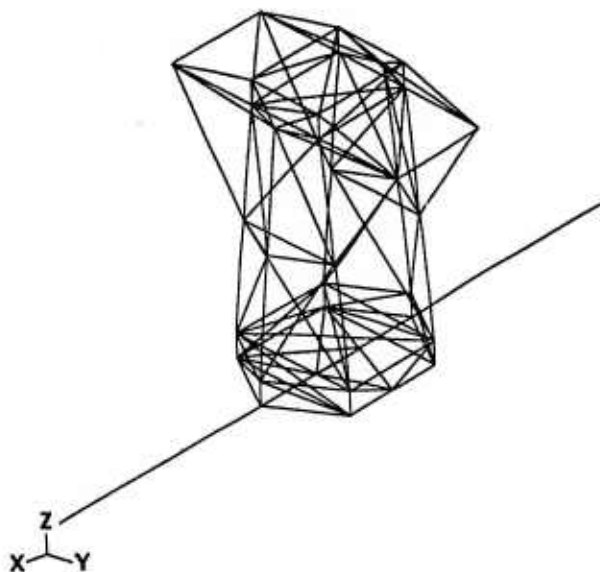


Fig. 4-9 Computer-Graphic Display of CSDL
No. 2 (All Beam Elements Shown)

4. TECHNOLOGY PRIMER

4.5.1 THE CSDL NO. 2 STRUCTURAL MODEL AND DISTURBANCES

To complete the structural scenario, two perturbation models were also included in the CSDL No. 2 design. Combined lumped-mass perturbations and beam stiffness perturbations are obtained by changing the thickness of the 25-cm diameter graphite epoxy hollow tubes used in the metering truss. The locations of these perturbations are shown in Fig. 4-10, and their specific descriptions are given in Tables 4-2 and 4-3, where P_0 denotes the nominal model and P_2 and P_4 the perturbed models. The latter two models are used to evaluate the control laws designed for P_0 and, hence, provide a specific test for control-system robustness. The frequencies of the first 44 flexible modes for P_0 are given in Section 4.5.2, Table 4-4.* Natural damping was assumed to be 0.1 percent for all modes.

④ LUMPED MASS PERTURBATION

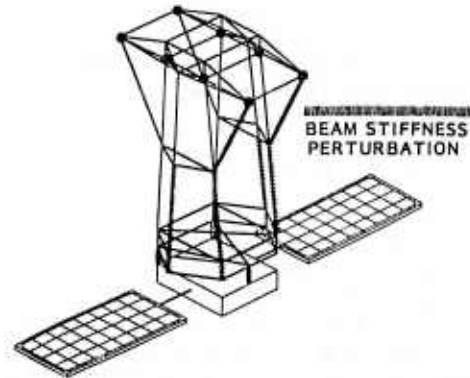


Fig. 4-10 CSDL No. 2 Model Perturbation (Qualitative)

Table 4-2
DESCRIPTION OF MEMBER PERTURBATIONS

MEMBER NO.	NODE A	NODE B	NOMINAL MODEL P_0	PERTURBED MODELS		PROPERTY 1	PROPERTY 2	PROPERTY 400 (NOMINAL)
				P_2	P_4			
76	8	14	400	1	1	25 cm dia x 0.10 cm	25 cm dia x 0.025 cm	25 cm dia x 0.05 cm
80	9	15	400	1	2	ROUND TUBE	ROUND TUBE	ROUND TUBE
81	11	17	400	1	1			
85	13	19	400	1	2	$A = 7.823 \times 10^{-4} \text{ m}^2$	$A = 1.962 \times 10^{-4} \text{ m}^2$	$I = 3.0496 \times 10^{-6} \text{ m}^4$
99	15	32	400	1	2			
101	17	33	400	1	2	$I = 6.063 \times 10^{-6} \text{ m}^4$	$I = 1.539 \times 10^{-6} \text{ m}^2$	$I = 3.0496 \times 10^{-6} \text{ m}^4$
						$J = 1.213 \times 10^{-5} \text{ m}^4$	$J = 3.059 \times 10^{-6} \text{ m}^4$	$J = 6.099 \times 10^{-6} \text{ m}^4$

Table 4-3
DESCRIPTION OF MASS PERTURBATIONS

NODE NO.	NOMINAL MODEL P_0	PERTURBED MODELS	
		P_2	P_4
27	375	350	375
28	375	350	375
29	375	350	375
30	375	350	375
32	500	500	550
33	500	500	450
34	250	300	300
35	250	250	200

*These were obtained using SPAR, a large-scale structural dynamics analysis program (available through the COSMIC library) whose detailed numerical procedures, structural reduction, eigen-computations, etc., are implemented differently than in NASTRAN. SPAR was used for comparison purposes, and for the first 68 modes, frequencies varied less than 0.1 percent compared with NASTRAN. In Table 4-4, modes 1 through 6 represent rigid-body modes.

4. TECHNOLOGY PRIMER

The disturbance model consists of two sinusoidal forces applied to a point on the upper optical structure and a point on the equipment section below the isolators, as shown subsequently in Fig 4-11. These forces simulate onboard vibrating equipment, and it is assumed that they act simultaneously.

4.5.2 The CSDL No. 2 Line-of-Sight Control Problem

To define a control problem for the CSDL No. 2 configuration, a performance metric is required. This is chosen to be the line-of-sight (LOS) error, i.e., the displacement of the image of a target when the structure deforms under the influence of the two onboard sinusoidal disturbances. The mathematical model giving the displacement law is described in Ref. 17, wherein it must be assumed that the coordinates x_1, y_1 of the image point are chosen to be zero.

The LOS error is a vector with components LOSX and LOSY in the focal plane, and is a function of the transverse defocus (X,Y). The defocus itself is denoted by Z, and together X, Y, Z are linear functions of the 16 optical variables:

$$x_p, y_p, x_t, y_t, x_f, y_f, z_p, z_s,$$

$$z_t, z_f, \theta x_p, \theta y_p, \theta x_s, \theta y_s, \theta x_t, \theta y_t,$$

where the $x_i, y_i, z_i, \theta x_i, \theta y_i$ refer to the translations and rotations in the global X, Y and Z directions of the primary (p), secondary (s), tertiary (t), and focal plane (f). These 16 optical variables are, in turn, linear functions of 21 variables which are X, Y, or Z coordinates of 12 particular nodes whose displacements control the geometry of the optical path. These 21 variables are therefore the physical coordinates of LOS and correspond to 21 degrees of freedom of the structure. Indeed, each of these physical coordinates can now be given its modal expansion in terms of the structure's mode shapes, and the resulting transformation:

$$\text{LOS} \rightarrow \text{OPTICAL VARIABLES} \rightarrow \text{PHYSICAL COORDINATES} \rightarrow \text{MODAL COORDINATES}$$

gives rise to the modal expansion of the LOS. More importantly, it suggests directly that, in order to control the LOS, one should control its physical coordinates where actuators can be placed. And indeed, the control actuators and their locations were chosen to correspond to these 21 degrees of freedom at the 12 particular nodes involved, as shown in Fig. 4-11.

4.5.2 THE CSDL NO. 2 LINE-OF-SIGHT CONTROL PROBLEM

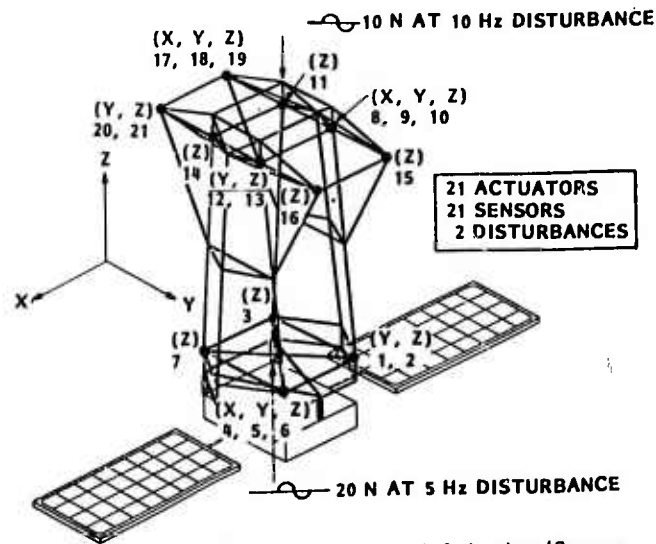


Fig. 4-11 Disturbances and Actuator/Sensor Locations for CSDL No. 2

The performance requirements are specified by the total LOS error defined as the quantity

$$\text{LOS} \triangleq \sqrt{(\text{LOSX})^2 + (\text{LOSY})^2}.$$

The contribution of each flexible mode to LOS can be calculated as follows. For simplicity, denote by ℓ_α ($\alpha=1,2$) the quantities $\ell_1 \triangleq \text{LOSX}$ and $\ell_2 \triangleq \text{LOSY}$. The expression of LOS in terms of its physical coordinates is then of the form

$$\begin{aligned} \ell_\alpha &= \sum_i \ell_{\alpha i} x_i \\ &= \sum_n \sum_i \ell_{\alpha i} \phi_{in} q_n \\ &\equiv \sum_n L_{\alpha n} q_n, \quad (L_{\alpha n} \equiv \sum_i \ell_{\alpha i} \phi_{in}) \end{aligned} \quad (4.83)$$

in which the modal expansion $x_i = \sum_n \phi_{in} q_n$ was used. The maximum value $S_{\alpha n}$ of $L_{\alpha n} q_n(t)$ represents the contribution of the n th mode to the components of the LOS error. The modal amplitude q_n is obtained from the structural transfer function defined in Eq. (4.8) of Section 4.2.1, and its maximum is the sum of the amplitudes corresponding to the two sinusoidal disturbance frequencies ω_k ($k=1,2$). Thus:

$$S_{\alpha n} \triangleq \max L_{\alpha n} q_n = \sum_{k=1,2} \frac{|L_{\alpha n} \phi_{kn} f_k|}{\sqrt{(\omega_k^2 - \omega_n^2)^2 + 4\zeta_n^2 \omega_k^2 \omega_n^2}} \quad (4.84)$$

where f_k denotes the magnitude of the k th disturbance. Finally, the contribution of the n th node to the LOS error is defined by

$$S_n = \sqrt{S_{1n}^2 + S_{2n}^2} \quad (4.85)$$

The control problem is to reduce the LOS error produced by the two steady-state disturbances to a value below a specified level. The disturbance magnitudes and the performance tolerances used in this analysis were based on preliminary CSDL estimates,* and are as follows:

Upper truss disturbance: 10 N at 10 Hz
 Lower truss disturbance: 20 N at 5 Hz
 LOS tolerance: 50×10^{-9} rad } Performance
 Defocus tolerance: 25×10^{-6} m } Requirements

Table 4-4 SYSTEM MODES AND THEIR CONTRIBUTIONS TO THE LINE-OF-SIGHT ERROR					
MODE NO.	NATURAL FREQ.	MODAL LOS ERROR (nrad)	MODE NO.	NATURAL FREQ.	MODAL LOS ERROR (nrad)
4	0.000	98	28	8.11	67
5	0.000	66	29	8.35	124
6	0.000	--	30	8.57	630
7	0.145	41	31	8.78	1
8	0.263	--	32	8.80	--
9	0.317	--	33	11.32	--
10	0.333	7	34	11.49	45
11	0.443	--	35	12.72	382
12	0.578	65	36	13.52	115
13	.581	12	37	13.71	334
14	1.22	113	38	14.16	37
15	1.30	--	39	15.65	59
16	1.34	175	40	16.07	35
17	1.72	6	41	16.52	47
18	1.81	--	42	16.74	48
19	1.81	--	44	17.15	87
20	1.88	--	44	17.82	30
21	2.36	633	45	19.07	93
22	2.98	365	46	23.77	3
23	3.17	--	47	24.41	39
24	3.38	815	48	25.91	17
25	5.16	--	49	26.27	--
26	5.26	143	50	26.36	200
27	7.87	--			

* These were subsequently revised, and in Ref. 17 they have been scaled up by a factor of 20. Since these quantities scale linearly, the control problem remains unchanged.

The LOS open-loop performance of CSDL No. 2, obtained from Eqs. (4.83), (4.84), and (4.85), is 972 nrad. The axial defocus already meets the requirements and, hence, is discarded from further consideration. The LOS error can be broken down into its modal components defined in Eq. (4.85) and listed in Table 4-4 for the first 44 flexible modes and 3 rigid-body rotational modes.

4.5.3 Control Design for CSDL No. 2

Active control is clearly required to meet the LOS requirements. Conventional vibration control imparts damping to all structural modes so as to reduce the overall response of the structure. Unfortunately, for steady-state disturbances, structural damping often fails to achieve the expected result and may even worsen the performance. As a test, 30 percent damping was assumed to be present in all modes. The total LOS error with damping was found to increase from 972 nrad to 1131 nrad. This phenomenon can be explained with reference to Fig. 4-12, which shows the ratios of transfer functions (LOS/disturbance) obtained, respectively, for the assumed 30 percent and the nominal 0.1 percent damping ratios. Near the disturbance frequencies, these ratios are larger than 1 in three cases out of four. Similar results are obtained when there are no rigid-body modes (Table 4-5).

Table 4-5 EFFECT OF PASSIVE DAMPING ON LOS PERFORMANCE		
	WITHOUT CONTROL (nrad)	WITH 30 PERCENT PASSIVE DAMPING
No Rigid-Body Modes	990	1,180
With Rigid-Body Modes	972	1,131

The conclusion to be drawn from this example is that damping augmentation does not work in all cases. Its effectiveness depends specifically upon the type of disturbance and the distribution of the modal frequencies in the disturbance spectrum. The approach which is taken here to solve the CSDL No. 2 control problem is based on the control-design method of Section 4.3. A quadratic performance criterion which contains explicitly the effect of the two disturbances is optimized. Thus, the LOS error due to these 5-Hz and 10-Hz disturbances is strongly reduced, while the overall system is stable.

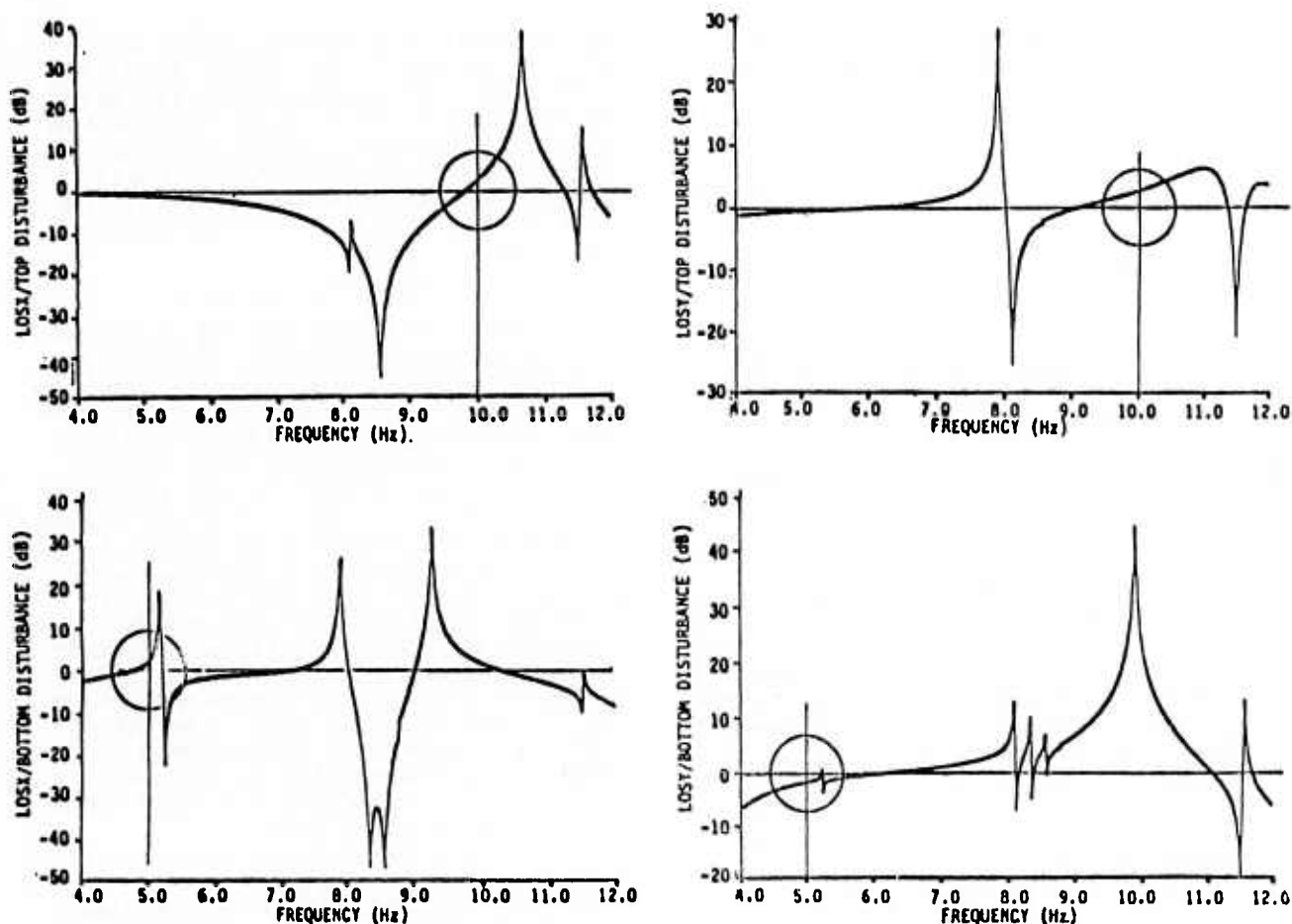


Fig. 4-12 Ratio of Transfer Functions (30% damping/0.1% damping) (See Text)

The overall procedure for a disturbance-rejecting controller design is shown in Fig. 4-13. As was stated in Section 4.5.2, 21 single degree-of-freedom force actuators were selected to control the physical coordinates of the LOS. These actuators are located at the structural nodes shown in Fig. 4-11. Correspondingly, 21 sensors collocated with these actuators and measuring displacement rates are introduced for the low-authority controller (LAC).

The high-authority controller (HAC) uses only three measurements: the two LOS errors (LOS_x and LOS_y) and the rigid-body angular rotation θ_z . This last measurement is necessary to control the attitude of the spacecraft about the z-axis, which is otherwise not observable through the line of sight. These measurements may be obtained directly by optical means or reconstructed from structural information and kinematics.

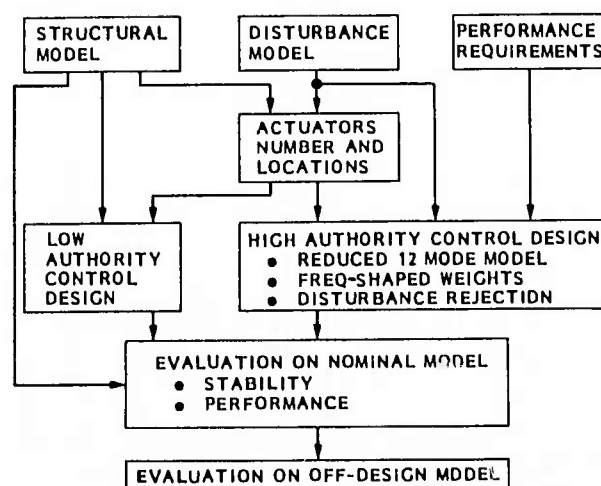


Fig. 4-13 Control Design Approach for Disturbance Rejection

Three modes (20, 33, and 49) were first discarded from the initial model because they were neither observable nor controllable. The evaluation model thus contains 3 rigid-body modes and 41 flexible modes. The reduced model was obtained by selecting ten modes with the highest controllability-observability product and the two modes with highest modal cost, as shown in Table 4-6. This 12-mode model (which includes the 3 rigid-body modes) is used for control design. Since the disturbances occur at the two discrete frequencies (5 and 10 Hz), the following state penalty is used in the design:

$$J = \int_{-\infty}^{\infty} [T(j\omega) [LOS_x^2 + LOS_y^2] + bu^T u] d\omega, \quad (4.86)$$

where the frequency-shaping weight is given by

$$T(j\omega) = \frac{4}{(\omega^2 - 100\pi^2)^2} + \frac{10}{(\omega^2 - 400\pi^2)^2}. \quad (4.87)$$

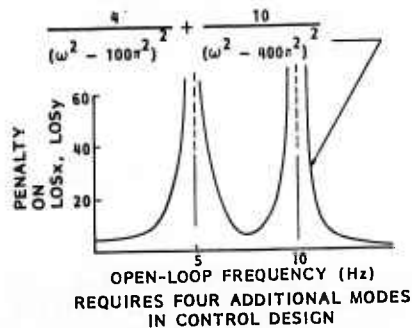


Fig. 4-14 Frequency-Shaped Weights for Disturbance Rejection

A plot of $T(j\omega)$ as a function of frequency is shown in Fig. 4-14. The control weight b is selected to ensure that the control effort in the closed loop is not excessive.

The 24 states of the reduced model are estimated by a Kalman filter to which the 8 additional states necessary for frequency shaping are appended. The overall structure of the controller/filter is shown in Table 4-7. The measurement vector y is used directly as input to the estimator. In the reduced model, this measurement is approximated by y_0 based on a reduced number of states. The quadratic weights used in the design are given in Table 4-8, and the resulting closed-loop filter and controller

Table 4-6
MODE SELECTION FOR HAC (12 MODES)

ORDERING BASED ON MODAL COST	ORDERING BASED ON CONTROL- LABILITY	ORDERING BASED ON OBS/CONTROLLABILITY PRODUCT
→ 24	21	→ 21
21	28	→ 30
30	30	→ 17
→ 22	17	→ 28
16	12	→ 4
26	11	→ 5
29	13	→ 6
14	4	→ 12
4		→ 13
28		→ 7
5		
→ : HAC MODES		

Table 4-7
FREQUENCY-SHAPED CONTROLLER/FILTER STRUCTURE

Reduced model for optimal control synthesis

$\dot{x} = F_0 x + G_0 u + I_0 w$	24-state model (12 modes)
$\dot{\xi} = \Omega \xi + M y_0$	8 frequency- shaping states (2 frequencies)
$z_0 = L_0 x$	3 measurements

Controller

$u = C_0 \hat{x} + C_\xi \xi$	21 controls
-------------------------------	-------------

Estimator

$\dot{\hat{x}} = F_0 \hat{x} + G_0 u + K(z - L_0 \hat{x})$	Kalman filter (24 states)
$\dot{\hat{\xi}} = \Omega \hat{\xi} + M z$	frequency- shaping states (8 states)
$u = C_0 \hat{x} + C_\xi \hat{\xi}$	control law (21 controls)

Table 4-8
CONTROL AND FILTER WEIGHTING USED IN THE DESIGN (NONZERO ELEMENTS)

State Penalty Weighting

AS (1, 1) = 1.000-04 AS (2, 2) = 1.000-04 AS (3, 3) = 1.000-04 AS (4, 4) = 1.000-04
 AS (5, 5) = 1.000-04 AS (6, 6) = 1.000-04 AS (27,27) = 1.000-03 AS (28,28) = 1.000-03
 AS (31,31) = 4.000+02 AS (32,32) = 4.000+02

Control Penalty Weighting

R (1, 1) = 2.000-11 R (1, 2) = 2.000-11 R (1, 3) = 2.000-11 R (1, 4) = 2.000-11
 R (1, 5) = 2.000-11 R (1, 6) = 2.000-11 R (1, 7) = 2.000-11 R (1, 8) = 2.000-11
 R (1, 9) = 2.000-11 R (1,10) = 2.000-11 R (1,11) = 2.000-11 R (1,12) = 2.000-11
 R (1,13) = 2.000-11 R (1,14) = 2.000-11 R (1,15) = 2.000-11 R (1,16) = 2.000-11
 R (1,17) = 2.000-11 R (1,18) = 2.000-11 R (1,19) = 2.000-11 R (1,20) = 2.000-11
 R (1,21) = 2.000-11

State Noise Distribution Used for Filter Design

D (1, 1) = 1.000-06 D (3, 2) = 1.000-06 D (5, 3) = 1.000-06 D (7, 4) = 1.000+00
 D (9, 5) = 1.000+00 D (11, 6) = 1.000+00 D (13, 7) = 1.000+00 D (15, 8) = 1.000+00
 D (17, 9) = 1.000+00 D (19,10) = 1.000+00 D (21,11) = 1.000+00 D (23,12) = 1.000+00

State Noise Covariance

W (1, 1) = 1.000-01 W (1, 2) = 1.000-01 W (1, 3) = 1.000-01 W (1, 4) = 1.000-04
 W (1, 5) = 1.000-04 W (1, 6) = 1.000-04 W (1, 7) = 1.000-04 W (1, 8) = 1.000-04
 W (1, 9) = 1.000-04 W (1,10) = 1.000-04 W (1,11) = 1.000-04 W (1,12) = 1.000-04

Measurement Distribution Matrix

M (1, 2) = 1.000+00 M (1, 8) = -2.577-07 M (1,10) = 7.361-04 M (1,12) = 2.416-06
 M (1,14) = 2.738-05 M (1,16) = 2.212-05 M (1,18) = 1.345-04 M (1,20) = 5.610-07
 M (1,22) = -4.273-04 M (1,24) = 1.867-02 M (2, 4) = 1.000+00 M (2, 8) = 3.254-04
 M (2,10) = -6.868-06 M (2,12) = 8.731-04 M (2,14) = -2.775-03 M (2,16) = 1.376-02
 M (2,18) = 2.734-06 M (2,20) = -4.542-04 M (2,22) = -1.702-05 M (2,24) = -1.139-05
 M (3, 6) = 1.000+00

Measurement Noise Covariance

V (1, 1) = 5.000-11 V (1, 2) = 5.000-11 V (1, 3) = 5.000-11

Table 4-9
CLOSED-LOOP HIGH-AUTHORITY-CONTROL (HAC)
DESIGN

MODE NO.	OPEN-LOOP FREQ. (Hz)	CLOSED-LOOP CONTROL DAMPING RATIO	STATE ESTIMATOR DAMPING RATIO
4	Rigid Body	0.74	0.70
5	Rigid Body	0.78	0.71
6	Rigid Body	0.73	0.71
7	0.145	0.009	0.247
12	0.578	0.014	0.039
13	0.581	0.012	0.046
17	1.72	0.021	0.017
21	2.36	0.127	0.044
22	2.99	0.001	0.001
24	3.39	0.001	0.001
28	8.118	0.004	0.001
30	8.57	0.046	0.005
FREQ. - SHAPING MODES	5.0 5.0 10.0 10.0	0.028 0.057 0.011 0.036	

damping ratios are given in Table 4-9. The HAC filter gains (matrix K_f) and control gains (matrix C), depicted subsequently in Fig. 4-17, are listed in Appendix B.

The LAC law is designed separately to minimize spillover. The model used for LAC synthesis includes the 12 modes used for HAC plus 10 additional modes chosen outside of the HAC bandwidth on the basis of their controllability. The HAC/LAC mode selection is shown in Table 4-10. The LAC control law is defined by the diagonal gain matrix C_L relating the 21 measured velocities at the actuator locations to the corresponding 21 actuator forces. These LAC gains are selected to provide approximately 3 percent damping in all modes. Because of variation in level of controllability from mode to mode, it is possible to achieve this condition only approximately. Table 4-11a shows the LAC control design, and Table 4-11b gives the LAC gains.

Table 4-10
MODE SELECTION FOR HIGH-AUTHORITY (HAC) AND LOW-AUTHORITY (LAC) CONTROL

DATE 021981

N	FREQ	LOSX (NRAD)	LOSX (NRAD)	LOS (NRAD)	DEFOCUS (MICRONS)
4	.000	98.566	.000	98.566	.0000
5	.000	.000	66.842	66.842	.0000
6	.000	.000	.000	.000	.0000
7	.145	.032	40.798	40.798	.0000
8	.263	.001	.599	.599	.0000
9	.317	.026	.007	.027	.0001
10	.333	6.570	.013	6.570	.0000
11	.443	.630	.111	.639	.0016
12	.578	65.020	.607	65.022	.0002
13	.581	.034	12.341	12.341	.0000
14	1.224	.487	112.637	112.638	.0000
15	1.300	.021	.858	.858	.0000
16	1.347	175.017	1.546	175.024	.0103
17	1.721	.060	6.044	6.045	.0001
18	1.818	.072	.018	.075	.0002
19	1.819	.011	.002	.011	.0000
20	1.889	.000	.000	.000	.0000
21	2.364	1.018	633.500	633.501	.0004
22	2.989	365.054	7.420	365.130	.0411
23	3.175	.025	1.499	1.500	.0000
24	3.386	1.007	815.537	815.537	.0008
25	5.161	.000	.001	.001	.0000
26	5.260	143.114	2.957	143.144	.0201
27	7.874	.000	.000	.000	.0000
28	8.110	16.368	65.251	67.273	.0075
29	8.355	124.302	.204	124.302	.0018
30	8.572	630.032	.384	630.032	.0360
31	8.785	1.046	.005	1.046	.0001
32	8.805	.004	.000	.004	.0000
33	11.321	.000	.001	.001	.0000
34	11.499	24.835	37.851	45.272	.0082
35	12.727	381.342	19.623	381.847	.5541
36	13.525	1.709	114.527	114.540	.0096
37	13.716	23.394	333.587	334.406	.0377
38	14.162	20.417	30.747	36.909	.0058
39	15.654	57.481	13.035	59.840	.0203
40	16.075	6.283	34.466	35.034	.0008
41	16.527	45.020	14.510	47.000	.0916
42	16.748	46.459	11.403	47.838	.1656
43	17.157	1.191	87.053	87.061	.0182
44	17.829	28.410	10.253	30.203	.0630
45	19.072	4.117	92.772	92.864	.0099
46	23.773	2.664	1.957	3.306	.0061
47	24.416	9.118	37.506	38.598	.0231
48	25.910	.380	17.413	17.417	.0048
49	26.272	.000	.000	.000	.0000
50	26.365	162.899	117.136	200.642	.0270

○ : 3 MODES DELETED FROM MODEL AND REPLACED
BY 3 RIGID BODY ROTATION MODES
(TOTAL MODES RETAINED: 44)

TOLERANCES:
LOS: 50 nrad
DEFOCUS: 15 μ m

4. TECHNOLOGY PRIMER

4.5.4 PERFORMANCE EVALUATION FOR CSDL NO. 2 NOMINAL AND PERTURBED MODELS

Table 4-11a					
CLOSED-LOOP LOW-AUTHORITY CONTROL (LAC) DESIGN					
MODE ¹ NO.	CLOSED-LOOP FREQUENCY (Hz)	DAMPING (%)	MODE NO.	CLOSED-LOOP FREQUENCY (Hz)	DAMPING (%)
1	0.000	0.0	25	5.161	0.1
2	0.000	0.0	26	5.260	0.1
3	0.000	0.0	27	7.874	0.1
4	0.000	100.0	28	8.139	7.6
5	0.000	100.0	29	8.355	0.1
6	0.000	100.0	30	8.561	6.5
7	0.151	40.5	31	8.785	0.1
8	0.259	25.4	32	8.805	0.1
9	0.293	100.0	33	11.516	3.0
10	0.336	3.1	34	12.780	3.5
11	0.359	2.8	35	13.525	0.1
12	0.543	100.0	36	13.721	2.7
13	0.574	20.1	37	14.162	1.7
14	0.583	8.2	38	15.712	2.0
15	1.224	0.1	39	16.103	1.6
16	1.302	0.6	40	16.557	3.5
17	1.345	0.4	41	16.635	2.4
18	1.739	11.7	42	17.150	4.2
19	1.818	0.1	43	17.738	3.6
20	1.819	0.1	44	18.994	3.2
21	2.246	31.9	45	23.825	0.9
22	2.989	0.1	46	24.351	4.9
23	3.175	0.1	47	25.893	0.7
24	3.386	0.1	48	26.328	3.1

¹ Closed-loop modes 1 through 6 correspond to attitude and attitude rate rigid-body modes.

Table 4-11b LAC GAINS C _L			
ACTUATOR NO.	GAIN N/ms ⁻¹	ACTUATOR NO.	GAIN N/ms ⁻¹
1	-548	12	-43.9
2	-8150	13	0.0
3	-9830	14	-3380
4	0.0	15	-7120
5	-458	16	-3850
6	-2380	17	-3450
7	-5470	18	-583
8	-12800	19	0.0
9	-220	20	-94.6
10	-6410	21	-3500
11	-6620		

4.5.4 Performance Evaluation for CSDL No. 2 Nominal and Perturbed Models

The HAC/LAC controller performance evaluation combines the HAC controller/filter equations (shown in Table 4-7), the LAC control law, and the 44-mode evaluation-model equations. The total system is of order 120. Stability is evaluated by determining the complex eigenvalues, which are summarized in Table 4-12. A significant feature of the design is that no pole has a lower damping ratio in closed loop than in open loop. The evaluation of the LOS error is obtained by computing the steady-state responses at 5 and 10 Hz using the complex equation:

$$\mathcal{L} = H_s(j\omega_k I - F_s)^{-1} I_s w_k, \quad j \equiv \sqrt{-1} \quad (4.88)$$

where \mathcal{L} is the LOS error vector (whose components have complex amplitudes), w_k is the magnitude of the disturbance at the frequency $\omega_k/2\pi$, and the matrices F_s , I_s and H_s correspond to the total closed-loop system defined by the equations

$$\dot{x}_s = F_s x_s + I_s w, \quad (4.89)$$

$$\mathcal{L} = H_s x_s$$

Table 4-12 CLOSED-LOOP POLES WITH HAC/LAC CONTROLLER					
CLOSED- LOOP MODE	FREQUENCY	DAMPING	CLOSED- LOOP MODE	FREQUENCY	DAMPING
1	.0309	0.7448	32	4.9331	0.0486
2	.0337	0.7071	33	5.0124	0.0303
3	.0337	0.7048	34	5.1613	0.0010
4	.0349	0.8741	35	5.2599	0.0010
5	.0441	0.7901	36	7.8743	0.0010
6	.0565	0.7883	37	8.1183	0.0011
7	.1147	0.5258	38	8.1344	0.0774
8	.1551	0.2400	39	8.3552	0.0010
9	.2428	0.2458	40	8.5529	0.1157
10	.2792	1.0000	41	8.5726	0.0047
11	.3341	0.0337	42	8.7853	0.0010
12	.3587	0.0276	43	8.8050	0.0010
13	.5584	1.0000	44	9.8678	0.0299
14	.5680	0.2134	45	9.8787	0.0069
15	.5786	0.0397	46	11.5158	0.0300
16	.5823	0.0463	47	12.7838	0.0362
17	.5854	0.0911	48	13.5252	0.0010
18	1.2236	0.0012	49	13.7254	0.0277
19	1.3020	0.0057	50	14.1829	0.0169
20	1.3450	0.0043	51	15.7052	0.0205
21	1.7216	0.0186	52	16.1059	0.0171
22	1.7413	0.1291	53	16.5566	0.0353
23	1.8178	0.0010	54	16.6335	0.0240
24	1.8188	0.0010	55	17.1482	0.0423
25	2.2428	0.4756	56	17.7449	0.0354
26	2.3678	0.0441	57	18.9932	0.0322
27	2.9885	0.0012	58	23.8244	0.0090
28	2.9886	0.0010	59	24.3511	0.0486
29	3.1753	0.0012	60	25.8923	0.0067
30	3.3860	0.0011	61	26.3284	0.0308
31	3.3864	0.0012			

4. TECHNOLOGY PRIMER

The magnitude of the vector sum of x-axis and y-axis LOS error is found to be 0.013 nrad.

The larger than four-order-of-magnitude reduction in the LOS error is in striking contrast to the relatively small closed-loop damping ratios, showing that large performance improvements do not necessarily require large increases in damping ratios. This significant result is indeed typical of the application of optimal control. It exemplifies the difference between the colocated LAC system which locally absorbs vibrational energy, and the HAC system which judiciously redistributes it, producing favorable cancellations so as to optimize the performance. However, this latter controller can be much more sensitive to model errors, and this sensitivity may be evaluated on perturbed models.

Evaluation on perturbed models. The two perturbed models P_2 and P_4 described in Section 4.5.1 are used to evaluate the previously described HAC/LAC controller. The transfer functions between the x-axis LOS error and the upper-disturbance input are compared in Fig. 4-15 for the nominal and the two perturbed models. There is a significant change in the P_2 transfer function around 10 Hz, where an interchange between modes 30 and 32 occurs. This can be seen in Table 4-13 where the LOS modal contributions are compared for the three models, allowing mode 30 to be tracked through the perturbations P_2 and P_4 . The controller is stable for perturbed model P_4 . However, stability with P_2 requires only the knowledge of the natural frequency of mode 30 (which had become mode 32 and was no longer

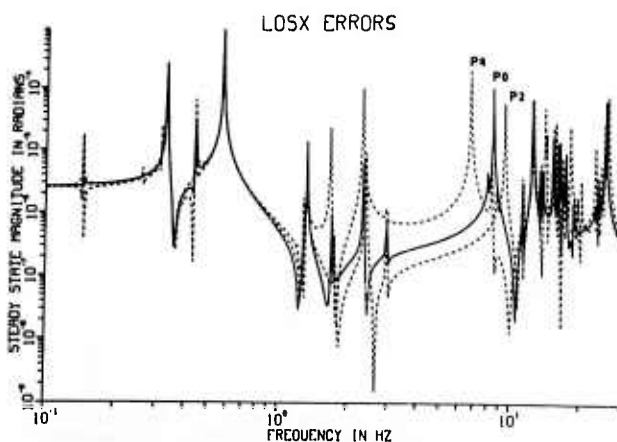


Fig. 4-15 LOSX Frequency Responses to Sinusoidal Disturbance of Upper-Support Truss, Nominal (P_0) and Perturbed (P_2 , P_4) Models

4.5.4 PERFORMANCE EVALUATION FOR CSDL NO. 2 NOMINAL AND PERTURBED MODELS

properly represented). LOS errors for the three models are compared in Table 4-14. Table 4-15 compares the open-loop performance to the closed-loop LOS errors. The improvement in performance for the perturbed models is of the same order of magnitude as for the nominal models.

Controller simplification. Because of the eight additional states required by the implementation of the frequency-shaping methods, the modified LQG problem from which control gains are obtained is of order 32. For practical implementation reasons, it may be desirable to reduce this order. The controller is simplified by setting the control and filter gains corresponding to various modes to zero. Table 4-16 shows

Table 4-13
FREQUENCY AND LOS OBSERVABILITY COMPARISONS -
NOMINAL AND PERTURBED MODELS

MODE NO.		OPEN-LOOP FREQ (Hz)			LOS MODAL COMPONENTS ^(*)		
		FOR MODEL			FOR MODEL		
FLEX #	CSDL #	P0	P2	P4	P0	P2	P4
1	7.	.145	.145	.145	.325	.330	.324
2	8.	.263	.262	.263	.214	.202	.218
3	9.	.317	.317	.317	.001	.001	.005
4	10.	.333	.333	.333	.229	.227	.230
5	11.	.443	.443	.443	.006	.001	.023
6	12.	.578	.576	.578	.736	.724	.746
7	13.	.581	.581	.581	.873	.875	.872
8	14.	1.224	1.224	1.224	.236	.213	.244
9	15.	1.300	1.301	1.300	.152	.047	.224
10	16.	1.347	1.347	1.347	.159	.149	.165
11	17.	1.721	1.769	1.695	2.775	2.046	3.096
12	18.	1.818	1.818	1.818	.001	.003	.004
13	19.	1.819	1.819	1.819	.012	.011	.013
14	20.	1.889	1.889	1.889	.001	.001	.001
15	21.	2.364	2.427	2.342	13.757	13.769	13.665
16	22.	2.989	2.969	2.989	.135	.118	.143
17	23.	3.175	3.175	3.175	.261	.275	.258
18	24.	3.386	3.386	3.386	.454	.476	.442
19	25.	5.161	5.161	5.161	.000	.000	.000
20	26.	5.260	5.260	5.260	.034	.027	.042
21	27.	7.874	7.874	6.863	.000	.000	12.721
22	28.	8.118	8.355	7.874	1.756	.064	.000
23	29.	8.355	8.705	8.355	.283	.003	.151
24	30.	8.572	8.805	8.463	10.668	.612	16.419
25	31.	8.785	8.851	8.765	.031	3.713	.020
26	32.	8.805	9.601	8.805	.052	15.290	.027
27	33.	11.321	11.321	11.321	.010	.002	.015
28	34.	11.499	11.571	11.467	2.237	2.034	2.708
29	35.	12.727	12.837	12.697	11.001	11.357	11.079
30	36.	13.525	13.525	13.524	.521	.431	1.027
31	37.	13.716	13.806	13.612	10.141	11.315	10.862
32	38.	14.162	14.280	14.147	7.145	4.350	6.026
33	39.	15.654	16.094	14.417	14.510	10.016	10.270
34	40.	16.075	16.553	14.710	10.623	14.871	7.460
35	41.	16.527	17.200	15.745	7.105	5.481	8.530
36	42.	16.748	18.585	16.571	3.952	15.542	11.507
37	43.	17.157	19.001	16.731	8.405	5.091	13.010
38	44.	17.829	19.351	17.265	3.440	1.096	3.928
39	45.	19.072	20.662	19.937	14.472	6.214	12.617
40	46.	23.773	25.180	23.839	20.120	25.158	25.064
41	47.	24.416	25.208	24.531	38.221	20.782	39.313
42	48.	25.910	25.934	26.043	12.027	34.604	9.150
43	49.	26.272	26.272	26.272	.000	.000	.000
44	50.	26.365	27.004	26.264	17.817	21.654	18.493

^(*) $(LOS)_n = 10^3 \sqrt{(LOSX)_n^2 + (LOS Y)_n^2}$ WHERE $(LOSX)_n$ ARE NTH ELEMENTS IN FIRST TWO ROWS OF LOS MATRIX

4. TECHNOLOGY PRIMER

4.5.4 PERFORMANCE EVALUATION FOR CSDL NO. 2 NOMINAL AND PERTURBED MODELS

Table 4-14 LOS ERROR AND CONTROL EFFORTS FOR NOMINAL AND PERTURBED MODELS				
		NOMINAL MODEL	P ₂	P ₄
LOS _x (nrad)	5 Hz	0.002	0.004	0.001
	10 Hz	0.005	0.007	0.004
LOS _y (nrad)	5 Hz	0.006	0.007	0.005
	10 Hz	0.004	0.004	0.004
Average Control Effort (N)		0.82	0.90	0.69

Table 4-15 COMPARISON OF OPEN-LOOP AND CLOSED-LOOP LOS ERRORS				
MODEL	OPEN LOOP (nrad)	CLOSED LOOP (nrad)	CLOSED LOOP AS A FRACTION OF OPEN LOOP	AVERAGE CONTROL EFFORT (NEWTONS)
Nominal	972	0.013	13 x 10 ⁻⁶	0.82
P ₂	1,740	0.016	9.2 x 10 ⁻⁶	0.90
P ₄	674	0.010	15 x 10 ⁻⁶	0.69

three simplified controllers (with orders 30, 26, and 20); the simplification does not degrade the LOS error significantly, and the control effort is also the same as for the full-order controller.

Note that when a 20th order controller is designed directly, the closed-loop system is unstable.

Robust controller. A robust controller may be designed so that knowledge of the natural frequency of mode 30 is not required for stability of perturbed model P₂. The robust design is obtained by increasing the control penalty and measurement noise covariance by a factor of ten. The robust controller is stable for all models. The closed-loop performance for P₂ degrades from 0.016 nrad to 0.046 nrad (see Fig. 4-16). This result illustrates the usual trade-off between maximum performance and robustness. Slightly relaxing the performance requirement can produce large improvements in system robustness.

Table 4-16 CLOSED-LOOP CONTROLLER SIMPLIFICATION				
CONTROLLER:	NOMINAL	1	2	3
MODES RETAINED IN MODEL (x)	RIGID	x	x	x
	RIGID	x	x	x
	RIGID	x	x	x
	0.145	x	x	
	0.578	x	x	
	0.581	x	x	
	1.72	x	x	x
	2.36	x	x	x
	2.99	x		
	3.39	x		
	8.12			
	8.57	x	x	x
COST	12.6	12.7	12.7	12.7
CONTROL EFFORT (N)	0.822	0.822	0.821	0.822
CONTROLLER ORDER	32	30	26	20

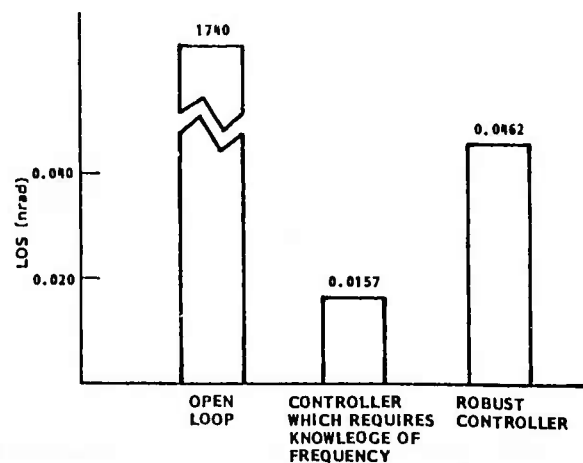


Fig. 4-16 A Robust Controller for P₂

4.5.5 Matrix Computational Algorithms for CSDL No. 2

Large space structure modeling, control design, and closed-loop evaluation require numerical solutions to high-order matrix problems. Standard digital computer procedures used successfully for small-scale problems are simply not applicable in the large space structure case because of high memory storage requirements and numerical instabilities. In addition, a significant part of the software is devoted to the manipulation and construction of the various large matrices involved in the control syntheses and evaluation procedures. The CSDL No. 2 model provides a good example to illustrate the size and type of the software operations needed for the control of large space structures.

In the CSDL No. 2 example: (a) 44 modes are used as the total model for the configuration; (b) two disturbances

$$w = \begin{bmatrix} w_1 \\ w_2 \end{bmatrix}$$

are assumed to be applied, each at a given structural node; and (c) 21 single DOF control actuators are placed on the structure. The state equations then take the form:

$$\dot{x} = \begin{matrix} 88 \times 1 \\ 88 \times 88 \end{matrix} F x + \begin{matrix} 88 \times 21 \\ 88 \times 21 \end{matrix} G u + \begin{matrix} 88 \times 2 \\ 88 \times 2 \end{matrix} \Gamma w, \quad (4.90)$$

where the matrix dimensions are included. The matrices G and Γ are of the form shown in Eq. (4.7) of Section 4.2.1.

Equation (4.90) represents only the initial formulation of the control problem: a large modal model of a disturbed structure to be controlled by a control vector as yet to be determined. For reasons given in Section 4.3, the controller design is carried out on a reduced-order model. For example, in the CSDL No. 2 configuration, only 12 modes were deemed as important for designing the required type of control. For this, one needs also the equation:

$$\dot{x}_0 = \begin{matrix} 24 \times 1 \\ 24 \times 24 \end{matrix} F_0 x_0 + \begin{matrix} 24 \times 21 \\ 24 \times 21 \end{matrix} G_0 u + \begin{matrix} 24 \times 2 \\ 24 \times 2 \end{matrix} \Gamma_0 w, \quad (4.91)$$

where those columns of Φ (appearing in G and Γ) corresponding to the discarded modes as well as the corresponding w_1 's in the matrix F given in Eq. (4.7) must be deleted.

Equations (4.90) and (4.91) together are only the first two equations (denoted by "PLANT" and

"REDUCED MODEL") in Fig. 4-17, which depicts the total set of system equations required for the disturbance-rejection control system. The third and fourth equations in Fig. 4-17 represent, respectively, the Kalman filter and the control equation. In these, the measurement matrices M are constructed from the LOS matrices L and L_0 , which, in turn, are derived from structural information (modal decomposition of LOS). The matrices F, G, and Γ (as discussed earlier) are also obtained from structural data (mode shapes), while the gain matrices K_1 , C, and C_L , which define the control laws, are obtained from modern optimal control synthesis computer programs. (Figure 4-18 shows the block diagram for the complete CSDL No. 2 control system.)

Closing the loop around the total system equations produces a "closed-loop dynamics" matrix F_s (Fig. 4-19) of dimension 120x120, corresponding to an aggregation of the 88 open-loop structural states with 32 filter states. Complex eigenvalues and eigenvectors of this large matrix need to be evaluated in order to obtain the steady-state solution of the differential equation

$$\dot{X} = F_s X + \begin{bmatrix} \Gamma \\ 0 \end{bmatrix} w \quad (4.92)$$

and to compute the associated transfer functions like those shown in Fig. 4-12. To obtain the closed-loop system performance, this solution X is substituted into the measurement equation (third equation of Fig. 4-19):

$$z = \begin{bmatrix} M \\ 0 \end{bmatrix} X, \quad (4.93)$$

where the three components of z are LOSX, LOSY, and DEFOCUS respectively. To obtain the control effort (forces), X is substituted into the control equation (second equation of Fig. 4.20):

$$u = CX + C_L G^T X, \quad (4.94)$$

where the two terms on the right-hand side, which correspond to the HAC and LAC control effort, can be evaluated separately.

In the above discussion, the path from the original structural concept (e.g., CSDL No. 2) to the final closed-loop evaluation model (Fig. 4-19) constitutes the dynamics and controls modeling process for controlled flexible spacecraft. Thus, in addition to the expertise

4. TECHNOLOGY PRIMER

4.5.5 MATRIX COMPUTATIONAL ALGORITHMS FOR CSDL NO. 2

$$\dot{\mathbf{x}} = \mathbf{F}\mathbf{x} + \mathbf{G}\mathbf{u} + \mathbf{\Gamma}\mathbf{w}$$

88x1 88x88 88x21 88x2

PLANT

$$\dot{\mathbf{x}}_0 = \mathbf{F}_0\mathbf{x}_0 + \mathbf{G}_0\mathbf{u} + \mathbf{\Gamma}_0\mathbf{w}$$

24x1 24x24 24x21 24x2

REDUCED MODEL

$$\begin{bmatrix} \dot{\hat{\mathbf{x}}}_0 \\ \dot{\hat{\boldsymbol{\xi}}} \end{bmatrix} = \mathbf{F}_1 \begin{bmatrix} \hat{\mathbf{x}}_0 \\ \hat{\boldsymbol{\xi}} \end{bmatrix} + \mathbf{G}_1\mathbf{u} + \mathbf{K}_1 \left\{ \begin{bmatrix} \mathbf{M} \\ \mathbf{\Lambda} \end{bmatrix} \mathbf{x} - \begin{bmatrix} \mathbf{M}_1 \\ \mathbf{\Lambda}_1 \end{bmatrix} \begin{bmatrix} \hat{\mathbf{x}}_0 \\ \hat{\boldsymbol{\xi}} \end{bmatrix} \right\}$$

24x1 24x24 24x21 32x11 3x88 3x32 8x88 8x32

FREQUENCY-SHAPED KALMAN FILTER

$$\mathbf{u} = \mathbf{C} \begin{bmatrix} \hat{\mathbf{x}}_0 \\ \hat{\boldsymbol{\xi}} \end{bmatrix} + \mathbf{C}_L \mathbf{G}^T \mathbf{x}$$

21x32 21x21

CONTROL

DISTURBANCE FREQUENCIES: $\omega_1/2\pi = 5 \text{ Hz}$, $\omega_2/2\pi = 10 \text{ Hz}$

WHERE:

$$\mathbf{F}_1 \equiv \begin{bmatrix} \mathbf{F}_0 & \mathbf{O} \\ \mathbf{\Lambda}_0 & \mathbf{\Omega} \end{bmatrix}, \quad \mathbf{\Omega} \equiv \begin{bmatrix} 0 & 0 & 1 & 0 \\ 0 & 0 & 0 & 1 \\ -\omega_1^2 & 0 & 0 & 0 \\ 0 & -\omega_2^2 & 0 & 0 \end{bmatrix}, \quad \mathbf{\Lambda} \equiv \begin{bmatrix} \mathbf{O} \\ \mathbf{L} \\ \mathbf{O} \\ \mathbf{L} \end{bmatrix}, \quad \mathbf{\Lambda}_0 \equiv \begin{bmatrix} \mathbf{O} \\ \mathbf{L}_0 \\ \mathbf{O} \\ \mathbf{L}_0 \end{bmatrix}, \quad \text{AND} \quad \begin{cases} \mathbf{K}_1 \equiv \begin{bmatrix} \mathbf{K} & \mathbf{O} \\ \mathbf{\Lambda}_1 & \mathbf{O} \\ \mathbf{M}_1 & \mathbf{O} \end{bmatrix} \\ \mathbf{\Lambda}_1 \equiv \begin{bmatrix} \mathbf{\Lambda}_0 & \mathbf{O} \\ \mathbf{\Lambda}_0 & \mathbf{O} \end{bmatrix} \\ \mathbf{M}_1 \equiv \begin{bmatrix} \mathbf{M}_0 & \mathbf{O} \end{bmatrix} \end{cases}$$

\mathbf{L} IS THE LOS MATRIX GIVEN BY $\begin{bmatrix} \text{LOSX} \\ \text{LOSY} \end{bmatrix} = \mathbf{L} \mathbf{x}$; \mathbf{L}_0 IS THE REDUCED LOS MATRIX GIVEN BY $\begin{bmatrix} \text{LOSX} \\ \text{LOSY} \end{bmatrix} = \mathbf{L}_0 \mathbf{x}_0$

\mathbf{M} IS THE MEASUREMENT MATRIX GIVEN BY $\begin{bmatrix} \text{LOSX} \\ \text{LOSY} \\ \theta_z \end{bmatrix} = \mathbf{M} \mathbf{x}$; \mathbf{M}_0 IS THE REDUCED MEASUREMENT MATRIX GIVEN BY $\begin{bmatrix} \text{LOSX} \\ \text{LOSY} \\ \theta_z \end{bmatrix} = \mathbf{M}_0 \mathbf{x}_0$

Fig. 4-17 Total System Equations (CSDL No. 2 Control System)

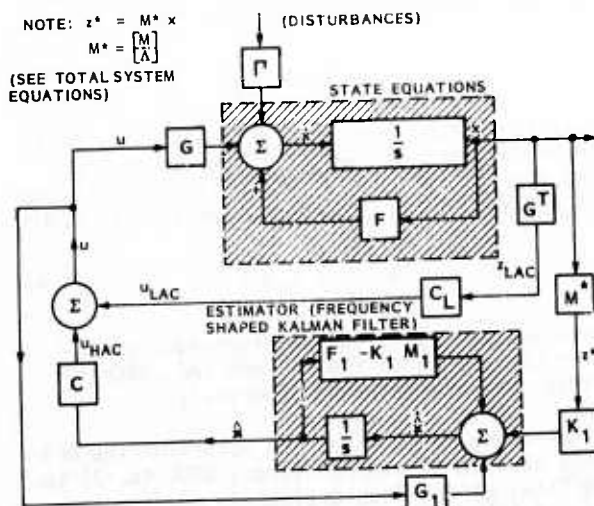


Fig. 4-18 Block Diagram for Combined HAC/LAC Control System

$$\dot{\mathbf{x}} = \mathbf{F}_s \mathbf{x} + \begin{bmatrix} \mathbf{\Gamma} \\ \mathbf{O} \end{bmatrix} \mathbf{w}$$

120x1 120x120 88x2 32x2

$$\mathbf{u} = \mathbf{C}_s \mathbf{x}$$

21x1 21x120

$$\mathbf{z} = \begin{bmatrix} \mathbf{M} & \mathbf{O} \end{bmatrix} \mathbf{x}$$

3x1 3x88 3x32

$$\mathbf{F}_s \equiv \begin{bmatrix} \mathbf{F} + \mathbf{G}\mathbf{C}_L\mathbf{G}^T & \mathbf{G}\mathbf{C} \\ \mathbf{K}\mathbf{M}^* \begin{bmatrix} \mathbf{O} \\ \mathbf{\Lambda} \end{bmatrix} + \mathbf{G}_1\mathbf{C}_L\mathbf{G}^T & \begin{bmatrix} \mathbf{F}_0 & \mathbf{O} \\ \mathbf{O} & \mathbf{\Omega} \end{bmatrix} + \mathbf{G}_1\mathbf{C} - \mathbf{K}\mathbf{M}_1 \end{bmatrix}$$

120x120 88x88 88x88 88x32

$$\mathbf{C}_s = \begin{bmatrix} \mathbf{C}_L \mathbf{G}^T & \mathbf{C} \end{bmatrix}$$

21x120 21x21 21x88 21x32

Fig. 4-19 Closed-Loop System/Evaluation Model (CSDL No. 2 Control System)

4. TECHNOLOGY PRIMER

4.5.5 MATRIX COMPUTATIONAL ALGORITHMS FOR CSDL NO. 2

required to design and synthesize modern optimal control systems, an extensive "preparation of a structure for controls" process is also an essential part of the vibration control technology for flexible spacecraft. Control design involves extensive manipulation of large matrices (e.g., construction, modification, partitioning,

aggregation, algebraic operations, complex eigenanalysis, etc.) which must be carried out in a large-scale digital computer. Referencing structural dynamics data files must be done in such a way that any change in the files (due to model refinement, design modification, etc.) allows one to repeat the entire process rapidly.

5. PROGRAM CONCLUSIONS AND RECOMMENDATIONS

Section 5 PROGRAM CONCLUSIONS AND RECOMMENDATIONS

The control design and successful performance evaluation activities for the CSDL No. 2 nominal and perturbed models make it possible now to draw several important conclusions regarding the model itself and the control strategy required to address disturbance rejection for LSS. These conclusions relate to: (1) the adequacy and value of the CSDL No. 2 model as a generic test-bed for the important class of LSS control problems dealing with disturbance rejection; (2) the evaluation of the various possible control strategies in terms of the physical interpretation of what the corresponding optimal controllers actually do. These two issues will be discussed in turn.

Generic Value of the CSDL No. 2 Model. The CSDL No. 2 structural model, together with its onboard disturbances and LOS performance metric, has emerged as an excellent example of a structure embodying the essential generic characteristics of LSS according to the criteria established in Section 4.1.2. Two important characteristics need further discussion to dispel common misconceptions regarding the nature of the disturbance rejection problem and the relevance of large size models to the control synthesis for actual LSS.

The CSDL No. 2 control problem, formulated by DARPA in Phase 1A, brought to light a new class of generic LSS problems dealing with sinusoidal steady-state disturbance rejection which are different from the initial conditions/transient vibration problems addressed earlier in Phase 1. While damping augmentation (via neoclassical or modern control techniques) was adequate in that case, early and brief experimentation on CSDL No. 2 with this type of controller indicated the inadequacy of such an approach because of the structure's "stubborn refusal" to yield satisfactory performance with any reasonable robustness, control effort, or number of actuators. From the point of view of the damping augmentation approach, CSDL No. 2 may have seemed ill-designed and inadequate to represent a Control-Configured Vehicle (CCV). However, the fallacy of this notion became apparent when the basic physics of the problem was examined and the control problem reformulated to take it into account. The distinction between free oscillations and forced vibrations, which is at the core of the control design problem, was indeed well illustrated in the CSDL No. 2 model.

The second important and valuable characteristic of CSDL No. 2 is the large order of the model

coupled with the assumed parameter uncertainty - both of which constitute the central challenge in the LSS control problem. This characteristic mandates the design of reduced-order controllers because practical implementation of full-order controllers is not feasible at present, and because, even if it were, the unavoidable uncertainties in the higher modes would make it excessively parameter-sensitive. In addition, CSDL No. 2 clearly established the need for large-scale computational capability in any real application.

Insofar as modeling/fidelity issues might be raised* with the CSDL No. 2 model (i.e., lumped-mass versus extended rigid-body modeling of the mirrors, idealized plate-inertias versus box-inertias for the equipment section, etc.), the authors of this report cannot endorse any of them as meaningful technical challenges. Such changes would modify somewhat the numerical values of frequencies and modes of the open-loop model, but are of no consequence for control theory methodology and have no impact on the generic LSS control problem. By contrast, generalization of the sinusoidal disturbance model to a more complex model (specified by its power spectral density) poses a useful challenge worth resolving in Phase II. While this disturbance model change may require some refinement of the frequency-shaping technique, the important questions here concern performance reduction and the need for onboard system identification of the disturbances.

Finally, the LOS performance metric must be given as much importance in the controller design as in the structural design of an optical spacecraft. The use of the LOS in the performance index J (see Eq. 4-86) is a natural consequence of the CSDL No. 2 control problem. Actuator selection and location is based directly on the decomposition of the LOS error into nodal displacements of the structure. In general, for more complex optical systems, there will be additional optical characteristics (e.g., higher order aberrations or their Zernike polynomial representations) which need to be controlled, and it can be expected that the associated performance metrics and optical algorithms will be used in the cost functions, actuator selection, and controller designs for such systems. As a step toward establishing the purview of a yet-to-be characterized CCV

*VCOSS Kick-Off Meeting, September 29, 1981.

5. PROGRAM CONCLUSIONS AND RECOMMENDATIONS

technology, the optical and control design should be integrated as early as possible. In particular, the definition of actuators and sensors must take into account the geometries of the optical train and that of the supporting structure. After this early integration of spacecraft instrumentation for combined mission and control objectives, the more difficult questions of CCV structural re-design can be addressed.

Physical Interpretations of Control Strategies. The initial considerations in controller design stem from the control objective and the nature of the disturbance. There are several generic ways of addressing the problem, and these are summarized below:

1. Destroy the disturbance at the source
2. Lock all the structural nodes by active means
3. Lock only those nodes contributing to the LOS error
4. Lock the LOS directly by optimally modifying the motions of the contributing nodes

Method 1 involves either vibration isolation or directly opposing the disturbance by appropriate actuators at the disturbance location. This may not be feasible in practice and is outside the scope of the present study.

Method 2, which has been used with success in transient vibration suppression, is the consequence of using modal control techniques. Because all nodal displacements are linear superpositions of structural modes, strong control of the principal modes (e.g., high modal damping) will result in quieting down all the structural nodes. In the case of forced vibrations, this method may require unwarranted large

control efforts. In addition, strong performance and robustness requirements may lead to an excessive number of actuators. For CSDL No. 2, which has 51 nodes, this could involve as many as $51 \times 3 = 153$ actuators. Since the performance (LOS) depends only on 21 degrees of freedom (d.o.f.'s) distributed among 12 structural nodes, a more reasonable approach is to concentrate the control effort on these 21 d.o.f.'s. This is the basis for Method 3.

Method 3 could be envisioned as an active locking of all the optical surfaces while the rest of the structure still undergoes forced vibrations. However, since in CSDL No. 2 there are only two optical d.o.f.'s of interest (i.e., LOSX and LOSY), better use can be made of the 21 actuators required to lock the 21 nodal d.o.f.'s of the LOS.

Method 4 is the one developed in the present study, and it exploits the redundancy of the 21 actuators. In this method, the actuators do not attempt to lock the corresponding nodal d.o.f.'s. Rather, they act in such a way that the combined motions at these 21 d.o.f.'s result in a locked LOS. With such a control, the structure still appears to be vibrating while the LOS is essentially still. This seemingly complicated solution is obtained rather simply by the optimal formulation of the control problem when the cost function has been properly formulated to embody the nature of the required performance. A side benefit of the optimal control technique is the guarantee that, for a given LOS error, the actuators will not fight each other but rather will cooperate so as to minimize the total control effort. (See Note 1.)

It is important to note that the new class of frequency-shaped cost controllers designed to

Note 1. This property is very typical of optimal solutions for redundant systems of actuators. Optimal formulations provide a powerful tool for achieving concurrent objectives when the degree of redundancy is large enough. An example of this occurs in multiple CMG systems for high-torque attitude maneuvering. In the corresponding nonlinear optimal control problem, the cost functions are based on geometrical operators whose counterpart would be the optics in LSS problems such as CSDL No. 2. The optimal solution in this case produces collective motions of the CMGs satisfying two concurrent objectives: (a) the torque required for the present maneuver is being produced at the same time that, (b) the CMG cluster is reconfiguring itself optimally for the next maneuver. As in the previous case, this seemingly complicated solution is obtained relatively simply from the optimal formulation of the control problem. The analogy between the CMG and the LOS control problem arises from the redundancy of the actuation system which allows null-motions to occur. For CMGs these are collective motions which produce no torque, while for LSS they are the structural motions which leave the LOS invariant. For CSDL No. 2, where 21 actuators control a 2-d.o.f. LOS, there remains a 19-parameter family of motions available to control higher-order optical aberrations. It appears likely that (moderately) redundant actuation may become a necessary part of the generic approach for LSS forced vibration problems.

5. PROGRAM CONCLUSIONS AND RECOMMENDATIONS

address the steady-state disturbance rejection problem is still an integral part of the originally formulated two-level HAC/LAC approach. This approach combines noncollocated state-estimator implementations for high performance with colocated output feedback for spillover management. In the CSDL No. 2 problem, damping considerations are essentially absent in the HAC design (other than required for stability). The LAC design is primarily intended to

stabilize the HAC controller in its roll-off region where the HAC-unmodeled modes are also very poorly known, and, for this reason, the LAC synthesis is almost a statistical method for spillover correction. Finally, the role of the frequency shaping of the LOS cost is to put emphasis on the LOS error at the disturbance frequencies, thereby reducing the control gains and desensitizing the controller to plant parameter errors.

ACOSS Phase 1A provided the needed technical bridge between theoretical ideas developed in Phase 1 and analytical/computational sophistication and experimental verification needed to proceed to proof-of-concept level demonstration. The basic validity of combining colocated output feedback with noncollocated state-estimator mechanizations needed for high performance was established. The possibility of very high performance for certain Control-Configured Vehicle (CCV) applications was demonstrated conclusively. Finally, these methods were realized in simple hardware conceptually not unlike that required for actual space structures applications,

lending credibility to the possibility of practical implementations.

Unresolved issues still remain, however. The process of model reduction needs much refinement, both in procedural organization and in connection with system robustness evaluation. Robustness measures need further definition, and levels of achievable robustness need to be investigated. Finally, system identification methods necessary to evaluate robustness and experimental performance must be further developed and tested.

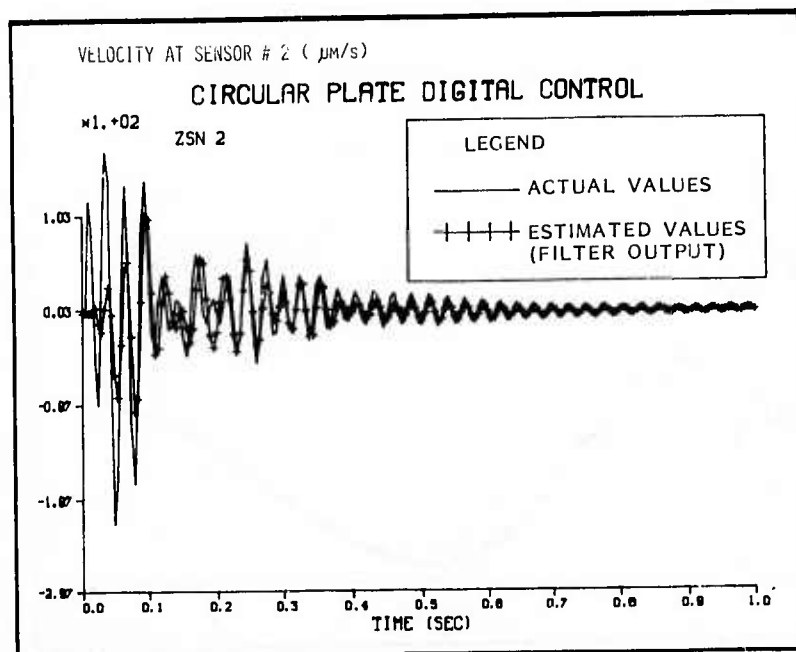
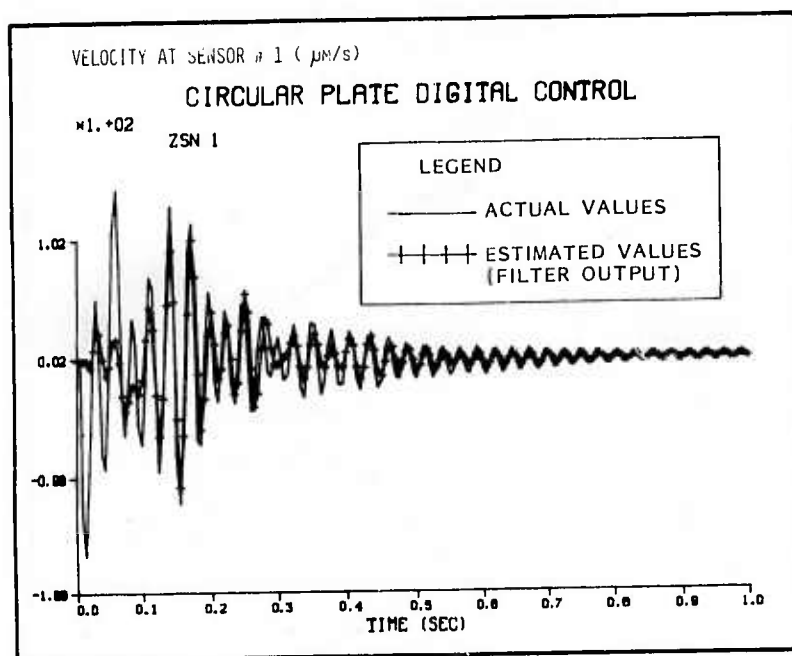
REFERENCES

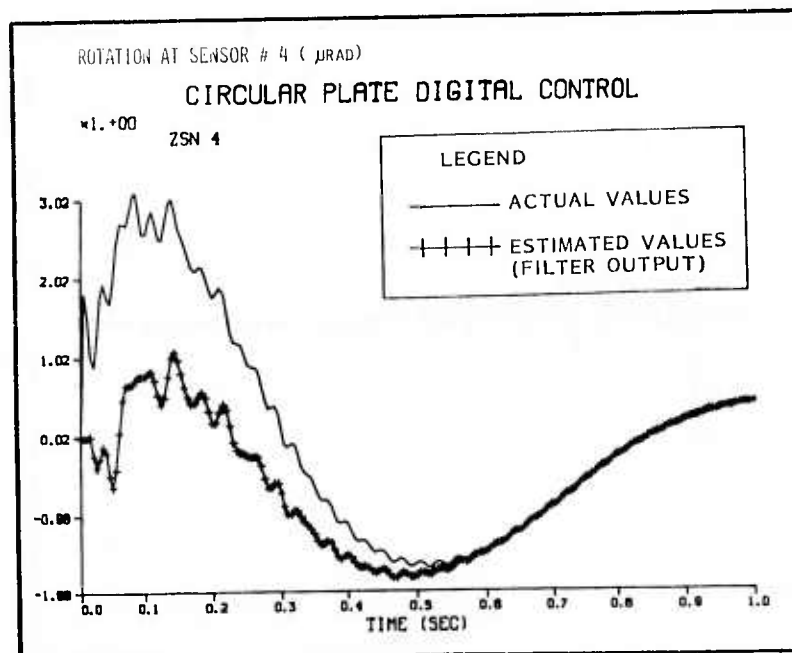
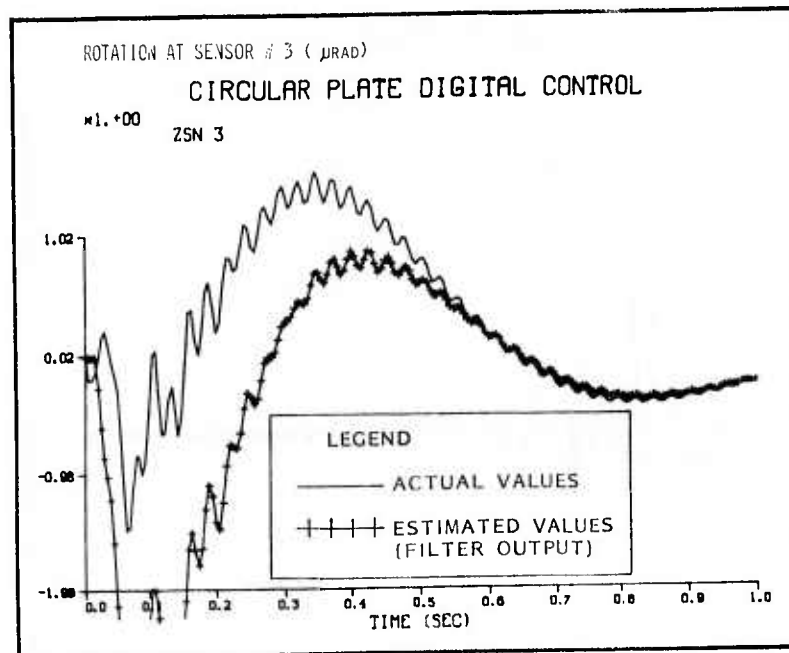
REFERENCES

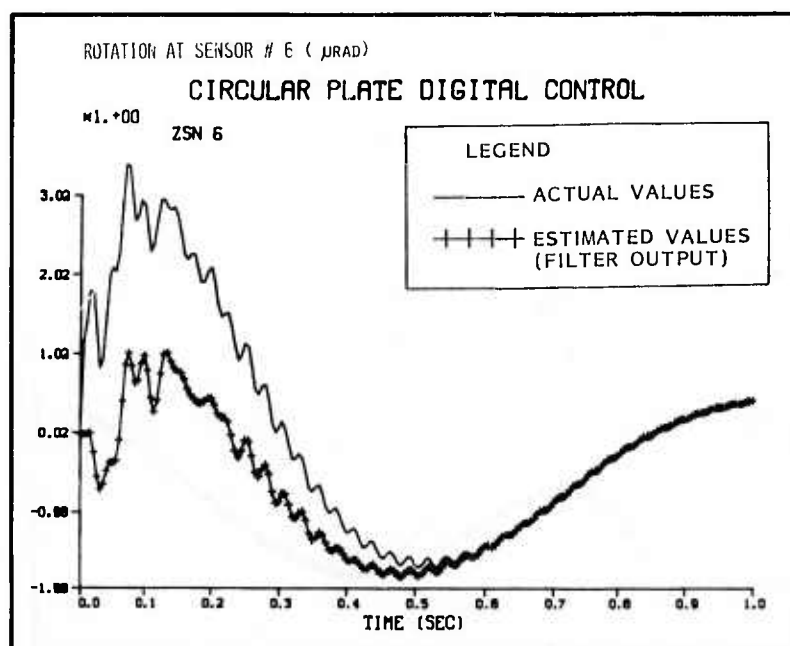
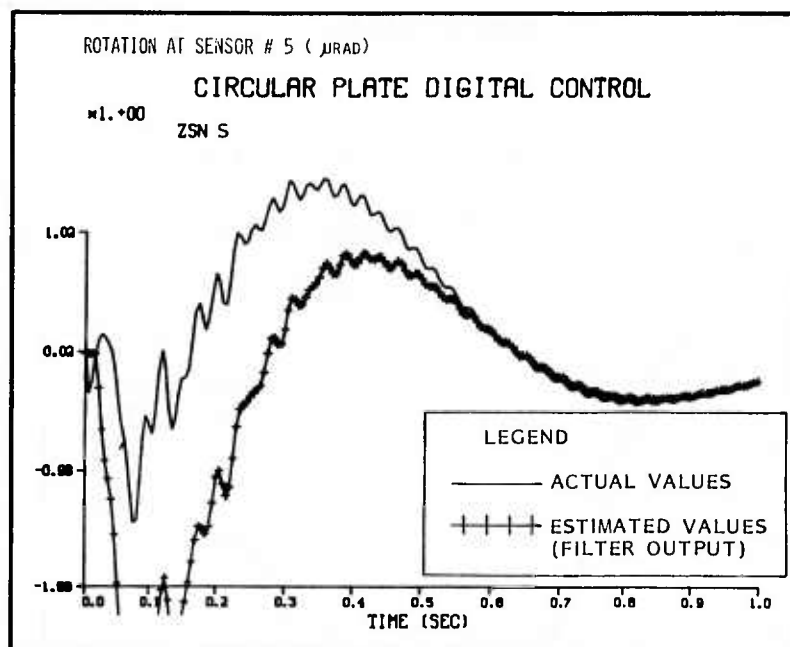
1. "ACOSS THREE (Active Control of Space Structures) Phase I," LMSC Final Technical Report, RADC-TR-80-131, May 1980.
2. M. Balas, "Modal Control of Certain Flexible Dynamic Systems," SIAM Journal of Control and Optimization, Vol. 16, 1978, pp. 450-462.
3. J. S. Przemieniecki, Theory of Matrix Structural Analysis, McGraw-Hill, New York, 1968, p. 316.
4. W. Hooker and G. Margulies, "The Dynamical Attitude Equations for an N-BODY Satellite," J. Astron. Sci., Vol. XII, 1965, pp. 123-128.
5. W. Hooker, "A Set of r Dynamical Equations for an Arbitrary Satellite Having r Rotational Degrees of Freedom," AIAA J., Vol. 8, No. 7, 1970, pp. 1205-1207.
6. "Dynamics of Spacecraft Structures, Shock and Vibration Computer Programs," SVM-10, The Shock and Vibration Information Center, United States Department of Defense, 1975, pp. 48-50, 60-61.
7. T. R. Kane and D. A. Levinson, "Formulation of Equations of Motion for Complex Spacecraft," AIAA J. of Guid. and Control, Vol. 3, No. 3, May-June 1980, pp. 234-238.
8. J.-N. Aubrun and G. Margulies, Gyrodampers for Large Space Structures, NASA Contractor Report 159171, Langley Research Center, Feb. 1979 (see Appendix A by D. A. Levinson).
9. R. E. Skelton, "Cost Decomposition of Linear Systems with Application to Model Reduction," International J. of Control, Dec. 1980.
10. C. T. Chen, Introduction to Linear System Theory, Holt, Rinehart and Winston, Inc., New York, 1970.
11. J.-N. Aubrun, N. K. Gupta, M. G. Lyons, and G. Margulies, "Large Space Structures Control: An Integrated Approach," AIAA Guidance and Control Conference Paper No. 79-1764, Boulder, CO, Aug. 6-8, 1979.
12. J.-N. Aubrun and G. Margulies, Low Authority Control Synthesis for Large Space Structures, NASA CR-3495, Langley Research Center, Jan. 1982.
13. J.-N. Aubrun, "Theory of the Control of Structures by Low-Authority Controllers," AIAA Conference on Large Space Platforms: Future Needs and Capabilities, Paper No. 78-1689, Los Angeles, CA, Sept. 1978; also in AIAA J. of Guid. and Control, Vol. 3, No. 5, 1980, pp. 444-451.
14. N. K. Gupta, "Frequency-Shaped Cost Functionals: Extensions of Linear-Quadratic-Gaussian Design Methods," AIAA J. of Guid. and Control, Vol. 3, No. 6, Nov.-Dec. 1980, pp. 529-535.
15. J.-N. Aubrun, M. G. Lyons, G. Margulies, A. Arbel, and N. K. Gupta, "Stability Augmentation for Flexible Space Structures," 18th IEEE Decision and Control Conference, Ft. Lauderdale, FL, Dec. 12-14, 1979.
16. P. C. Hughes and R. E. Skelton, "Controllability and Observability for Flexible Spacecraft," AIAA J. of Guid. and Control, Vol. 3, No. 5, Sept.-Oct. 1980, pp. 452-459.
17. R. Strunce, et al., "Active Control of Space Structures: Interim Report," Charles Stark Draper Laboratory Report R-1404, Oct. 1980.

Appendix A

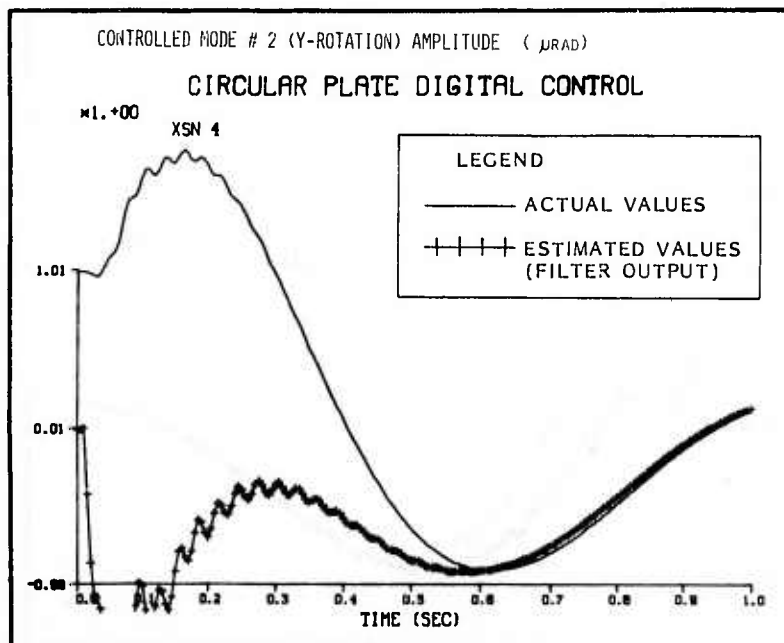
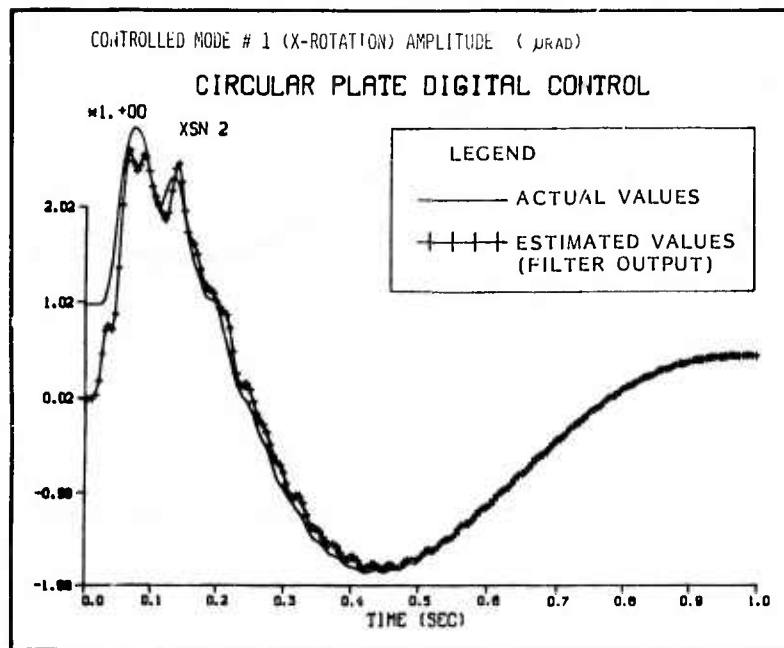
CIRCULAR PLATE EXPERIMENT - SIMULATION RESULTS

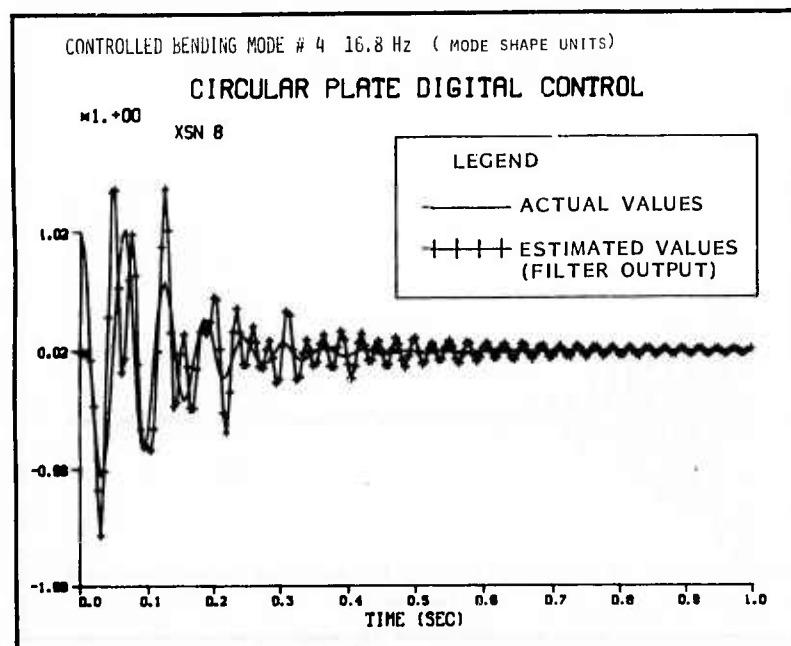
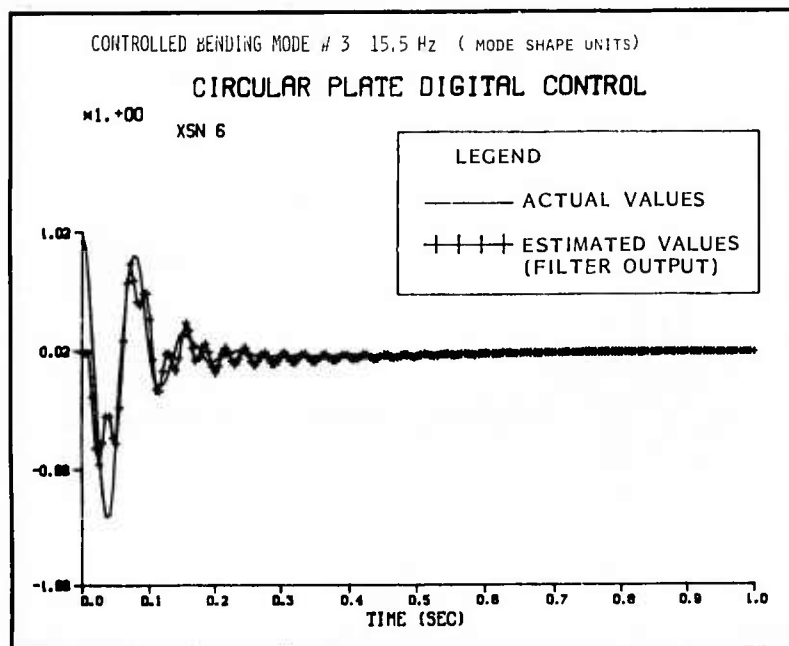
VELOCITY SENSOR OUTPUTS

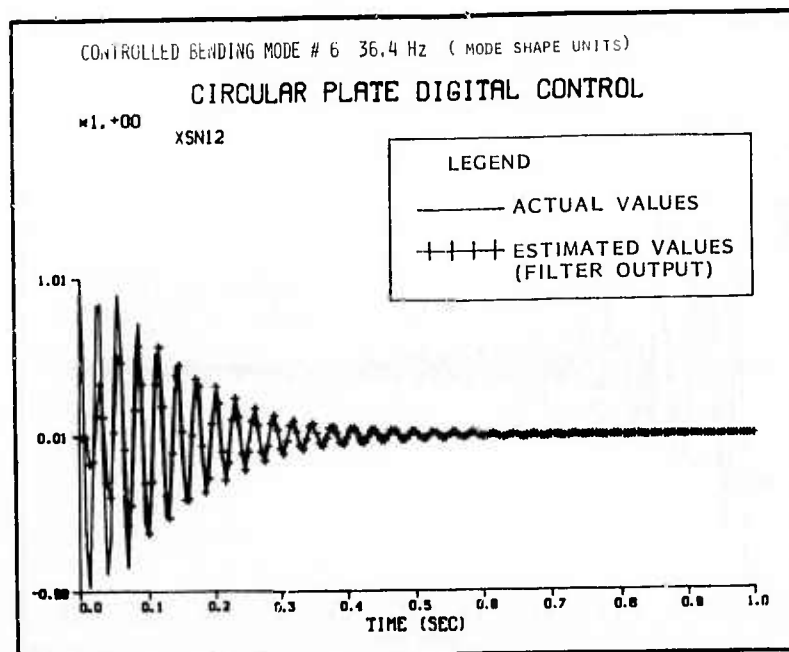
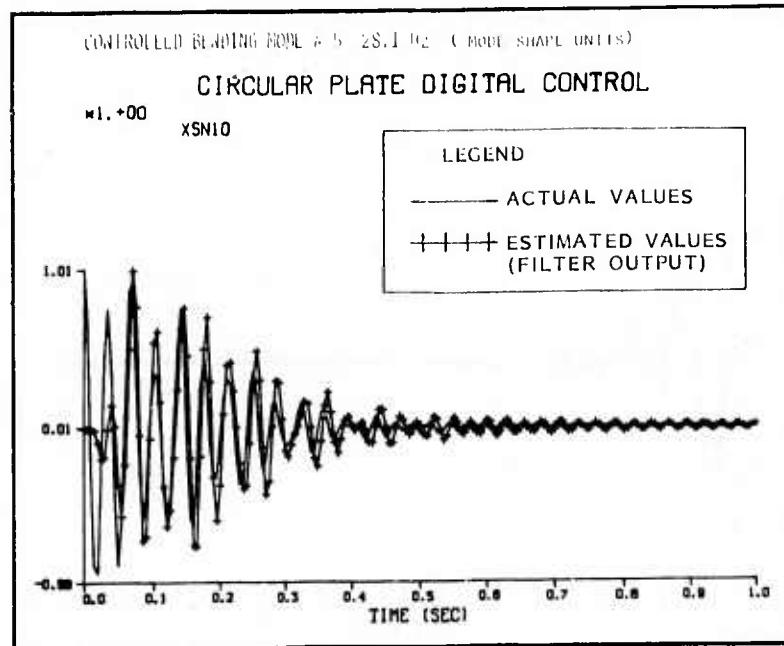
OPTICAL SENSOR OUTPUTS

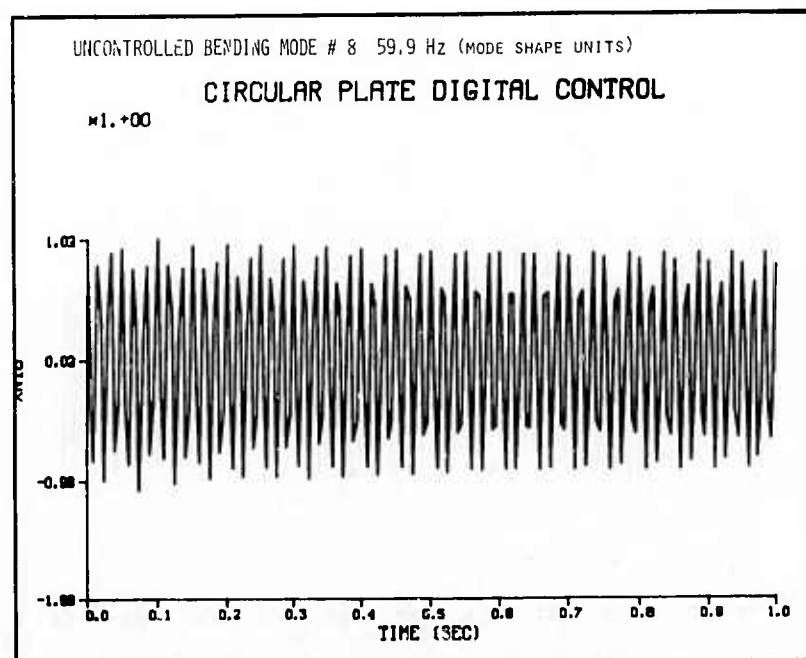
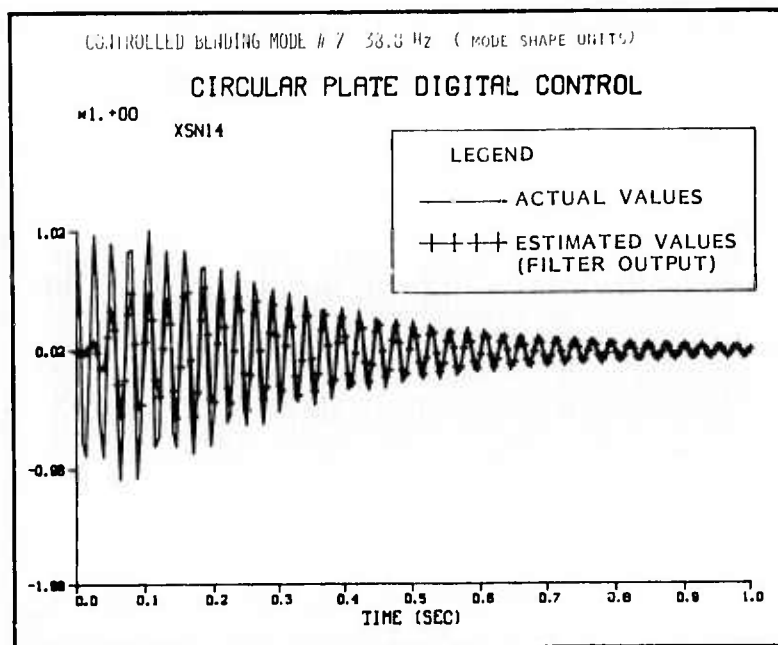


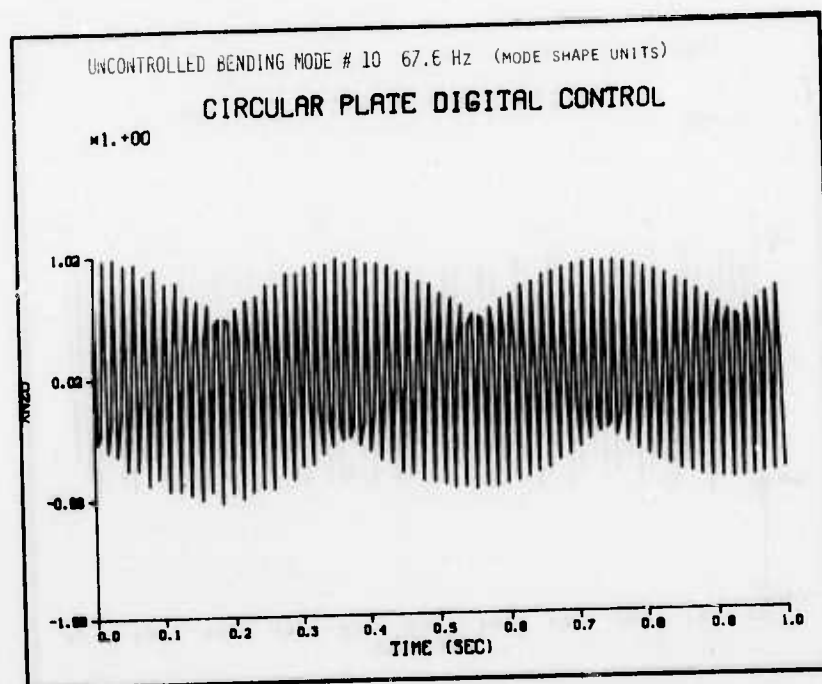
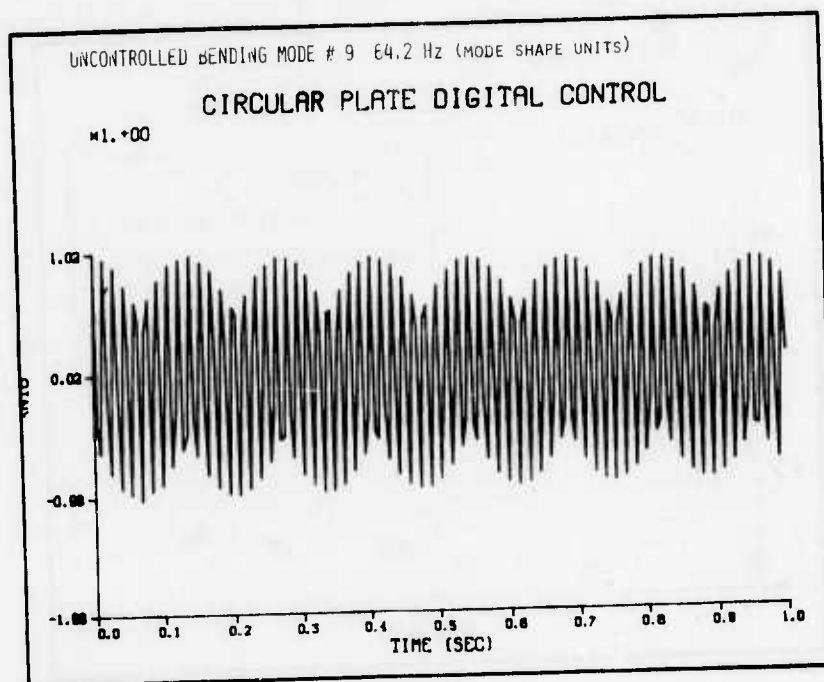
MODAL AMPLITUDES

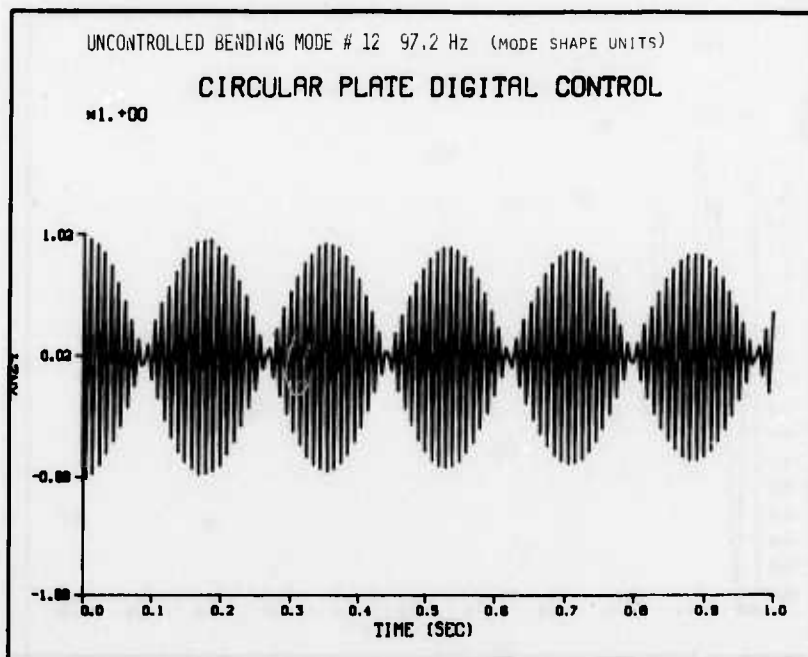
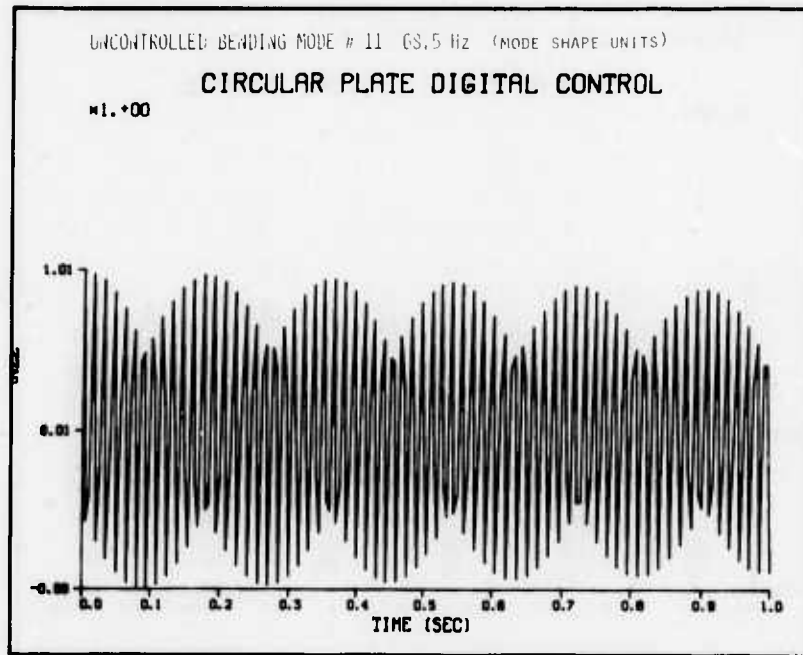


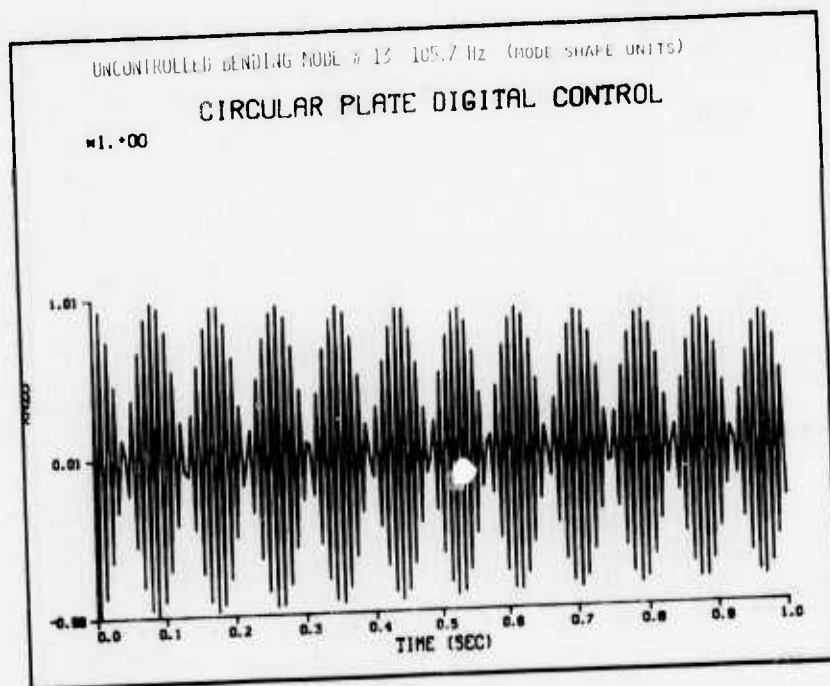
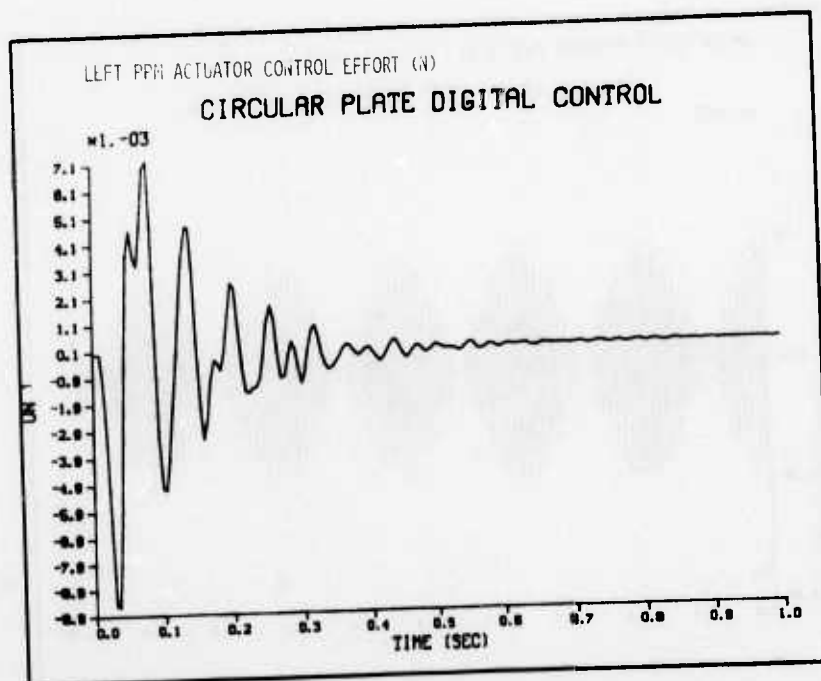


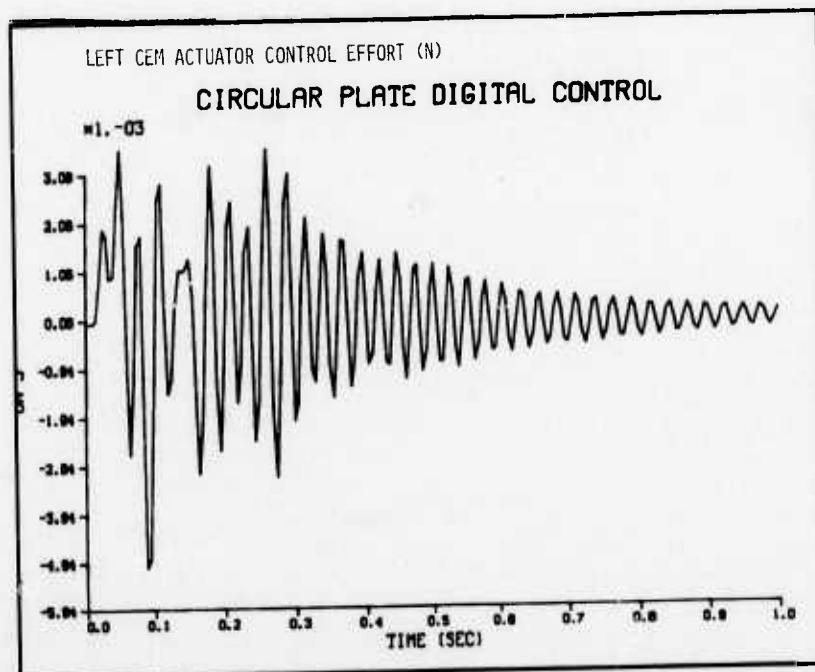
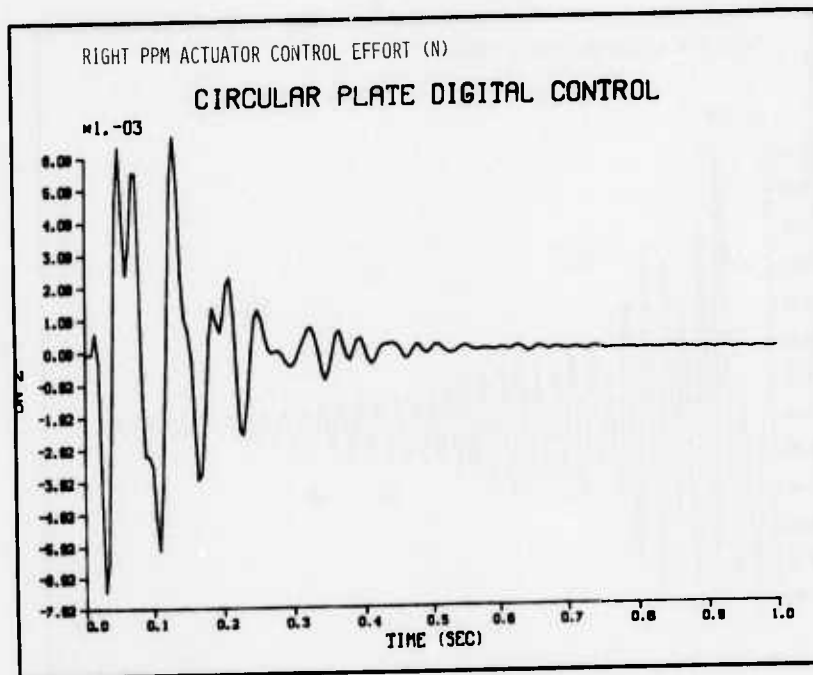


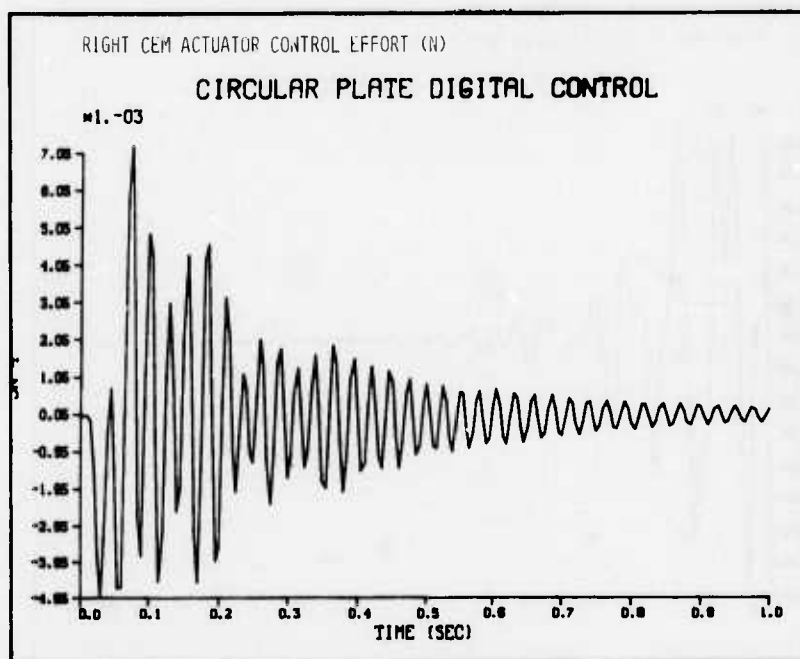






CONTROL EFFORTS





Appendix B

HAC GAIN MATRICES

 THE G MATRIX (88 BY 21)

	1	2	3	4	5	6	7	8	9	10
1	4.931E-06	3.907E-06	-4.849E-06	0	4.931E-06	3.907E-06	-4.849E-06	0	-1.258E-05	2.158E-06
2	0	0	0	0	0	0	0	0	0	0
3	-4.576E-07	3.273E-06	3.273E-06	-5.119E-06	4.576E-07	-3.273E-06	-3.273E-06	1.148E-05	-4.576E-07	3.273E-06
4	0	0	0	0	0	0	0	0	0	0
5	-7.848E-06	4.576E-07	4.576E-07	-9.400E-06	7.848E-06	-4.576E-07	-4.576E-07	-3.188E-06	-7.848E-06	4.576E-07
6	0	0	0	0	0	0	0	0	0	0
7	6.740E-05	-1.520E-03	-1.507E-03	1.946E-03	-6.628E-05	1.521E-03	1.507E-03	-6.035E-03	8.661E-05	-1.517E-03
8	0	0	0	0	0	0	0	0	0	0
9	-4.615E-03	9.353E-04	7.917E-04	-7.844E-03	4.612E-03	-9.354E-04	-7.911E-04	-1.574E-03	-4.944E-03	9.175E-04
10	0	0	0	0	0	0	0	0	0	0
11	-2.582E-04	-5.140E-03	-5.175E-03	2.359E-06	-2.581E-04	-5.140E-03	-5.175E-03	-3.486E-08	-3.288E-04	-5.152E-03
12	0	0	0	0	0	0	0	0	0	0
13	-4.927E-03	-7.887E-04	1.479E-03	1.084E-06	-4.930E-03	-7.889E-04	1.480E-03	-4.465E-09	-3.893E-04	-3.367E-04
14	0	0	0	0	0	0	0	0	0	0
15	2.786E-04	7.798E-03	7.885E-03	-7.174E-06	2.784E-04	7.798E-03	7.885E-03	1.040E-07	4.498E-04	7.831E-03
16	0	0	0	0	0	0	0	0	0	0
17	1.557E-02	2.626E-03	-4.516E-03	-6.149E-05	1.558E-02	2.607E-03	-4.546E-03	2.331E-06	1.257E-03	1.212E-03
18	0	0	0	0	0	0	0	0	0	0
19	-3.792E-04	-3.451E-03	-3.544E-03	1.705E-02	4.813E-04	3.468E-03	3.515E-03	-4.789E-04	-5.916E-04	-3.473E-03
20	0	0	0	0	0	0	0	0	0	0
21	-6.065E-05	8.113E-05	1.475E-04	4.850E-04	6.065E-05	-8.125E-05	-1.471E-04	-3.086E-04	6.402E-05	9.512E-05
22	0	0	0	0	0	0	0	0	0	0
23	1.041E-03	5.915E-04	-4.105E-04	2.902E-03	-1.041E-03	-5.880E-04	4.074E-04	-6.370E-04	-1.227E-03	4.700E-04
24	0	0	0	0	0	0	0	0	0	0
25	-1.307E-03	5.226E-04	1.456E-03	1.259E-05	-1.310E-03	5.220E-04	1.456E-03	-1.622E-07	7.509E-04	6.857E-04
26	0	0	0	0	0	0	0	0	0	0
27	1.006E-02	6.255E-03	1.399E-04	1.505E-02	-1.007E-02	-6.240E-03	-1.608E-04	-2.878E-03	-3.566E-03	5.596E-03
28	0	0	0	0	0	0	0	0	0	0
29	-2.154E-05	7.625E-05	9.212E-05	-1.265E-06	-2.101E-05	7.662E-05	9.217E-05	1.064E-07	1.469E-05	8.128E-05
30	0	0	0	0	0	0	0	0	0	0
31	1.972E-04	3.582E-05	-5.378E-05	7.511E-06	1.890E-04	2.892E-05	-5.561E-05	-1.567E-06	1.349E-05	2.022E-05
32	0	0	0	0	0	0	0	0	0	0
33	3.590E-03	-1.105E-02	-1.294E-02	-2.081E-03	-3.614E-03	1.106E-02	1.293E-02	3.545E-03	-1.746E-03	-1.169E-02
34	0	0	0	0	0	0	0	0	0	0
35	4.064E-04	-2.260E-04	-3.931E-04	-2.038E-05	4.052E-04	-2.269E-04	-3.919E-04	-7.419E-08	-2.646E-04	-2.157E-04
36	0	0	0	0	0	0	0	0	0	0
37	-9.101E-04	-7.139E-05	3.561E-04	-6.900E-04	9.149E-04	7.102E-05	-3.546E-04	-2.210E-05	4.665E-05	-2.514E-05
38	0	0	0	0	0	0	0	0	0	0
39	-1.191E-04	3.799E-04	3.925E-04	-5.232E-05	1.195E-04	-3.810E-04	-3.923E-04	-4.185E-05	4.717E-05	4.009E-04
40	0	0	0	0	0	0	0	0	0	0
41	-2.175E-08	6.695E-08	4.810E-08	-2.104E-08	2.160E-08	-6.758E-08	-4.808E-08	-1.372E-09	6.763E-09	7.306E-08
42	0	0	0	0	0	0	0	0	0	0
43	-3.331E-05	3.507E-05	1.425E-05	5.453E-06	-3.311E-05	3.532E-05	1.394E-05	8.103E-08	2.200E-05	1.707E-05
44	0	0	0	0	0	0	0	0	0	0
45	-1.035E-07	-1.706E-07	-1.795E-07	-2.069E-07	9.386E-08	1.472E-07	1.744E-07	-4.482E-08	3.625E-08	2.419E-07
46	0	0	0	0	0	0	0	0	0	0
47	1.516E-03	7.889E-03	4.343E-03	4.007E-03	-1.281E-03	-7.338E-03	-4.189E-03	1.194E-03	-7.914E-04	-2.633E-03
48	0	0	0	0	0	0	0	0	0	0
49	-4.465E-05	-1.861E-04	1.699E-05	-8.016E-06	-4.500E-05	-1.884E-04	1.508E-05	1.742E-06	2.646E-05	1.551E-05
50	0	0	0	0	0	0	0	0	0	0
51	-6.038E-03	-1.090E-02	-1.497E-03	4.897E-05	-5.972E-03	-1.119E-02	-1.527E-03	2.401E-04	3.907E-03	2.415E-03
52	0	0	0	0	0	0	0	0	0	0
53	8.393E-06	2.121E-05	2.138E-06	-8.314E-07	8.185E-06	2.135E-05	2.026E-06	-2.590E-07	-5.330E-06	6.684E-08
54	0	0	0	0	0	0	0	0	0	0
55	2.440E-05	3.144E-05	3.493E-06	1.106E-07	2.500E-05	3.297E-05	3.483E-06	-8.481E-07	-1.041E-05	-6.146E-06
56	0	0	0	0	0	0	0	0	0	0
57	5.372E-04	-5.240E-04	-2.335E-03	-5.021E-04	-3.436E-04	3.114E-03	-1.962E-03	1.504E-02	1.385E-03	-7.346E-04
58	0	0	0	0	0	0	0	0	0	0
59	2.289E-04	-6.329E-03	1.603E-02	6.933E-04	-4.007E-04	-4.286E-03	1.614E-02	1.616E-03	8.106E-04	-2.736E-03
60	0	0	0	0	0	0	0	0	0	0
61	-3.716E-05	-2.196E-04	7.538E-04	1.111E-05	4.598E-05	2.099E-04	-6.789E-04	1.130E-04	6.276E-06	-1.554E-04
62	0	0	0	0	0	0	0	0	0	0
63	1.194E-03	2.582E-03	-1.420E-02	-1.157E-04	-1.557E-03	-1.642E-03	1.154E-02	-3.402E-03	1.549E-03	3.081E-03
64	0	0	0	0	0	0	0	0	0	0
65	-7.384E-04	5.092E-03	-2.654E-03	-1.134E-03	2.178E-03	-1.116E-02	1.070E-02	6.365E-03	-1.136E-02	-8.554E-05
66	0	0	0	0	0	0	0	0	0	0
67	-1.960E-03	1.052E-02	-1.072E-02	8.840E-04	-1.494E-03	9.613E-03	-1.110E-02	1.343E-03	-1.940E-03	-2.503E-03
68	0	0	0	0	0	0	0	0	0	0
69	1.649E-03	-7.453E-03	1.057E-02	-4.347E-03	-1.711E-03	5.795E-03	-1.016E-02	-2.526E-03	3.095E-03	-2.101E-04
70	0	0	0	0	0	0	0	0	0	0
71	1.789E-03	1.262E-03	5.820E-03	2.772E-04	1.928E-03	-4.253E-03	5.633E-03	-1.052E-02	-6.118E-04	1.113E-02
72	0	0	0	0	0	0	0	0	0	0

THE G

MATRIX (88 BY 21)

	1	2	3	4	5	6	7	8	9	10
73	-2.384D-03	7.476D-03	-7.482D-03	-4.977D-04	-2.069D-03	-2.943D-03	-9.053D-03	-1.012D-02	1.032D-03	-3.130D-03
74	0	0	0	0	0	0	0	0	0	0
75	-1.850D-03	-1.538D-03	-1.191D-02	-6.748D-04	9.576D-04	4.300D-03	1.049D-02	-5.583D-03	1.898D-03	-1.037D-02
76	0	0	0	0	0	0	0	0	0	0
77	5.521D-03	-2.281D-02	2.088D-03	4.022D-04	5.093D-03	-1.861D-02	1.380D-03	-2.885D-04	-3.386D-03	-2.685D-03
78	0	0	0	0	0	0	0	0	0	0
79	1.925D-03	-2.092D-02	8.072D-03	2.882D-03	-2.530D-03	2.427D-02	-9.095D-03	-1.136D-03	-4.895D-03	2.455D-03
80	0	0	0	0	0	0	0	0	0	0
81	-1.036D-03	-4.072D-03	-5.683D-03	-6.522D-04	-1.905D-03	-8.282D-03	-1.248D-02	-2.946D-03	4.618D-04	1.608D-02
82	0	0	0	0	0	0	0	0	0	0
83	1.544D-03	8.355D-03	1.497D-02	1.306D-03	3.422D-04	-2.652D-03	-4.452D-03	-1.030D-02	-2.643D-03	-3.733D-02
84	0	0	0	0	0	0	0	0	0	0
85	1.417D-04	2.238D-03	4.727D-03	6.905D-04	1.172D-04	-3.732D-04	-3.221D-03	9.227D-03	-5.788D-04	-8.217D-03
86	0	0	0	0	0	0	0	0	0	0
87	1.238D-03	1.749D-03	7.806D-03	7.052D-04	2.541D-03	3.188D-03	7.821D-03	-7.613D-03	4.911D-03	1.226D-02
88	0	0	0	0	0	0	0	0	0	0
	11	12	13	14	15	16	17	18	19	20
1	-3.097D-06	-1.258D-05	2.156D-06	-3.097D-06	8.286D-06	8.286D-06	0	-1.258D-05	-9.227D-06	-1.258D-05
2	0	0	0	0	0	0	0	0	0	0
3	3.273D-06	4.576D-07	-3.273D-06	-3.273D-06	3.273D-06	-3.273D-06	1.296D-05	-4.576D-07	3.273D-06	4.576D-07
4	0	0	0	0	0	0	0	0	0	0
5	4.576D-07	7.848D-06	-4.576D-07	-4.576D-07	4.576D-07	-4.576D-07	2.232D-05	-7.848D-06	4.576D-07	7.848D-06
6	0	0	0	0	0	0	0	0	0	0
7	-1.510D-03	-8.696D-05	1.517D-03	1.510D-03	-1.521D-03	1.522D-03	-6.313D-03	8.542D-05	-1.504D-03	-8.536D-05
8	0	0	0	0	0	0	0	0	0	0
9	8.049D-04	4.941D-03	-9.180D-04	-8.050D-04	1.042D-03	-1.043D-03	1.452D-02	-4.945D-03	6.931D-04	4.945D-03
10	0	0	0	0	0	0	0	0	0	0
11	-5.172D-03	-3.290D-04	-5.152D-03	-5.172D-03	-5.132D-03	-5.132D-03	2.594D-07	-3.289D-04	-5.195D-03	-3.290D-04
12	0	0	0	0	0	0	0	0	0	0
13	1.026D-03	-3.896D-04	-3.366D-04	1.027D-03	-1.928D-03	-1.929D-03	-3.986D-07	-3.892D-04	2.617D-03	-3.894D-04
14	0	0	0	0	0	0	0	0	0	0
15	7.879D-03	4.502D-04	7.831D-03	7.879D-03	7.786D-03	7.786D-03	-5.702D-07	4.501D-04	7.933D-03	4.504D-04
16	0	0	0	0	0	0	0	0	0	0
17	-3.095D-03	1.250D-03	1.190D-03	-3.124D-03	6.249D-03	6.236D-03	-1.037D-05	1.256D-03	-8.125D-03	1.248D-03
18	0	0	0	0	0	0	0	0	0	0
19	-3.540D-03	5.986D-04	3.481D-03	3.519D-03	-3.405D-03	3.446D-03	1.473D-03	-5.928D-04	-3.611D-03	6.008D-04
20	0	0	0	0	0	0	0	0	0	0
21	1.417D-04	-6.462D-05	-9.552D-05	-1.408D-04	6.075D-05	-6.123D-05	-5.088D-04	5.993D-05	1.824D-04	-5.937D-05
22	0	0	0	0	0	0	0	0	0	0
23	-3.139D-04	1.214D-03	-4.719D-04	3.093D-04	1.359D-03	-1.356D-03	3.566D-03	-1.241D-03	-1.100D-03	1.242D-03
24	0	0	0	0	0	0	0	0	0	0
25	1.313D-03	7.492D-04	6.854D-04	1.313D-03	-4.694D-05	-4.880D-05	1.111D-07	7.545D-04	2.054D-03	7.542D-04
26	0	0	0	0	0	0	0	0	0	0
27	8.348D-04	3.482D-03	-5.614D-03	-8.592D-04	1.120D-02	-1.118D-02	1.006D-02	-3.670D-03	-3.982D-03	3.680D-03
28	0	0	0	0	0	0	0	0	0	0
29	9.188D-05	1.452D-05	8.164D-05	9.197D-05	7.055D-05	7.113D-05	-3.752D-07	1.484D-05	1.041D-04	1.468D-05
30	0	0	0	0	0	0	0	0	0	0
31	-3.712D-05	1.675D-05	1.362D-05	-3.955D-05	8.797D-05	7.721D-05	4.315D-06	1.329D-05	-1.043D-04	1.663D-05
32	0	0	0	0	0	0	0	0	0	0
33	-1.365D-02	1.752D-03	1.171D-02	1.361D-02	-1.074D-02	1.073D-02	9.011D-03	-1.582D-03	-1.535D-02	1.541D-03
34	0	0	0	0	0	0	0	0	0	0
35	-4.356D-04	-2.607D-04	-2.166D-04	-4.344D-04	4.295D-05	4.231D-05	1.218D-06	-2.709D-04	-7.068D-04	-2.695D-04
36	0	0	0	0	0	0	0	0	0	0
37	3.355D-04	-4.233D-05	2.556D-05	-3.333D-04	-4.294D-04	4.289D-04	-2.385D-04	4.800D-05	6.967D-04	-4.853D-05
38	0	0	0	0	0	0	0	0	0	0
39	4.587D-04	-4.609D-05	-4.019D-04	-4.568D-04	3.927D-04	-3.920D-04	-2.007D-04	4.393D-05	5.086D-04	-4.210D-05
40	0	0	0	0	0	0	0	0	0	0
41	7.989D-08	-5.967D-09	-7.332D-08	-7.938D-08	8.593D-08	-8.536D-08	-3.024D-08	7.054D-09	8.408D-08	-6.309D-09
42	0	0	0	0	0	0	0	0	0	0
43	4.037D-05	2.081D-05	1.731D-05	4.067D-05	-1.199D-05	-1.179D-05	-3.293D-07	2.388D-05	7.190D-05	2.344D-05
44	0	0	0	0	0	0	0	0	0	0
45	-3.336D-08	-2.489D-08	-2.386D-07	2.989D-08	1.055D-06	-1.023D-06	-1.971D-07	3.047D-06	-5.390D-07	9.668D-06
46	0	0	0	0	0	0	0	0	0	0
47	4.835D-03	6.128D-04	2.515D-03	-4.675D-03	-2.206D-02	2.125D-02	3.407D-03	-5.008D-04	1.809D-02	-2.508D-04
48	0	0	0	0	0	0	0	0	0	0
49	-7.362D-05	3.944D-05	1.816D-05	-7.555D-05	2.472D-04	2.648D-04	-2.494D-06	2.051D-05	-2.373D-04	2.241D-05
50	0	0	0	0	0	0	0	0	0	0
51	-3.075D-03	4.580D-03	2.568D-03	-3.059D-03	2.023D-02	2.074D-02	-5.153D-04	3.629D-03	-1.440D-02	3.638D-03
52	0	0	0	0	0	0	0	0	0	0
53	1.045D-05	-6.394D-06	-5.448D-08	1.024D-05	-2.890D-05	-2.890D-05	6.377D-07	-4.556D-06	3.031D-05	-4.534D-06
54	0	0	0	0	0	0	0	0	0	0

APPENDIX B

 THE G MATRIX (88 BY 21)

	11	12	13	14	15	16	17	18	19	20	
55	6.468E-06	-1.234E-05	-6.645E-06	6.617E-06	-5.339E-05	-5.563E-05	1.726E-06	-9.787E-06	3.550E-05	-9.753E-06	
56	0	0	0	0	0	0	0	0	0	0	
57	2.433E-03	-3.810E-03	-5.931E-04	1.312E-03	1.076E-03	-2.064E-03	-1.777E-02	6.496E-03	9.527E-04	-5.113E-03	
58	0	0	0	0	0	0	0	0	0	0	
59	-8.906E-03	-2.902E-03	-2.503E-03	-1.109E-02	1.656E-03	1.541E-03	2.402E-05	4.543E-04	-5.222E-03	-3.976E-03	
60	0	0	0	0	0	0	0	0	0	0	
61	-5.591E-04	-1.564E-05	1.309E-04	5.314E-04	1.300E-04	-1.384E-04	-1.563E-05	-2.946E-05	-3.067E-04	1.121E-05	
62	0	0	0	0	0	0	0	0	0	0	
63	1.159E-02	-1.892E-03	-2.386E-03	-1.115E-02	-3.348E-03	3.613E-03	2.704E-03	2.031E-03	4.639E-03	-1.725E-03	
64	0	0	0	0	0	0	0	0	0	0	
65	-2.087E-03	1.473E-02	-7.641E-04	2.832E-03	1.691E-03	-1.968E-03	-1.563E-02	-1.036E-02	-5.407E-03	1.139E-02	
66	0	0	0	0	0	0	0	0	0	0	
67	-2.991E-03	1.136E-03	-6.766E-04	-2.604E-03	-9.204E-04	-3.665E-03	-8.405E-04	-6.176E-04	1.012E-02	3.201E-03	
68	0	0	0	0	0	0	0	0	0	0	
69	-1.406E-03	-3.691E-03	-1.235E-04	-3.204E-04	5.262E-03	-2.199E-03	1.492E-03	1.244E-03	-1.592E-02	-6.043E-04	
70	0	0	0	0	0	0	0	0	0	0	
71	4.871E-03	-3.971E-03	4.195E-03	8.797E-03	-1.381E-02	-7.686E-03	-5.180E-03	8.284E-04	-1.661E-02	-4.628E-04	
72	0	0	0	0	0	0	0	0	0	0	
73	-9.753E-03	-8.335E-04	-1.024E-02	-6.617E-03	5.999E-03	1.471E-02	-5.922E-03	3.444E-03	8.834E-03	3.683E-03	
74	0	0	0	0	0	0	0	0	0	0	
75	-9.154E-03	-2.286E-03	9.347E-03	7.448E-03	1.369E-02	-1.246E-02	-6.123E-05	3.030E-03	2.620E-02	-1.972E-03	
76	0	0	0	0	0	0	0	0	0	0	
77	7.434E-03	-4.507E-03	-1.249E-03	6.551E-03	2.551E-03	1.429E-03	4.969E-04	-2.145E-03	2.901E-02	-2.810E-03	
78	0	0	0	0	0	0	0	0	0	0	
79	6.875E-03	6.657E-03	-3.245E-03	-8.581E-03	-1.214E-03	1.664E-03	-3.618E-03	-3.610E-03	1.296E-02	6.379E-03	
80	0	0	0	0	0	0	0	0	0	0	
81	-7.603E-04	2.131E-04	3.905E-02	-6.677E-03	-1.909E-03	-4.554E-03	-1.748E-04	2.529E-03	2.554E-04	7.605E-03	
82	0	0	0	0	0	0	0	0	0	0	
83	3.279E-03	1.565E-05	1.389E-02	-3.592E-03	3.591E-03	-1.385E-03	6.000E-06	1.742E-03	-1.839E-03	4.297E-03	
84	0	0	0	0	0	0	0	0	0	0	
85	-3.462E-03	2.070E-03	5.730E-03	2.184E-04	6.620E-04	-3.486E-04	3.751E-04	6.370E-03	2.286E-03	4.923E-03	
86	0	0	0	0	0	0	0	0	0	0	
87	-2.933E-02	3.532E-04	-1.840E-04	-1.806E-02	-2.933E-03	-1.080E-03	-2.084E-04	9.928E-03	1.273E-02	-5.094E-04	
88	0	0	0	0	0	0	0	0	0	0	

	21	
1	-9.227E-06	
2	0	
3	-3.273E-06	
4	0	
5	-4.576E-07	
6	0	
7	1.503E-03	
8	0	
9	-6.904E-04	
10	0	
11	-5.195E-03	
12	0	
13	2.618E-03	
14	0	
15	7.933E-03	
16	0	
17	-8.162E-03	
18	0	
19	3.558E-03	
20	0	
21	-1.824E-04	
22	0	
23	1.107E-03	
24	0	
25	2.055E-03	
26	0	
27	4.023E-03	
28	0	
29	1.040E-04	
30	0	
31	-1.026E-04	
32	0	
33	1.537E-02	
34	0	
35	-7.063E-04	
36	0	

 THE G MATRIX (88 BY 21)

	21
37	-7.0160-04
38	0
39	-5.0960-04
40	0
41	-8.4370-08
42	0
43	7.1810-05
44	0
45	5.3420-07
46	0
47	-1.7970-02
48	0
49	-2.5540-04
50	0
51	-1.5120-02
52	0
53	3.0830-05
54	0
55	3.8120-05
56	0
57	7.2780-04
58	0
59	-6.0670-03
60	0
61	2.7150-04
62	0
63	-3.4440-03
64	0
65	2.2210-03
66	0
67	1.5440-02
68	0
69	1.5520-02
70	0
71	-7.8020-03
72	0
73	1.9430-02
74	0
75	-2.7170-02
76	0
77	2.4020-02
78	0
79	-1.4680-02
80	0
81	1.4910-03
82	0
83	1.0190-03
84	0
85	-9.1280-04
86	0
87	7.5990-03
88	0

APPENDIX B

THE M MATRIX (3 BY 88)

1	2	3	4	5	6	7	8	9	10
0	1.000E+00	0	0	0	0	0	-2.577E-07	0	3.527E-07
0	0	0	1.000E+00	0	0	0	3.254E-04	0	-2.141E-04
0	0	0	0	0	1.000E+00	0	0	0	0
11	12	13	14	15	16	17	18	19	20
0	-1.291E-06	0	-2.290E-04	0	6.019E-06	0	7.361E-04	0	2.416E-06
0	-3.468E-07	0	4.425E-07	0	1.066E-06	0	-6.868E-06	0	8.731E-04
0	0	0	0	0	0	0	0	0	0
21	22	23	24	25	26	27	28	29	30
0	-1.021E-06	0	3.749E-06	0	-1.590E-04	0	2.738E-05	0	-9.646E-07
0	-2.360E-04	0	-1.517E-04	0	-1.404E-06	0	-2.775E-03	0	2.413E-07
0	0	0	0	0	0	0	0	0	0
31	32	33	34	35	36	37	38	39	40
0	1.174E-05	0	2.212E-05	0	1.345E-04	0	-4.340E-06	0	5.610E-07
0	-2.402E-06	0	1.376E-02	0	2.734E-06	0	-2.605E-04	0	-4.542E-04
0	0	0	0	0	0	0	0	0	0
41	42	43	44	45	46	47	48	49	50
0	7.711E-10	0	-3.388E-05	0	2.015E-08	0	-4.273E-04	0	2.830E-04
0	-8.610E-08	0	-7.001E-07	0	-1.359E-07	0	-1.703E-03	0	4.642E-07
0	0	0	0	0	0	0	0	0	0
51	52	53	54	55	56	57	58	59	60
0	1.867E-02	0	-3.145E-05	0	-5.243E-05	0	-1.227E-03	0	1.099E-02
0	-1.139E-05	0	1.580E-07	0	-2.438E-07	0	1.871E-03	0	-5.653E-04
0	0	0	0	0	0	0	0	0	0
61	62	63	64	65	66	67	68	69	70
0	7.772E-06	0	-7.094E-04	0	3.953E-03	0	-1.415E-02	0	1.905E-03
0	5.207E-04	0	-1.012E-02	0	5.953E-03	0	3.209E-03	0	1.045E-02
0	0	0	0	0	0	0	0	0	0
71	72	73	74	75	76	77	78	79	80
0	-6.819E-03	0	3.838E-03	0	1.150E-04	0	3.236E-03	0	-6.416E-04
0	-2.198E-03	0	-9.420E-04	0	-8.405E-03	0	-1.168E-03	0	-1.446E-02
0	0	0	0	0	0	0	0	0	0
81	82	83	84	85	86	87	88		
0	-2.266E-02	0	9.029E-03	0	2.627E-04	0	-1.447E-02		
0	1.665E-02	0	3.714E-02	0	1.202E-02	0	-1.040E-02		
0	0	0	0	0	0	0	0		

 THE K MATRIX (24 BY 3)

	1	2	3
1	4.472D-02	1.957D-06	1.221D-16
2	3.005D-01	-2.469D-05	5.248D-16
3	-1.957D-06	4.472D-02	2.604D-16
4	-5.284D-05	3.429D-01	4.551D-15
5	-3.207D-17	2.754D-18	4.472D-02
6	-5.465D-17	-1.893D-17	2.991D-01
7	-5.122D-01	7.158D+02	6.609D-12
8	-1.143D+00	1.327D+03	1.311D-12
9	1.655D+02	-1.663D+00	1.321D-11
10	3.770D+02	-2.153D+00	-8.417D-13
11	4.579D-01	3.118D+02	1.844D-12
12	2.127D+00	3.689D+02	-4.233D-13
13	1.390D+00	1.364D+01	-6.376D-13
14	1.249D+00	-1.230D+02	-1.143D-13
15	-6.004D-01	2.268D+02	1.273D-13
16	1.604D-01	9.177D+01	-7.497D-14
17	5.336D+00	9.712D-01	-4.154D-11
18	9.972D+00	1.928D-01	-2.809D-12
19	5.433D-02	-8.481D+01	-1.527D-12
20	2.542D-02	-2.072D+01	-5.675D-13
21	4.285D+00	-1.736D+01	9.050D-13
22	-1.517D+00	-6.078D+00	3.546D-13
23	1.655D+01	4.325D-01	2.942D-13
24	2.111D+01	-1.443D-02	9.743D-15

APPENDIX B

THE C MATRIX (21 BY 32)

	1	2	3	4	5	6	7	8	9	10
1	-2.580D+03	1.162D+04	-1.734D+03	-2.917D+03	3.581D+03	6.109D+02	-5.933D-02	-9.349D-01	-2.357D+00	8.860D+00
2	-2.419D+03	2.183D+04	-1.168D+03	1.486D+04	6.027D+02	5.209D+01	7.060D-01	5.053D+00	-1.014D+00	1.625D+01
3	1.860D+03	3.596D+03	-1.116D+03	1.615D+04	6.108D+02	5.309D+01	7.281D-01	5.479D+00	5.216D-01	2.316D+00
4	-1.092D+01	1.552D+01	2.790D+03	4.799D+03	3.131D+03	6.051D+02	-2.740D-02	1.275D+00	5.739D-03	-1.066D-02
5	-2.559D+03	1.141D+04	1.738D+03	2.913D+03	-3.581D+03	-6.109D+02	6.128D-02	9.274D-01	-2.376D+00	8.672D+00
6	-2.405D+03	2.195D+04	1.168D+03	-1.494D+04	-6.024D+02	-5.206D+01	-7.049D-01	-5.088D+00	-9.757D-01	1.656D+01
7	1.874D+03	3.393D+03	1.116D+03	-1.615D+04	-6.107D+02	-5.308D+01	-7.279D-01	-5.481D+00	5.629D-01	2.401D+00
8	1.654D+01	-4.459D+02	-1.161D+04	-5.897D+03	4.415D+03	5.701D+02	5.519D-01	-1.130D+00	1.618D-02	-3.026D-01
9	5.308D+03	-6.872D+03	-1.443D+03	1.639D+03	3.600D+03	6.132D+02	4.989D-02	5.569D-01	1.819D-01	-5.699D+00
10	-6.873D+02	-5.140D+03	-1.165D+03	1.502D+04	6.022D+02	5.200D+01	7.057D-01	5.110D+00	-4.963D-02	-3.816D+00
11	1.028D+03	6.630D+03	-1.003D+03	1.717D+04	6.099D+02	5.295D+01	7.646D-01	5.809D+00	2.323D-01	4.639D+00
12	5.352D+03	-8.193D+03	1.439D+03	-1.633D+03	-3.600D+03	-6.132D+02	-5.142D-02	-5.504D-01	2.187D-01	-6.654D+00
13	-6.835D+02	-5.274D+03	1.161D+03	-1.503D+04	-6.023D+02	-5.201D+01	-7.071D-01	-5.113D+00	-1.755D-02	-3.693D+00
14	1.048D+03	6.306D+03	1.008D+03	-1.713D+04	-6.097D+02	-5.293D+01	-7.628D-01	-5.801D+00	2.793D-01	4.649D+00
15	-1.813D+03	-4.217D+04	-1.245D+03	1.360D+04	5.917D+02	5.066D+01	6.702D-01	4.658D+00	2.767D-01	-3.095D+01
16	-1.857D+03	-4.183D+04	1.246D+03	-1.347D+04	-5.925D+02	-5.073D+01	-6.718D-01	-4.594D+00	2.735D-01	-3.049D+01
17	-5.080D+01	1.128D+03	-6.860D+03	-1.074D+04	-7.288D+03	-1.423D+03	4.070D-01	-2.776D+00	-2.888D-02	8.990D-01
18	5.287D+03	-6.301D+03	-1.465D+03	1.435D+03	3.600D+03	6.132D+02	4.301D-02	4.903D-01	1.661D-01	-5.275D+00
19	2.652D+03	3.040D+04	-8.417D+02	1.929D+04	6.184D+02	5.401D+01	8.243D-01	6.496D+00	2.776D-01	2.194D+01
20	5.283D+03	-6.322D+03	1.466D+03	-1.396D+03	-3.600D+03	-6.133D+02	-4.311D-02	-4.738D-01	1.669D-01	-5.270D+00
21	2.668D+03	3.073D+04	8.369D+02	-1.943D+04	-6.179D+02	-5.397D+01	-8.246D-01	-6.556D+00	3.242D-01	2.247D+01
	11	12	13	14	15	16	17	18	19	20
1	-1.043D-01	-2.397D+00	-3.533D+00	1.231D+01	-9.626D+00	-5.765D+01	-1.596D-01	2.186D+00	1.959D-01	5.572D-01
2	2.061D+00	1.376D+01	-8.116D+00	-5.464D+01	4.716D+01	2.007D+02	-2.042D-01	3.883D+00	-1.369D+00	-1.879D+00
3	2.144D+00	1.482D+01	-5.788D+00	-6.099D+01	5.172D+01	2.306D+02	5.867D-03	5.203D-01	-1.388D+00	-2.154D+00
4	-2.717D+00	3.786D+00	-8.286D+00	-1.539D+01	1.377D+01	3.041D+01	3.405D-04	7.640D-03	-4.165D-01	-9.685D-02
5	1.053D-01	2.435D+00	3.482D+00	-1.159D+01	9.726D+00	5.824D+01	-1.529D-01	2.146D+00	-2.018D-01	-5.224D-01
6	-2.063D+00	-1.372D+01	8.049D+00	5.617D+01	-4.719D+01	-2.005D+02	-2.159D-01	3.886D+00	1.306D+00	1.945D+00
7	-2.144D+00	-1.481D+01	5.795D+00	6.115D+01	-5.170D+01	-2.304D+02	-6.545D-03	4.712D-01	1.388D+00	2.158D+00
8	-4.389D-01	-3.419D+00	3.238D+00	1.470D+01	-1.636D+01	-4.009D+01	1.378D-03	-7.582D-02	4.625D-01	-1.884D-01
9	2.391D-01	1.511D+00	1.040D+00	-7.237D+00	5.434D+00	3.382D+01	1.053D-01	-1.416D+00	-1.260D-01	-3.995D-01
10	2.069D+00	1.383D+01	-7.864D+00	-5.644D+01	4.863D+01	2.017D+02	4.653D-02	-8.423D-01	-1.348D+00	-1.613D+00
11	2.241D+00	1.574D+01	-6.463D+00	-6.453D+01	5.490D+01	2.433D+02	-2.874D-02	1.086D+00	-1.484D+00	-2.258D+00
12	-2.401D-01	-1.550D+00	-9.629D-01	6.717D+00	-5.488D+00	-3.403D+01	1.145D-01	-1.646D+00	1.299D-01	3.725D-01
13	-2.071D+00	-1.388D+01	7.894D+00	5.623D+01	-4.874D+01	-2.022D+02	3.257D-02	-8.750D-01	1.351D+00	1.602D+00
14	-2.237D+00	-1.567D+01	6.445D+00	6.474D+01	-5.473D+01	-2.424D+02	-4.094D-02	1.015D+00	1.479D+00	2.268D+00
15	1.964D+00	1.253D+01	-9.903D+00	-5.209D+01	4.582D+01	1.658D+02	3.444D-01	-7.141D+00	-1.315D+00	-6.639D-01
16	-1.959D+00	-1.262D+01	9.987D+00	4.931D+01	-4.580D+01	-1.663D+02	3.205D-01	-7.077D+00	1.321D+00	5.405D-01
17	-1.167D+00	-7.955D+00	-8.595D-01	3.594D+01	-3.261D+01	-1.470D+02	-1.659D-02	1.969D-01	8.309D-01	1.072D+00
18	2.203D-01	1.331D+00	1.158D+00	-6.470D+00	4.758D+00	3.131D+01	1.002D-01	-1.317D+00	-1.074D-01	-3.886D-01
19	2.414D+00	1.765D+01	-5.028D+00	-7.200D+01	6.055D+01	2.859D+02	-2.072D-01	5.082D+00	-1.602D+00	-3.077D+00
20	-2.177D-01	-1.334D+00	-1.143D+00	5.890D+00	-4.636D+00	-3.130D+01	9.825D-02	-1.321D+00	1.056D-01	3.844D-01
21	-2.421D+00	-1.761D+01	4.963D+00	7.455D+01	-6.065D+01	-2.863D+02	-2.223D-01	5.114D+00	1.660D+00	3.187D+00
	21	22	23	24	25	26	27	28	29	30
1	-9.419D-01	-1.566D+01	4.146D+01	2.652D+02	-3.533D+07	2.939D+06	-8.245D+05	1.424D+05	-2.964D+06	2.004D+06
2	-4.127D+00	-3.117D+01	7.347D+01	4.102D+02	-6.386D+07	-1.970D+07	-1.578D+06	-2.025D+06	-5.839D+06	-1.019D+07
3	-2.260D+00	-5.734D+00	9.724D+00	2.999D+01	-8.968D+06	-2.035D+07	-2.544D+05	-1.959D+06	-9.844D+05	-1.123D+07
4	-1.367D+00	7.939D-01	1.195D-01	-6.631D+00	-6.658D+04	-6.082D+06	-4.289D+03	-7.757D+05	1.264D+03	-2.848D+06
5	-4.318D-01	-1.773D+01	4.068D+01	2.643D+02	-3.468D+07	-2.805D+06	-8.082D+05	-1.466D+05	-2.922D+06	-2.033D+06
6	1.679D+00	-2.868D+01	7.383D+01	4.444D+02	-6.425D+07	1.969D+07	-1.572D+06	2.021D+06	-5.867D+06	1.019D+07
7	1.943D+00	-1.811D+00	9.080D+00	4.625D+01	-8.430D+06	2.037D+07	-2.312D+05	1.955D+06	-9.183D+05	1.122D+07
8	9.137D-02	-1.775D-01	-1.467D+00	-1.058D+01	1.282D+06	5.331D+06	3.051D+04	5.885D+05	1.195D+05	3.056D+06
9	5.488D-01	1.042D+01	-2.687D+01	-1.700D+02	2.275D+07	-1.980D+06	5.311D+05	-1.157D+05	1.933D+06	-1.269D+06
10	-7.685D-02	5.739D+00	-1.606D+01	-8.101D+01	1.422D+07	-1.804D+07	3.660D+05	-1.615D+06	1.375D+06	-1.068D+07
11	-2.622D+00	-1.015D+01	2.045D+01	9.478D+01	-1.818D+07	-2.163D+07	-4.751D+05	-2.097D+06	-1.792D+06	-1.191D+07
12	4.257D-01	1.320D+01	-3.116D+01	-1.960D+02	2.652D+07	1.888D+06	6.245D+05	1.192D+05	2.295D+06	1.286D+06
13	6.119D-01	7.461D+00	-1.653D+01	-9.301D+01	1.454D+07	1.801D+07	3.706D+05	1.620D+06	1.402D+06	1.071D+07
14	1.967D+00	-5.970D+00	1.940D+01	1.108D+02	-1.729D+07	2.165D+07	-4.423D+05	2.090D+06	-1.694D+06	1.187D+07
15	6.727D+00	5.597D+01	-1.354D+02	-6.991D+02	1.190D+08	-1.361D+07	3.026D+06	-7.446D+05	1.131D+07	-1.039D+07
16	-2.337D+00	5.335D+01	-1.343D+02	-7.820D+02	1.183D+08	1.298D+07	2.959D+06	7.437D+05	1.117D+07	1.042D+07
17	-3.231D-01	-5.160D-01	3.806D+00	1.687D+01	-3.311D+06	1.106D+07	-6.395D+04	9.059D+05	-2.851D+05	6.880D+06
18	4.597D-01	9.646D+00	-2.499D+01	-1.600D+02	2.111D+07	-1.778D+06	4.900D+05	-1.039D+05	1.760D+06	-1.118D+06
19	-7.236D+00	-4.227D+01	9.610D+01	4.781D+02	-8.486D+07	-2.603D+07	-2.180D+06	-2.807D+06	-8.175D+06	-1.291D+07
20	5.310D-01	1.076D+01	-2.501D+01	-1.594D+02	2.113D+07	1.755D+06	4.914D+05	1.267D+05	1.796D+06	1.086D+06
21	4.218D+00	-3.599D+01	9.724D+01	5.622D+02	-8.598D+07	2.661D+07	-2.168D+06	2.830D+06	-8.222D+06	1.290D+07
	31	32								
1	8.718D+05	1.602D+05								
2	1.295D+06	-1.081D+06								
3	7.834D+04	-1.167D+06								

APPENDIX B

THE C. MATRIX (21 BY 32)

	31	32
4	1.160D+04	-3.703D+05
5	8.480D+05	-1.642D+05
6	1.281D+06	1.080D+06
7	5.964D+04	1.167D+06
8	-2.416D+04	4.351D+05
9	-5.731D+05	-1.069D+05
10	-2.372D+05	-1.185D+06
11	2.872D+05	-1.242D+06
12	-6.403D+05	1.098D+05
13	-2.423D+05	1.187D+06
14	2.603D+05	1.239D+06
15	-2.138D+06	-1.298D+06
16	-2.081D+06	1.300D+06
17	7.117D+04	7.412D+05
18	-5.415D+05	-8.849D+04
19	1.455D+06	-1.244D+06
20	-5.386D+05	8.207D+04
21	1.440D+06	1.241D+06

**Best
Available
Copy**

addresses	number of copies
RADC/OOSE	10
RADC/TSL GRIF-155 AFB NY 13441	1
RADC/DAP GRIF-155 AFB NY 13441	2
ADMINISTRATOR DEF TECH INF CTR ATTN: DTIC-DDA CAMERON STA 3G 5 ALEXANDRIA VA 22314	12
Lockheed Missiles & Space Co., Inc. Lockheed Palo Alto Research Laboratory 3251 Hanover St., Palo Alto, CA 94304	5
Charles Stark Draper Labs 555 Technology Square Cambridge, MA 02139	5
Charles Stark Draper Lab Attn: Dr. Keto Soosar 555 Technology Square R.S. -95 Cambridge, MA 02139	1
Charles Stark Draper Lab Attn: Dr. J.B. Linn 555 Technology Square Cambridge, MA 02139	1

Charles Stark Draper Lab
Attn: Mr. R. Strince
555 Technology Square
M.S.-60
Cambridge, MA 02139

Charles Stark Draper Lab
Attn: Dr. Daniel R. Hegg
555 Technology Square
M.S. -60
Cambridge, MA 02139

ARPA/MIS
1400 Wilson Blvd
Arlington, VA 22209

ARPA/STO
Attn: Lt Col A. Herzberg
1400 Wilson Blvd
Arlington, VA 22209

ARPA/STO
Attn: Maj E. Dietz
1400 Wilson Blvd
Arlington, VA 22209

Riverside Research Institute
Attn: Dr. R. Kappesser
Attn: Mr. A. Devilliers
1701 N. Ft. Myer Drive Suite 711
Arlington, VA 22209

Riverside Research
Attn: HALO Library, Mr. Bob Passut
1701 N. Ft. Myer Drive
Arlington, VA 22209

itek Corp
Optical Systems Division
10 Anguire Rd.
Lexington, MA 02173

Perkin Elmer Corp
Attn: Mr. H. Levenstein
Electro Optical Division
Main Avenue
Norwalk, CT 06856

1

Hughes Aircraft Company
Attn: Mr. George Speak
M.S. 8-156
Culver City, CA 90230

1

Hughes Aircraft Company
Attn: Mr. Ken Beale
Sentinela Beale Sts
Culver City, CA 90230

1

Air Force Flight Dynamics Lab
Attn: Dr. Lynn Rogers
Wright Patterson AFB, OH 45433

1

AFWL/F130
Attn: Mr. Jerome Pearson
Wright Patterson AFB, OH 45433

1

Air Force Wright Aero Lab. F133
Attn: Capt Paul Wren
Wright Patterson AFB, OH 45433

1

Air Force Institute of Technology
Attn: Prof. R. Calico/ENY
Wright Patterson AFB, OH 45433

1

Aerospace Corp.
Attn: Dr. G.I. Tseng
2350 E. El Segundo Blvd
El Segundo, CA 90245

2

Aerospace Corp.
Attn: Mr. J. Mosich
2300 E. El Segundo Blvd
El Segundo, CA 90245

Aerospace Corp/Bldg 125/1054
Attn: Mr. Steve Surrin
Advanced Systems Tech Div.
2400 E El Segundo Blvd
El Segundo, CA 90245

65/30/YLVS
Attn: Mr. Lawrence Weeks
P.O. Box 92900
Worldway Postal Center
Los Angeles CA 90009

65/YCS
Attn: YCPI/Capt Sajewski
P.O. Box 92900
Worldway Postal Center
Los Angeles, CA 90009

Grumman Aerospace Corp
Attn: Mr. A. Mendelson
South Oyster Bay Road
Bethpage, NY 11714

DUSD&E/LS
Attn: Mr. A. Bertapelli
Room 3D136
Pentagon, Washington, DC 20301

Jet Propulsion Laboratory
Attn: Mr. D.B. Schaechter
4800 Oak Grove Drive
Pasadena, CA 91103

MIT/Lincoln Laboratory
Attn: S. Wright
P.O. Box 73
Lexington, MA 02173

MIT/Lincoln Laboratory
Attn: Dr. D. Hyland
P.O. Box 73
Lexington, MA 02173

1

MIT/Lincoln Laboratory
Attn: Dr. N. Smith
P.O. Box 73
Lexington, MA 02173

1

Control Dynamics Co.
Attn: Dr. Sherman Seltzer
221 East Side Square, Suite 1B
Mantoloking, NJ 08051

1

Lockheed Space Missile Corp.
Attn: A. A. Woods, Jr., 0762-E6
P.O. Box 504
Sunnyvale, California 94088-3504

5

Lockheed Missiles Space Co.
Attn: Mr. Paul Williamson
3251 Hanover St.
Palo Alto, CA 94304

1

General Dynamics
Attn: Ray Halstenberg
Convair Division
5001 Kearny Villa Rd
San Diego, CA 92123

1

SII
Attn: Mr. R.C. Stroud
20005 Stevens Creek Blvd.
Sunnyvale, CA 95014

1

NASA Langley Research Ctr
Attn: Dr. G. Horner
Attn: Dr. Card
Langley Station Bldg 12933 W/S 230
Hampton, VA 23060

2

NASA Johnson Space Center
Attn: Robert Miland
MS. 2A
Houston, TX 77058

1

McDonald Douglas Corp
Attn: Mr. Read Johnson
Douglas Missile Space Systems Div
5301 Bulsa Ave
Huntington Beach, CA 92607

1

Integrated Systems Inc.
Attn: Dr. N. K. Gupta and M.G. Lyons
151 University Avenue, Suite 400
Palo Alto, California 94301

2

Boeing Aerospace Company
Attn: Mr. Leo Cline
P.O. Box 3999
Seattle, WA 98124
MS 8 W-23

1

TRW Defense Space Sys Group Inc.
Attn: Ralph Iwens
Bldg 82/2054
One Space Park
Redondo Beach, CA 90278

1

TRW
Attn: Mr. Len Pincus
Bldg R-5, Room 2031
Redondo Beach, CA 90278

1

Department of the Navy
Attn: Dr. K.T. Alfrend
Naval Research Laboratory
Code 7920
Washington, DC 20375

1

Airesearch Manuf. Co. of Calif.
Attn: Mr. Oscar Buchmann
2525 West 190th St.
Torrance, CA 90509

1

Analytic Decisions, Inc.
Attn: Mr. Gary Glaser
1401 Wilson Blv.
Arlington, VA 22209

1

Ford Aerospace & Communications Corp.
Drs. I. P. Leliakov and P. Barba, MS/G80
3939 Fabian way
Palo Alto, California 94304

1

Center for Analysis
Attn: Mr. Jim Justice
13 Corporate Plaza
Newport Beach, CA 92660

1

General Research Corp.
Attn: Mr. G. R. Curry
P.O. Box 3587
Santa Barbara, CA 93105

1

General Research Corp
Attn: Mr. Thomas Zakrzewski
7655 Old Springhouse Road
McLean, VA 22101

1

Institute of Defense Analysis
Attn: Dr. Hans Wolfhard
400 Army Navy Drive
Arlington, VA 22202

1

Karman Sciences Corp.
Attn: Dr. Walter E. Ware
1500 Garden of the Gods Road
P.O. Box 7463
Colorado Springs, CO 80933

1

1
MRJ, Inc.
10400 Eaton Place
Suite 300
Fairfax, VA 22030

1
Photon Research Associates
Attn: Mr. Jim Myer
P.O. Box 1318
La Jolla, CA 92038

1
Rockwell International
Attn: Russell Loftman (Space Systems Group)
(Mail Code - SL50)
12214 Lakewood Blvd.
Downey, CA 90241

1
Science Applications, Inc.
Attn: Mr. Richard Ryan
3 Preston Court
Bedford, MA 01730

1
U.S. Army Missile Command
Attn: DRSMI-RAS/Mr. Fred Haak
Redstone Arsenal, AL

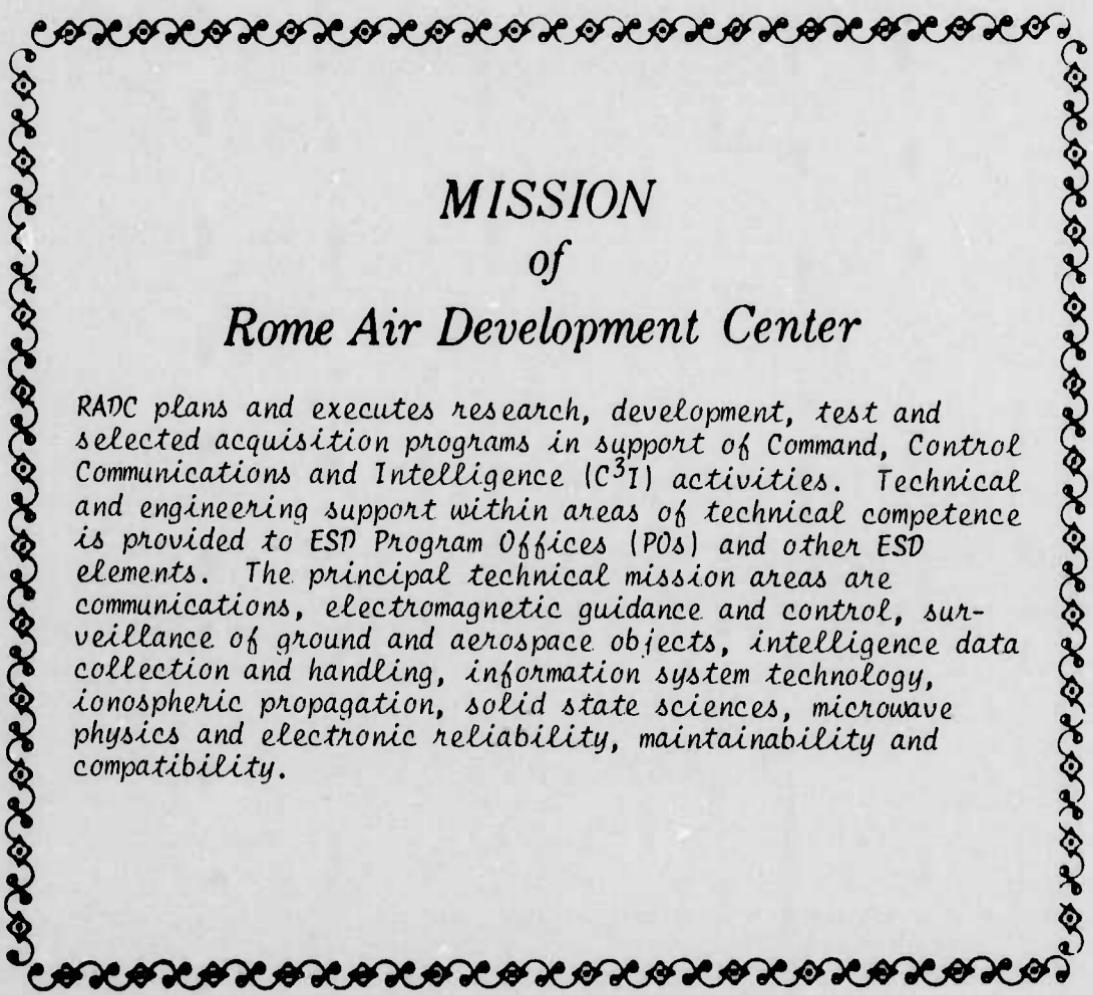
1
Naval Electronic Systems Command
Attn: Mr. Charles Good
PME-100-4
National Center 1
Washington, DC 20360

2
Lockheed Palo Alto Research Laboratory
Attn: Dr. J. N. Aubrun, 0752-56
3251 Hanover Street
Palo Alto, California 94304-1187

1
U.S. Army/DARCOM
Attn: Mr. Bernie Chasnov
AMC Bldg
5001 Eisenhower Ave
Alexandria, VA 22333

Honeywell Inc.
Attn: Mr. Thomas B. Cunningham
Attn: Mr. Michael F. Barrett
2600 Ridgway Parkway MN 17-2375
Minneapolis, MN 55413

2



*MISSION
of
Rome Air Development Center*

RADC plans and executes research, development, test and selected acquisition programs in support of Command, Control Communications and Intelligence (C³I) activities. Technical and engineering support within areas of technical competence is provided to ESD Program Offices (POs) and other ESD elements. The principal technical mission areas are communications, electromagnetic guidance and control, surveillance of ground and aerospace objects, intelligence data collection and handling, information system technology, ionospheric propagation, solid state sciences, microwave physics and electronic reliability, maintainability and compatibility.